2026-06-16

þÿ µ - U n i f o r m l y C o n v e r g e n t N u m e
Schemes for Singularly Perturbed
þÿ P a r a b o l i c C o n v e c t i o n D i f f u s i o
Problems with Boundary Turning Point

Yimesgen, Mehari Kebede

BAHIR DAR UNIVERSITY
College of Science
Department of Mathematics

ε- Uniformly Convergent Numerical Schemes for Singularly Perturbed Parabolic Convection–Diffusion Problems with Boundary Turning Point

By
Yimesgen Mehari Kebede

June 16, 2026
Bahir Dar, Ethiopia

BAHIR DAR UNIVERSITY
College of Science
Department of Mathematics

ε- Uniformly Convergent Numerical Schemes for Singularly Perturbed Parabolic Convection–Diffusion Problems with Boundary Turning Point ***By***

Yimesgen Mehari Kebede

Advisor: Awoke Andargie (PhD, Prof.)
Co-Advisor: Endalew Getnet (PhD, Assoc. Prof.)

A dissertation submitted to the Department of Mathematics, College of Science, Bahir Dar University in partial fulfilment of the requirements for the degree of Doctor of Philosophy in Applied Mathematics.

June 16, 2026
Bahir Dar, Ethiopia

Declaration

This is to certify that the dissertation entitled "ε- Uniformly Convergent Numerical Schemes for Singularly Perturbed Parabolic Convection–Diffusion Problems with Boundary Turning Point," submitted in partial fulfillment of the requirements for the degree of Doctor of Philosophy, Department of Mathematics, Bahir Dar University, is a record of original work carried out by me and has never been submitted to this or any other institution to get any other degree or certificate. The help and assistance I received during the course of this study have been acknowledged.

Yimesgen Mehari Kebede	______________	______________
Name of PhD student	Signature	Date

Bahir Dar University

College of Science

Department of Mathematics

Approval of Dissertation for Oral defense

We here by certify that we have supervised, read, and evaluated this dissertation titled "ε- Uniformly Convergent Numerical Schemes for Singularly Perturbed Parabolic Convection–Diffusion Problems with Boundary Turning Point " by Mr. Yimesgen Mehari Kebede prepared under our guidance. We recommend that Yimesgen Mehari Kebede is approved for the degree of Doctor of Philosophy in Applied Mathematics.

Prof. Awoke Andargie Tirune	____________	____________
Main Supervisor's Name	Signature	Date
Dr. Endalew Getnet Tsega	____________	____________
Co-Supervisor's Name	Signature	Date

Bahir Dar University

College of science

Department of Mathematics

Approval of Dissertation For Defense Result

We here by certify that we have examined this dissertation entitled "ε- Uniformly Convergent Numerical Schemes for Singularly Perturbed Parabolic Convection–Diffusion Problems with Boundary Turning Point " by Yimesgen Mehari Kebede. We recommend that Yimesgen Mehari Kebede is approved for the degree of Doctor of Philosophy in Applied Mathematics.

Board of Examiners

Prof. Gemechis File Duressa	______________	______________
External Examiner's Name	Signature	Date
Dr. Getachew Adamu Derese	______________	______________
Internal Examiner's Name	Signature	Date
Dr. Hunegaw Dessie Asress	______________	______________
Chair Person's Name	Signature	Date

Acknowledgment

First and for most, I would like to express my thankfulness to the Almighty God for providing me the strength, knowledge, ability, sufficient opportunity, and enabling me to start and finish this research work.

Secondly, I would like to express my deepest appreciation to my advisor, **Prof. Awoke Andargie** for his continuous support of my Ph.D. study and research, for his patience, motivation, interest, comments, and immense knowledge. His guidance helped me during all the research and writing for this dissertation. I also would like to thank my co-advisor, **Dr. Endalew Getnet** for his guidance, kind comments, and encouragement throughout my research work, from begging to end. Besides my advisors, I thank my course instructor, Dr. Birlew Belayneh, and my friend Dr. Dagnachew Mengstie and Bahir Dar University department of mathematics staff members for their encouragement, insightful comments, and questions.

Special thanks go to my wife, Anchinesh Amlak; my sister, Adanech Amlak; and my children, Betselot Yimesgen and Mekdes Yimesgen, for their patience, encouragement, and for giving me sufficient time and support throughout my research work. I am also deeply grateful to my parents, brothers, sisters, classmates, friends, and fellow candidates for their motivation and support in various aspects of my academic journey.

Finally, I would like to express my sincere gratitude to Bahir Dar University and Wollo University, KIOT, for providing the necessary facilities, resources, and financial support, both directly and indirectly, for my research work. I am also thankful to all those who have supported and encouraged me in one way or another toward the successful completion of this research.

Contents

Abbreviations

Abbreviation	Meaning
BTP	Boundary turning point.
$DDEs$	Differential-difference equations.
FDM	Finite difference method.
FMM	Fitted mesh method.
FOM	Fitted operator method.
$NSFDM$	Non-standard finite difference method.
$ODEs$	Ordinary differential equations.
$PDEs$	Partial differential equations.
$RPPs$	Regular perturbation problems.
$SPDEs$	Singularly perturbed differential equations.
$SPDDEs$	Singularly perturbed differential-difference equations.
$SPPDDEs$	Singularly perturbed parabolic differential-difference equations.
$SPPPDEs$	Singularly perturbed parabolic partial differential equations.
$SPPs$	Singularly perturbed problems.
SP-BTP	Singularly perturbed boundary turning point.
$1D$	One-dimensional problems.
$2D$	Two-dimensional problems.
$3D$	Three-dimensional problems.

Nomenclature

Symbol	Description
$\varepsilon, c_\varepsilon$	perturbation parameters.
τ	large time delay.
ω	transition parameter.
σ	fitting factor (artificial viscosity).
p	order of the turning point.
δ, μ	small delay and advance parameters, respectively.
$\Omega, \overline{\Omega}$	spatial domain and its closure.
$D_x^-, D_x^+, D_x^0, \delta_x^2, D_x^- D_x^+$	standard finite difference operators in x used to approximate first- and second-order derivatives.
$\Lambda, \overline{\Lambda}$	temporal domain and its closure.
$\mathcal{D}, \overline{\mathcal{D}}$	solution domain and its closure, $\Omega \times \Lambda$.
$\partial\mathcal{D}$	boundary of the solution domain.
$\Gamma_b, \Gamma_l, \Gamma_r$	base, left, and right boundaries of the solution domain.
h, k	mesh sizes in spatial and temporal discretization, respectively.
N, M	number of mesh intervals in the spatial and temporal domains, respectively.
T	terminal time of the temporal domain.
$\mathcal{L}_\varepsilon, \hat{\mathcal{L}}_\varepsilon, \hat{\mathcal{L}}_\varepsilon^N$	continuous, semi-discrete, and fully discrete operators, respectively.
$u(x,t), u^j(x), U_i^j$	continuous, semi-discrete, and fully discrete solutions, respectively.

Symbol	Description
$v, w, V^j, W^j, V_i^j, W_i^j$	regular and singular components of u, U^j, and U_i^j, respectively.
$C^{2,1}$	functions continuously differentiable up to second order in space and first order in time.
$O(\cdot)$, $o(\cdot)$	order notations.
$\lvert \cdot \rvert$	absolute value.
$\lVert \cdot \rVert$ or $\lVert \cdot \rVert_\infty$	maximum (supremum) norm over the domain $\mathcal{D}$.
$e_\varepsilon^{N,M}$	maximum pointwise error.
$e^{N,M}$	parameter-uniform error estimate.
$R_\varepsilon^{N,M}$	pointwise rate of convergence.
$R^{N,M}$	parameter-uniform rate of convergence.

List of Tables

List of Figures

List of Publications/Communicated

In this study the following research papers are published, accepted or submitted to some reputable journals:

1. Y.M. Kebede, A.A. Tiruneh, E.G. Tsega, Crank–Nicolson Method for Singularly Perturbed Unsteady Parabolic Problem With Multiple Boundary Turning Points, Adv. Math. Phys., 2024, **2024**(1), pp.4895771.

2. Y.M. Kebede, A.A. Tiruneh, E.G. Tsega, Non-standard Finite-Difference Scheme for Singularly Perturbed Parabolic Convection-Diffusion Problem with Boundary Turning Points, J. Math. Model., 2025, **13**(1), pp.85–103.

3. Y.M. Kebede, A.A. Tiruneh, E.G. Tsega, Fitted Operator Method for Singularly Perturbed Delay Parabolic Problems With Boundary Turning Points, Int. J. Math. Math. Sci., 2025, **2025**(1), pp.5581971.

4. Y.M. Kebede, A.A. Tiruneh, E.G. Tsega, Layer-Resolving Mesh Method for Convection-Diffusion Delay Problems with Boundary Turning Points, J. Math. Model., 2025, pp.900–923.

5. Y.M. Kebede, A.A. Tiruneh, E.G. Tsega, Hybrid Fitted Mesh Strategy for Singularly Perturbed Time-Dependent Convection-Diffusion Problems Featuring Boundary Turning Points, Int. J. Math. Math. Sci., 2025, pp.951–975.

6. Second-Order Convergence Scheme for Singularly Perturbed Unsteady Problems with Boundary Turning Point **In press**.

7. Nonstandard Finite Difference Method for Singularly Perturbed Parabolic Convection–diffusion Problems with Deviating Arguments and Boundary Turning Points **Under Review**.

8. Layer-Resolving Mesh Numerical Method for Singularly Perturbed Parabolic Convection-diffusion Turning Point problems with Deviating argument **Under Review**.

Abstract

In this dissertation, fitted operator and fitted mesh numerical methods are developed for singularly perturbed parabolic differential and differential-difference equations with boundary turning points. These problems are typically modeled by partial differential equations and differential-difference equations in which a small parameter ε multiplies the highest-order derivative and the convection coefficient vanishes at the boundary, giving rise to boundary turning points. Due to the presence of the perturbation parameter, the solution exhibits a multi-scale character, often featuring a thin transition layer where it varies abruptly, while away from the layer the solution behaves smoothly and changes gradually. Standard numerical methods on uniform meshes are generally unable to provide reliable approximations in such cases. The proposed methods in each chapter are ε-uniform, achieve better order of convergence and provide reliable solutions. The fitted operator numerical method is developed based on both the exponentially fitted operator approach and the non-standard finite difference method on uniform meshes. For the fitted mesh schemes, the well-known piecewise-uniform Shishkin mesh is employed to accurately resolve the layers. Additionally, a post-processing technique (Richardson extrapolation) is used to enhance the accuracy of some of the developed methods. To validate the theoretical findings and demonstrate the accuracy of the proposed approaches, extensive numerical results are presented in tables and graphs for various mesh sizes, perturbation parameters ε, and orders of turning point p. The stability and convergence of the schemes are rigorously established using the discrete minimum principle, consistency arguments, and a priori error bounds, leading to ε-uniform convergence results. All simulations in this dissertation are performed using MATLAB. The results demonstrate the effectiveness of the proposed schemes and show improved accuracy and convergence compared to some existing methods.

Chapter 1

General Introduction

In this chapter, we present an overview of singularly perturbed problems (SPPs), with a particular focus on singularly perturbed parabolic partial differential and differential-difference equations with boundary turning points. To provide a coherent flow to the dissertation, the chapter begins with the background of the study, including representative models, common solution methods, and a review of relevant literature. This is followed by a discussion of the research objectives, significance of the study, specific problems addressed in this study, the procedures to do this research, and the overall organization of the dissertation.

1.1 Background of the Study

Singular perturbation problems (SPPs) represent a class of mathematical problems that frequently arise across a wide range of scientific and engineering disciplines. Over time, the study of SPPs has grown significantly and continues to provide valuable insights for addressing complex challenges in these fields. In fluid dynamics, SPPs model high Reynolds number flows, where viscous effects are confined to narrow boundary layers. In wave mechanics and turbulence modeling, they help describe fluctuating motions in wave–current systems. In heat and mass transfer, particularly in nuclear and chemical engineering, they are used to simulate diffusion with reaction, convective transport, and related phenomena. Additionally, quantum physics and electroanalytical chemistry often involve models exhibiting singular perturbation characteristics due to disparities in interaction scales [114].

SPPs are typically identified by differential or differential-difference equations that include very small parameters multiplying the highest-order derivatives. These small parameters lead to sharp changes, rapid transitions, and interactions between different scales in the system. A well-known example of an SPP is the Navier–Stokes equation in fluid dynamics [25],

$$\frac{\partial(u^2+p)}{\partial x}+\frac{\partial(uv)}{\partial y}=\frac{1}{Re}\left(\frac{\partial^2 u}{\partial x^2}+\frac{\partial^2 v}{\partial y^2}\right) \tag{1.1}$$

with suitable initial and boundary conditions. Here u and v are the velocity components along the x and y directions and p is pressure. The parameter 'Re' is called 'Reynolds number'. For sufficiently large $Re \gg 1$, the equation (1.1) will be transformed in to a singularly perturbed differential equation. The term singular perturbation (SP) was first introduced in the 1940s by Wasow [132], and SP problems are generally characterized by dynamics operating on multiple scales and their solution contain layer. Ludwig Prandtl introduced the terminology boundary layer at the Third International Congress of Mathematicians in Heidelberg in 1904 [96]. A boundary layer is a narrow region within the boundary of the domain of a differential equation where the solution changes rapidly compared to the rest of the domain. Outside this region, called the outer region, the solution varies slowly. In physical problems (such as fluid flow, heat transfer, or diffusion), the boundary layer represents a thin region adjacent to a boundary or an interface where physical quantities like velocity, temperature, or concentration experience steep gradients due to viscous, conductive, or diffusive effects.

Perturbation problems are generally classified into two main categories: regular perturbation problems (RPPs) and singular perturbation problems (SPPs). In an RPP, the behavior of the solution remains essentially unchanged as the perturbation parameter ε approaches zero; that is, setting $\varepsilon = 0$ in the governing equation does not significantly alter the nature of the solution. In contrast, an SPP exhibits markedly different behavior when $\varepsilon \to 0$ and when $\varepsilon = 0$; the limiting process leads to qualitative changes in the solution.

Generally, a parameter–dependent problem P_ε is called regularly perturbed if its solution $u_\varepsilon(x)$ satisfies $u_\varepsilon \to u_0$ uniformly on its domain as $\varepsilon \to 0$, where u_0 is the solution of the reduced problem P_0. If this uniform convergence fails, the problem is called singularly perturbed.

Several formal characterizations of singularly perturbed problems have been proposed in the literature:

- In. [79]:

  The term "singular perturbation" arises because the nature of the differential equation changes completely in the limiting case when the perturbation parameter becomes zero.

- In [106]:

  Singularly perturbed problems are differential equations (ordinary or partial) that depend on a small positive parameter ε, whose solutions approach a discontinuous limit as $\varepsilon \to$

0. Such problems are described as singularly perturbed, with ε acting as the perturbation parameter.

Singular perturbation problems also can be classified into two categories:

1. *Cumulative type* (oscillatory solutions), where the perturbation's effect becomes significant only after long times

2. *Boundary layer type*, characterized by solutions with rapid variations in narrow regions

This dissertation focuses on boundary layer problems, which are particularly relevant in fluid dynamics and heat transfer applications.

1.1.1 Locations of Layers

The solutions of SPDEs have a layer behaviour usually in a narrow region in which its position varies from problem to problem, so it is not possible to develop a generic method which can be applied to different classes of SPPs. Mathematically, we first consider a singularly perturbed boundary value problem,

$$P_\varepsilon : \quad \begin{cases} -\varepsilon u''(x) + p(x)u'(x) + q(x)u(x) = g(x), \quad a < x < b, \\ u(a) = \alpha, u(b) = \beta. \end{cases} \tag{1.2}$$

where $0 < \varepsilon \ll 1$, and $p(x)$, $q(x)$, and $g(x)$ are sufficiently smooth functions. Assuming that, for each ε, the problem P_ε has a unique smooth solution $u_\varepsilon(x)$, we aim to construct approximations of $u_\varepsilon(x)$ for small values of ε. The solution $u_\varepsilon(x)$ of P_ε depends on ε as well as on the boundary conditions. We obtain the so-called reduced problem P_0 having solution u_0 by putting $\varepsilon = 0$ in (1.2):

$$P_0 : \quad \begin{cases} p(x)u_0'(x) + q(x)u_0(x) = g(x), \quad a < x < b, \\ u_0(a) = \alpha, u_0(b) = \beta. \end{cases} \tag{1.3}$$

The reduced solution $u_0(x)$ may fail to satisfy both boundary conditions simultaneously. This mismatch signals the presence of boundary layers in the solution of the full problem.

For a layperson, natural questions may arise:

- Does the problem (1.2) have a limiting solution as $\varepsilon \to 0$, i.e., does $\lim_{\varepsilon \to 0} u_\varepsilon(x)$ exist?

- If yes, then:

  i Does this solution satisfy equation (1.3), i.e., does $\lim_{\varepsilon \to 0} u_\varepsilon(x) = u_0(x)$ hold true?

  ii Which of the boundary conditions will be satisfied by the limiting solution?

The boundary layer is formed near the boundary of the domain where the solution of the reduced problem fails to satisfy the prescribed boundary condition.

- In [105], the location of the boundary layer is defined as follows: Let $u(x)$ be the solution of equation (1.2), and let $x = a$, where $a \in \{0, 1\}$, denote a boundary point. The point $x = a$ is said to be a boundary layer point if the following inequality holds:

$$\lim_{x \to a} \lim_{\varepsilon \to 0} u(x) \neq \lim_{\varepsilon \to 0} \lim_{x \to a} u(x).$$

Table 1.1 below shows the nature and location of the layer for the problem (1.2) [50].

Table 1.1: Summary of locations of layers

<table>
<tr><td>Conditions on $p(x)$ and $q(x)$</td><td>Type and location of layers</td></tr>
<tr><td colspan="2">Non-turning point problem ($p(x) \neq 0$, $q(x) \geq 0$)</td></tr>
<tr><td>$p(x) < 0$
$p(x) > 0$</td><td>Boundary layer at $x = a$.
Boundary layer at $x = b$.</td></tr>
<tr><td colspan="2">Reaction-diffusion problem ($p(x) = 0$)</td></tr>
<tr><td>$q(x) > 0$
$q(x) < 0$
$q(x)$ changes sign</td><td>Boundary layers at $x = a$ and $x = b$.
Rapidly oscillating solution.
Classical turning point.</td></tr>
<tr><td colspan="2">Turning point problem ($p'(x) \neq q(x), \quad q(x) \geq 0 \ \forall x \in [a, b]$, and $p(d) = 0 \quad$ for some $d \in (a, b)$)</td></tr>
<tr><td>$p'(d) < 0$
$p'(d) > 0$</td><td>No boundary layers; interior layer at $x = d$.
Boundary layers at $x = a$ and $x = b$.</td></tr>
<tr><td colspan="2">Discontinuous convection coefficient ($p(x) = 0$, $g(x)$ discontinuous at $d \in (a, b)$)</td></tr>
<tr><td></td><td>Boundary layers at $x = a$ and $x = b$, and
interior layers on both sides of $x = d$.</td></tr>
</table>

1.1.2 Singularly Perturbed Turning Point Problems

Singularly perturbed turning point problems form a special class of singularly perturbed differential equations in which the convection (or transport) coefficient vanishes at certain points in the domain, called turning points. These problems typically involve a small positive parameter ε multiplying the highest-order derivative, leading to sharp layer behavior in parts of the solution. Turning points introduce significant mathematical complexity, as they cause qualitative changes in the solution behavior and layer structure, such as transitions from exponential growth to decay, or vice versa [130, 90]. The singularly perturbed turning point problems are attractive to both applied mathematicians and pure mathematicians due to the fact that the solutions exhibit some interesting behavior, such as boundary layer, interior layer and resonance phenomena [1, 18, 33]. In particular, singularly perturbed turning point problem received much attention in the literature due to the complexity involved in finding uniformly valid asymptotic expansions. Some authors, such as Jindge [48], O'Malley [88, 89], Smith [115], Wasow [129], and Watts [133] studied the qualitative aspects of these problems, namely existence, uniqueness and asymptotic behavior of the solution. For multiple turning point problems, one can see [127, 128]. Kevorkian and Cole [55] constructed an asymptotic expansion for turning point problems by using the variational approach given by Grassman and Matkowsky [38]. For a detailed treatment of the theory of singularly perturbed ordinary differential equations (ODEs) with turning points, the reader is referred to the works cited in [74, 1, 18, 32, 33, 46, 53, 64, 70, 87, 71, 81, 27, 113, 128].

SPPs with turning points arise as mathematical models for various physical phenomena. Among these, the problem with interior turning points represents the one-dimensional version of stationary convection-diffusion problems with a dominant convective term and a speed field that changes its sign in the catch basin. On the other hand, boundary turning point problems arise in geophysics [44] , in the modelling of thermal boundary layers in laminar flow [109], drift-diffusion equation of semiconductor device [95] and modeling of transport phenomena [113]. The problem from [44] models heat flow and mass transport near an oceanic rise. It is a single boundary turning point problem due to the assumption of a linear velocity distribution. However, if a higher-order velocity distribution is considered, the problem becomes one with multiple boundary turning points [109]. Turning point problems are particularly relevant in aerodynamics, where flow transitions between subsonic and supersonic regimes, and in plasma physics, where internal interfaces (turning points) create sharp transition layers [22, 30, 119]. A deep understanding of singularly perturbed turning point problems is essential for designing reliable numerical schemes that can accurately simulate complex physical systems characterized by strong convective effects and multiscale behavior.

Mathematically, consider the singularly perturbed two-point boundary value problem[128]

$$-\varepsilon u''(x) \pm x^p b(x)\, u'(x) + c(x)\, u(x) = f(x), \quad x \in [s, 1], \tag{1.4}$$

with boundary conditions

$$u(s) = A, \quad u(1) = B,$$

where $0 < \varepsilon \ll 1$, $p \in \mathbb{N}$, and $s = 0$ or $s = -1$. We assume

$$b(x) > 0, \quad c(x) \geq 0, \quad x \in [s, 1].$$

The coefficient $x^p b(x)$ vanishes only at $x = 0$, creating an isolated turning point.

- When $s = 0$, the turning point lies at the boundary and we refer to it as a boundary turning point.
- When $s = -1$, the turning point is in the interior and is called an interior turning point.
- If $p = 1$, the turning point is termed a simple turning point.
- If $p \geq 2$, it is referred to as a multiple turning point, since not only $x^p b(x)$ but also its first derivative vanish at $x = 0$.
- In the case of plus sign of $x^p b(x)$, it is called a repulsive turning point (diverging flow).
- In the case of minus sign of $x^p b(x)$, it is called an attractive turning point (converging flow).

Another turning point model example extensively studied in the literature is

$$\varepsilon y''(x) + p(x)y'(x) - q(x)y(x) = f(x), \quad x \in (c, d), \tag{1.5}$$

with boundary conditions

$$y(c) = \alpha, \quad y(d) = \beta,$$

where $c < 0$, $d > 0$, $0 < \varepsilon \ll 1$, and $y, p, q, f \in C^\infty[c, d]$ are real-valued scalar functions. We assume that $p(x)$ has a single simple zero in $[c, d]$. Without loss of generality, we take $p(0) = 0$. Then, $x = 0$ is called a turning point for problem (1.5).

A priori bounds for solutions to interior turning point problems were established in several studies [1, 18, 33]. In particular, it was shown that the bound is independent of the singular perturbation parameter ε if and only if the reaction coefficient $q(x)$ is positive at the turning point. Furthermore, it was demonstrated that the ratio

$$k = \frac{q(x)}{p_x(x)}\Big|_{x=0}$$

plays a fundamental role in determining the behavior of the solution. If $k < 0$, the solution remains smooth near the turning point, and two exponential outflow boundary layers typically form at both endpoints of the domain. In this case, the turning point is sometimes called a diverging flow or expansion turning point. Conversely, if $k > 0$, then generally no boundary layers form at the boundaries; instead, an interior layer develops at the turning point, whose nature depends sensitively on the value of k. For $0 < k < 1$, the interior layer is referred to as a cusp layer because it can be approximated by a cusp-like function shape. The interior turning point in this regime is also called a converging flow or compression turning point. This type of interior layer turning point problem has been thoroughly analyzed by Farrell [33].

Interior turning point problems naturally arise, for example, as linearized one-dimensional slices of fluid flow problems containing regions of recirculation. In inviscid fluid dynamics, a diverging flow turning point corresponds to a sonic point, while a converging flow turning point corresponds to a shock point. An interesting special case occurs when $q(x) = 0$ at the turning point. In this situation, the solution exhibits the so-called Ackerberg–O'Malley resonance phenomenon [3], which involves a non-standard interaction between inner and outer expansions and requires even more careful analytical treatment. For further detailed discussions and rigorous analysis, one can refer to [1, 3, 18, 33].

1.1.3 Singularly Perturbed Parabolic Differential-Difference Equations with Turning Point

Mathematical models that account for both the present state and the historical evolution of a system are essential in numerous areas of science and engineering. Such models arise in feedback control theory, where delays naturally represent signal transmission times and actuator response lags [17, 56]. They also appear in epidemiology, where incubation periods are captured in disease dynamics [24]; in biology, for modeling processes such as cell cycles, immune responses, and haematopoiesis [65, 116]. These systems are typically governed by functional differential equations, commonly referred to as delay differential equations (DDEs) or differential-difference equations [17, 43, 56]. In the life sciences, delays often correspond to hidden variables, such as unobserved biochemical processes, that embed memory effects into system dynamics [11]. As noted in [36], even seemingly small delays can substantially alter system behavior, potentially leading to inaccurate predictions if ignored. Although delay differential equations (DDEs) are sometimes approximated by ordinary differential equations (ODEs) for analytical or computational simplicity, such approximations risk neglecting critical dynamic features.

As [56] warns:

"Small delays can have large effects."

In contrast to ODEs where the evolution of the state variable $x(t)$ depends solely on its current value DDEs incorporate both present and past states, providing a more accurate and realistic framework for modeling systems with memory. Singularly perturbed differential-difference equations (SPDDEs) involve a small perturbation parameter multiplying the highest-order derivative, combined with at least one delay (negative shift) or advance (positive shift) term. These shift terms can appear either in time or space. When the delay is in time, the problem is referred to as a singularly perturbed time-delay partial differential equation (SPTDDE), when in space, as a space-shift partial differential equation.

A defining feature in some SPDDEs is the presence of a turning point a point in the domain where the convection coefficient vanishes and may change sign. These turning point properties introduce significant analytical and numerical challenges compared to singular perturbation problems without turning points, due to possible changes in the qualitative behaviour of solutions. When delays or advances are present, the complexity of the problem increases substantially. Time delays are particularly important in biological systems, such as population dynamics, epidemiology, immunology, physiology and neural networks [126, 9, 23]. In these settings, delays capture effects like maturation periods (gestation period), infection incubation, immune responses, and other hidden physiological or behavioural processes.

Singularly perturbed space-shift PDEs (advanced or delayed in space) also arise in modeling microscale heat transfer [110], membrane diffusion [61], and neuronal activity in response to random synaptic inputs [118]. In all these cases, both the small perturbation parameter and the shift (delay or advance) terms play critical roles in accurately capturing system dynamics and reproducing layer behavior.

A general form of a singularly perturbed parabolic differential-difference equation (SPDDE) with turning points on $x \in (c, d), \quad t > 0$ is given by

$$\varepsilon u_{xx}(x,t)+a(x,t)u_x(x,t)-b(x,t)u(x,t)-u_t(x,t) = \begin{cases} f\big(x,t,u(x,t),u(x-\delta,t),u(x+\mu,t)\big), & \text{(space shifts)}, \\ g\big(x,t,u(x,t),u(x,t-\tau)\big), & \text{(time delay)}, \end{cases} \tag{1.6}$$

where $0 < \varepsilon \ll 1$ is a small perturbation parameter, and μ, δ represent spatial shift parameters (with δ corresponding to a negative shift or delay and μ to a positive shift or advance) and τ is time delay parameter. A point $\bar{x} \in [c, d]$ at which $a(\bar{x}, t) = 0$ for some fixed time t is called a turning point at time t. If this zero coincides with a boundary point, it is referred to as a boundary turning point, if it lies strictly within the domain, it is called an interior turning point.

When τ, μ and δ are zero, equation (1.6) reduces to a singularly perturbed parabolic partial differential equation.

- If the shifts τ,μ and δ are small relative to ε, they can often be approximated via Taylor expansions, simplifying numerical schemes.
- If the shifts are comparable to or larger than ε, they may generate additional interior or boundary layers, and require special treatment to ensure that shifted arguments coincide with discretization nodes.

1.1.4 Some Well-known Singularly Perturbed Model Problems

Some singular perturbation models that simulate real-world problems are listed below:

1. **Heat and Mass Transfer Near Oceanic Rises** [44]

   For one-dimensional (along the stagnation point streamline), non-dissipative steady flow, the heat transport equation is given by

$$K\frac{d^2T}{dz^2} + \rho C_v v(z)\frac{dT}{dz} - \rho\alpha g v(z)T = 0, \tag{1.7}$$

   where

$$\begin{aligned}
\alpha &- \text{coefficient of thermal expansion,}\\
\rho &- \text{density of the medium,}\\
C_v &- \text{specific heat at constant volume,}\\
g &- \text{gravitational acceleration,}\\
K &- \text{thermal conductivity,}\\
v(z) &- \text{velocity distribution,}\\
T &- \text{temperature.}
\end{aligned}$$

   Introducing a non-dimensional distance

$$\zeta = \frac{\alpha g}{C_v} z,$$

and approximate the velocity distribution by retaining only the linear term, so that equation (1.7) becomes

$$\varepsilon \frac{d^2T}{d\zeta^2} + \zeta \frac{dT}{d\zeta} - \zeta T = 0, \tag{1.8}$$

where

$$\varepsilon = \frac{K(\alpha g/C_v)^3}{\alpha \rho g a_1}$$

is a dimensionless parameter. Equation (1.8) is solved subject to the boundary conditions

$$\zeta = 0 \quad (z = 0): \quad T = T_0, \tag{1.9}$$

$$\zeta = p \quad (z = l): \quad T = T_1, \tag{1.10}$$

where $p = \frac{\alpha g}{C_v} l$, and l is the depth from which upward displacement begins.

2. The resonant turning point problem[131]

   The resonant turning point problem arises in the context of a time-independent Fokker–Planck equation for a one-dimensional dynamical system with state-independent random perturbations and is given by

$$\varepsilon^2 \frac{d^2\varphi}{dx^2} + b(x)\frac{d\varphi}{dx} = 0, \quad \varphi(0,\varepsilon) = A, \quad \varphi(1,\varepsilon) = B, \quad x \in (0,1), \tag{1.11}$$

   where $0 < \varepsilon \ll 1$ and $b(x)$ denotes a gradient field.

   Under the assumptions that $b'(x)$ is strictly negative throughout the interval $[0,1]$ and $b(r_0) = 0$ for some $0 < r_0 < 1$, the above problem is known as a resonant turning point problem.

   The point $x = r_0$ at which $b(x)$ vanishes is called the turning point, and it separates regions where the convective field $b(x)$ changes sign.

3. **The Neuron Variability Model**

   In 1965, a mathematical model was developed for describing the time evolution trajectories of membrane potential for neuron variability [117]. In 1967, the author generalized his model to handle a distribution of postsynaptic potential amplitudes [118]. The determination of the expected time for the generation of action potentials in nerve cells by random synaptic inputs in the dendrites can be modeled as a first-exit time problem.

   A generalized form of Stein's neuron variability model was proposed in 1991 in terms of singularly perturbed parabolic differential-difference equations (SPPDDEs) to describe the time evolution trajectories of the membrane potential [83].

$$\frac{\partial u}{\partial t} = \frac{\sigma^2}{2}\frac{\partial^2 u}{\partial x^2} + (\mu_D - x\tau)\frac{\partial u}{\partial x} + \lambda_s u(x + a_s, t) + \omega_s u(x + i_s, t) - (\lambda_s + \omega_s)u(x, t), \tag{1.12}$$

where the first derivative term accounts for the exponential decay between two consecutive jumps caused by the input processes. The membrane potential (u) decays exponentially to the resting level with a membrane time constant τ. The parameters μ_D and σ are the diffusion moments of a Wiener process characterizing the influence of dendritic synapses on cell excitability. The excitatory input contributes to the membrane potential by an amplitude a_s with intensity λ_s, and similarly, the inhibitory input contributes by an amplitude i_s with intensity ω_s. This model provides a framework for studying the time evolution of membrane potential trajectories. However, deriving an exact solution of this model for physiologically acceptable parameters is extremely difficult [124]. Consequently, the study of the model relies heavily on numerical methods.

4. **Processing of Metal Sheets**

   The processing of metal sheets is modeled by the following singularly perturbed partial differential equation:

$$\frac{\partial u}{\partial t} = D\frac{\partial^2 u}{\partial x^2} + v(f(u(x, t - \rho)))\frac{\partial u}{\partial x} + a[g(u(x, t - \rho)) - u(x, t)], \quad 0 < x < 1, \tag{1.13}$$

   where u denotes the distribution of the temperature in the metal sheet having velocity v and is heated by the source g, the speed of the controller introduces a fixed delay of length ρ [8].

In this dissertation, we develop and analysis parameter uniform numerical schemes for 1D time dependent SPPDEs with simple and higher order boundary turning point.

1.1.5 Methods of Solution for Singularly Perturbed Problems

In general, solutions of singularly perturbed problems (SPPs), with or without turning points, exhibit rapid variations within narrow region(s) called layers and smooth behaviour elsewhere. This multi-scale nature, involving both slow and fast dynamics, renders such problems inherently stiff and challenging to approximate the solution. SPPs are typically analyzed using two complementary approaches: asymptotic analysis and numerical methods. Asymptotic techniques provide qualitative insight by constructing approximate solutions valid in different regions of the domain. These involve outer expansions, valid away from layers, and inner expansions, capturing sharp gradients within layers using stretched variables. The solutions are then combined using the matched asymptotic expansion method to form a uniformly valid approximation across the entire domain. Near turning points, specialized methods such as the WKB (Wentzel–Kramers–Brillouin) or Airy-type expansions are employed to describe local behavior accurately [86, 130]. However, these approaches can be technically challenging, especially when multiple turning points or strong nonlinearities are present, making it difficult to determine inner scalings and perform accurate matching.

The matched asymptotic expansion method, originally developed by Prandtl in 1905 for boundary-layer problems in fluid dynamics [45], remains one of the most widely used asymptotic tools. Other important asymptotic techniques include the method of multiple scales, which introduces separate fast and slow variables to construct uniformly valid approximations for problems with widely differing scales [19, 45, 78, 91]. Despite their strengths, purely analytical asymptotic methods may not always be practical, particularly for complex or highly nonlinear problems. Consequently, numerical methods play a crucial role in resolving SPPs. Standard numerical schemes such as finite difference, finite element, and finite volume methods often fail to resolve sharp layers accurately on uniform meshes unless an impractically fine discretization is used [105, 90, 79]. To overcome this challenge, parameter-uniform numerical methods have been developed. These methods are designed to provide convergence rates that are independent of the perturbation parameter ε, ensuring reliable accuracy even as ε becomes very small. The key idea behind these methods is to incorporate information about the layer structure either through mesh adaptation or through modifications to the numerical scheme itself.

Definition 1.1. *[105](**ε-uniformly convergent:**) Consider a family of mathematical problems parameterized by a singular perturbation parameter ε, where $0 < \varepsilon \leq 1$. Assume that each problem in the family has a unique solution denoted by $u(x_i, t_j)$ and U_i^j be a numerical approximation of $u(x_i, t_j)$ obtained by a numerical method with h and k are mesh size of spatial and time directions respectively. The numerical method is said to be $\varepsilon-$uniformly convergent, if*

$$\sup_{0<\epsilon\leq 1} \max_{i,j} |u(x_i, t_j) - U_i^j| \leq C(h^{p_1} + k^{p_2}),$$

where C independent of ε, and p_1 and p_2 are positive real numbers called order of convergence in space and time variables, respectively.

A central strategy in parameter-uniform methods is the use of layer-adapted meshes, such as Shishkin and Bakhvalov meshes, which place more grid points in regions where layers are expected. These meshes enable standard finite difference or finite element discretizations to achieve uniform accuracy without requiring global mesh refinement. It requires the prior information about the location and width of the boundary layer. Another approach involves fitted operator methods, where the discrete operators are carefully constructed to account for the expected asymptotic behavior of the solution, effectively capturing layer phenomena even on simpler meshes. For comprehensive discussions on the theory and construction of parameter-uniform methods, see, for example, [105, 62, 77].

The fitted operator methods can be broadly classified into two categories based on the formulation of the numerical scheme: non-standard finite difference methods (NSFDMs) and fitted operator finite difference methods (FOFDMs). In NSFDMs, a uniform mesh is used, and a specially constructed denominator function is introduced in the discretization of the diffusion term using exact finite difference techniques to account for the perturbation parameter [76, 75]. This approach is versatile and can be extended to higher-dimensional and nonlinear singularly perturbed problems, with several studies addressing two- and three-dimensional cases [92, 93]. On the other hand, FOFDMs also employ a uniform mesh but incorporate an exponential fitting parameter derived from the asymptotic behavior of the solution to effectively capture rapid variations within boundary layers. This method was first introduced in [26]. However, this method is generally limited to linear one-dimensional problems and is not effective for nonlinear or higher-dimensional cases.

In this dissertation, we develop and analyse fitted operator and fitted mesh numerical methods to solve time-dependent singularly perturbed convection-diffusion differential equations (SPCD-DEs) and singularly perturbed convection-diffusion differential-difference equations (SPPCD-DDEs) with boundary turning point. Various simple and computationally efficient fitted numerical methods are formulated, analyzed, and shown to provide more accurate solutions than some existing methods.

1.1.6 Literature Review

As highlighted in numerous studies, research on singularly perturbed problems (SPPs) has received significant attention over the decades. Several survey articles have comprehensively reviewed the asymptotic and numerical analysis of SPPs, covering singular perturbation models and the corresponding numerical methods developed over different periods [52, 50, 51, 49, 111, 104]. These studies addressed various aspects of SPPs, including stabilization techniques, adaptive methods, fitted mesh approaches, turning point problems, and interior layer phenomena. In the present work, the studies summarized in these surveys are not discussed in detail; however, they are referenced whenever necessary in relation to specific topics.

To obtain accurate numerical solutions for SPPs, various ε-uniformly convergent methods have been developed. Two major classes of such methods are the fitted operator methods and the fitted mesh methods. The fitted operator approach was initially introduced for relaxation-type problems and later extended and analyzed for ordinary differential equations (ODEs) [26, 47]. Similarly, fitted mesh methods were constructed and justified for elliptic equations [12]. Following these foundational developments, extensive research has been devoted to constructing ε-uniformly convergent numerical methods for both singularly perturbed ordinary differential equations (SPODEs) and singularly perturbed partial differential equations (SPPDEs). Several fitted operator and fitted mesh approaches have subsequently been proposed and analyzed for SPODEs [6, 7, 34, 94, 121, 10, 82, 21]. In the context of PDEs, the first ε-uniformly convergent finite difference schemes in the maximum norm were developed for both fitted operator and fitted mesh frameworks [31, 5, 63, 112].

In the following three subsections, the focus is on recently conducted research on singularly perturbed partial differential equations that are directly related to the present work.

1.1.6.1 Singularly Perturbed Parabolic Convection-Diffusion Equations with BTP

Singularly perturbed turning point problems have received considerable attention since the late 1960s [111]. Various numerical methods have been proposed for solving singularly perturbed parabolic convection–diffusion problems with turning points subject to Dirichlet and Robin boundary conditions.

A singularly perturbed parabolic convection–diffusion problem with a boundary turning point of the form

$$\varepsilon\frac{\partial^2 u(x,t)}{\partial x^2}+a(x,t)\frac{\partial u(x,t)}{\partial x}-b(x,t)u(x,t)-\frac{\partial u(x,t)}{\partial t}=f(x,t), \qquad (x,t)\in\mathcal{D}=(0,1)\times(0,T] \quad (1.14)$$

subject to the initial–boundary conditions

$$\begin{cases} u(x,0)=s(x) \text{ on } S_x:=(x,0):0\le x\le 1,\\ u(0,t)=q_0(t) \text{ on } S_0:=(0,t):0\le t\le T,\\ u(1,t)=q_1(t) \text{ on } S_1:=(1,t):0\le t\le T, \end{cases} \quad (1.15)$$

has been widely investigated in the literature [28]. Here,

$$0<\varepsilon\ll 1,$$

and

$$a(x,t) = a_0(x,t)x^p, \qquad p \geq 1, \qquad a_0(x,t) \geq \alpha > 0, \qquad b(x,t) \geq \beta > 0,$$

for all $(x,t) \in \bar{D}$.

A first-order ε-uniform numerical method based on the standard upwind finite difference scheme on a fitted piecewise-uniform mesh for space discretization and the implicit Euler method on a uniform mesh for time discretization was proposed and analyzed [28]. Many subsequent studies have been based on the problem defined by Equations (1.14)–(1.15). Several numerical approaches have subsequently been developed using different combinations of temporal and spatial discretization techniques. These include implicit Euler methods combined with cubic B-spline collocation methods on Shishkin meshes [39], Crank–Nicolson methods combined with upwind finite difference schemes on Shishkin meshes [60], and implicit Euler methods together with fitted mesh schemes improved through Richardson extrapolation techniques [68]. Hybrid finite difference schemes combining central difference and midpoint upwind methods on piecewise-uniform Shishkin meshes have also been proposed and analyzed [69].

Further developments include numerical schemes employing generalized Shishkin meshes with Richardson extrapolation to improve convergence orders [134], adaptive layer-resolving meshes generated through monitor functions [58], and extrapolated upwind methods on piecewise-uniform meshes [107]. In addition, parameter-uniform methods combining Crank–Nicolson time discretization with exponentially fitted operator techniques on uniform meshes have also been investigated [123]. Although this class of problems has been extensively studied, most existing methods are based primarily on fitted mesh techniques and generally achieve only first-order convergence before the application of extrapolation techniques. Moreover, most studies focus mainly on simple boundary turning point problems to describe the overall behavior of the solution. Therefore, the construction of fitted numerical schemes that are uniformly higher-order accurate simultaneously in both space and time variables remains a significant open problem.

1.1.6.2 Singularly Perturbed Parabolic Delay Partial Differential Equations with BTP

A singularly perturbed parabolic convection–diffusion time delay problem with a boundary turning point of the form

$$\varepsilon \frac{\partial^2 u(x,t)}{\partial x^2} + a(x,t)\frac{\partial u(x,t)}{\partial x} - b(x,t)u(x,t) - d(x,t)\frac{\partial u(x,t)}{\partial t} = f(x,t) + c(x,t)u(x,t-\tau), \quad (1.16)$$

subject to the initial and boundary conditions

$$\begin{cases} u(x,t) = s(x,t), & (x,t) \in [-1,1] \times [-\tau, 0], \\ u(-1,t) = q_0(t), \quad u(1,t) = q_1(t), & t \in [0,T], \end{cases} \tag{1.17}$$

has been investigated in [135], where $0 < \varepsilon \ll 1$ is the perturbation parameter and $\tau > 0$ is the delay parameter. Moreover,

$$a(x,t) = -a_0(x,t)x^p,$$

with $p \geq 1$ being a non-negative odd integer, $a_0(x,t) \geq \alpha > 0$, $b(x,t) \geq \beta > 0$, and $c(x,t) > 0$ for all $(x,t) \in \bar{\mathcal{D}}$. A fitted mesh method based on an upwind finite difference scheme on a non-uniform mesh was proposed and analyzed. The resulting scheme achieved almost first-order convergence in both the spatial and temporal variables before extrapolation.

Another singularly perturbed parabolic convection–diffusion time delay problem with a boundary turning point of the form

$$\varepsilon \frac{\partial^2 u(x,t)}{\partial x^2} + a(x,t)\frac{\partial u(x,t)}{\partial x} - b(x,t)u(x,t) - \frac{\partial u(x,t)}{\partial t} = f(x,t) + c(x,t)u(x,t-\tau), \tag{1.18}$$

subject to the initial and boundary conditions

$$\begin{cases} u(x,t) = s(x,t), & (x,t) \in [0,1] \times [-\tau, 0], \\ u(0,t) = q_0(t), \quad u(1,t) = q_1(t), & t \in [0,T], \end{cases} \tag{1.19}$$

was studied in [100], where $0 < \varepsilon \ll 1$ is the perturbation parameter and $\tau > 0$ is the delay parameter. Furthermore,

$$a(x,t) = a_0(x,t)x^p,$$

with $p \geq 1$, $a_0(x,t) \geq \alpha > 0$, $b(x,t) \geq \beta > 0$, and $c(x,t) > 0$ for all $(x,t) \in \bar{\mathcal{D}}$. To approximate the solution, a numerical method consisting of a backward Euler scheme for time discretization on a uniform mesh and a hybrid spatial discretization combining midpoint upwind and central difference schemes on a modified Shishkin mesh was proposed. The temporal convergence order was further improved using the Richardson extrapolation technique. Existing studies on singularly perturbed parabolic delay partial differential equations (PDEs) with boundary turning points remain relatively limited and have generally achieved only first-order accuracy prior to extrapolation. Therefore, the construction of schemes that are ε-uniformly convergent and higher-order accurate (second order or higher) simultaneously in both spatial and temporal variables remains a significant open problem.

1.1.6.3 Singularly Perturbed Parabolic Convection-Diffusion Turning Point Problems with General Shifts

A singularly perturbed parabolic differential–difference equation with a boundary turning point and deviating arguments of the form

$$\varepsilon\frac{\partial^2 u(x,t)}{\partial x^2}+a(x,t)\frac{\partial u(x,t)}{\partial x}-b(x,t)u(x-\delta,t)-c(x,t)u(x,t)-d(x,t)u(x+\mu,t)-\frac{\partial u(x,t)}{\partial t}=f(x,t), \tag{1.20}$$

subject to the initial and boundary conditions

$$\begin{cases} u(x,0)=u_0(x), & \forall x\in s_x,\\ u(x,t)=\phi(x,t), & \forall (x,t)\in\Omega_l=\{(x,t):-\delta\le x\le 0;\ t\in\Lambda\},\\ u(x,t)=\psi(x,t), & \forall (x,t)\in\Omega_r=\{(x,t):1\le x\le 1+\mu;\ t\in\Lambda\}, \end{cases} \tag{1.21}$$

on the domain $D=\Omega\times\Lambda=(0,1)\times(0,T]$, for a fixed $T>0$, was investigated in [99]. Here, $a(x,t)=a_0(x,t)x^p$, with $p\ge 1$ for all $(x,t)\in\bar{D}$, and $0<\varepsilon\ll 1$ is the perturbation parameter. They proposed a first-order ε-uniform numerical method consisting of the implicit Euler method in time on a uniform mesh and the standard upwind finite difference method on a non-uniform mesh of Shishkin type in space.

To the best of our knowledge, the only existing study addressing singularly perturbed parabolic differential-difference equations with boundary turning points and deviating arguments is the work by Rai and Sharma [99]. However, the proposed numerical scheme achieves only first-order accuracy and does not investigate the more complex case of higher-order turning points (i.e., $p\ge 2$ in the coefficient $a(x,t)=a_0(x,t)x^p$). Therefore, the development of robust, high-order numerical schemes that maintain ε-uniform convergence, as well as a systematic analysis of how higher-order turning points (where $p\ge 2$) affect the solution structure and numerical approximation, remains an open and significant avenue for future research.

Generally, this literature review clearly demonstrates that singularly perturbed parabolic partial differential-difference equations with turning point problems remain an active and evolving area of research in singular perturbation studies. In particular, time-dependent turning point problems involving large time lags, small spatial delays, as well as non-delay cases have been largely unexplored, with existing schemes limited to first-order accuracy at best and most works focused on single boundary turning point problems. To conclude this survey, it is evident that very limited effort has been devoted to developing and analysing robust numerical methods for the governing turning point problems considered in this dissertation. Therefore, this study aims to fill this gap by proposing a reliable numerical technique for those turning point problems that have not been extensively addressed in the existing literature.

1.2 Research Objectives

Numerical methods are the heart and soul of modern science and technology. One of the goals of numerical methods is to obtain an approximate solution for mathematical problems that are difficult or impossible to solve analytically. Besides this, there are some mathematical problems, such as singularly perturbed problems, that requires further investigation than other regular problems because of the singular perturbation parameter. It is well known that classical numerical schemes on uniform meshes fail to converge uniformly with respect to the singular perturbation parameter. The efficiency of a numerical method is determined by its accuracy, simplicity in computing the discrete solution, and its insensitivity to the parameters of the given problem.It is desirable to construct numerical methods whose convergence is uniform with respect to the perturbation parameter. This motivates us to develop ε-uniformly convergent numerical methods for solving singularly perturbed parabolic differential and differential-difference equations with boundary turning point.

1.2.1 General Objective

The main objective of this dissertation is to develop, ε-uniformly convergent numerical schemes for singularly perturbed parabolic convection-diffusion problems with boundary turning point.

1.2.2 Specific Objectives

The specific objectives of this dissertation are to:

1. Develop a nonstandard finite difference (NSFD) scheme for solving singularly perturbed turning point problems given in Eqs. (1.15) and (1.20).

2. Construct a hybrid fitted mesh numerical scheme for solving singularly perturbed parabolic differential equations (SPPDEs) with boundary turning point in Eqs. (1.15), (1.18), and (1.20).

3. Formulate an exponentially fitted operator numerical scheme for solving singularly perturbed parabolic delay differential equations (SPPDDEs) with a boundary turning point in Eq. (1.18).

4. Analyze the stability and ε-uniform convergence of the proposed numerical schemes.

1.3 Significant of the Study

Although the numerical treatment of singularly perturbed problems (SPPs) has been extensively studied over the years, the numerical analysis of singularly perturbed parabolic differential delay equations (SPPDDEs) with turning points remains in its early stages. The development higher order of uniformly convergent numerical methods for SPPs with turning point continues to be an active area of research, and the numerical techniques currently available still require significant improvement. Therefore, it is essential to design numerical schemes that are simple to construct, more accurate than conventional methods, and exhibit uniform convergence with higher order accuracy.

In this dissertation, we proposed different parameter-uniform numerical methods to solve such problems. The results and techniques developed herein:

- Provide some background information for other researchers who work on this area.
- Offer an alternative method for solving singularly perturbed delay and non-delay problems,
- Enhance the advancement of the literature in this research domain.
- Introduce the application of numerical methods in different field of studies.

1.4 Scope of the Study

This dissertation is focused on developing and analyzing numerical methods for solving singularly perturbed parabolic partial differential equations with turning point of the following form:

1. **Singularly Perturbed Parabolic Convection-Diffusion Problem with Turning Point**

Consider the one-dimensional time-dependent singularly perturbed parabolic partial differential equation defined on the domain $\mathcal{D} = (0,1) \times (0,T]$:

$$\varepsilon \frac{\partial^2 u(x,t)}{\partial x^2} + a(x,t)\frac{\partial u(x,t)}{\partial x} - b(x,t)u(x,t) - \frac{\partial u(x,t)}{\partial t} = f(x,t), \quad (x,t) \in \mathcal{D}, \tag{1.22}$$

subject to the initial and boundary conditions:

$$\begin{cases} u(x,0) = s(x), & x \in [0,1], \\ u(0,t) = q_0(t), & t \in [0,T], \\ u(1,t) = q_1(t), & t \in [0,T], \end{cases} \tag{1.23}$$

where $0 < \varepsilon \ll 1$ is a small positive perturbation parameter.

To guarantee the well-posedness and uniqueness of the solution, it is assumed that all functions involved in Eqs. (1.22)–(1.23) are sufficiently smooth and bounded on the closure of $\mathcal{D}$. Specifically, the convection coefficient is given by $a(x,t) = a_0(x,t)x^p$, where $p \geq 1$, $a_0(x,t) \geq \alpha > 0$, and $b(x,t) \geq \beta > 0$ for all $(x,t) \in \overline{\mathcal{D}}$. Consequently, the solution exhibits a boundary layer near the left end of the spatial domain. Due to the vanishing of the convection coefficient at $x = 0$, this point serves as a turning point. In particular, when $p = 1$, $x = 0$ is referred to as a simple (first-order) turning point; for $p > 1$, it is termed a higher-order (or multiple) turning point.

2. **Singularly Perturbed Time-Delay Parabolic Convection-Diffusion Problem with Turning Point**

Consider the singularly perturbed time-delay parabolic convection-diffusion problem defined on the domain $\mathcal{D} = (0,1) \times (0,T)$:

$$\varepsilon \frac{\partial^2 u(x,t)}{\partial x^2} + a(x,t)\frac{\partial u(x,t)}{\partial x} - b(x,t)u(x,t) - c(x,t)\frac{\partial u(x,t)}{\partial t} = f(x,t) + d(x,t)u(x,t-\tau), \tag{1.24}$$

subject to the initial and boundary conditions:

$$\begin{cases} u(x,t) = s(x,t), & (x,t) \in [0,1] \times [-\tau, 0], \\ u(0,t) = q_0(t), & t \in [0,T], \\ u(1,t) = q_1(t), & t \in [0,T], \end{cases} \tag{1.25}$$

where $0 < \varepsilon \ll 1$ is a small perturbation parameter and $\tau > 0$ is a fixed delay parameter satisfying

$T = k\tau$ with $k > 1$ an integer. To guarantee the well-posedness and uniqueness of the solution, it is assumed that all functions involved in Eqs. (1.24)–(1.25) are sufficiently smooth and bounded on the closure of $\mathcal{D}$. In particular, the convection coefficient is taken as $a(x,t) = a_0(x,t)x^p$, where $p \geq 1$ and $a_0(x,t) \geq \alpha > 0$. Additionally, $b(x,t) \geq \beta > 0$ for all $(x,t) \in \overline{\mathcal{D}}$. The vanishing of the convection coefficient $a(x,t)$ at $x = 0$ introduces a turning point. Specifically, when $p = 1$, the problem has a simple (first-order) turning point at $x = 0$; for $p > 1$, it is classified as a higher-order turning point problem. The presence of the delay term $u(x, t - \tau)$, potentially inducing memory effects.

3. **Singularly Perturbed Parabolic Convection–Diffusion Turning-Point Problems with General Shifts**

   Consider the singularly perturbed parabolic partial differential equation with general shifts on the reaction terms, defined on the domain $\mathcal{D} = \Omega \times \Lambda = (0,1) \times (0,T]$ for a fixed $T > 0$:

$$\frac{\partial u(x,t)}{\partial t} - \varepsilon \frac{\partial^2 u(x,t)}{\partial x^2} - a(x,t)\frac{\partial u(x,t)}{\partial x} + b(x,t)u(x-\delta,t) + c(x,t)u(x,t) + d(x,t)u(x+\mu,t) = f(x,t), \tag{1.26}$$

   subject to the initial and boundary conditions:

$$\begin{cases} u(x,0) = u_0(x), & 0 \leq x \leq 1 \\ u(x,t) = \phi(x,t), & (x,t) \in \Omega_l = \{(x,t) : -\delta \leq x \leq 0,\ t \in \Lambda\}, \\ u(x,t) = \psi(x,t), & (x,t) \in \Omega_r = \{(x,t) : 1 \leq x \leq 1+\mu,\ t \in \Lambda\}, \end{cases} \tag{1.27}$$

   where $0 < \varepsilon \ll 1$ is a small perturbation parameter. The convection coefficient is given by $a(x,t) = a_0(x,t)x^p$, with $p \geq 1$ and $a_0(x,t)$ sufficiently smooth and bounded on $\bar{\Omega}$. The delay and advance parameters $\delta(\varepsilon)$ and $\mu(\varepsilon)$ are small and assumed to be of order $o(\varepsilon)$.

   To guarantee the existence and uniqueness of a solution, it is assumed that all functions appearing in Eqs. (1.26)–(1.27) are sufficiently smooth, bounded, and independent of ε.

1.5 Mathematical Procedures

In this section, the fundamental mathematical procedures employed to achieve the objectives of the study are outlined as follows:

1. Description of the problems.

2. Analysis of the properties of the continuous solution.

3. Development of numerical schemes for the considered problems.

4. Stability and convergence analysis of the developed schemes.

5. Design of algorithms and implementation of the methods in code.

6. Testing of the methods using numerical examples.

7. Presentation of the results using tables and figures.

8. Discussion and conclusion based on the theoretical findings and numerical outcomes.

1.6 Organization of the Dissertation

This dissertation consists of eight chapters. Chapter 1 presents the background of the study, a comprehensive literature review, the objectives, significance, scope of the study, the mathematical procedures, and an outline of the dissertation. Chapters 2 and 3 focus on the development and analysis of non-standard finite difference (NSFD) method on uniform mesh and hybrid numerical scheme on Shishkin mesh respectively for solving singularly perturbed parabolic convection–diffusion problems with boundary turning point, as described by Eqs. (1.22)–(1.23). Chapters 4 and 5 deals with the design and implementation an exponentially fitted operator and a hybrid numerical schemes, respectively to address singularly perturbed parabolic convection–diffusion problems with large time lag and boundary turning point, modeled by Eqs. (1.24)–(1.25). Chapters 6 and 7 deals with the design and implementation of non-standard finite difference method and a layer-resolving mesh method, respectively to address singularly perturbed parabolic convection–diffusion turning-point problems with general shifts, as modeled by Eqs. (1.26)–(1.27). Finally, Chapter 8 provides a general discussion, concluding remarks, and recommendations for future research.

Chapter 2

Nonstandard Finite Difference Scheme for Singularly Perturbed Parabolic Convection-Diffusion Problems with Boundary Turning Point

This chapter proposes a numerical scheme for solving singularly perturbed unsteady convection-diffusion problems exhibiting boundary turning point. The proposed scheme uses the Crank–Nicolson method in time and a nonstandard finite difference method in space on uniform meshes. Furthermore, Richardson extrapolation is applied to enhance the spatial order of convergence. The resulting scheme is shown to be uniformly convergent with respect to the perturbation parameter ε, and achieves second-order accuracy in both space and time. The numerical results are compared with some previous findings available in the literature.

2.1 Introduction

Singularly perturbed convection-diffusion equations with turning points form a special class of singularly perturbed differential equations in which the convection (or transport) coefficient vanishes at certain points in the domain, called turning points. Depending on the sign and variation of the convection coefficient, together with the nature of the problem, these equations may exhibit left boundary layers, right boundary layers, or interior layers. In this chapter, we considered problems with a left boundary layer and turning point.

This problem arises in the modeling of processes of convective transport of a diffusing substance (heat, matter) for the case in which the rate of flow from one of the boundaries is proportional to the distance from the boundary [113]. The model problems of this chapter corresponds to the flow directed outward the left boundary of the domain with a stop of the flow on this boundary. This class of problems also models the heat flow and mass transport near oceanic rises [44] and appears in the modeling of thermal boundary layers in laminar flow [109]. The problem in [44] is a single boundary turning point problem because of the assumption that the velocity distribution is linear. If one allows for higher orders of velocity distribution, then the boundary turning point becomes multiple. Multiple (second-order) boundary turning point problems are given in ([109], Chapter 12), and drift-diffusion equation of semiconductor device [95].

As discussed in Chapter 1, when the perturbation parameter ε is small, the standard numerical techniques for solving singularly perturbed boundary turning point (SP-BTP) problems become unstable and cannot produce reliable results. Therefore, it requires advanced numerical method which converges to the exact solution with independent of the perturbation parameter. The purpose of this chapter is to construct and analyse a parameter uniform numerical scheme which presents relatively rapid convergence and accuracy for solving the problems considered in [59] using Crank-Nicolson method in time and Nonstandard finite difference methods (NSFDMs) in space with uniform meshes. NSFDMs nowadays, are playing a crucial role in the development of reliable numerical methods to solve singularly perturbed problems. These NSFDMs are designed using the exact finite difference scheme, and the denominator function should be complicated. There are no general guidelines for doing so, but the advantage of this method is that it is straightforward to implement and extendable to higher-dimensional problems. However, the following important rules have been discovered by Mickens [75].

Rule 1: The orders of the discrete derivatives should be equal to the orders of the corresponding derivatives in the differential equation. When the orders of the discrete derivatives are higher than those in the differential equation, numerical instabilities in the form of oscillations often appear.

Rule 2: Denominator functions for the discrete derivatives must, in general, be expressed in terms of more complicated functions of the step sizes than those conventionally used.

Rule 3: Nonlinear terms should be replaced by nonlocal discrete representations.

Rule 4: Special conditions that hold for the solutions of the differential equations should also hold for the solutions of the finite difference scheme.

Rule 5: The scheme should not introduce extraneous or spurious solutions.

Rule 6: For differential equations having $n \geq 3$ terms, it is generally useful to construct finite difference schemes for various sub-equations composed of m terms, where $m < n$; then combine all the schemes together into an overall consistent finite difference model.

2.2 Description of the Problem

Consider the singularly perturbed parabolic convection-diffusion initial boundary value problem in the rectangular domain $\mathcal{D} = \Omega \times \Lambda = (0,1) \times (0,T]$, for some finite positive T of the form:

$$\mathcal{L}_\varepsilon u(x,t) \equiv \varepsilon \frac{\partial^2 u(x,t)}{\partial x^2} + a(x,t)\frac{\partial u(x,t)}{\partial x} - b(x,t)u(x,t) - \frac{\partial u(x,t)}{\partial t} = f(x,t), \quad (x,t) \in \mathcal{D}, \tag{2.1}$$

subject to the initial and boundary conditions:

$$\begin{cases} u(x,0) = u_0(x), & \text{on} \quad \Gamma_b = \overline{\Omega} \times \{0\}, \\ u(0,t) = \phi(t), & \text{on} \quad \Gamma_l = \{0\} \times \overline{\Lambda}, \\ u(1,t) = \psi(t), & \text{on} \quad \Gamma_r = \{1\} \times \overline{\Lambda}, \end{cases} \tag{2.2}$$

where $0 < \varepsilon \ll 1$ is the perturbation parameter; Γ_l, Γ_b and Γ_r are the left, bottom and right sides of the domain $\mathcal{D}$ respectively. The boundary of the domain is defined as $\partial\mathcal{D} = \Gamma_l \cup \Gamma_b \cup \Gamma_r$. We assume that $a(x,t), b(x,t), f(x,t)$ are smooth and bounded functions on $\overline{\mathcal{D}}$, and $\phi(t), \psi(t), u_0(x)$ are smooth and bounded on their respective domains and independent of ε. Furthermore, we suppose that

$$a(x,t) = a_0(x,t)x^p, p \geq 1, a_0(x,t) \geq \alpha > 0, \quad b(x,t) \geq \beta > 0, \quad \forall (x,t) \in \overline{\mathcal{D}}.$$

Problem (2.1) is related to the flow problem when directed towards the left side Γ_l of the domain, and the flow stops at this boundary. These problems arise in modeling heat flow and mass transport near an oceanic rise [44], and in developing the models of thermal boundary layers in laminar flow [109].

As the coefficient $a(x,t)$ of the convection term vanishes at $x = 0$, the problem (2.1) is called a problem with a boundary turning point. It covers two aspects: the turning point for $p = 1$ is referred to as a simple turning point (assuming the linear velocity distribution), and it is a multiple turning point when $p > 1$ (for higher orders of velocity distribution).

The reduced problem obtained by taking $\varepsilon = 0$ in (2.1) is the following first-order hyperbolic PDE.

$$\begin{cases} a(x,t)\dfrac{\partial v_0(x,t)}{\partial x} - b(x,t)v_0(x,t) - \dfrac{\partial v_0(x,t)}{\partial t} = f(x,t), & (x,t) \in \mathcal{D}, \\ v_0(x,t) = u(x,t), & (x,t) \in \Gamma_b \cup \Gamma_l. \end{cases} \tag{2.3}$$

The left side Γ_l and all other lines parallel to Γ_l are the characteristic curves of the reduced problem when $a(0,t) = 0$, $b(0,t) > 0$. Consequently, the resulting boundary layer functions are called parabolic boundary layer functions. These are characterized by the boundary values $u(0,t)$ at the left side Γ_l. It has been observed that the left lateral surface and the characteristic curve of (2.3) do not intersect. However, their deviation increases in the vertical direction, moving away from the lateral boundary (see [40, 108]). An exponential (regular) boundary layer function arises due to the inconsistency between the boundary value $u_0(t)$ and the value being transported along the characteristic at the intersection point (if $a(x,t) > 0$, $\forall (x,t) \in \mathcal{D}$, then every characteristic intersects Γ_b at one point). In general, a parabolic boundary layer of width $\mathcal{O}(\sqrt{\varepsilon})$ appears in the solution to problem (2.1) in the neighbourhood of Γ_l as $\varepsilon \to 0$ [59].

The following compatibility and the above smoothness conditions ensure the existence of a unique solution to problem (2.1):

$$u_0(0) = \phi(0), \quad u_0(1) = \psi(0), \tag{2.4}$$

and

$$\begin{cases} \varepsilon\frac{\partial^2 u_0(0)}{\partial x^2} + a(0,0)\frac{\partial u_0(0)}{\partial x} - b(0,0)u_0(0) - \frac{\partial \phi(0)}{\partial t} = f(0,0), \\ \varepsilon\frac{\partial^2 u_0(1)}{\partial x^2} + a(1,0)\frac{\partial u_0(1)}{\partial x} - b(1,0)u_0(1) - \frac{\partial \psi(0)}{\partial t} = f(1,0), \end{cases} \tag{2.5}$$

2.3 Properties of the Continuous Solution

Lemma 2.1 (Continuous Minimum Principle). *Let $F(x,t)$ be a sufficiently smooth function defined on $\mathcal{D}$ such that $F(x,t) \geq 0$, $\forall (x,t) \in \partial\mathcal{D}$ and $\mathcal{L}_\varepsilon F(x,t) \leq 0$, $\forall (x,t) \in \mathcal{D}$. Then $F(x,t) \geq 0, \forall (x,t) \in \overline{\mathcal{D}}$.*

Proof. Suppose that there exist $(y,z) \in \overline{\mathcal{D}}$ such that $F(y,z) = \min\limits_{(x,t)\in\overline{\mathcal{D}}} F(x,t) < 0$. Since $F(x,t) \geq 0$ on

$\partial\mathcal{D}$, it follows that $(y,z) \notin \partial\mathcal{D}$. Since $\digamma(y,z) = \min_{(x,t)\in\overline{\mathcal{D}}} \digamma(x,t)$ which implies $\frac{\partial \digamma}{\partial t}(y,z) = 0, \quad \frac{\partial \digamma}{\partial x}(y,z) = 0$ and $\frac{\partial^2 \digamma}{\partial x^2}(y,z) \geq 0$. Thus, $\mathcal{L}_\varepsilon \digamma(y,z) = \varepsilon \frac{\partial^2 \digamma}{\partial x^2}(y,z) + a(y,z)\frac{\partial \digamma}{\partial x}(y,z) - b(y,z)\digamma(y,z) - \frac{\partial \digamma}{\partial t}(y,z) = -b(y,z)\digamma(y,z) > 0$, since $b(y,z) \geq \beta > 0$ and $\digamma(y,z) < 0$. This contradicts the assumption $\mathcal{L}_\varepsilon \digamma(x,t) \leq 0, \quad \forall (x,t) \in \mathcal{D}$. Therefore, $\digamma(x,t) \geq 0$ for all $(x,t) \in \overline{\mathcal{D}}$. □

Lemma 2.2 (Stability Estimate). *Let $u(x,t)$ be the solution of problem (2.1). Then,*

$$\|u\|_{\overline{\mathcal{D}}} \leq \|u\|_{\partial\mathcal{D}} + \frac{\|f\|_{\overline{\mathcal{D}}}}{\beta}.$$

Proof. Define the barrier functions $\eth^{\pm}(x,t) = \|u\|_{\partial\mathcal{D}} + \frac{\|f\|_{\overline{\mathcal{D}}}}{\beta} \pm u(x,t)$.

On the boundary $\partial\mathcal{D}$, we have $\eth^{\pm}(x,t) = \|u\|_{\partial\mathcal{D}} + \frac{\|f\|_{\overline{\mathcal{D}}}}{\beta} \pm u(x,t) \geq 0$.

In the interior of $\mathcal{D}$,

$$\begin{aligned}
\mathcal{L}_\varepsilon \eth^{\pm}(x,t) &= -b(x,t)\big(\|u\|_{\partial\mathcal{D}} + \tfrac{\|f\|_{\overline{\mathcal{D}}}}{\beta}\big) \pm \mathcal{L}_\varepsilon u(x,t) \\
&= -b(x,t)\big(\|u\|_{\partial\mathcal{D}} + \tfrac{\|f\|_{\overline{\mathcal{D}}}}{\beta}\big) \pm f(x,t) \\
&\leq -\beta\big(\|u\|_{\partial\mathcal{D}} + \tfrac{\|f\|_{\overline{\mathcal{D}}}}{\beta}\big) \pm \|f\|_{\overline{\mathcal{D}}} \\
&= -\beta\|u\|_{\overline{\mathcal{D}}} - \|f\|_{\overline{\mathcal{D}}} \pm \|f\|_{\overline{\mathcal{D}}} \leq 0
\end{aligned}$$

Then, by Lemma 2.1, $\eth^{\pm}(x,t) \geq 0$ for all $(x,t) \in \overline{\mathcal{D}}$. This implies $\|u(x,t)\|_{\overline{\mathcal{D}}} \leq \|u\|_{\partial\mathcal{D}} + \frac{\|f\|_{\overline{\mathcal{D}}}}{\beta}, \quad \forall (x,t) \in \overline{\mathcal{D}}$. □

Lemma 2.3. *Let $u(x,t)$ be the sufficiently smooth solution of the problem (2.1)–(2.2). Then,*

$$|u(x,t) - u_0(x)| \leq Ct, \tag{2.6}$$

$$|u(x,t) - \psi(t)| \leq C(1-x), \tag{2.7}$$

for all $(x,t) \in \overline{\mathcal{D}}$, where C is a positive constant independent of ε.

Proof. To prove (2.6), define $v(x,t) = u(x,t) - u_0(x)$. Then, $\mathcal{L}_\varepsilon v(x,t) = \mathcal{L}_\varepsilon(u(x,t) - u_0(x))$. Using (2.1), we obtain $\mathcal{L}_\varepsilon v(x,t) = f(x,t) - \mathcal{L}_\varepsilon u_0(x)$, where $\mathcal{L}_\varepsilon u_0(x) = \varepsilon u_0''(x) + a(x,t)u_0'(x) - b(x,t)u_0(x)$. The initial and boundary conditions become $v(x,0) = u(x,0) - u_0(x) = 0$, and $v(0,t) = \phi(t) - u_0(0), \qquad v(1,t) = \psi(t) - u_0(1)$.

Choose the barrier function

$$\Psi^{\pm}(x,t) = Ct \pm v(x,t),$$

where C is a sufficiently large positive constant. Since $\Psi^{\pm}(x,0) = 0$, and v is bounded on the lateral boundaries, we have $\Psi^{\pm}(x,t) \geq 0 \quad$ on $\partial\mathcal{D}$. Now, $\mathcal{L}_\varepsilon(Ct) = C + b(x,t)Ct \geq C$. Further, $|\mathcal{L}_\varepsilon v(x,t)| = |f(x,t) - \mathcal{L}_\varepsilon u_0(x)| \leq C$, for some constant C independent of ε. Hence, $\mathcal{L}_\varepsilon \Psi^{\pm}(x,t) = \mathcal{L}_\varepsilon(Ct) \pm \mathcal{L}_\varepsilon v(x,t) \geq 0$. Therefore, by the minimum principle 2.1, $\Psi^{\pm}(x,t) \geq 0 \quad$ in $\overline{\mathcal{D}}$. Consequently, $|v(x,t)| \leq Ct$, which implies $|u(x,t) - u_0(x)| \leq Ct$. Next, to prove (2.7), define $w(x,t) = u(x,t) - \psi(t)$. Then, $\mathcal{L}_\varepsilon w(x,t) = f(x,t) - \mathcal{L}_\varepsilon \psi(t)$, where $\mathcal{L}_\varepsilon \psi(t) = -b(x,t)\psi(t) - \psi_t(t)$. The boundary conditions become $w(1,t) = u(1,t) - \psi(t) = 0$. Choose the barrier function $\Phi^{\pm}(x,t) = C(1-x) \pm w(x,t)$, where C is sufficiently large. Since $\Phi^{\pm}(1,t) = 0$, and w is bounded on the remaining boundaries, we have $\Phi^{\pm}(x,t) \geq 0 \quad$ on $\partial\mathcal{D}$. Moreover, $\mathcal{L}_\varepsilon(C(1-x)) = Ca(x,t) + Cb(x,t)(1-x) \geq C$, for sufficiently large C, because $a(x,t) \geq 0, \quad b(x,t) \geq \beta > 0$. Also, $|\mathcal{L}_\varepsilon w(x,t)| \leq C$. Hence, $\mathcal{L}_\varepsilon \Phi^{\pm}(x,t) \geq 0$. Applying the minimum principle 2.1 again yields $|w(x,t)| \leq C(1-x)$. Therefore, $|u(x,t) - \psi(t)| \leq C(1-x)$. □

Remark 2.1. *To prove the next theorem, we adopt the assumption of Ng-Stynes in [85] that the convection coefficient $a = a(x)$ depends only on the spatial variable x in the domain $\mathcal{D}$.*

The following theorem gives the bounds for the mixed derivatives of u.

Theorem 2.1. *The solution $u(x,t)$ of problem (2.1) satisfies the following bounds for $0 \leq i + 3j \leq 4$:*

$$\left| \frac{\partial^{i+j} u(x,t)}{\partial x^i \partial t^j} \right| \leq C\Big(1 + \varepsilon^{-i/2} \exp\big(-x\sqrt{\tfrac{\alpha}{\varepsilon}}\big)\Big), \quad (x,t) \in \overline{\mathcal{D}}.$$

Proof. For $i = 0$, on the boundaries $x = 0$ and $x = 1$ of $\overline{\mathcal{D}}$, we have $u = 0$, thus $u_t = 0$. On the initial boundary $t = 0$, we also have $u = 0$, hence $u_x = 0$ and $u_{xx} = 0$. From equation (2.1), it follows that $u_t(x,0) = f(x,0)$. Since f is bounded, there exists a constant K_1 such that $|u_t| \leq K_1$.

Now consider the operator

$$\mathcal{L}_\varepsilon u(x,t) \equiv \varepsilon u_{xx} + a(x,t)u_x - b(x,t)u - u_t = f.$$

It can be rewritten as:

$$\mathcal{L}_\epsilon u(x,t) \equiv \varepsilon u_{xx} + (au)_x - (a_x + b)u - u_t = f.$$

Now, applying this operator to u_t and using the remark yields

$$\begin{aligned}\mathcal{L}_\epsilon u_t(x,t) &= \varepsilon u_{txx} + (au_t)_x - (a_x+b)u_t - u_{tt} \quad as \quad a = a(x)\\ &= \varepsilon u_{txx} + au_{tx} - bu_t - u_{tt}\\ &= \left(\varepsilon u_{xx} + au_x - bu - u_t\right)_t + b_t u\\ &= f_t(x,t) + b_t u.\end{aligned} \tag{2.8}$$

Since f and b are smooth and bounded on the domain $\mathcal{D}$, Lemmas2.1 and 2.2 yields $\mathcal{L}_\varepsilon u_t \leq K_2$ and thus $|u_t| \leq C \quad \text{on} \quad \overline{\mathcal{D}}$. To bound the derivatives of the solution in the spatial domain, consider the cases for a fixed $j = 0$.

For $i = 0$, from Lemma 2.2 we have $|u| \leq C$. For $i = 1$, following the arguments in[54], construct the neighbourhood of $I = (0, \sqrt{\varepsilon}), \ \ \forall r \in I$. For some $r^* \in I$ by mean value theorem, we have

$$u_x(r^*) = \frac{u(\sqrt{\varepsilon}) - u(0)}{\sqrt{\varepsilon}} = \varepsilon^{-1/2}|u(\sqrt{\varepsilon}) - u(0)| \leq C\varepsilon^{-1/2}\|u\|.$$

Now, rewriting equation (2.1) as

$$\varepsilon u_{xx} + (au)_x - (a_x+b)u - u_t = f,$$

we get

$$\varepsilon u_{xx} + (au)_x = f + (a_x+b)u + u_t.$$

Integrating from r^* to r, we have

$$(\varepsilon u_x + au)\big|_{r^*}^{r} = \int_{r^*}^{r} \left[f + (a_x+b)u + u_t\right] dx \leq C\int_{r^*}^{r} \left(\|f\| + \|u\| + \|u_t\|\right) dx \leq C\sqrt{\varepsilon}.$$

Thus,

$$\varepsilon u_x(r,t) + a(r,t)u(r,t) \leq \varepsilon u_x(r^*,t) + a(r^*,t)u(r^*,t) + C\sqrt{\varepsilon}.$$

Since for $r \in (0, \sqrt{\varepsilon})$, we have $|a(r,t)| = |a_0(r,t)r^p| \leq C\varepsilon^{p/2}$, using the above bound on $u_x(r^*)$, we obtain

$$|u_x(r,t)| \leq |u_x(r^*,t)| + \frac{|a(r,t)u(r,t)|}{\varepsilon} + \frac{|a(r^*,t)u(r^*,t)|}{\varepsilon} + C\varepsilon^{-1/2}.$$

Hence,

$$|u_x(r,t)| \leq C\varepsilon^{-1/2} + C\varepsilon^{p/2-1} + C\varepsilon^{p/2-1} + C\varepsilon^{-1/2} \leq C\varepsilon^{-1/2} \leq C\big(1+\varepsilon^{-1/2}\exp\Big(-x\sqrt{\tfrac{\alpha}{\varepsilon}}\Big)\big).$$

The bound for $i = 1$ is thus established.

In a similar fashion, higher-order spatial and mixed derivatives can be bounded by repeated differentiation of the original equation and using analogous arguments. $\square$

2.4 Derivation of the Numerical Method

In this section, we discretize the continuous problem (2.1). First, it is discretized in the temporal direction using the Crank-Nicolson scheme on a uniform mesh. Some essential properties of the solution to the semi-discrete problem are given. Then, NSFD method is applied on the spatial direction on uniform mesh.

2.4.1 Temporal Discretization

The temporal domain $\overline{\Lambda}$ is discretized with a uniform mesh of size Δt: $\overline{\Lambda}^M = \{t_j = jk,\ j = 0,1,\ldots,M,\ \Delta t = \frac{T}{M}\}$, where M is the number of mesh intervals in temporal direction. Using the Crank–Nicolson method, we have:

$$\begin{cases} \varepsilon u_{xx}^{j+1/2} + a^{j+1/2}(x)u_x^{j+1/2} - b^{j+1/2}(x)u^{j+1/2}(x) - D_t^- u^{j+1}(x) = f^{j+1/2}(x), \\ u(0,t_{j+1}) = \phi(t_{j+1}), \quad u(1,t_{j+1}) = \psi(t_{j+1}), \quad 0 \leq j \leq M-1, \\ u(x,0) = u_0(x), \quad x \in \Omega, \end{cases} \tag{2.9}$$

where

$$\begin{cases} D_t^- u^{j+1}(x) = \dfrac{u^{j+1}(x) - u^j(x)}{\Delta t}, u^{j+1/2}(x) = \dfrac{u^{j+1}(x) + u^j(x)}{2}, f^{j+1/2}(x) = \dfrac{f^{j+1}(x) + f^j(x)}{2}, \\ a^{j+1/2}(x) = \dfrac{a^{j+1}(x) + a^j(x)}{2}, b^{j+1/2}(x) = \dfrac{b^{j+1}(x) + b^j(x)}{2}. \end{cases}$$

The time semi-discretized problem (2.9) can be rewritten as:

$$
\begin{cases}
\hat{\mathcal{L}}_\varepsilon u^{j+1}(x) = g^{j+1}(x), \quad 0 \le j \le M-1, \\
u(0, t_{j+1}) = \phi(t_{j+1}), \quad u(1, t_{j+1}) = \psi(t_{j+1}), \quad 0 \le j \le M-1, \\
u(x, 0) = u_0(x), \quad x \in \Omega,
\end{cases}
\tag{2.10}
$$

where

$$
\begin{cases}
\hat{\mathcal{L}}_\varepsilon u^{j+1}(x) = \frac{\varepsilon}{2}(u_{xx})^{j+1} + \frac{a^{j+1}(x)}{2}(u_x)^{j+1} - \frac{c^{j+1}(x)}{2}u^{j+1}(x), \\
g^{j+1}(x) = f^{j+1/2}(x) - \frac{\varepsilon}{2}(u_{xx})^j - \frac{a^j(x)}{2}(u_x)^j + \frac{d^j(x)}{2}u^j(x), \\
c^{j+1}(x) = b^{j+1}(x) + \frac{2}{\Delta t}, \\
d^j(x) = b^j(x) - \frac{2}{\Delta t}.
\end{cases}
$$

The semi-discrete operator $\hat{\mathcal{L}}_\varepsilon$ satisfies the following lemma.

Lemma 2.4 (**Semi-discrete Minimum Principle**). *Suppose the function $\theta^{j+1}(x)$ satisfies $\theta^{j+1}(0) \ge 0$, $\theta^{j+1}(1) \ge 0$, and $\hat{\mathcal{L}}_\varepsilon \theta^{j+1}(x) \le 0 \quad \forall x \in \Omega$. Then, $\theta^{j+1}(x) \ge 0 \quad \forall x \in \overline{\Omega}$ and $j = 0, 1, 2, \dots, M-1$.*

Proof. Let $\ell \in \Omega$ be such that $\theta^{j+1}(\ell) = \min_{x\in\Omega} \theta^{j+1}(x) < 0$. This implies $(\theta^{j+1})'(\ell) = 0$ and $(\theta^{j+1})''(\ell) \ge 0$. Then we have:

$$
\hat{\mathcal{L}}_\varepsilon \theta^{j+1}(\ell) = \frac{\varepsilon}{2}(\theta^{j+1})''(\ell) + \frac{a^{j+1}(\ell)}{2}(\theta^{j+1})'(\ell) - \frac{c^{j+1}(\ell)}{2}\theta^{j+1}(\ell) > 0,
$$

since $c^{j+1}(\ell) = b^{j+1}(\ell) + \frac{2}{\Delta t} \ge \beta + \frac{2}{\Delta t} > 0$. This contradicts the assumption that $\hat{\mathcal{L}}_\varepsilon \theta^{j+1}(x) \le 0$. Therefore, $\theta^{j+1}(x) \ge 0$ on $\overline{\Omega}$. □

Lemma 2.5 (**Stability Estimate**). *Let u^{j+1} be the solution of the discrete problem at time level t_{j+1}. If $u^{j+1}(0) \ge 0$ and $u^{j+1}(1) \ge 0$, then the following stability estimate holds:*

$$
\left|u^{j+1}(x)\right| \le \max\{\left|u^{j+1}(0)\right|, \left|u^{j+1}(1)\right|\} + \max_{x\in\bar{\Omega}} \frac{\left|\hat{\mathcal{L}}_\epsilon u^{j+1}(x)\right|}{\beta}.
$$

Proof. We prove the lemma using a discrete comparison principle (barrier function technique).

Define two barrier functions:

$$
\Psi^{\pm}(x) = M \pm u^{j+1}(x),
$$

where the constant M is chosen as

$$M = \max\{\left|u^{j+1}(0)\right|, \left|u^{j+1}(1)\right|\} + \max_{x\in\bar{\Omega}} \frac{\left|\hat{\mathcal{L}}_\epsilon u^{j+1}(x)\right|}{\beta}.$$

Our goal is to show that $\Psi^{\pm}(x) \geq 0$ for all $x \in \bar{\Omega}$, which directly implies $\left|u^{j+1}(x)\right| \leq M$, yielding the desired estimate.

Step 1: Boundary values. At the boundaries $x = 0$ and $x = 1$, we have by construction:

$$\Psi^{\pm}(0) = M \pm u^{j+1}(0) \geq \max\{\left|u^{j+1}(0)\right|, \left|u^{j+1}(1)\right|\} \pm u^{j+1}(0) \geq 0.$$

The same inequality holds for $\Psi^{\pm}(1)$. Hence, $\Psi^{\pm}(0) \geq 0$ and $\Psi^{\pm}(1) \geq 0$.

Step 2: Action of the discrete operator. Consider the action of the discrete operator $\hat{\mathcal{L}}_\epsilon$ on $\Psi^{\pm}$. By linearity,

$$\hat{\mathcal{L}}_\epsilon \Psi^{\pm}(x) = \hat{\mathcal{L}}_\epsilon M \pm \hat{\mathcal{L}}_\epsilon u^{j+1}(x).$$

Since M is a constant, the discrete operator acting on it reduces to $\hat{\mathcal{L}}_\epsilon M = \beta M$ (this follows from the form of the operator, e.g., $\hat{\mathcal{L}}_\varepsilon u^{j+1}(x) = \frac{\varepsilon}{2}(u_{xx})^{j+1} + \frac{a^{j+1}(x)}{2}(u_x)^{j+1} - \frac{c^{j+1}(x)}{2}u^{j+1}(x)$ with $c^{j+1}(x) = b^{j+1}(x) + \frac{2}{\Delta t} \geq \beta > 0$). Therefore,

$$\hat{\mathcal{L}}_\epsilon \Psi^{\pm}(x) = -\beta M \pm \hat{\mathcal{L}}_\epsilon u^{j+1}(x).$$

Step 3: Sign of the discrete operator. Using the definition of M, we have $\beta M \geq \left|\hat{\mathcal{L}}_\epsilon u^{j+1}(x)\right|$ for all x. Consequently,

$$\hat{\mathcal{L}}_\epsilon \Psi^{\pm}(x) = -\beta M \pm \hat{\mathcal{L}}_\epsilon u^{j+1}(x) \leq -\beta M - \left|\hat{\mathcal{L}}_\epsilon u^{j+1}(x)\right| \leq 0.$$

Thus, $\hat{\mathcal{L}}_\epsilon \Psi^{\pm}(x) \leq 0$ for all interior grid points $x \in \Omega$. Since the discrete operator $\hat{\mathcal{L}}_\epsilon$ satisfies a discrete minimum principle (as established in Lemma 2.4), a function with non-negative boundary values and on which the operator yields a negative result must be non-negative everywhere in the domain.

We have shown:

- $\Psi^{\pm}(0) \geq 0$, $\Psi^{\pm}(1) \geq 0$,

- $\hat{\mathcal{L}}_\epsilon \Psi^{\pm}(x) \le 0$ for all $x \in \Omega$.

Therefore, by the discrete minimum principle, $\Psi^{\pm}(x) \ge 0$ for all $x \in \bar{\Omega}$.

Since $\Psi^{\pm}(x) = M \pm u^{j+1}(x) \ge 0$, it follows that

$$-M \le u^{j+1}(x) \le M \quad \text{for all } x \in \bar{\Omega},$$

which is equivalent to

$$\left|u^{j+1}(x)\right| \le M = \max\{\left|u^{j+1}(0)\right|, \left|u^{j+1}(1)\right|\} + \max_{x\in\bar{\Omega}} \frac{\left|\hat{\mathcal{L}}_\epsilon u^{j+1}(x)\right|}{\beta}.$$

This completes the proof. □

Next, we analyse the error in time semi-discretization. The local truncation error measures the consistency of the numerical scheme and is defined as the residual obtained when the exact solution is substituted into the discrete operator. It represents the error introduced in a single time step:

$$e_{j+1}(x) = \hat{\mathcal{L}}_\varepsilon\, u(x, t_{j+1}) - g^j(x),$$

where $u(x, t_{j+1})$ denotes the exact solution of (2.10) where as global error describes the accumulation of the local truncation errors over all time levels and quantifies the difference between the exact solution and the numerical approximation:

$$E_j(x) = u(x, t_j) - u^j(x),$$

where $u(x, t_j)$ and $u^j(x)$ denote the exact and numerical solutions of (2.10), respectively.

The convergence of the scheme is established by deriving appropriate bounds for both the local truncation error and the global error. The following two lemmas provide estimates for the local truncation error and the global error, respectively.

Lemma 2.6. *Suppose that*

$$\left|\frac{\partial^i u}{\partial t^i}\right| \le C, \quad (x,t) \in \overline{\mathcal{D}}, \quad \forall i \in \{0, 1, 2\}.$$

The local truncation error at the $(j+1)^{th}$ time step is given by

$$|e_{j+1}| \le C(\Delta t)^3.$$

Proof. Using Taylor series expansions around $t_{j+1/2} = t_j + \Delta t/2$, we have:

$$u(x,t_{j+1}) = u(x,t_{j+1/2}) + \frac{\Delta t}{2} u_t(x,t_{j+1/2}) + \frac{1}{2!}\left(\frac{\Delta t}{2}\right)^2 u_{tt}(x,t_{j+1/2}) + O((\Delta t)^3), \tag{2.11}$$

$$u(x,t_j) = u(x,t_{j+1/2}) - \frac{\Delta t}{2} u_t(x,t_{j+1/2}) + \frac{1}{2!}\left(\frac{\Delta t}{2}\right)^2 u_{tt}(x,t_{j+1/2}) + O((\Delta t)^3). \tag{2.12}$$

Subtracting (2.12) from (2.11), we obtain

$$\frac{u(x,t_{j+1}) - u(x,t_j)}{\Delta t} = u_t(x,t_{j+1/2}) + O(\Delta t^2). \tag{2.13}$$

Substituting Eq. (2.13) to Eq. (2.1), we have:

$$\begin{aligned}\frac{u(x,t_{j+1}) - u(x,t_j)}{\Delta t} &= \varepsilon u_{xx}(x,t_{j+\frac{1}{2}}) + a(x,t_{j+\frac{1}{2}}) u_x(x,t_{j+\frac{1}{2}}) \\ &\quad - b(x,t_{j+\frac{1}{2}}) u(x,t_{j+\frac{1}{2}}) - f(x,t_{j+\frac{1}{2}}) + O\big((\Delta t)^2\big)\,.\end{aligned}$$

Additionally, we use the identity:

$$u(x,t_{j+1/2}) = \frac{u(x,t_{j+1}) + u(x,t_j)}{2} + O(\Delta t^2).$$

This leads to the following approximation:

$$\hat{\mathcal{L}}_\epsilon u(x,t_{j+1}) \equiv \frac{\varepsilon}{2} u_{xx}(x,t_{j+1}) + \frac{a(x,t_{j+1})}{2} u_x(x,t_{j+1}) - \frac{c(x,t_{j+1})}{2} u(x,t_{j+1}) = g(x,t_{j+1}) + O((\Delta t)^3), \tag{2.14}$$

where $c(x,t) = b(x,t) + \frac{2}{\Delta t}$. From the discrete operator equation (e.g., Eq. (2.10)) and Eq. (2.14), the local truncation error satisfies:

$$\hat{\mathcal{L}}_\epsilon e_{j+1}(x) = O((\Delta t)^3), \quad \text{with } e_{j+1}(0) = e_{j+1}(1) = 0.$$

Hence, it follows that:

$$\|e_{j+1}\| \leq C(\Delta t)^3.$$

□

Theorem 2.2. *Under the assumptions of Lemma 2.6, the global error $E_j = u(x,t_j) - u^j(x)$ satisfies the* *estimate*

$$\|E_j\| \le C(\Delta t)^2, \qquad 0 \le j \le \frac{T}{\Delta t},$$

where $u(x,t_j)$ *and* $u^j(x)$ *denote the exact and numerical solutions of* (2.10)*, respectively.*

Proof. The local error estimate up to the j^{th} time level gives the global error at the j^{th} time level.

$$\begin{aligned}
\|E_j\| &= \|\sum_{i=1}^{j} e_i\|, \;\; j \le \frac{T}{\Delta t} \\
&\le ||e_1|| + ||e_2|| + ||e_3|| + ... + ||e_j|| \\
&\le C_1(j)(\Delta t)^3 \quad \text{(using Lemma 2.6)} \\
&\le C_1 T(\Delta t)^2 \text{ as } \; j.\Delta t \le T \\
&\le C(\Delta t)^2, \;\; C = C_1 T.
\end{aligned}$$

□

Theorem 2.3. *The solution* $u^{j+1}(x)$ *of the semi-discrete problem* (2.10) *and its derivatives satisfy the bound*

$$\left|\frac{d^k u^{j+1}(x)}{dx^k}\right| \le C\left(1 + \varepsilon^{-k/2}\exp\left(-x\sqrt{\tfrac{\alpha}{\varepsilon}}\right)\right), \quad x \in \Omega_x, \quad 0 \le k \le 4,$$

where C *is a constant independent of* ε *and* Δt*.*

Proof. Consider the semi-discrete problem

$$\hat{\mathcal{L}}_\varepsilon u^{j+1}(x) = g^{j+1}(x),$$

where

$$\begin{cases}
\hat{\mathcal{L}}_\varepsilon u^{j+1}(x) = \dfrac{\varepsilon}{2}(u_{xx})^{j+1} + \dfrac{a^{j+1}(x)}{2}(u_x)^{j+1} - \dfrac{c^{j+1}(x)}{2}u^{j+1}(x), \\
c^{j+1}(x) = b^{j+1}(x) + \dfrac{2}{\Delta t}, b^{j+1}(x) \ge \beta > 0, c^{j+1}(x) \ge \beta + \dfrac{2}{\Delta t} > 0.
\end{cases}$$

For $k = 0$, applying the continuous minimum principle to the operator $\hat{\mathcal{L}}_\varepsilon$, together with the boundedness of $g^{j+1}(x)$, gives

$$|u^{j+1}(x)| \le C, \qquad x \in \Omega_x.$$

Next, we estimate the spatial derivatives. Using arguments similar to those in [54], consider the interval

$$I = (0, \sqrt{\varepsilon}).$$

By the mean value theorem, there exists some $r^* \in I$ such that

$$u_x^{j+1}(r^*) = \frac{u^{j+1}(\sqrt{\varepsilon}) - u^{j+1}(0)}{\sqrt{\varepsilon}}.$$

Hence,

$$|u_x^{j+1}(r^*)| \leq C\varepsilon^{-1/2}\|u^{j+1}\|. \tag{2.15}$$

Now rewrite the semi-discrete equation as

$$\frac{\varepsilon}{2}u_{xx}^{j+1} + \frac{1}{2}(a^{j+1}u^{j+1})_x - \frac{1}{2}(a_x^{j+1} + c^{j+1})u^{j+1} = g^{j+1}(x).$$

Thus,

$$\frac{\varepsilon}{2}u_{xx}^{j+1} + \frac{1}{2}(a^{j+1}u^{j+1})_x = g^{j+1}(x) + \frac{1}{2}(a_x^{j+1} + c^{j+1})u^{j+1}.$$

Integrating from r^* to r, where $r \in (0, \sqrt{\varepsilon})$, we obtain

$$\int_{r^*}^{r} \left(\frac{\varepsilon}{2}u_{xx}^{j+1} + \frac{1}{2}(a^{j+1}u^{j+1})_x\right) dx = \int_{r^*}^{r} \left(g^{j+1}(x) + \frac{1}{2}(a_x^{j+1} + c^{j+1})u^{j+1}\right) dx.$$

Therefore,

$$\left(\frac{\varepsilon}{2}u_x^{j+1} + \frac{1}{2}a^{j+1}u^{j+1}\right)\Big|_{r^*}^{r} \leq C\sqrt{\varepsilon}.$$

Hence,

$$\varepsilon u_x^{j+1}(r) + a^{j+1}(r)u^{j+1}(r) \leq \varepsilon u_x^{j+1}(r^*) + a^{j+1}(r^*)u^{j+1}(r^*) + C\sqrt{\varepsilon}.$$

Since

$$a^{j+1}(x) = a_0^{j+1}(x)x^p, \qquad p \geq 1,$$

we have

$$|a^{j+1}(r)| \leq C\varepsilon^{p/2}, \qquad r \in (0, \sqrt{\varepsilon}).$$

Using (2.15), we obtain

$$
\begin{aligned}
|u_x^{j+1}(r)| &\leq |u_x^{j+1}(r^*)| + \frac{|a^{j+1}(r^*)u^{j+1}(r^*)|}{\varepsilon} + \frac{|a^{j+1}(r)u^{j+1}(r)|}{\varepsilon} + C\varepsilon^{-1/2} \\
&\leq C_1\varepsilon^{-1/2} + C_2\varepsilon^{p/2-1} + C_3\varepsilon^{p/2-1} + C\varepsilon^{-1/2} \\
&\leq C\varepsilon^{-1/2}.
\end{aligned}
$$

Since the layer occurs near $x = 0$, the exponential decay factor may be included to obtain

$$
|u_x^{j+1}(x)| \leq C\left(1 + \varepsilon^{-1/2}\exp\left(-x\sqrt{\frac{\alpha}{\varepsilon}}\right)\right).
$$

Thus, the estimate holds for $k = 1$.

For higher-order derivatives, differentiate the semi-discrete equation repeatedly with respect to x. Using the boundedness of the coefficients and the previously established derivative estimates, together with standard induction arguments, we obtain

$$
\left|\frac{d^k u^{j+1}(x)}{dx^k}\right| \leq C\left(1 + \varepsilon^{-k/2}\exp\left(-x\sqrt{\frac{\alpha}{\varepsilon}}\right)\right), \qquad 2 \leq k \leq 4.
$$

Hence,

$$
\left|\frac{d^k u^{j+1}(x)}{dx^k}\right| \leq C\left(1 + \varepsilon^{-k/2}\exp\left(-x\sqrt{\tfrac{\alpha}{\varepsilon}}\right)\right), \quad 0 \leq k \leq 4.
$$

□

2.4.2 Spatial Discretization

The theoretical foundation of the non-standard discrete modeling method lies in the development of the exact finite difference method. In [75], Mickens presented a set of techniques and rules for constructing non-standard finite difference methods (NSFDMs) for various types of model problems. For a problem of the form given in (2.1), to construct an exact finite difference scheme, one can consider the lower bounds of the coefficients and focus on the homogeneous part of the corresponding ordinary differential equation, as given by (2.10):

$$
\varepsilon u_{xx} + \alpha u_x = 0. \tag{2.16}
$$

The space domain $\overline{\Omega} = [0, 1]$ is discretized using uniform space length h: $\overline{\Omega}^N = \left\{x_i = ih,\ i = 0(1)N,\ h = \frac{1}{N}\right\}$, where N is the number of mesh intervals in the spatial discretization. The finite difference scheme that replaces h^2 by a non-negative denominator function Υ^2 in Eq. (2.16) is:

$$\varepsilon \frac{u_{i+1} - 2u_i + u_{i-1}}{\Upsilon_i^2} + \alpha \frac{u_{i+1} - u_i}{h} = 0. \tag{2.17}$$

We can find Υ_i^2 using the following procedure. First, we rewrite equation (2.16) equivalently as a first-order coupled system of differential equations:

$$\frac{du}{dx} = y, \tag{2.18}$$

$$\frac{dy}{dx} = -\frac{\alpha}{\varepsilon} y. \tag{2.19}$$

From (2.19) we have $y(x) = \exp\left(-\frac{\alpha}{\varepsilon} x\right)$. By applying a first-order difference scheme to (2.18):

$$y_i = \frac{u_{i+1} - u_i}{h} = \exp\left(-\frac{\alpha}{\varepsilon} x_i\right), \tag{2.20}$$

then substituting (2.20) into (2.17), we obtain the denominator function:

$$\Upsilon_i^2 = \frac{h\varepsilon}{\alpha}\left(\exp\left(\frac{h\alpha}{\varepsilon}\right) - 1\right) \equiv h^2 + \mathcal{O}\left(\frac{h^3}{\varepsilon}\right).$$

So equation (2.17) becomes:

$$\varepsilon \frac{u_{i+1} - 2u_i + u_{i-1}}{\frac{\varepsilon h}{\alpha}\left(\exp\left(\frac{\alpha h}{\varepsilon}\right) - 1\right)} + \alpha \frac{u_{i+1} - u_i}{h} = 0.$$

Therefore, the denominator function $\Upsilon^2 = \frac{h\varepsilon}{\alpha}\left(\exp\left(\frac{\alpha h}{\varepsilon}\right) - 1\right)$ can replace h^2. Using this denominator function for the variable coefficient problem, we write:

$$\Upsilon_{i,j+1}^2 = \frac{\varepsilon h}{a_i^{j+1}}\left(\exp\left(\frac{h a_i^{j+1}}{\varepsilon}\right) - 1\right), \tag{2.21}$$

2.4.3 Full Discrete Scheme

Using denominator function Eq. (2.21) into the semi-discrete scheme Eq. (2.10), the full discrete scheme becomes:

$$\begin{aligned}\hat{\mathcal{R}}_{\varepsilon}^{N}U^{j+1}(x_i) \equiv \frac{\varepsilon}{2}\frac{u_{i+1}^{j+1}-2u_i^{j+1}+u_{i-1}^{j+1}}{\Upsilon_{i,j+1}^2}+\frac{a_i^{j+1}}{2}\frac{u_{i+1}^{j+1}-u_i^{j+1}}{h} \quad -\left(\frac{b_i^{j+1}}{2}+\frac{1}{\Delta t}\right)u_i^{j+1}=H_i^{j+1},\\ u_0^{j+1}=\phi(t_{j+1}), \quad u_N^{j+1}=\psi(t_{j+1}), \quad u_i^0=u_0(x_i),\end{aligned} \tag{2.22}$$

for $i=1,\dots,N-1$, $j=0,\dots,M-1$, where

$$H_i^{j+1}=-\frac{\varepsilon}{2}\frac{u_{i+1}^{j}-2u_i^{j}+u_{i-1}^{j}}{\Upsilon_{i,j}^2}-\frac{a_i^{j}}{2}\frac{u_{i+1}^{j}-u_i^{j}}{h}+\left(\frac{b_i^{j}}{2}-\frac{1}{\Delta t}\right)u_i^{j}+\frac{f_i^{j+1}+f_i^{j}}{2}.$$

After rearranging the terms in (2.22), we arrive at the following recurrence relation:

$$r_i^- u_{i-1}^{j+1}+r_i^c u_i^{j+1}+r_i^+ u_{i+1}^{j+1}=s_i^- u_{i-1}^{j}+s_i^c u_i^{j}+s_i^+ u_{i+1}^{j}+\frac{f_i^{j+1}+f_i^{j}}{2}, \tag{2.23}$$

where the coefficients are given by:

$$\begin{cases} r_i^- = \dfrac{\varepsilon}{2\Upsilon_{i,j+1}^2},\\ r_i^c = -\left(\dfrac{\varepsilon}{\Upsilon_{i,j+1}^2}+\dfrac{a_i^{j+1}}{2h}+\dfrac{b_i^{j+1}}{2}+\dfrac{1}{\Delta t}\right),\\ r_i^+ = \dfrac{\varepsilon}{2\Upsilon_{i,j+1}^2}+\dfrac{a_i^{j+1}}{2h}, \end{cases} \qquad \begin{cases} s_i^- = -\dfrac{\varepsilon}{2\Upsilon_{i,j}^2},\\ s_i^c = \dfrac{\varepsilon}{\Upsilon_{i,j}^2}+\dfrac{a_i^{j}}{2h}+\dfrac{b_i^{j}}{2}-\dfrac{1}{\Delta t},\\ s_i^+ = -\left(\dfrac{\varepsilon}{2\Upsilon_{i,j}^2}+\dfrac{a_i^{j}}{2h}\right). \end{cases}$$

Since $|r_i^c|>|r_i^-|+|r_i^+|$, the tri-diagonal system (2.23) is strictly diagonally dominant. As a result, the solution is unique. To solve this system, we employed the matrix inverse method.

2.5 Convergence Analysis

Lemma 2.7 (Discrete Minimum Principle). *Let the mesh function u_i^{j+1} satisfy $u_0^{j+1}\geq 0, u_N^{j+1}\geq 0$ and $\hat{\mathcal{L}}_{\epsilon}^{N}u_i^{j+1}\leq 0$, $\forall i=1,2,\dots,N-1$. Then, $u_i^{j+1}\geq 0,\ \ \forall i=0,1,\dots,N$.*

Proof. If $s\in\{0,1,\dots,N\}$ with $u_s^{j+1}=\min\limits_{0\leq i\leq N}u_i^{j+1}<0$, then $s\neq 0$ and $s\neq N$. Also, we have

$(u_{s+1}^{j+1} - u_s^{j+1}) > 0$ and $(u_{s-1}^{j+1} - u_s^{j+1}) > 0$. Thus,

$$\begin{aligned}
\hat{\mathcal{L}}_\epsilon^N u_s^{j+1} &= \frac{\varepsilon}{2}\frac{(u_{s+1}^{j+1} - 2u_s^{j+1} + u_{s-1}^{j+1})}{\Upsilon^2} + \frac{a_s^{j+1}}{2}\frac{(u_{s+1}^{j+1} - u_s^{j+1})}{h} - \left(\frac{b_s^{j+1}}{2} + \frac{1}{\Delta t}\right) u_s^{j+1} \\
&= \frac{\varepsilon}{2}\frac{(u_{s+1}^{j+1} - u_s^{j+1}) + (u_{s-1}^{j+1} - u_s^{j+1})}{\Upsilon^2} + \frac{a_s^{j+1}}{2}\frac{(u_{s+1}^{j+1} - u_s^{j+1})}{h} - \left(\frac{b_s^{j+1}}{2} + \frac{1}{\Delta t}\right) u_s^{j+1} > 0,
\end{aligned}$$

which is a contradiction. Hence the result follows. □

Lemma 2.8 (**Stability Estimate**). *The solution u_i^{j+1} of (2.23) satisfies the bound*

$$\left|u_i^{j+1}\right| \le \frac{1}{\beta}\|\hat{\mathcal{L}}_\epsilon^N u_i^{j+1}\| + \max\left(|\psi(t_{j+1})|, |\phi(t_{j+1})|\right).$$

Proof. Define the barrier functions

$$\daleth_{i,j+1}^{\pm} = \frac{1}{\beta}\|\hat{\mathcal{L}}_\epsilon^N u_i^{j+1}\| + \max\left(|\psi(t_{j+1})|, |\phi(t_{j+1})|\right) \pm u_i^{j+1}.$$

At the boundary points, we have:

$$\daleth_{0,j+1}^{\pm} = \frac{1}{\beta}\|\hat{\mathcal{L}}_\epsilon^N u_0^{j+1}\| + \max\left(|\psi(t_{j+1})|, |\phi(t_{j+1})|\right) \pm u_0^{j+1} \ge 0,$$

$$\daleth_{N,j+1}^{\pm} = \frac{1}{\beta}\|\hat{\mathcal{L}}_\epsilon^N u_N^{j+1}\| + \max\left(|\psi(t_{j+1})|, |\phi(t_{j+1})|\right) \pm u_N^{j+1} \ge 0.$$

Now, for interior points, we apply the discrete operator to $\daleth_{i,j+1}^{\pm}$. Using linearity and the definition of the operator $\hat{\mathcal{L}}_\epsilon^N$, we compute:

$$\begin{aligned}
\hat{\mathcal{L}}_\epsilon^N \daleth_{i,j+1}^{\pm} &= \frac{\varepsilon}{2}\delta_x^2 \daleth_{i,j+1}^{\pm} + \frac{a_i^{j+1}}{2} D_x^+ \daleth_{i,j+1}^{\pm} - \left(\frac{b_i^{j+1}}{2} + \frac{1}{\Delta t}\right) \daleth_{i,j+1}^{\pm} \\
&= -\left(\frac{b_i^{j+1}}{2} + \frac{1}{\Delta t}\right)\left(\frac{1}{\beta}\|\hat{\mathcal{L}}_\epsilon^N u_i^{j+1}\| + \max\left(|\psi(t_{j+1})|, |\phi(t_{j+1})|\right)\right) \pm \hat{\mathcal{L}}_\epsilon^N (u_i^{j+1}) \\
&= -\left(\frac{b_i^{j+1}}{2} + \frac{1}{\Delta t}\right)\left(\frac{1}{\beta}\|\hat{\mathcal{L}}_\epsilon^N u_i^{j+1}\| + \max\left(|\psi(t_{j+1})|, |\phi(t_{j+1})|\right)\right) \pm \hat{\mathcal{L}}_\epsilon^N u_i^{j+1}.
\end{aligned}$$

Since $\left(\frac{b_i^{j+1}}{2} + \frac{1}{\Delta t}\right) \geq \beta > 0$, we have:

$$\hat{\mathcal{L}}_\epsilon^N \daleth_{i,j+1}^{\pm} \leq -\beta\left(\frac{1}{\beta}\|\hat{\mathcal{L}}_\epsilon^N u_i^{j+1}\| + \max\left(|\psi(t_{j+1})|, |\phi(t_{j+1})|\right)\right) \pm \hat{\mathcal{L}}_\epsilon^N u_i^{j+1} \leq 0.$$

Hence, $\hat{\mathcal{L}}_\epsilon^N \daleth_{i,j+1}^{\pm} \leq 0$ at all interior nodes, and $\daleth_{i,j+1}^{\pm} \geq 0$ at the boundaries.

By applying the discrete maximum principle (Lemma 2.7), we conclude that

$$\daleth_{i,j+1}^{\pm} \geq 0 \quad \text{for all } i,$$

which implies

$$\left|u_i^{j+1}\right| \leq \frac{1}{\beta}\left|\hat{\mathcal{L}}_\epsilon^N u_i^{j+1}\right| + \max\left(|\psi(t_{j+1})|, |\phi(t_{j+1})|\right).$$

□

Lemma 2.9. *For $\varepsilon \to 0$ and for a fixed mesh, it holds that*

$$\lim_{\varepsilon\to 0} \frac{\exp\left(-x_i\sqrt{\frac{\alpha}{\varepsilon}}\right)}{(\sqrt{\varepsilon})^s} = 0, \quad s \in \mathbb{Z}^+, \quad \textit{and} \quad \varepsilon\left|1 - \frac{h^2}{\xi^2}\right| \leq Ch.$$

Proof. Note that

$$\frac{\exp\left(-x_i\sqrt{\frac{\alpha}{\varepsilon}}\right)}{(\sqrt{\varepsilon})^s} \leq \frac{\exp\left(-h\sqrt{\frac{\alpha}{\varepsilon}}\right)}{(\sqrt{\varepsilon})^s}, \quad \text{for } i = 1, 2, \ldots, N.$$

Let $\eta = \dfrac{1}{\sqrt{\varepsilon}}$. Then we have:

$$\lim_{\varepsilon\to 0} \frac{\exp\left(-h\sqrt{\frac{\alpha}{\varepsilon}}\right)}{(\sqrt{\varepsilon})^s} = \lim_{\eta\to\infty} \frac{\eta^s}{\exp(h\sqrt{\alpha}\eta)}.$$

Applying L'Hôpital's Rule s times, we obtain:

$$\lim_{\eta\to\infty} \frac{\eta^s}{\exp(h\sqrt{\alpha}\eta)} = \lim_{\eta\to\infty} \frac{s!}{(h\sqrt{\alpha})^s \exp(h\sqrt{\alpha}\eta)} = 0.$$

Now, consider the second part:

$$\varepsilon\left|1 - \frac{h^2}{\xi^2}\right| = \varepsilon\left|1 - \frac{h^2}{\frac{\varepsilon h}{\alpha}\left(\exp\left(\frac{\alpha h}{\varepsilon}\right) - 1\right)}\right| = \alpha h\left|\frac{\varepsilon}{\alpha h} - \frac{1}{\exp\left(\frac{\alpha h}{\varepsilon}\right) - 1}\right|.$$

Let $\sigma = \dfrac{\alpha h}{\varepsilon}$. Then:

$$\varepsilon \left| 1 - \frac{h^2}{\xi^2} \right| = \alpha h \left(\frac{1}{\sigma} - \frac{1}{\exp(\sigma) - 1} \right).$$

Taking limits:

$$\lim_{\sigma \to 0} \alpha h \left(\frac{1}{\sigma} - \frac{1}{\exp(\sigma) - 1} \right) = \frac{1}{2} \alpha h, \quad \lim_{\sigma \to \infty} \alpha h \left(\frac{1}{\sigma} - \frac{1}{\exp(\sigma) - 1} \right) = 0.$$

Thus, for all $\sigma \in (0, \infty)$, we have

$$\varepsilon \left| 1 - \frac{h^2}{\xi^2} \right| \leq Ch,$$

for some constant $C > 0$, which completes the proof. □

Theorem 2.4. *Let $u^{j+1}(x_i)$ and u_i^{j+1} be the solutions of (2.10) and (2.23), respectively. Then the error bound at the $(j+1)^{th}$ time level is given by*

$$\sup_{0 < \varepsilon \leq 1} \left\| u^{j+1}(x_i) - u_i^{j+1} \right\| \leq CN^{-1}, \qquad i = 0(1)N.$$

Proof. The truncation error in the spatial discretization is

$$\begin{aligned} \left| \hat{\mathcal{L}}_\varepsilon^N \left(u^{j+1}(x_i) - u_i^{j+1} \right) \right| &= \left| \hat{\mathcal{L}}_\varepsilon u^{j+1}(x_i) - \hat{\mathcal{L}}_\varepsilon^N u_i^{j+1} \right| \\ &\leq \left| \varepsilon \left(\frac{d^2}{dx^2} - \delta_x^2 \right) u_i^{j+1} + a_i^{j+1} \left(\frac{d}{dx} - D^+ \right) u_i^{j+1} \right|, \end{aligned}$$

where

$$\delta_x^2 u_i^{j+1} = \frac{u_{i+1}^{j+1} - 2u_i^{j+1} + u_{i-1}^{j+1}}{\Upsilon^2}, \quad D^+ u_i^{j+1} = \frac{u_{i+1}^{j+1} - u_i^{j+1}}{h}.$$

Using Taylor expansions and Theorem 2.3, we get:

$$\begin{aligned} \left| \hat{\mathcal{L}}_\varepsilon u^{j+1}(x_i) - \hat{\mathcal{L}}_\varepsilon^N u_i^{j+1} \right| &\leq \left| \varepsilon \left(1 - \frac{h^2}{\Upsilon^2} \right) \frac{d^2 u^{j+1}}{dx^2}(x_i) - a^{j+1}(x_i) \frac{h^2}{6} \frac{d^3 u^{j+1}}{dx^3}(x_i) - a^{j+1}(x_i) \frac{\varepsilon h^4}{12 \Upsilon^2} \frac{d^4 u^{j+1}}{dx^4}(x_i) \right| \\ &\leq C \left[h \left(1 + \varepsilon^{-1} e^{-x_i \sqrt{\beta/\varepsilon}} \right) + h^2 \left(1 + \varepsilon^{-3/2} e^{-x_i \sqrt{\beta/\varepsilon}} \right) \right]. \end{aligned}$$

Then, by Lemma 2.9, we obtain

$$\sup_{0 < \varepsilon \leq 1} \left\| u^{j+1}(x_i) - u_i^{j+1} \right\| \leq CN^{-1}.$$

□

Theorem 2.5. *The solution u_i^{j+1} in (2.23) converges uniformly to the solution $u(x_i, t_{j+1})$ in (2.1) and its error bound is given by*

$$\sup_{0<\varepsilon\leq 1} \left\| u(x_i, t_{j+1}) - u_i^{j+1} \right\| \leq C(N^{-1} + (\Delta t)^2), \quad i = 0(1)N, \quad j = 0(1)M.$$

Proof. The scheme's uniform convergence is based on Theorems 2.2 and 2.4. We justify it as follows

$$\sup_{0<\varepsilon\leq 1} \left\| u(x_i, t_{j+1}) - u_i^{j+1} \right\| \leq \sup_{0<\varepsilon\leq 1} \left\| u(x_i, t_{j+1}) - u^{j+1}(x_i) \right\| + \sup_{0<\varepsilon\leq 1} \left\| u^{j+1}(x_i) - u_i^{j+1} \right\| \leq C(\Delta t)^2 + N^{-1}).$$

□

2.5.1 Richardson Extrapolation

To enhance the spatial convergence order, we apply the Richardson extrapolation technique as follows.

Let $\mathcal{D}^{N,M} \subset \mathcal{D}^{2N,M}$, where $\mathcal{D}^{2N,M}$ is the mesh obtained by bisecting the spatial step size h. Denote the numerical solution on $u^{2N,M}$ by $\overline{u}_i^j$. According to the error estimate established in Theorem 2.5, we have:

$$\left\| u(x_i, t_{j+1}) - u_i^{j+1} \right\| \leq C((\Delta t)^2 + h). \tag{2.24}$$

Since inequality (2.24) holds for any $(\Delta t)^2, h > 0$, we may express the pointwise error as

$$u(x_i, t_{j+1}) - u_i^{j+1} = C((\Delta t)^2 + h) + R^{N,M}, \quad \forall (x_i, t_{j+1}) \in \mathcal{D}^{N,M}, \tag{2.25}$$

where $R^{N,M} = \mathcal{O}((\Delta t)^3 + h^2)$ represents the higher-order remainder terms. This leads to the refined estimate

$$\left\| u(x_i, t_{j+1}) - u_i^{j+1} \right\| \leq C((\Delta t)^2 + h) + \mathcal{O}((\Delta t)^3 + h^2). \tag{2.26}$$

Similarly, for the mesh $\mathcal{D}^{2N,M}$ with halved spatial step size $h/2$, we have

$$u(x_i, t_{j+1}) - \overline{u}_i^{j+1} = C((\Delta t)^2 + \tfrac{h}{2}) + R^{2N,M}, \quad \forall (x_i, t_{j+1}) \in \mathcal{D}^{2N,M}, \tag{2.27}$$

where $R^{2N,M} = \mathcal{O}((\Delta t)^3 + h^2)$. As proved in [42], the extrapolated approach based on space discretization eliminates the leading order error term and provides second order uniform accuracy in space. Following the approach in [42], we eliminate the leading-order spatial error by subtracting a scaled version of Eq. (4.7) from Eq. (4.3):

$$u(x_i, t_{j+1}) - \left(2\overline{u}_i^{j+1} - u_i^{j+1}\right) = Ck^2 + \mathcal{O}((\Delta t)^3 + h^2).$$

We thus define the Richardson extrapolated solution as

$$(u_i^{j+1})_{\text{ext}} := 2\overline{u}_i^{j+1} - u_i^{j+1}, \tag{2.28}$$

which improves the spatial order of accuracy by one. The resulting approximation $(u_i^{j+1})_{\text{ext}}$ is more accurate than either u_i^{j+1} or $\overline{u}_i^{j+1}$ alone.

To quantify the truncation error of this extrapolated solution, we write

$$\begin{aligned} u(x_i, t_{j+1}) - (u_i^{j+1})_{\text{ext}} &= u(x_i, t_{j+1}) - \left[2\overline{u}_i^{j+1} - u_i^{j+1}\right] \\ &= 2\left(u(x_i, t_{j+1}) - \overline{u}_i^{j+1}\right) - \left(u(x_i, t_{j+1}) - u_i^{j+1}\right). \end{aligned} \tag{2.29}$$

Combining Eqs. (2.25), (2.27), and (2.29), we establish the following result.

Theorem 2.6. *Let $u(x_i, t_{j+1})$ be the exact solution and $(u_i^{j+1})_{ext}$ be the Richardson extrapolated numerical solution to problem (2.1). Then the extrapolated scheme satisfies the error estimate:*

$$\sup_{0<\varepsilon\leq 1} \left\| u(x_i, t_{j+1}) - (u_i^{j+1})_{ext} \right\| \leq C((\Delta t)^2 + N^{-2}),$$

where C is a constant independent of the mesh sizes $h = N^{-1}$, (Δt), and the perturbation parameter ε.

2.6 Numerical Results and Discussion

To validate the theoretical results established in this chapter, we perform numerical experiments using the proposed scheme on the problem given in (2.1). Specifically, we considered three numerical examples to verify the applicability and effectiveness of the proposed scheme.

The exact solution is unavailable for the model problems below, so the double mesh principle is used to estimate the maximum pointwise error before and after extrapolation. Specifically, the error is defined by

$$\begin{aligned} e_\varepsilon^{N,M} &= \max_{0\leq i\leq N,\, 0\leq j\leq M} \left| u^{N,M}(x_i, t_j) - u^{2N,2M}(x_{2i}, t_{2j}) \right|, \\ (e_\varepsilon^{N,M})_{\text{ext}} &= \max_{0\leq i\leq N,\, 0\leq j\leq M} \left| (u^{N,M}(x_i, t_j))_{\text{ext}} - (u^{2N,2M}(x_{2i}, t_{2j})_{\text{ext}} \right|, \end{aligned}$$

respectively.

The rate of convergence is given by

$$R_\varepsilon^{N,M} = \log_2\left(\frac{e_\varepsilon^{N,M}}{e_\varepsilon^{2N,2M}}\right).$$

Furthermore, we calculate the ε-uniform maximum pointwise error $e^{N,M}$ and the corresponding ε-uniform rate of convergence $R^{N,M}$ as follow

$$\begin{aligned} e^{N,M} &= \max_\varepsilon e_\varepsilon^{N,M}, \\ R^{N,M} &= \log_2\left(\frac{e^{N,M}}{e^{2N,2M}}\right). \end{aligned}$$

Example 2.1. *Consider the following singularly perturbed boundary turning point problem [136]:*

$$\begin{aligned} &\varepsilon u_{xx}(x,t) + x^p u_x(x,t) - u(x,t) - u_t(x,t) = -1 + x^2, && (x,t) \in \mathcal{D}, \\ &u(x,0) = (1-x)^2, && 0 \le x \le 1, \\ &u(0,t) = t^2 + 1, \quad u(1,t) = 0, && 0 \le t \le 1. \end{aligned}$$

Table 2.1: $e^{N,M}$ and $p^{N,M}$ for Example 2.1 for $p = 1$ with Richardson extrapolation

$\varepsilon \downarrow$	$M = N \rightarrow$	2^5	2^6	2^7	2^8	2^9	2^{10}
	10^{-1}	3.0696e-05	7.9049e-06	2.0056e-06	5.0511e-07	1.2674e-07	3.1690e-08
		1.9572	1.9787	1.9894	1.9947	1.9997	
	10^{-3}	4.6927e-04	1.1958e-04	2.8999e-05	5.6951e-06	8.5996e-07	2.1500e-07
		1.9724	2.0440	2.3482	2.7274	1.9992	
	10^{-5}	4.6927e-04	1.1969e-04	3.0220e-05	7.5922e-06	1.9027e-06	4.7570e-07
		1.9711	1.9857	1.9929	1.9965	1.9999	
	10^{-7}	4.6927e-04	1.1969e-04	3.0220e-05	7.5922e-06	1.9027e-06	4.7570e-07
		1.9711	1.9857	1.9929	1.9965	1.9999	
	$\vdots$	$\vdots$	$\vdots$	$\vdots$	$\vdots$	$\vdots$	$\vdots$
	10^{-9}	4.6927e-04	1.1969e-04	3.0220e-05	7.5922e-06	1.9027e-06	4.7570e-07
		1.9711	1.9857	1.9929	1.9965	1.9999	
PM:	$e^{M,N}$	4.6927e-04	1.1969e-04	3.0220e-05	7.5922e-06	1.9027e-06	4.7570e-07
		1.9711	1.9857	1.9929	1.9965	1.9999	
In [136]:	$e^{M,N}$	9.449e-04	2.345e-04	6.424e-05	1.721e-05	4.778e-06	
		2.011	1.868	1.900	1.849		

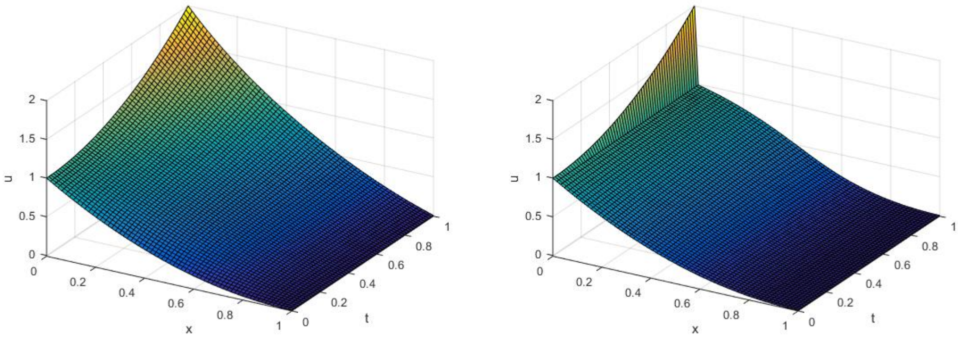

(a) $\varepsilon = 2^{-1}$ (b) $\varepsilon = 2^{-20}$

Figure 2.1: The effect of ε using 3D view for Example 2.1 for $p = 2$.

Example 2.2. *Consider the following singularly perturbed boundary turning point problem [59]:*

$$
\begin{aligned}
&\varepsilon u_{xx}(x,t) + (2-x^2)x^p u_x(x,t) - (1+x)u(x,t) - u_t(x,t) = 10e^{-t}t^2 x(x-1), && (x,t) \in \mathcal{D},\\
&u(x,0) = 1 - x, && 0 \le x \le 1,\\
&u(0,t) = t^2 + 1, \quad u(1,t) = 0, && 0 \le t \le 1.
\end{aligned}
$$

Table 2.2: Comparison of $e^{N,M}$ and $p^{N,M}$ for Example 2.2 when $p = 1$ before extrapolation

$\varepsilon \downarrow$	$M = N \rightarrow$	2^5	2^6	2^7	2^8	2^9	2^{10}
	10^{-1}	1.8509e-03	9.8145e-04	5.0132e-04	2.6880e-04	1.3284e-04	6.6435e-05
		0.9152	0.9691	0.9131	1.0102	0.9996	
	10^{-3}	3.0268e-03	1.5854e-03	8.1157e-04	3.9626e-04	1.5460e-04	7.7300e-05
		0.9329	0.9661	1.0343	1.3579	0.9999	
	10^{-5}	3.0268e-03	1.5854e-03	8.1084e-04	4.1001e-04	2.0616e-04	1.0308e-04
		0.9330	0.9673	0.9837	0.9919	0.9999	
	10^{-7}	3.0268e-03	1.5854e-03	8.1084e-04	4.1001e-04	2.0616e-04	1.0308e-04
		0.9330	0.9673	0.9837	0.9919	0.9999	
	$\vdots$	$\vdots$	$\vdots$	$\vdots$	$\vdots$	$\vdots$	
	10^{-9}	3.0268e-03	1.5854e-03	8.1084e-04	4.1001e-04	2.0616e-04	1.0308e-04
		0.9330	0.9673	0.9837	0.9919	0.9999	
PM:	$e^{M,N}$	3.0268e-03	1.5854e-03	8.1084e-04	4.1001e-04	2.0616e-04	1.0308e-04
		0.9330	0.9673	0.9837	0.9919	0.9999	
In [59]:	$e^{M,N}$	7.81e-02	4.21e-02	2.19e-02	1.12e-02	5.63e-03	
		0.89	0.94	0.97	0.99		

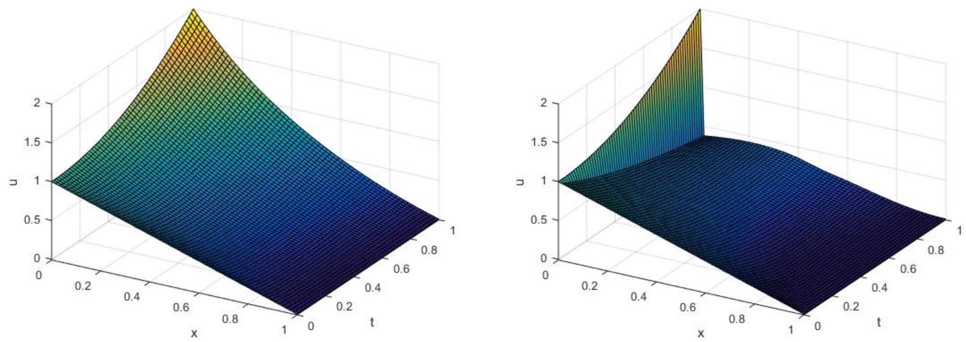

(a) $\varepsilon = 2^{-1}$ (b) $\varepsilon = 2^{-20}$

Figure 2.2: The effect of ε using 3D view for Example 2.2 for $p = 3$.

Example 2.3. *Consider the following singularly perturbed boundary turning point problem [66]*

$$\varepsilon u_{xx}(x,t) + x^p u_x(x,t) - (x+p)u(x,t) - u_t(x,t) = e^{-t}p(x^2-1), \quad (x,t) \in \mathcal{D},$$

$$u(x,0) = (1-x)^2, \;\; 0 \le x \le 1, \quad u(0,t) = t^2+1, \;\; u(1,t) = 0, \quad 0 \le t \le 1.$$

Table 2.3: Comparison $e_\varepsilon^{N,M}$ and $p_\varepsilon^{N,M}$ for Example 2.3 with $\varepsilon = 2^{-15}$ and for different values of p after extrapolation

$p \downarrow M = N \rightarrow$	2^5	2^6	2^7	2^8	2^9
	Proposed Method				
1	4.0553e-04	1.0988e-04	2.8833e-05	7.3965e-06	1.8754e-06
	1.8839	1.9301	1.9628	1.9796	
2	7.8643e-04	2.1700e-04	5.7212e-05	1.4743e-05	3.7449e-06
	1.8576	1.9233	1.9563	1.9770	
3	1.1504e-03	3.2208e-04	8.5415e-05	2.2060e-05	5.6109e-06
	1.8366	1.9149	1.9531	1.9751	
	Method in [66]		.	.	.
1	1.0563e-3	3.3846e-4	1.0488e-4	3.2120e-5	9.7653e-6
	1.6419	1.6903	1.7071	1.7177	
2	4.8912e-3	1.9672e-3	6.8809e-4	2.2846e-4	7.2656e-5
	1.3140	1.5155	1.5907	1.6528	
3	6.3012e-3	2.5303e-3	8.9776e-4	2.9678e-4	9.4708e-5
	1.3163	1.4949	1.5969	1.6479	

The maximum absolute errors and their corresponding rates of convergence for the proposed method, applied to Example 2.1 and Example 2.2 with $p = 1$, are presented in Table 2.1 and Table 2.2, respectively. From these tables, it can be observed that for fixed mesh parameters, as $\varepsilon \to 0$, the maximum absolute error remains approximately constant. Moreover, as the mesh is refined, the maximum absolute error decreases,

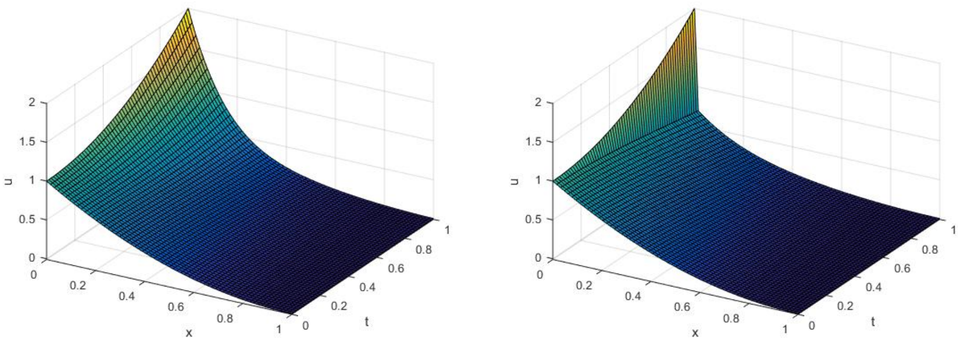

(a) $\varepsilon = 2^{-4}$ (b) $\varepsilon = 2^{-15}$

Figure 2.3: Surface plots of the numerical solution for Example 2.3 and $p = 1$.

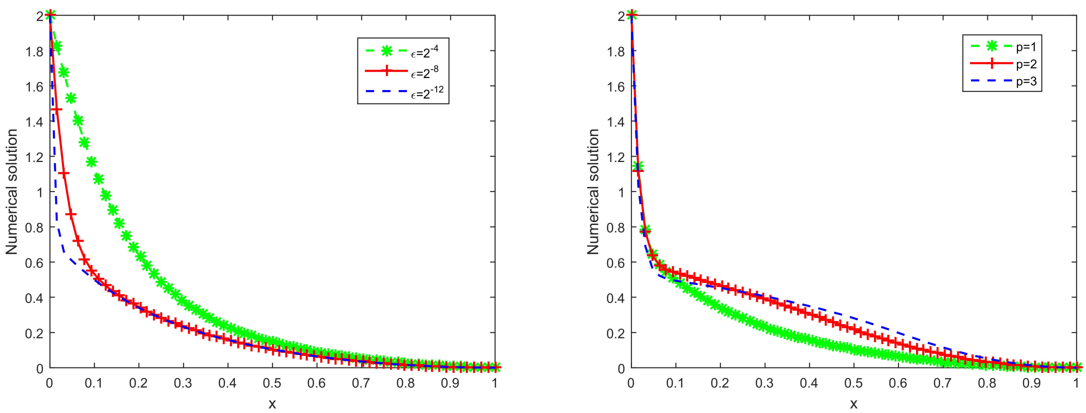

(a) $p = 1$ (b) $\varepsilon = 2^{-10}$

Figure 2.4: Numerical solution profile for Example 2.3 for different ε and p values.

confirming that the scheme is ε-uniformly convergent. Furthermore, Table 2.1 and Table 2.2 also provide a comparison of the proposed method with those reported in [136] and [59], using Examples 2.1 and 2.2, respectively. The results clearly demonstrate that the proposed method achieves higher accuracy and a better order of convergence. Additionally, Table 2.3 compares the maximum absolute errors and the corresponding orders of convergence for various p values, showing that the proposed method better in both accuracy and convergence rate than the method in [66].

Surface plots for each example are presented in Figures 2.1, 2.2, and 2.3 for various values of the singular perturbation parameter ε. These figures show that the solution develops a pronounced left boundary layer in the spatial domain, which is a characteristic feature of singularly perturbed convection–diffusion problems. The numerical solution profiles for different values of ε and p are displayed in Figure 2.4 to illustrate the influence of both the perturbation parameter and the convection exponent on the solution behavior. Figure 2.4a demonstrates that as $\varepsilon \to 0$, the solution exhibits an increasingly sharp boundary layer near $x = 0$, accompanied by a corresponding reduction in the layer width. This behavior is consistent with the theoretical property that the boundary layer thickness is primarily governed by ε.

Moreover, variations in the parameter p, which appears in the convection coefficient, modify the strength and spatial variation of the convective term. As p increases, the convection effect becomes more pronounced near the boundary, leading to changes in the gradient of the solution and slight adjustments in the layer profile. However, the asymptotic thickness of the boundary layer remains predominantly controlled by ε.

2.7 Conclusion

In this chapter, a parameter-uniform numerical method has been proposed for solving singularly perturbed parabolic convection–diffusion equations with boundary turning point. These problems are characterized by stiffness due to the presence of a small perturbation parameter ε and the existence of boundary turning point. The solution exhibits a left boundary layer in the spatial domain. The developed scheme combines a non-standard finite difference method for spatial discretization with the Crank–Nicolson method for temporal integration, both applied on uniform meshes. Numerical results, supported by figures and tables, illustrate the solution's behavior as ε varies. The method is stable and achieves second-order ε-uniform convergence. Furthermore, as order of turning points p varies the scheme's stability and order of convergence are not affected. The performance of the scheme is investigated by comparing the results with some published papers. Overall, the proposed method offers improved accuracy and ε-uniform convergence rate.

Chapter 3

Hybrid Numerical Scheme for Singularly Perturbed Parabolic Convection-Diffusion Problems with Boundary Turning Point

This chapter addresses the problem presented in Chapter 2 by developing a numerical method based on a fitted mesh approach. A hybrid finite difference scheme is formulated on a Shishkin mesh, employing the Crank–Nicolson method for time discretization and a combination of midpoint upwind and central differences for spatial discretization. The midpoint upwind scheme is applied in the outer region, while the central difference is used within the boundary layer to ensure an oscillation-free solution. The proposed scheme is ε-uniformly convergent in the maximum norm with almost second-order accuracy. Its stability is established using the discrete minimum principle and truncation error bounds. Numerical results from three model examples confirm the theoretical findings.

3.1 Introduction

It is well established in the literature that standard finite difference methods do not exhibit uniform convergence when applied to singularly perturbed problems on uniform mesh [78, 80]. These methods typically converge only when the mesh size is considerably smaller than the perturbation parameter (ε), which significantly increases the computational cost. Furthermore, they are often not uniformly well-conditioned and can be sensitive to perturbations in the input data. To accurately capture the layer structure at a low computational cost, a mesh adaptation technique offers advantages over a uniform mesh. There are several approaches for adapting the mesh through the redistribution of mesh points, among which the Bakhvalov and Shishkin meshes are notable examples. The simplest non-uniform mesh, which places more mesh points in the boundary layer region than in the outer region—namely, the piecewise-uniform mesh proposed by Shishkin—is sufficient for the construction of an ε-uniform method. It is attractive due to its simplicity and is adequate for handling a wide variety of singularly perturbed problems. The purpose of this work is to construct and analyze a higher-order ε-uniform numerical scheme for a singularly perturbed convection–diffusion problem with boundary turning points. The proposed hybrid scheme combines the central finite difference method and the midpoint upwind scheme on a piecewise Shishkin mesh in the spatial direction, and employs the Crank–Nicolson method in the temporal direction. The advantage of the present method over those presented in [59, 66, 123] lies in its second-order accuracy in both time and space variables, as well as its improved overall accuracy.

3.2 Definition of the Problem

Consider the singularly perturbed parabolic convection–diffusion problem with a boundary turning point introduced in Chapter 2.

3.3 Properties of the Continuous Solution

The governing problem considered in this chapter coincides with the model problem studied in Chapter 2. Hence, the analytical properties of the continuous solution discussed earlier remain applicable. To avoid repetition, the corresponding results are omitted here and will be referred to whenever needed in the subsequent analysis.

3.4 Derivation of the Numerical Method

3.4.1 Temporal Discretization

In this subsection, the temporal discretization is omitted since it is identical to the discretization presented in Subsection 2.4.1 of Chapter 2. Therefore, we directly consider the semi-discrete form of the continuous problem (2.1). The semi discrete solution u_i^{j+1} of problem (2.10) can be decomposed into regular and singular components as

$$u^{j+1}(x) = v^{j+1}(x) + w^{j+1}(x).$$

The bounds on these components are given in the following theorem (see [20]).

Theorem 3.1. *The solution $u^{j+1}(x)$ and its derivatives satisfy the bound*

$$\left|\frac{d^k u^{j+1}(x)}{dx^k}\right| \le C\Big(1 + \varepsilon^{-k/2}\exp\big(-x\sqrt{\tfrac{\alpha}{\varepsilon}}\big)\Big), \quad x \in \Omega_x, \quad 0 \le k \le 4.$$

Moreover, the regular and singular components satisfy

$$\left|\frac{d^k v^{j+1}(x)}{dx^k}\right| \le C\left(1 + \varepsilon^{3-k/2}\right), \quad x \in \Omega_x, \quad 0 \le k \le 4,$$

and

$$\left|\frac{d^k w^{j+1}(x)}{dx^k}\right| \le C\varepsilon^{-k/2}\exp\big(-x\sqrt{\tfrac{\alpha}{\varepsilon}}\big), \quad x \in \Omega_x, \quad 0 \le k \le 4.$$

Proof. Assume the asymptotic expansion for the regular component:

$$v^{j+1}(x) = v_0^{j+1}(x) + \varepsilon v_1^{j+1}(x) + \varepsilon^2 v_2^{j+1}(x) + \varepsilon^3 v_r^{j+1}(x),$$

where $y^{j+1}(x) = v_0^{j+1}(x) + \varepsilon v_1^{j+1}(x) + \varepsilon^2 v_2^{j+1}(x)$.

The leading-order term $v_0^{j+1}(x)$ satisfies the reduced problem $\frac{a^{j+1}(x)}{2}\frac{dv_0^{j+1}}{dx} - \frac{c^{j+1}(x)}{2}v_0^{j+1}(x) = g^{j+1}(x)$, subject to the appropriate reduced boundary condition.

For $m = 1, 2$, the correction terms satisfy

$$\frac{a^{j+1}(x)}{2}\frac{dv_m^{j+1}}{dx} - \frac{c^{j+1}(x)}{2}v_m^{j+1}(x) = -\frac{1}{2}\frac{d^2 v_{m-1}^{j+1}}{dx^2},$$

with homogeneous boundary conditions.

The remainder term $v_r^{j+1}(x)$ satisfies

$$\hat{\mathcal{L}}_\varepsilon v_r^{j+1}(x) = -\frac{\varepsilon^3}{2}\frac{d^2 v_2^{j+1}}{dx^2}.$$

Since $v_m^{j+1}(x)$, $m = 0, 1, 2$, are solutions of reduced first-order problems with sufficiently smooth bounded coefficients, standard theory yields

$$\left|\frac{d^k v_m^{j+1}(x)}{dx^k}\right| \leq C, \qquad 0 \leq k \leq 4.$$

Using the stability estimate and the minimum principle for the remainder problem, together with standard singular perturbation arguments, one obtains

$$\left|\frac{d^k v_r^{j+1}(x)}{dx^k}\right| \leq C\varepsilon^{-k/2}, \qquad 0 \leq k \leq 4.$$

Consequently,

$$\begin{aligned}\left|\frac{d^k v^{j+1}(x)}{dx^k}\right| &= \left|\frac{d^k}{dx^k}\left(v_0^{j+1} + \varepsilon v_1^{j+1} + \varepsilon^2 v_2^{j+1} + \varepsilon^3 v_r^{j+1}\right)\right| \\ &\leq C\left(1 + \varepsilon^{3-k/2}\right), \qquad 0 \leq k \leq 4.\end{aligned}$$

Next, we estimate the singular component $w^{j+1}(x)$. Construct the barrier functions

$$\Phi^{\pm}(x) = C\exp\left(-x\sqrt{\frac{\alpha}{\varepsilon}}\right) \pm w^{j+1}(x),$$

where C is chosen sufficiently large such that $\Phi^{\pm}(0) \geq 0, \qquad \Phi^{\pm}(1) \geq 0$. Since $c^{j+1}(x) = b^{j+1}(x) + \frac{2}{\Delta t} \geq \beta + \frac{2}{\Delta t} > 0$, it follows that $\hat{\mathcal{L}}_{\varepsilon}\Phi^{\pm}(x) \leq 0$. Therefore, by the semi-minimum principle 2.4, $\Phi^{\pm}(x) \geq 0, \qquad x \in \Omega_x$, which implies

$$|w^{j+1}(x)| \leq C\exp\left(-x\sqrt{\frac{\alpha}{\varepsilon}}\right).$$

Differentiating the singular component equation repeatedly and applying standard derivative estimates for singularly perturbed problems yields

$$\left|\frac{d^k w^{j+1}(x)}{dx^k}\right| \leq C\varepsilon^{-k/2}\exp\left(-x\sqrt{\frac{\alpha}{\varepsilon}}\right), \qquad 0 \leq k \leq 4.$$

Finally, since $u^{j+1}(x) = v^{j+1}(x) + w^{j+1}(x)$, we obtain

$$\begin{aligned}\left|\frac{d^k u^{j+1}(x)}{dx^k}\right| &\leq \left|\frac{d^k v^{j+1}(x)}{dx^k}\right| + \left|\frac{d^k w^{j+1}(x)}{dx^k}\right| \\ &\leq C\left(1 + \varepsilon^{-k/2}\exp\left(-x\sqrt{\frac{\alpha}{\varepsilon}}\right)\right), \qquad 0 \leq k \leq 4.\end{aligned}$$

□

3.4.2 Spatial Discretization

In this subsection, we describe the construction of the piecewise-uniform Shishkin mesh for discretizing the spatial domain, and analyze the behavior of the difference scheme applied to semi-discretized problem (2.10). Due to the presence of a boundary layer near $x = 0$ in problem (2.1), the mesh must be refined in the neighborhood of $x = 0$. To construct the piecewise-uniform mesh, we divide the domain $[0, 1]$ into two subintervals:

$$[0, 1] = [0, \omega] \cup (\omega, 1],$$

where $\omega \in (0, 1)$ is a suitably chosen mesh transition parameter, typically depending on the perturbation parameter ε and the number of mesh intervals N. Each subinterval is partitioned uniformly into $N/2$ mesh intervals, resulting in a total of N mesh intervals. The mesh points are given by $\overline{\Omega}^N = \{0 = x_0, x_1, \ldots, x_{N/2} = \omega, x_{N/2+1}, \ldots, x_N = 1\}$, where

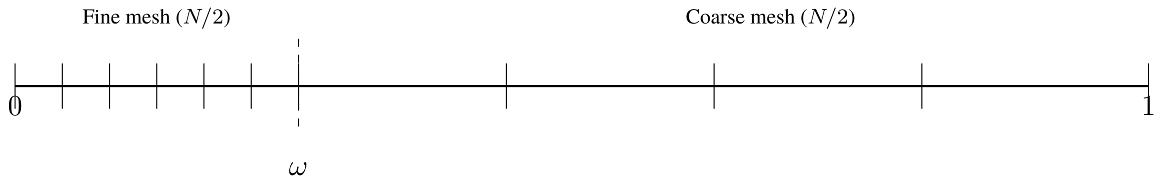

Figure 3.1: Shishkin mesh on the interval $[0, 1]$ with transition point ω

$$x_i = \begin{cases} i\dfrac{2\omega}{N}, & \text{for } i = 0, 1, \ldots, \dfrac{N}{2}, \\ \omega + \left(i - \dfrac{N}{2}\right)\dfrac{2(1-\omega)}{N}, & \text{for } i = \dfrac{N}{2} + 1, \ldots, N, \end{cases}$$

and $N \geq 4$ is a positive even integer.

The transition point ω, which separates the coarse and fine regions of the mesh, is defined by

$$\omega = \min\left\{\frac{1}{2}, \frac{2\sqrt{\varepsilon}}{\sqrt{\alpha}} \ln N\right\}. \tag{3.1}$$

Based on the definition of x_i, the spatial step sizes for $i = 0, 1, 2, \ldots, N$ are given by:

$$h_i = x_{i+1} - x_i = \begin{cases} h = \dfrac{2\omega}{N}, & \text{for } i = 0, 1, \ldots, \dfrac{N}{2} - 1, \\ H = \dfrac{2(1-\omega)}{N}, & \text{for } i = \dfrac{N}{2}, \ldots, N - 1, \end{cases}$$

where h and H denote the mesh widths in the intervals $[0, \omega]$ and $(\omega, 1]$, respectively. From these expressions, it follows that $N^{-1} \leq H \leq 2N^{-1}, \quad h = \frac{2\sqrt{\varepsilon}}{\sqrt{\alpha}} \ln N$. A uniform mesh can be obtained by choosing $\omega = \dfrac{1}{2}$.

In analysing the error, we use $\sqrt{\varepsilon} \leq CN^{-1}$ and $\omega = \frac{2\sqrt{\varepsilon}}{\sqrt{\alpha}} \ln N$, otherwise one can proceed with classical way. We propose a numerical scheme to solve (2.1), which consists of Crank-Nicolson for time derivative, and hybrid scheme for spatial derivatives. The hybrid scheme is a combination of central difference scheme in the inner region $[0, \omega]$ and the midpoint upwind scheme in the outer region $(\omega, 1]$.

3.4.3 Full Discrete Scheme

The proposed full discrete scheme is:

$$\frac{1}{2}\left(\hat{\mathcal{L}}^N_{\varepsilon,\text{hy}} U_i^{j+1} + \hat{\mathcal{L}}^N_{\varepsilon,\text{hy}} U_i^j\right) = \begin{cases} \frac{1}{2}\left(f_i^{j+1} + f_i^j\right), & 1 \leq i \leq N/2, \\ \frac{1}{2}\left(f_{i+\frac{1}{2}}^{j+1} + f_{i+\frac{1}{2}}^j\right), & N/2 < i \leq N-1, \end{cases} \tag{3.2}$$

$$\begin{aligned} &U_0^{j+1} = \phi(t_{j+1}), U_N^{j+1} = \psi(t_{j+1}), j \in \{0, 1, 2, ..., M-1\}, \\ &U_i^0 = u_0(x_i), i \in \{1, 2, ..., N-1\}, \end{aligned}$$

where

$$\hat{\mathcal{L}}^N_{\varepsilon,\text{hy}} U_i^{j+1} = \begin{cases} \hat{\mathcal{L}}^N_{\varepsilon,\text{cen}} U_i^{j+1} = \varepsilon D_x^+ D_x^- U_i^{j+1} + a_i^{j+1} D_x^0 U_i^{j+1} - \left(b_i^{j+1} + \dfrac{2}{\Delta t}\right) U_i^{j+1}, & \text{for } 1 \leq i \leq N/2, \\ \hat{\mathcal{L}}^N_{\epsilon,\text{mu}} U_i^{j+1} = \varepsilon D_x^+ D_x^- U_i^{j+1} + a_{i+\frac{1}{2}}^{j+1} D_x^+ U_i^{j+1} - \left(b_{i+\frac{1}{2}}^{j+1} + \dfrac{2}{\Delta t}\right) U_{i+\frac{1}{2}}^{j+1}, & \text{for } N/2 < i \leq N-1, \end{cases} \tag{3.3}$$

and

$$\hat{\mathcal{L}}^N_{\varepsilon,\text{hy}} U_i^j = \begin{cases} \hat{\mathcal{L}}^N_{\varepsilon,\text{cen}} U_i^j = \varepsilon D_x^+ D_x^- U_i^j + a_i^j D_x^0 U_i^j - \left(b_i^j - \dfrac{2}{\Delta t}\right) U_i^j, & \text{for } 1 \leq i \leq N/2, \\ \hat{\mathcal{L}}^N_{\epsilon,\text{mu}} U_i^{j+1} = \varepsilon D_x^+ D_x^- U_i^j + a_{i+\frac{1}{2}}^j D_x^+ U_i^j - \left(b_{i+\frac{1}{2}}^j - \dfrac{2}{\Delta t}\right) U_{i+\frac{1}{2}}^j, & \text{for } N/2 < i \leq N-1, \end{cases}$$

where $\hat{\mathcal{L}}^N_{\epsilon,\text{up}}$ is the midpoint upwind scheme and $\hat{\mathcal{L}}^N_{\epsilon,\text{cen}}$ is the central difference scheme.

The difference operators are defined by;

$$\begin{cases} D_x^+D_x^-U_i^{j+1} = \dfrac{2(D^+ - D^-)}{\hat{h}}U_i^{j+1}, \\ D_x^0U_i^{j+1} = \dfrac{U_{i+1}^{j+1} - U_{i-1}^{j+1}}{\hat{h}}, \end{cases} \quad \text{and} \quad \begin{cases} D_x^+U_i^{j+1} = \dfrac{U_{i+1}^{j+1} - U_i^{j+1}}{h_{i+1}}, \\ D_x^-U_i^{j+1} = \dfrac{U_i^{j+1} - U_{i-1}^{j+1}}{h_i}, \quad \hat{h}_i = h_i + h_{i+1}. \end{cases}$$

In the above equations, the mid-point values are given by $a_{i+\frac{1}{2}}^{j+1} = \frac{a_{i+1}^{j+1}+a_i^{j+1}}{2}$, $c_{i+\frac{1}{2}}^{j+1} = \frac{q_{i+1}^{j+1}+q_i^{j+1}}{2}$, $f_{i+\frac{1}{2}}^{j+1} = \frac{f_{i+1}^{j+1}+f_i^{j+1}}{2}$, and $U_{i+\frac{1}{2}}^{j+1} = \frac{U_{i+1}^{j+1}+U_i^{j+1}}{2}$.

After rearranging the terms in (3.2), we obtained the following system.

$$\begin{cases} \hat{\mathcal{L}}_{\varepsilon,\text{hy}}^N \equiv y_i^-U_{i-1}^{j+1} + y_i^cU_i^{j+1} + y_i^+U_{i+1}^{j+1} = H_i^j, & i \in \{1,2,...,N-1\}, \quad j \in \{0,1,2,...,M-1\}, \\ U_0^{j+1} = \phi(t_{j+1}), U_N^{j+1} = \psi(t_{j+1}), & j \in \{0,1,2,...,M-1\}, \\ U_i^0 = u_0(x_i), i \in \{1,2,...,N-1\}, \end{cases} \tag{3.4}$$

where the coefficients are given by;

$$\begin{cases} y_i^- = \dfrac{2\varepsilon}{\hat{h}_ih_i} - \dfrac{a_i^{j+1}}{\hat{h}_i}, \\ y_i^c = -\dfrac{2\varepsilon}{h_ih_{i+1}} - (b_i^{j+1} + \frac{2}{\Delta t}), \\ y_i^+ = \dfrac{2\varepsilon}{\hat{h}_ih_{i+1}} + \dfrac{a_i^{j+1}}{\hat{h}_i}, \quad i = 1,2,...,\frac{N}{2}, \end{cases} \qquad \begin{cases} y_i^- = \dfrac{2\varepsilon}{\hat{h}h_i}, \\ y_i^c = -\dfrac{2\varepsilon}{h_ih_{i+1}} - \dfrac{a_{i+\frac{1}{2}}^{j+1}}{h_{i+1}} - \frac{1}{2}\left(b_{i+\frac{1}{2}}^{j+1} + \dfrac{2}{\Delta t}\right), \\ y_i^+ = \dfrac{2\varepsilon}{\hat{h}h_{i+1}} + \dfrac{a_{i+\frac{1}{2}}^{j+1}}{h_{i+1}} - \frac{1}{2}\left(b_{i+\frac{1}{2}}^{j+1} + \dfrac{2}{\Delta t}\right), i = \frac{N}{2}+1,...,N-1, \end{cases} \tag{3.5}$$

and

$$H_i^j = \begin{cases} \left(f_i^{j+1} + f_i^j\right) - \varepsilon D_x^+D_x^-U_i^j + a_i^jD_x^0U_i^j - \left(b_i^j - \dfrac{2}{\Delta t}\right)U_i^j, & 1 \le i \le N/2, \\ \left(f_{i+\frac{1}{2}}^{j+1} + f_{i+\frac{1}{2}}^j\right) - \varepsilon D_x^+D_x^-U_i^j + a_{i+\frac{1}{2}}^jD_x^-U_i^j - \left(b_{i+\frac{1}{2}}^j - \dfrac{2}{\Delta t}\right)U_{i+\frac{1}{2}}^j, & N/2 < i \le N-1, \end{cases}$$

The coefficient matrix in Eq.(3.4) gives $(N-1)\times(N-1)$ tri-diagonal system of equations with unknowns $U_1, U_2, ..., U_{N-1}$ which can be solved using matrix inversion method.

3.5 Uniform Convergence Analysis

Lemma 3.1. *For $N \geq N_0 \geq 8$, there exists $\alpha > 0$ such that*

$$\left(\|b\| + \frac{2}{\Delta t}\right) \leq \alpha N_0, \quad \textit{and} \quad \frac{N_0}{(\ln N_0)^2} \geq 4\omega_0^2\|a\|.$$

Then, we have

$$y_i^- > 0, \quad y_i^+ > 0, \quad \textit{for} \quad 1 \leq i \leq N-1,$$

$$|y_i^-| + |y_i^+| < |y_i^c|, \quad \textit{for} \quad 1 < i < N-1,$$

$$|y_1^+| < |y_1^c|, \quad \textit{and} \quad |y_{N-1}^-| < |y_{N-1}^c|.$$

Proof. From Equations (3.5), it is clear that

$$y_i^- > 0, \quad \text{for} \quad \frac{N}{2} \leq i < N-1,$$

$$y_i^+ > 0, \quad \text{for} \quad 1 \leq i \leq \frac{N}{2}.$$

Now, we have to prove

$$y_i^- > 0, \quad \text{for} \quad 1 \leq i \leq \frac{N}{2}, \quad \text{and} \quad y_i^+ > 0, \quad \text{for} \quad \frac{N}{2} < i < N-1.$$

From Equation (3.5), one can write

$$\begin{aligned}
y_i^- &= \left(\frac{2\varepsilon}{\hat{h}_i h_i} - \frac{a_i^{j+1}}{\hat{h}_i}\right) \geq \left(\frac{2\varepsilon}{\hat{h}_i h_i} - \frac{\|a_0\| x_i^p}{\hat{h}_i}\right) = \left(\frac{N^2}{16\omega_0^2 \ln^2 N} - \frac{\|a_0\|(\sum_{i=1}^{N/2} h_i)^p}{2h_i}\right) \\
&= \left(\frac{N^2}{16\omega_0^2 \ln^2 N} - \frac{\|a_0\|(\frac{N}{2} h_i)^p}{2h_i}\right) = \left(\frac{N^2}{16\omega_0^2 \ln^2 N} - \frac{\|a_0\| N^p h^{p-1}}{2^{p+1}}\right) = \left(\frac{N^2}{16\omega_0^2 \ln^2 N} - \frac{\|a_0\| N^p (\frac{2\omega}{N})^{p-1}}{2^{p+1}}\right) \\
&= \left(\frac{N^2}{16\omega_0^2 \ln^2 N} - \frac{\|a_0\| N(\omega)^{p-1}}{4}\right), \text{since} \quad \omega = \min\{1/2, \omega_0\sqrt{\varepsilon}\ln N\} \implies \omega \leq \frac{1}{2} \\
&\geq \frac{N}{16\omega_0^2}\left(\frac{N}{\ln^2 N} - \frac{4\omega_0^2\|a_0\|}{2^{p-1}}\right), \quad p = 1, 2, 3, \ldots.
\end{aligned}$$

Since for $N \geq N_0 \geq 8$, $\frac{N}{\ln^2 N} - \frac{N_0}{\ln^2 N_0} \geq 0$, it follows that $y_i^- > 0$ for $1 \leq i \leq \frac{N}{2}$, when $\frac{N_0}{\ln^2 N_0} \geq 4\omega_0^2\|a_0\|$.

Here, we consider the domain $(\omega, 1]$, and using $H \leq 2N^{-1}$ in Equation ((3.5), we have

$$y_i^+ = \frac{2\varepsilon}{\hat{h}h_{i+1}} + \frac{a_{i+\frac{1}{2}}^{j+1}}{h_{i+1}} - \frac{1}{2}\left(b_{i+\frac{1}{2}}^{j+1} + \frac{2}{\Delta t}\right) \geq \frac{\|a_0\| x_i^p}{H} - \frac{1}{2}\left(\|b\| + \frac{2}{\Delta t}\right) = \frac{\|a_0\|(\sum_{i=N/2}^{N} H)^p}{H} - \frac{1}{2}\left(\|b\| + \frac{2}{\Delta t}\right)$$
$$= \frac{\|a_0\|(\frac{N}{2}H)^p}{H} - \frac{1}{2}\left(\|b\| + \frac{2}{\Delta t}\right) \geq \frac{1}{2}\left(\alpha N - (\|b\| + \frac{2}{\Delta t})\right), \quad \frac{N}{2} \leq i < N-1.$$

Therefore, for $N \geq N_0$, we have

$$y_i^+ > 0, \quad \text{for } \frac{N}{2} < i < N-1, \quad \text{when} \quad \alpha N_0 \geq \|b\|_\infty + \frac{2}{\Delta t}.$$

From Equations (3.5), one can easily show that

$$|y_1^+| < |y_1^c| \quad \text{and} \quad |y_{N-1}^-| < |y_{N-1}^c|.$$

Now, for $1 < i \leq \frac{N}{2}$, we have

$$\begin{aligned} |r_i^-| + |r_i^+| &= \left| \frac{2\varepsilon}{h_i \hat{h}_i} - \frac{a_i^{j+1}}{\hat{h}_i} \right| + \left| \frac{2\varepsilon}{h_{i+1}\hat{h}_i} + \frac{a_i^{j+1}}{\hat{h}_i} \right| \\ &= \frac{2\varepsilon}{h_i \hat{h}_i} - \frac{a_i^{j+1}}{\hat{h}_i} + \frac{2\varepsilon}{h_{i+1}\hat{h}_i} + \frac{a_i^{j+1}}{\hat{h}_i} \quad (\text{since } r_i^-, r_i^+ > 0) \\ &= \frac{2\varepsilon}{h_i h_{i+1}} \quad (\text{using } \hat{h}_i = h_i + h_{i+1}). \end{aligned}$$

However, we also have:

$$|y_i^c| = \left| -\frac{2\varepsilon}{h_i h_{i+1}} - \left(b_i^{j+1} + \frac{2}{\Delta t}\right) \right| = \frac{2\varepsilon}{h_i h_{i+1}} + b_i^{j+1} + \frac{2}{\Delta t}.$$

Hence, $|y_i^-| + |y_i^+| < |y_i^c|$, and for $\frac{N}{2} < i < N-1$, we get

$$|y_i^-| + |y_i^+| = \frac{2\varepsilon}{\hat{h}h_i} + \frac{2\varepsilon}{\hat{h}h_{i+1}} + \frac{a_{i+\frac{1}{2}}^{j+1}}{h_{i+1}} - \frac{1}{2}\left(b_{i+\frac{1}{2}}^{j+1} + \frac{2}{\Delta t}\right) < |y_i^c|,$$

□

Remark 3.1. *From the lemma 3.1 the matrix associated with the discrete operator $\hat{\mathcal{L}}_{\varepsilon,hy}^N$ in Eq. (3.2) is strictly diagonally dominance and so has a unique solution. The operator $\hat{\mathcal{L}}_{\varepsilon,hy}^N$ in Eq. (3.2) satisfies the following* *minimum principle. Hence the scheme (3.2) is uniformly stable in the maximum norm.*

Lemma 3.2. ***(Discrete minimum Principle)*** *Assume that* $U_0^{j+1} \geq 0, U_N^{j+1} \geq 0$ *and* $\hat{\mathcal{L}}_{\varepsilon,hy}^N U_i^{j+1} \leq 0$, *for* $1 \leq i \leq N-1$. *Then* $U_i^{j+1} \geq 0 \quad$ *for* $\quad 1 \leq i \leq N$ *and* $1 \leq j < M$.

Proof. The proof follows using Lemma 3.1 and Remark 3.1. □

Lemma 3.3 (Discrete Stability Estimate)**.** *The solution* u_i^{j+1} *of the discrete problem* (3.4) *satisfies the bound*

$$|u_i^{j+1}| \leq \max_{\partial\mathcal{D}^{M,N}} \left|u(x_i, t_{j+1})\right| + \frac{T}{\beta} \left\| \hat{\mathcal{L}}_{\epsilon,hy}^N u_i^{j+1} \right\|, \qquad (x_i, t_j) \in \mathcal{D}^{N,M}.$$

Proof. We construct the following barrier functions:

$$Z^{\pm}(x_i, t_{j+1}) = \max_{\partial\mathcal{D}^{M,N}} \left|U(x_i, t_{j+1})\right| + \frac{T}{\beta} \left\| \hat{\mathcal{L}}_{\epsilon,\text{hy}}^N U_i^{j+1} \right\| \pm U_i^{j+1}.$$

Using the discrete minimum principle, Lemma 3.2 we obtain

$$Z^{\pm}(x_i, t_{j+1}) \geq 0 \quad \text{for all } (x_i, t_j) \in D_{N,M},$$

which yields the desired estimate. □

To prove $\varepsilon-$uniform error estimates on singular components, the following barrier function are constructed;

$$\varphi_i^n = \begin{cases} \prod_{k=1}^{i} \left(1 + \frac{\mu h_k}{\sqrt{\varepsilon}}\right)^{-1}, & 1 \leq i \leq N; \\ 1, & i = 0; \end{cases}$$

where $\mu = \sqrt{\alpha}$ is a constant. Also,

$$\begin{cases} \varphi_{i-1}^n = \left(1 + \frac{\mu h_i}{\sqrt{\varepsilon}}\right)^{-1} \varphi_i^n, & 1 \leq i \leq N; \\ \varphi_{i+1}^n = \left(1 + \frac{\mu h_{i+1}}{\sqrt{\varepsilon}}\right)^{-1} \varphi_i^n, & 1 \leq i \leq N-1. \end{cases}$$

Lemma 3.4. *The barrier function* φ_i^n *satisfies the following inequalities:*

$$\hat{\mathcal{L}_\epsilon^N} \varphi_i^n \leq -\frac{C}{\sqrt{\varepsilon}} \varphi_i^n \quad \textit{for} \quad 1 \leq i \leq N$$

Proof. Consider the barrier function

$$\varphi_i^n = \begin{cases} \prod_{k=1}^{i} \left(1 + \frac{\mu h_k}{\sqrt{\varepsilon}}\right)^{-1}, & 1 \le i \le N, \\ 1, & i = 0, \end{cases}$$

where $\mu = \sqrt{\alpha}$. From its definition,

$$\varphi_{i-1}^n = \left(1 + \frac{\mu h_i}{\sqrt{\varepsilon}}\right) \varphi_i^n, \qquad \varphi_{i+1}^n = \left(1 + \frac{\mu h_{i+1}}{\sqrt{\varepsilon}}\right)^{-1} \varphi_i^n.$$

First, consider $1 \le i \le N/2$, where the central difference operator is used:

$$\hat{\mathcal{L}}_{\varepsilon,\text{cen}}^N \varphi_i^n = \varepsilon D_x^+ D_x^- \varphi_i^n + a_i^{j+1} D_x^0 \varphi_i^n - \left(b_i^{j+1} + \frac{2}{\Delta t}\right) \varphi_i^n.$$

Using the neighboring relations, $\frac{\varphi_{i+1}^n - \varphi_i^n}{h_{i+1}} = -\frac{\mu}{\sqrt{\varepsilon}\left(1+\frac{\mu h_{i+1}}{\sqrt{\varepsilon}}\right)} \varphi_i^n$, and $\frac{\varphi_i^n - \varphi_{i-1}^n}{h_i} = -\frac{\mu}{\sqrt{\varepsilon}} \varphi_i^n$.

Hence, $\varepsilon D_x^+ D_x^- \varphi_i^n \le -\frac{C_1}{\sqrt{\varepsilon}} \varphi_i^n$. Also, $|D_x^0 \varphi_i^n| = \left|\frac{\varphi_{i+1}^n - \varphi_{i-1}^n}{\hat{h}_i}\right| \le \frac{C}{\sqrt{\varepsilon}} \varphi_i^n$, which gives $a_i^{j+1} D_x^0 \varphi_i^n \le \frac{C_2}{\sqrt{\varepsilon}} \varphi_i^n$. Since $b_i^{j+1} \ge \beta > 0$, $-\left(b_i^{j+1} + \frac{2}{\Delta t}\right) \varphi_i^n \le -C_3 \varphi_i^n$. Therefore, $\hat{\mathcal{L}}_{\varepsilon,\text{cen}}^N \varphi_i^n \le -\frac{C}{\sqrt{\varepsilon}} \varphi_i^n$.

For $N/2 < i \le N-1$, the midpoint upwind operator is used:

$$\hat{\mathcal{L}}_{\varepsilon,\text{mu}}^N \varphi_i^n = \varepsilon D_x^+ D_x^- \varphi_i^n + a_{i+\frac{1}{2}}^{j+1} D_x^+ \varphi_i^n - \left(b_{i+\frac{1}{2}}^{j+1} + \frac{2}{\Delta t}\right) \varphi_{i+\frac{1}{2}}^n.$$

Since $D_x^+ \varphi_i^n = -\frac{\mu}{\sqrt{\varepsilon}\left(1+\frac{\mu h_{i+1}}{\sqrt{\varepsilon}}\right)} \varphi_i^n < 0$, the convection term is nonpositive. Thus, $\hat{\mathcal{L}}_{\varepsilon,\text{mu}}^N \varphi_i^n \le -\frac{C}{\sqrt{\varepsilon}} \varphi_i^n$. Hence, for all $1 \le i \le N$, $\hat{\mathcal{L}}_\varepsilon^N \varphi_i^n \le -\frac{C}{\sqrt{\varepsilon}} \varphi_i^n$. For further details, the reader is referred to [100]. $\square$

Lemma 3.5. *The mesh function φ_i^n satisfies the following inequality:*

$$e^{-\mu x_i/\sqrt{\varepsilon}} \le \prod_{k=1}^{i} \left(1 + \frac{\mu h_k}{\sqrt{\varepsilon}}\right)^{-1} = \varphi_i^n, \quad \textit{for all} \quad 0 \le i \le N,$$

and on Shishkin mesh, mesh function also satisfies the following inequality:

$$\prod_{k=1}^{i} \left(1 + \frac{\mu h_k}{\sqrt{\varepsilon}}\right)^{-1} \le \begin{cases} CN^{-4i/N}, & 0 < i \le \frac{N}{2}; \\ CN^{-2}, & \frac{N}{2} \le i < N. \end{cases}$$

Proof. We are given the mesh function

$$\varphi_i^n = \prod_{k=1}^{i} \left(1 + \frac{\mu h_k}{\sqrt{\varepsilon}}\right)^{-1},$$

and aim to establish two inequalities.

1. Lower Bound:

We aim to prove:

$$\prod_{k=1}^{i} \left(1 + \frac{\mu h_k}{\sqrt{\varepsilon}}\right)^{-1} \geq e^{-\mu x_i/\sqrt{\varepsilon}}, \quad \text{for all } 0 \leq i \leq N.$$

Taking the logarithm of both sides:

$$\ln\left(\prod_{k=1}^{i} \left(1 + \frac{\mu h_k}{\sqrt{\varepsilon}}\right)^{-1}\right) = -\sum_{k=1}^{i} \ln\left(1 + \frac{\mu h_k}{\sqrt{\varepsilon}}\right).$$

Using the inequality $\ln(1+z) \leq z$ for $z > -1$, which holds since $\mu, h_k > 0$, we get:

$$-\sum_{k=1}^{i} \ln\left(1 + \frac{\mu h_k}{\sqrt{\varepsilon}}\right) \geq -\sum_{k=1}^{i} \frac{\mu h_k}{\sqrt{\varepsilon}} = -\frac{\mu}{\sqrt{\varepsilon}} \sum_{k=1}^{i} h_k = -\frac{\mu x_i}{\sqrt{\varepsilon}}.$$

Taking exponential both sides:

$$\prod_{k=1}^{i} \left(1 + \frac{\mu h_k}{\sqrt{\varepsilon}}\right)^{-1} \geq e^{-\mu x_i/\sqrt{\varepsilon}}.$$

2. Upper Bound on Shishkin Mesh:

We now prove:

$$\prod_{k=1}^{i} \left(1 + \frac{\mu h_k}{\sqrt{\varepsilon}}\right)^{-1} \leq \begin{cases} CN^{-4i/N}, & 0 < i \leq \frac{N}{2}; \\ CN^{-2}, & \frac{N}{2} \leq i < N. \end{cases}$$

In $[0, \omega]$, the fine mesh size: $h_k \approx \frac{2\omega}{N} = \mathcal{O}(N^{-1} \ln N)$, In $[\omega, 1]$, the coarse mesh size: $h_k \approx \mathcal{O}(N^{-1})$.

Case 1: $0 < i \leq \frac{N}{2}$ (fine mesh)

Here, $h_k \approx \frac{2\omega}{N}$, and $\omega = \mathcal{O}\left(\frac{\sqrt{\varepsilon}}{\mu}\ln N\right)$, so

$$\frac{\mu h_k}{\sqrt{\varepsilon}} \approx \frac{2\omega\mu}{N\sqrt{\varepsilon}} \approx \frac{4\ln N}{N}.$$

Thus,

$$\prod_{k=1}^{i}\left(1+\frac{\mu h_k}{\sqrt{\varepsilon}}\right)^{-1} \leq \left(1+\frac{4\ln N}{N}\right)^{-i}.$$

Using the inequality $\left(1+\frac{a}{N}\right)^{-N} \leq e^{-a}$, we get:

$$\left(1+\frac{4\ln N}{N}\right)^{-i} = \left[\left(1+\frac{4\ln N}{N}\right)^{-N}\right]^{i/N} \leq e^{-4\ln N\cdot i/N} = N^{-4i/N}.$$

Therefore,

$$\prod_{k=1}^{i}\left(1+\frac{\mu h_k}{\sqrt{\varepsilon}}\right)^{-1} \leq CN^{-4i/N}.$$

Case 2: $\frac{N}{2} \leq i < N$ (coarse mesh)

Here, $h_k \approx \mathcal{O}(1/N)$, and the number of terms is at most N. Thus:

$$1+\frac{\mu h_k}{\sqrt{\varepsilon}} \geq 1+\frac{c}{N}, \quad \text{for some constant } c > 0.$$

So,

$$\prod_{k=1}^{i}\left(1+\frac{\mu h_k}{\sqrt{\varepsilon}}\right)^{-1} \leq \left(1+\frac{c}{N}\right)^{-N/2} \leq e^{-c/2} \leq CN^{-2}.$$

□

Theorem 3.2. *Let $u_i(t)$ and $U_i(t)$ be the solutions of the continuous and discrete problem respectively. Then, the truncation error of the proposed scheme satisfy the following bounds;*

$$\sup_{0<\varepsilon\leq 1}|u_i(t)-U_i(t)| \leq \begin{cases} CN^{-2}\ln^2 N & \text{for} \quad i=0,1,...,N/2, \\ CN^{-1}(\varepsilon+N^{-1}), & \text{for} \quad i=N/2+1,...,N \end{cases}$$

where C is a constant independent of ε and the mesh parameter N.

Proof. We prove this theorem by decomposing the numerical solution U_i^N in Eq.(3.4) into regular and singular components, similar to the continuous problem, as:

$$U_i^j = V_i^j + W_i^j \quad \text{on the domain } \mathcal{D}^{N,M}.$$

Therefore, the pointwise error of the discrete solution at each mesh point (x_i, t_j) is decomposed as:

$$u_i^j - U_i^j = v_i^j - V_i^j + w_i^j - W_i^j. \tag{3.6}$$

We now estimate the truncation error separately for the regular and singular components. First, for the regular component:

$$\hat{\mathcal{L}}_{\varepsilon,\text{hy}}^N (v - V)_i^j = \begin{cases} \left| \varepsilon \left(D_x^+ D_x^- - \dfrac{\partial^2}{\partial x^2} \right) v_i^j + a_i^j \left(D_x^0 - \dfrac{\partial}{\partial x} \right) v_i^j \right|, & i \leq N/2, \\ \left| \varepsilon \left(D_x^+ D_x^- - \dfrac{\partial^2}{\partial x^2} \right) v_i^j + a_{i+\frac{1}{2}}^j \left(D_x^+ - \dfrac{\partial}{\partial x} \right) v_i^j \right. & \\ \quad \left. - q_{i+\frac{1}{2}}^j \left(\dfrac{v_i^j + v_{i+1}^j}{2} - v_{i+\frac{1}{2}}^j \right) \right|, & i > N/2, \end{cases}$$

This satisfies the inequality:

$$\hat{\mathcal{L}}_{\varepsilon,\text{hy}}^N (v - V)_i^j \leq \begin{cases} Ch_i \left(\varepsilon \displaystyle\int_{x_{i-1}}^{x_{i+1}} |v_{xxxx}| \, dx + h_i \int_{x_{i-1}}^{x_{i+1}} |v_{xxx}| \, dx \right), & \text{for } i \leq N/2, \\ C \left(\varepsilon \displaystyle\int_{x_{i-1}}^{x_{i+1}} |v_{xxx}| \, dx + h_{i+1} \int_{x_i}^{x_{i+1}} (|v_{xxx}| + |v_{xx}| + |v_x|) \, dx \right), & \text{for } i > N/2. \end{cases}$$

Alternatively, the inequality can be expressed as:

$$\hat{\mathcal{L}}_{\varepsilon,\text{hy}}^N (v - V)_i^j \leq \begin{cases} C \left[h_i (h_i + h_{i+1}) (\varepsilon |v_{xxxx}| + |v_{xxx}|) \right], & i \leq N/2, \\ C \left[\varepsilon (h_i + h_{i+1}) |v_{xxx}| + h_{i+1}^2 (|v_{xxx}| + |v_{xx}| + |v_x|) \right], & i > N/2. \end{cases}$$

Using the derivative bounds of the regular component (Theorem 3.1), we obtain

$$\hat{\mathcal{L}}_{\varepsilon,\text{hy}}^N (v - V)_i^j \leq \begin{cases} CN^{-2} \quad \text{for} \quad i = 0, 1, ..., N/2, \\ CN^{-1}(\varepsilon + N^{-1}), \quad \text{for} \quad i = N/2 + 1, ..., N. \end{cases} \tag{3.7}$$

Applying Lemma 3.2, we get

$$|(v-V)_i^j| \leq \begin{cases} CN^{-2} \quad \text{for} \quad i=0,1,...,N/2, \\ CN^{-1}(\varepsilon+N^{-1}), \quad \text{for} \quad i=N/2+1,...,N. \end{cases} \tag{3.8}$$

Next, we estimate the truncation error for the singular component. First, consider the outer layer region $[\omega, 1]$. In this region, both w and W are small. Consider the following barrier functions:

$$\Psi^{\pm}(x_i, t_j) = C\varphi_i^j \pm W(x_i, t_j) \quad \forall (x_i, t_j) \in \mathcal{D}^{N,M};$$

where $C = |W(x_0, t_j)|$. We observe that

$$\begin{aligned} \Psi^{\pm}(x_0, t_j) &= C\varphi_0^j \pm W(x_0, t_j) = C \pm W(x_0, t_j) \geq 0, \\ \Psi^{\pm}(x_N, t_j) &= C\varphi_N^j \geq 0, \\ \hat{\mathcal{L}}_{\varepsilon,\text{hy}}^{N,M}\Psi^{\pm}(x_i, t_j) &= C\hat{\mathcal{L}}_{\varepsilon,\text{hy}}^{N,M}\varphi_i^j \pm \hat{\mathcal{L}}_{\varepsilon,\text{hy}}^{N,M}W(x_i, t_j) = C\hat{\mathcal{L}}_{\varepsilon,\text{hy}}^{N,M}\varphi_i^j \leq 0. \end{aligned}$$

Using Lemma 3.2, the following estimate is obtained:

$$|W(x_i, t_j)| \leq C\varphi_i^j = C\prod_{j=1}^{i}\left(1 + \frac{\mu h_j}{\sqrt{\varepsilon}}\right)^{-1}.$$

Using the triangle inequality and Theorem 3.1, we have

$$\begin{aligned} |\left(w-W\right)(x_i, t_j)| &\leq |w(x_i, t_j)| + |W(x_i, t_j)| \leq C\exp\left(-\frac{\sqrt{\alpha}}{\sqrt{\varepsilon}}x_i\right) + C\prod_{k=i}^{i}\left(1 + \frac{\sqrt{\alpha}h_k}{\sqrt{\varepsilon}}\right)^{-1} \\ &\leq C\prod_{k=1}^{i}\left(1 + \frac{\sqrt{\alpha}h_k}{\sqrt{\varepsilon}}\right)^{-1} + C\prod_{k=i}^{i}\left(1 + \frac{\sqrt{\alpha}h_k}{\sqrt{\varepsilon}}\right)^{-1} = C\prod_{k=1}^{i}\left(1 + \frac{\sqrt{\alpha}h_k}{\sqrt{\varepsilon}}\right)^{-1}. \end{aligned}$$

Using Lemma 3.5, the error bound in the outer region is given by

$$|\left(w-W\right)(x_i, t_j)| \leq CN^{-2}, \quad (x_i, t_j) \in [\sigma, 1] \times (0, T].$$

For the inner layer region $(x_i, t_j) \in [0, \omega] \times (0, T]$, the truncation error becomes

$$\begin{aligned}
\hat{\mathcal{L}}^N_{\varepsilon,\text{hy}}(w-W)(x_i,t_j) &\le Ch_i \left[\int_{x_{i-1}}^{x_{i+1}} (\varepsilon|w_{xxxx}| + |w_{xxx}|)\, dx \right] \le C\frac{h_i}{\varepsilon^{3/2}} \left[\int_{x_{i-1}}^{x_{i+1}} \exp\left(-\sqrt{\frac{\alpha}{\varepsilon}}x\right)\, dx \right] \\
&\le C\frac{h_i}{\sqrt{\alpha\varepsilon}} \left[\exp\left(-\sqrt{\frac{\alpha}{\varepsilon}}x_{i+1}\right) - \exp\left(-\sqrt{\frac{\alpha}{\varepsilon}}x_{i-1}\right) \right] \\
&= C\frac{h_i}{\sqrt{\alpha\varepsilon}} \left[\exp\left(-\sqrt{\frac{\alpha}{\varepsilon}}x_i\right) \left\{ \exp\left(\sqrt{\frac{\alpha}{\varepsilon}}h\right) - \exp\left(-\sqrt{\frac{\alpha}{\varepsilon}}h\right) \right\} \right] \\
&= C\frac{h_i}{\sqrt{\alpha\varepsilon}} \left[\exp\left(-\sqrt{\frac{\alpha}{\varepsilon}}x_i\right) \sinh\left(\sqrt{\frac{\alpha}{\varepsilon}}h\right) \right].
\end{aligned}$$

Using the assumption in Lemma 3.1, we have $\sqrt{\frac{\alpha}{\varepsilon}}h \le 2$. Since $\sinh\nu \le C\nu$ for $0 \le \nu \le 2$, it follows that

$$\sinh\left(\sqrt{\frac{\alpha}{\varepsilon}}h\right) \le \sqrt{\frac{\alpha}{\varepsilon}}h.$$

Therefore, the above expression becomes

$$\hat{\mathcal{L}}^N_{\varepsilon,\text{hy}}(w-W)^j_i \le C\frac{h^2}{\varepsilon^{3/2}} \exp\left(-\sqrt{\frac{\alpha}{\varepsilon}}x_i\right) \le C\frac{N^{-2}\ln^2 N}{\sqrt{\varepsilon}}\varphi^n_i \quad \text{(by Lemma 3.5).} \tag{3.9}$$

Considering the barrier functions

$$\psi^{\pm}_j(x_i) = C\left[N^{-2} + (N^{-2}\ln^2 N)\prod_{k=1}^{N}\left(1 + h_k\sqrt{\frac{\alpha}{\varepsilon}}\right)^{-1} \right]\varphi^j_i \pm (w-W)(x_i,t_j),$$

we observe that

$$\psi^{\pm}_j(x_0) \ge 0, \quad \psi^{\pm}_j(x_N) \ge 0,$$

and by Lemma 3.4,

$$\hat{\mathcal{L}}^N_{\varepsilon,\text{hy}}\psi^{\pm}_j(x_i) \le 0.$$

Applying the discrete minimum principle, the barrier functions satisfy $\psi^{\pm}_j(x_i) \ge 0$. Using the discrete barrier functions above and Lemma 3.2, we obtain

$$|(w-W)(x_i,t_j)| \le CN^{-2}\ln^2 N.$$

Combining the errors for the regular and singular components yields the required result. $\square$

Theorem 3.3. *The solution U^j_i of the fully discrete scheme (3.2) converges uniformly to the solution $u(x,t)$*

of (2.1)*and the error estimate is given by*

$$\sup_{0<\varepsilon\leq 1}\left|u(x_i,t_j)-U_i^j\right|\leq C(N^{-2}\ln^2 N+(\Delta t)^2), i=0,1,2,...,N,\ \ j=0,1,2,...,M,$$

where C is constant independent of ε and the parameters N and Δt.

Proof. The proof is derived from the bounds established in Theorems 2.2 and 3.2. □

3.6 Numerical Results and Discussion

To test the accuracy of the proposed scheme, we carried out the three model examples for different values of the mesh size and the perturbation parameter ε. Also, the maximum absolute error ($e_\varepsilon^{M,N}$) and the rate of convergence ($R_\varepsilon^{M,N}$) are evaluated.

We used the double mesh principle to estimate the maximum absolute error and rate of convergence of the current approach when the exact solution to the given problem is unknown. To determine an approximation of the maximum absolute error and the rate of convergence at the specified mesh points, we applied the formula in Chapter 2 in Section 2.6.

Example 3.1. *Consider the singularly perturbed boundary turning point problem in [59]*

$$\varepsilon u_{xx}(x,t)+(2-x^2)x^p u_x(x,t)-(1+x)u(x,t)-u_t(x,t)=10t^2e^{-t}x(x-1),\ \ (x,t)\in D.$$
$$u(x,0)=1-x,\ \ 0\leq x\leq 1,\ \ u(0,t)=1+t^2,\ \ u(1,t)=0,\ \ 0\leq t\leq 1$$

Example 3.2. *Consider the singularly perturbed boundary turning points problem in [66, 123]*

$$\varepsilon u_{xx}(x,t)+x^p u_x(x,t)-(x+p)u(x,t)-u_t(x,t)=p(x^2-1)e^{-t},\ \ (x,t)\in\mathcal{D},$$
$$u(x,0)=(1-x)^2,\ \ 0\leq x\leq 1,\ \ u(0,t)=1+t^2,\ \ u(1,t)=0,\ \ 0\leq t\leq 1.$$

Example 3.3. *Consider the singularly perturbed boundary turning point problem [59]*

$$\varepsilon u_{xx}(x,t)+x^p u_x(x,t)-u(x,t)-u_t(x,t)=x^2-1,\ \ (x,t)\in D.$$
$$u(x,0)=0,\ \ 0\leq x\leq 1,\ \ u(0,t)=t,\ \ u(1,t)=0,\ \ 0\leq t\leq 1$$

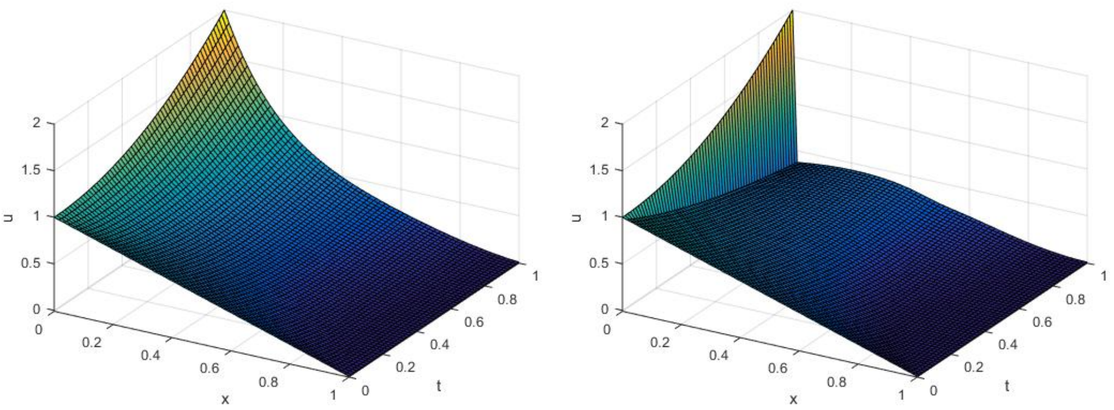

(a) $\varepsilon = 10^{-1}$ (b) $\varepsilon = 10^{-4}$

Figure 3.2: Surface plots of the numerical solution for Example 3.1 with $M = N = 64$ and $p = 3$.

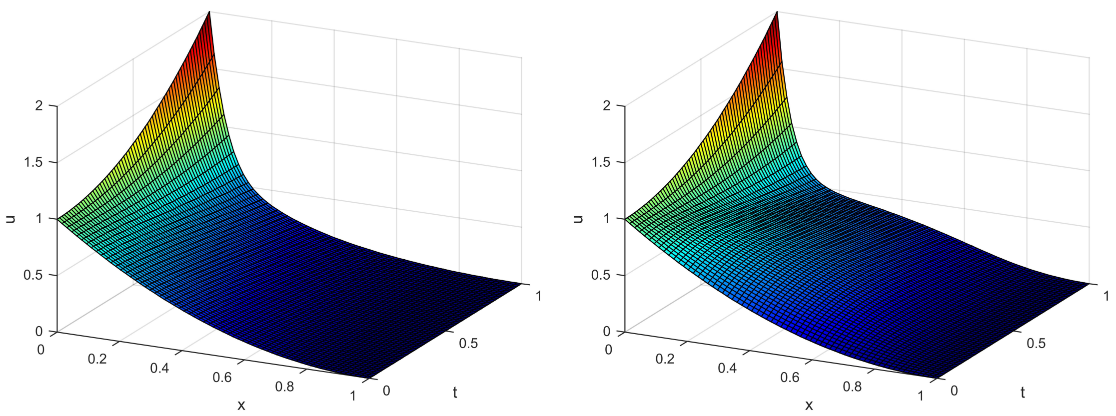

(a) $p = 1$ (b) $p = 3$

Figure 3.3: Surface plots of the numerical solution for Example 3.2 with $M = N = 64$ and $\varepsilon = 10^{-2}$.

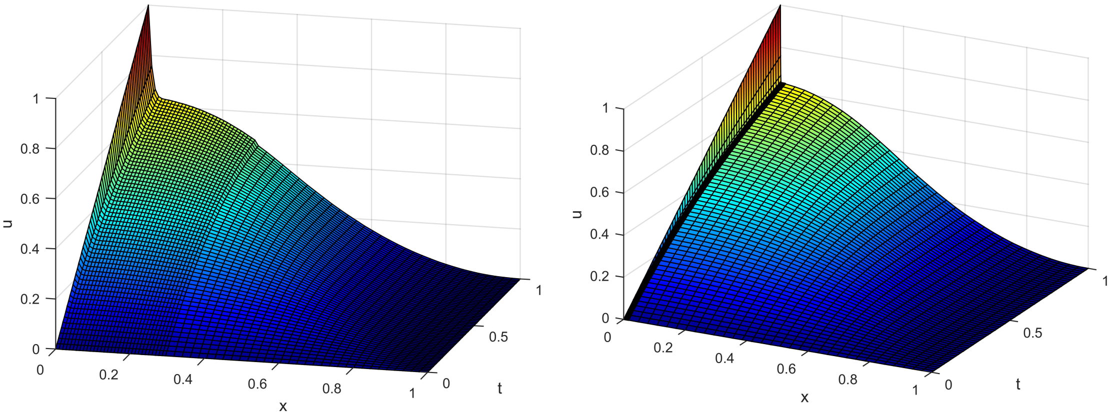

(a) $\varepsilon = 10^{-3}$ (b) $\varepsilon = 10^{-6}$

Figure 3.4: Surface plots of numerical solution for Example 3.3 $N = M = 64$ for $p = 1$ at different time levels

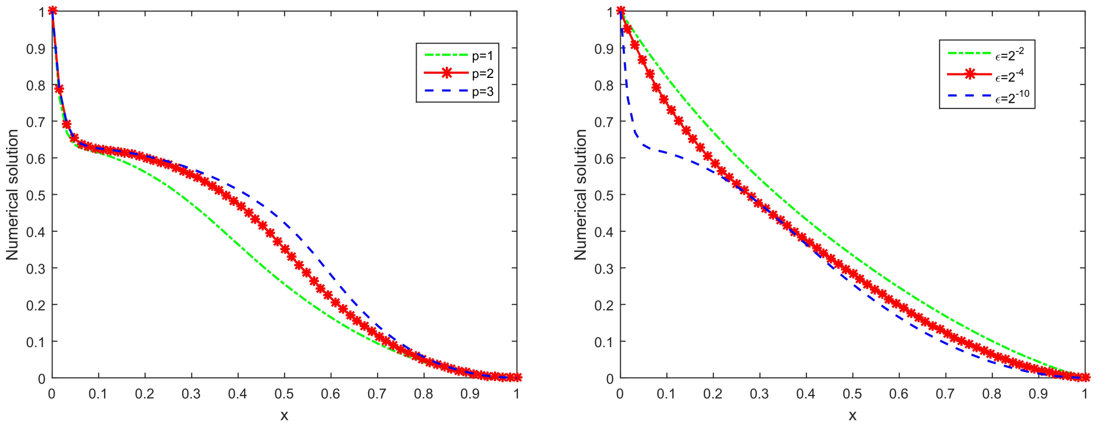

(a) $\varepsilon = 2^{-10}$ (b) $p = 1$

Figure 3.5: Numerical solution profile for Example 3.3 $N = M = 64$.

Table 3.1: Maximum absolute error and rate of convergence for Example 3.1 for $p = 1$

$\varepsilon \downarrow M = N \rightarrow$	32	64	128	256	512	1024
10^{-1}	5.7582e-04	1.5074e-04	3.8268e-05	9.6017e-06	2.4096e-06	6.0423e-07
	1.9336	1.9778	1.9948	1.9945	1.9956	
10^{-3}	6.1835e-04	1.6479e-04	4.2469e-05	1.0769e-05	2.7092e-06	6.8012e-07
	1.9078	1.9562	1.9795	1.9909	1.9941	
10^{-5}	6.2267e-04	1.6625e-04	4.2915e-05	1.0899e-05	2.7460e-06	6.8945e-07
	1.9052	1.9538	1.9772	1.9888	1.9938	
10^{-7}	6.2310e-04	1.6639e-04	4.2960e-05	1.0912e-05	2.7498e-06	6.9041e-07
	1.9049	1.9535	1.9770	1.9886	1.9937	
10^{-9}	6.2315e-04	1.6641e-04	4.2964e-05	1.0914e-05	2.7502e-06	6.9050e-07
	1.9049	1.9535	1.9770	1.9886	1.9937	
$\vdots$	$\vdots$	$\vdots$	$\vdots$	$\vdots$	$\vdots$	$\vdots$
10^{-15}	6.2315e-04	1.6641e-04	4.2964e-05	1.0914e-05	2.7502e-06	6.9050e-07
	1.9049	1.9535	1.9770	1.9886	1.9937	
PM: $e^{M,N}$	6.2315e-04	1.6641e-04	4.2964e-05	1.0914e-05	2.7502e-06	6.9050e-07
	1.9049	1.9535	1.9770	1.9886	1.9937	
In Chap 2: $e^{M,N}$	3.0268e-03	1.5854e-03	8.1084e-04	4.1001e-04	2.0616e-04	1.0308e-04
	0.9330	0.9673	0.9837	0.9919	0.9999	
In [59]: $e^{M,N}$	7.815e-02	4.21e-02	2.19e-02	1.12e-02	5.63e-03	
	0.89	0.94	0.97	0.99		

Table 3.2: Maximum absolute error and rate of convergence for Example 3.2 for $p = 1$

$\varepsilon \downarrow M = N \rightarrow$	32	64	128	256	512	1024
10^{-1}	3.0042e-04	8.0264e-05	2.0589e-05	5.1929e-06	1.3067e-06	3.2776e-07
	1.9042	1.9629	1.9872	1.9906	1.9952	
10^{-3}	3.2382e-04	8.7929e-05	2.2873e-05	5.8272e-06	1.4694e-06	3.6879e-07
	1.8808	1.9427	1.9728	1.9876	1.9942	
10^{-5}	3.2621e-04	8.8723e-05	2.3116e-05	5.8981e-06	1.4895e-06	3.7395e-07
	1.8784	1.9404	1.9706	1.9855	1.9938	
10^{-7}	3.2645e-04	8.8803e-05	2.3141e-05	5.9053e-06	1.4915e-06	3.7447e-07
	1.8782	1.9402	1.9704	1.9852	1.9937	
10^{-9}	3.2647e-04	8.8811e-05	2.3143e-05	5.9060e-06	1.4917e-06	3.7452e-07
	1.8782	1.9402	1.9703	1.9852	1.9937	
$\vdots$	$\vdots$	$\vdots$	$\vdots$	$\vdots$	$\vdots$	$\vdots$
10^{-15}	3.2647e-04	8.8811e-05	2.3143e-05	5.9060e-06	1.4917e-06	3.7452e-07
	1.8782	1.9402	1.9703	1.9852	1.9937	
PM: $e^{M,N}$	3.2647e-04	8.8811e-05	2.3143e-05	5.9060e-06	1.4917e-06	3.7452e-07
	1.8782	1.9402	1.9703	1.9852	1.9937	
In [66]: $e^{M,N}$	1.0568e-3	3.3876e-4	1.0496e-4	3.2143e-5	9.7722e-6	
	1.6413	1.6904	1.7073	1.7178		
In [123]: $e^{M,N}$	5.8935e-03	3.1304e-03	1.6083e-03	8.1279e-04		—-
	0.9128	0.9608	0.9846	—		

Table 3.3: Comparison of maximum absolute error and rate of convergence for Example 3.2 for $\varepsilon = 2^{-20}$ with different values of p

$p \downarrow M = N \rightarrow$	32	64	128	256	512
Proposed method					
2	6.3415e-04	1.7412e-04	4.5531e-05	1.1629e-05	2.9363e-06
	1.8648	1.9351	1.9691	1.9857	
4	1.2142e-03	3.4112e-04	9.0153e-05	2.3144e-05	5.8581e-06
	1.8316	1.9198	1.9617	1.9821	
6	1.7411e-03	5.0106e-04	1.3387e-04	3.4544e-05	8.7656e-06
	1.7970	1.9042	1.9543	1.9785	
8	2.2166e-03	6.5398e-04	1.7667e-04	4.5829e-05	1.1659e-05
	1.7610	1.8881	1.9468	1.9749	
Method in [67]	using $\Delta t = N^{-2}$		.	.	.
2	6.8958e-03	2.6028e-03	8.9736e-04	2.9563e-04	9.3628e-05
	1.4056	1.5363	1.6019	1.6588	
4	1.0798e-02	4.1593e-03	1.4298e-03	4.7267e-04	1.4992e-04
	1.3763	1.5405	1.5970	1.6566	
6	1.4830e-02	5.6392e-03	1.9774e-03	6.4986e-04	2.0631e-04
	1.3949	1.5119	1.6054	1.6553	
8	1.8505e-02	6.9617e-03	2.4979e-03	8.2754e-04	2.6298e-04
	1.4104	1.4787	1.5938	1.6539	

Table 3.4: Maximum absolute error and rate of convergence for Example 3.3 for $p = 1$

$\varepsilon \downarrow M = N \rightarrow$	32	64	128	256	512	1024
10^{-1}	3.3033e-04	8.4124e-05	2.1075e-05	5.2537e-06	1.3143e-06	3.2878e-07
	1.9733	1.9970	2.0041	1.9991	1.9991	
10^{-3}	3.5602e-04	9.2151e-05	2.3413e-05	5.8954e-06	1.4780e-06	3.7062e-07
	1.9499	1.9767	1.9896	1.9960	1.9960	
10^{-5}	3.5864e-04	9.2983e-05	2.3662e-05	5.9672e-06	1.4981e-06	3.7649e-07
	1.9475	1.9799	1.9874	1.9939	1.9939	
10^{-7}	3.5890e-04	9.3066e-05	2.3687e-05	5.9744e-06	1.5002e-06	3.7673e-07
	1.9472	1.9742	1.9872	1.9937	1.9936	
10^{-9}	3.5892e-04	9.3075e-05	2.3690e-05	5.9752e-06	1.5004e-06	3.7676e-07
	1.9472	1.9741	1.9872	1.9936	1.9936	
$\vdots$	$\vdots$	$\vdots$	$\vdots$	$\vdots$	$\vdots$	$\vdots$
10^{-15}	3.5892e-04	9.3075e-05	2.3690e-05	5.9752e-06	1.5004e-06	3.7676e-07
	1.9472	1.9741	1.9872	1.9936	1.9936	
PM: $e^{M,N}$	3.5892e-04	9.3075e-05	2.3690e-05	5.9752e-06	1.5004e-06	3.7676e-07
	1.9472	1.9741	1.9872	1.9936	1.9936	
In [59]: $e^{M,N}$	1.24e-02	5.99e-03	2.94e-03	1.60e-03	8.57e-04	
	1.05	1.03	0.88	0.90		

The maximum absolute errors and the corresponding rates of convergence for the proposed method, applied to Example 3.1, and 3.2, and at $p = 1$, are presented in Tables 3.1 and 3.2 respectively. From these tables we demonstrates that the maximum absolute error remains essentially constant for a fixed mesh parameter as the singular perturbation parameter ε decreases to zero. Furthermore, as the mesh parameter increases, the maximum absolute error decreases, indicating that the proposed method is ε-uniformly convergent. In Table 3.3, comparison is made with different p values for a fixed ε and achieve better accuracy and rate of convergence. The results in each table also confirm the theoretical predictions. In addition, parameter-uniform maximum errors of the proposed method are compared with those of other existing methods in the literature (see [59, 66, 67, 123]) for each example. The results clearly show that the proposed method provides better accuracy and higher order of convergence.

Surface plots for each of Example 3.1, 3.2, and 3.3 are displayed in Figures 3.2, 3.3, and 3.4 for different values of the singular perturbation parameter ε and the turning point order p, respectively. Figure 3.2 illustrates the formation of a boundary layer near the left boundary of the spatial domain as ε decreases to zero. In Figure 3.3, it is observed that for a fixed ε, increasing p partially increases the pick of the graph. Figure 3.4 shows that as ε decreases, the mesh condenses near the layer region to better resolve the boundary layer. For a fixed perturbation parameter ε, increasing the turning point order p results in a thicker boundary layer, as shown in Figure 3.5a. Additionally, Figure 3.5b reveals that decreasing ε leads to the formation of a steep gradient in the vicinity of $x = 0$. Overall, the figures demonstrate that the solution exhibits a left boundary layer in the spatial domain, and as $\varepsilon \to 0$, the thickness of this boundary layer decreases.

3.7 Conclusion

In this chapter, we examine singularly perturbed convection–diffusion parabolic partial differential equations with boundary turning points. The solution to these problems exhibits a left boundary layer within the spatial domain. A numerical method is developed using a hybrid approach: the central difference scheme is applied in the boundary layer region, while the midpoint upwind scheme is used outside the layer region. Spatial discretization is carried out on a Shishkin-type mesh, and time discretization employs the Crank–Nicolson method on a uniform mesh. Figures and tables illustrate how the solution behaves for various values of the perturbation parameter. The results demonstrate the stability and parameter-uniform convergence of the proposed method, achieving second-order accuracy in time and second-order accuracy in space (with a logarithmic factor). The numerical solutions of the model examples are consistent with the theoretical findings. Furthermore, the proposed method provides improved accuracy compared to some existing approaches in the literature and yields better results than those presented in Chapter 2.

Chapter 4

Fitted Operator Numerical Method for Singularly Perturbed Delay Parabolic Convection-Diffusion Problems with Boundary Turning Point

This chapter introduces a numerical scheme designed to solve singularly perturbed parabolic convection-diffusion problems with multiple (higher order) boundary turning point and time lag. These problems are characterized by the presence of a small perturbation parameter, which, as it approaches zero, causes the solution to develop a steep gradient in the left region of the spatial domain. The proposed numerical scheme consists of the Crank-Nicolson method for temporal discretization, followed by an exponentially fitted operator finite difference method for the system of boundary value problems obtained from the temporal semi-discretization. Stability and parameter-uniform convergence, with second-order accuracy in time and first-order in space, are proven using the minimum principle and solution bounds. Two model problems demonstrate the method's efficiency, with numerical results supporting the theoretical analysis.

4.1 Introduction

Singularly perturbed delay partial differential equations (SPDPDEs) contain a small positive parameter ε multiplying the highest derivative and at least one delay argument. These problems are classified into space-shift and time-lag types, depending on whether the shift occurs in spatial or temporal variables. The small parameter ε may induce boundary layers, while the delay introduces a memory effect, making the solution dependent on past states. Singular perturbation problems with turning points (degeneracy) pose significant challenges and model diverse physical phenomena. Interior turning points correspond to convection-diffusion problems with sign-changing convective speed, while boundary turning points arise in geophysics [44] and thermal boundary layer modeling [109].

Standard finite difference methods on uniform meshes fail to capture narrow layers and turning point accurately as $\varepsilon \to 0$. This motivates advanced numerical schemes that ensure parameter-uniform convergence and accuracy independent of ε, delay parameters, and degeneracy. Exponentially fitted methods are widely employed to construct uniformly convergent numerical schemes for singularly perturbed problems. The exponential fitting parameter is derived from the asymptotic solution of the problem, and its form depends on the structure of the developed scheme. While these methods yield accurate and uniformly convergent results for one-dimensional linear problems, their applicability is limited for higher-dimensional and nonlinear problems [78]. Recent studies have investigated singularly perturbed parabolic differential equations (SPPDEs) with turning point [66, 59, 136, 67, 108]. However, uniformly convergent methods for problems with time delay with multiple turning point remain scarce.

To the best of our knowledge, only two parameter-uniform convergence numerical methods for SPDPDEs with multiple turning point have been proposed [100, 135], both employing the implicit Euler method in time and hybrid spatial schemes on Shishkin meshes. These achieve first-order temporal convergence, with second-order accuracy obtained via Richardson extrapolation. This work presents the first parameter-uniform scheme that combines exponentially fitted operators with the Crank–Nicolson method in time for SPDPDEs with higher-order boundary turning point. The use of central difference approximations for the spatial derivative on uniform meshes can lead to oscillations, which are suppressed here by introducing artificial viscosity into the diffusion term.

4.2 Description of the Problem

Consider the singularly perturbed parabolic convection-diffusion initial boundary value problem in the rectangular domain $\mathcal{D} = \Omega \times \Lambda = (0,1) \times (0,T]$, for some finite positive T of the form:[100]:

$$\mathcal{L}_\varepsilon u(x,t) \equiv \varepsilon \frac{\partial^2 u(x,t)}{\partial x^2} + a(x,t)\frac{\partial u(x,t)}{\partial x} - b(x,t)u(x,t) - \frac{\partial u(x,t)}{\partial t} = f(x,t) + c(x,t)u(x,t-\tau) = F(x,t), \quad (x,t) \in \mathcal{D}, \tag{4.1}$$

subject to the initial and boundary conditions:

$$\begin{cases} u(0,t) = \psi_l(t), & (0,t) \in \Gamma_l = \{(0,t) : 0 \leq t \leq 2\}, \\ u(1,t) = \psi_r(t), & (1,t) \in \Gamma_r = \{(1,t) : 0 \leq t \leq 2\}, \\ u(x,t) = \psi_b(x,t), & (x,t) \in \Gamma_b = \{(x,t) : 0 \leq x \leq 1, \ -\tau \leq t \leq 0\}. \end{cases} \tag{4.2}$$

where $0 < \varepsilon \ll 1$ is the perturbation parameter and $a(x,t) = a_0(x,t)x^p$, with $p \geq 1$. Also the delay parameter $\tau > 0$ such that $T = s\tau$ for positive integer s. We assume that $a_0(x,t), b(x,t), c(x,t)$ and $f(x,t)$ are smooth and bounded functions on $\overline{D}$, and $\psi_l(t), \psi_r(t), u_0(x)$ are smooth and bounded on their respective domains and independent of ε. The boundary of the domain is defined as $\partial\mathcal{D} = \Gamma_l \cup \Gamma_b \cup \Gamma_r$. Furthermore, we suppose that $a_0(x,t) \geq \alpha > 0, \quad b(x,t) \geq \beta > 0, c(x,t) \geq \gamma > 0 \quad \forall (x,t) \in \overline{\mathcal{D}}$. Under these assumptions, problem (4.1) exhibits a boundary layer near $x = 0$.

Problems of the form (4.1) are referred to as singularly perturbed problems (SPPs) with boundary turning point. The point $x = 0$ is identified as a turning point since the convective coefficient vanishes there. When $p > 1$, problem (4.1) is termed a multiple (higher-order) boundary turning point problem; otherwise, it is called a simple boundary turning point problem.

The existence and uniqueness of the solution are guaranteed by the above smoothness assumptions together with the following compatibility conditions:

$$\psi_b(0,0) = \psi_l(0), \quad \psi_b(1,0) = \psi_r(0), \tag{4.3}$$

and

$$\begin{cases} \varepsilon \dfrac{\partial^2 \psi_b(0,0)}{\partial x^2} + a(0,0)\dfrac{\partial \psi_b(0,0)}{\partial x} - b(0,0)\psi_b(0,0) - \dfrac{\partial \psi_l(0)}{\partial t} = f(0,0) + c(0,0)\psi_b(0,-\tau), \\ \varepsilon \dfrac{\partial^2 \psi_b(1,0)}{\partial x^2} + a(1,0)\dfrac{\partial \psi_b(1,0)}{\partial x} - b(1,0)\psi_b(1,0) - \dfrac{\partial \psi_r(0)}{\partial t} = f(1,0) + c(1,0)\psi_b(1,-\tau), \end{cases} \tag{4.4}$$

4.3 Bounds on the Solution and its Derivatives

Lemma 4.1 (Continuous Minimum Principle). *Let $\theta(x,t)$ be a sufficiently smooth function defined on $\mathcal{D}$ which satisfies $\theta(x,t) \geq 0, \quad \forall (x,t) \in \partial\mathcal{D}, \quad$ and $\quad \mathcal{L}_\varepsilon \theta(x,t) \leq 0, \quad \forall (x,t) \in \mathcal{D}$. Then, $\theta(x,t) \geq 0, \quad \forall (x,t) \in \bar{\mathcal{D}}$.*

Proof. Suppose there exists a point $(y,z) \in \bar{\mathcal{D}}$ such that

$$F(y,z) = \min_{(x,t)\in\bar{\mathcal{D}}} \theta(x,t) < 0.$$

Since $\theta(x,t) \geq 0$ on $\partial\mathcal{D}$, it follows that $(y,z) \notin \partial\mathcal{D}$, i.e., $(y,z) \in \mathcal{D}$. The condition $\theta(y,z) = \min_{\bar{\mathcal{D}}} \theta < 0$ implies

$$\frac{\partial\theta}{\partial t}(y,z) = 0, \quad \frac{\partial\theta}{\partial x}(y,z) = 0, \quad \frac{\partial^2\theta}{\partial x^2}(y,z) \geq 0.$$

Therefore,

$$\mathcal{L}_\varepsilon \theta(y,z) = \left(\varepsilon \frac{\partial^2\theta}{\partial x^2} + a\frac{\partial\theta}{\partial x} - b\theta - \frac{\partial\theta}{\partial t} \right)(y,z) > 0,$$

which contradicts the assumption that $\mathcal{L}_\varepsilon \theta(x,t) \leq 0$ for all $(x,t) \in \mathcal{D}$. Hence,

$$\theta(x,t) \geq 0, \quad \forall (x,t) \in \bar{\mathcal{D}}.$$

□

Lemma 4.2. *The solution of the problem* (4.1) *satisfies the following bound:*

$$|u(x,t) - \psi_b(x,t)| \leq Ct, \quad (x,t) \in \mathcal{D}.$$

Proof. Let us define

$$z(x,t) = \begin{cases} u(x,t) - \psi_b(x,t), & \text{for } -\tau \leq t \leq 0, \\ u(x,t) - \psi_b(x,0), & \text{for } 0 \leq t \leq T. \end{cases}$$

Then, $z(x,t)$ satisfies

$$\mathcal{L}_\varepsilon z(x,t) = g(x,t),$$

where

$$g(x,t) = f(x,t) + \mathcal{L}_\varepsilon \psi(x,0) + \gamma(x,t)\psi(x,-\tau) + \gamma(x,t)z(x,t-\tau).$$

We have

$$z(x,t) = u(x,t) - \psi_b(x,t) = \psi_b(x,t) - \psi_b(x,t) = 0 \quad \text{on } \partial\mathcal{D},$$

which gives

$$z(0,t) = \psi_l(t) - \psi_b(0,0), \quad z(1,t) = \psi_r(t) - \psi_b(1,0), \quad \text{for } t \in [0,T].$$

Then, using the compatibility condition at the corner point, we get

$$|z(0,t)| = C_1 t, \quad |z(1,t)| = C_2 t, \quad t \in [0,T],$$

for some constants C_1 and C_2. In addition, let

$$d(x,t) = \begin{cases} Ct, & \text{for } 0 \leq t \leq T, \\ 0, & \text{for } -\tau \leq t \leq 0. \end{cases}$$

From the above, we have

$$\mathcal{L}_\varepsilon d(x,t) = 1 + Ctb(x,t).$$

This results in

$$|\mathcal{L}_\varepsilon z(x,t)| \leq \mathcal{L}_\varepsilon d(x,t) \quad \text{on } D, \quad \text{and} \quad |z(x,t)| \leq d(x,t) \quad \text{on } \partial\mathcal{D} = \Gamma_l \cup \Gamma_r \cup \Gamma_b$$

As a result, using Lemma 4.1, we obtain

$$|z(x,t)| \leq d(x,t), \quad \text{on } D,$$

which implies

$$|z(x,t)| \leq Ct.$$

For more details, please refer to [37, p. 292].

□

Lemma 4.3. *The bound on the solution $u(x,t)$ of equation (4.1) is given by*

$$|u(x,t)| \leq C, \quad (x,t) \in \overline{\mathcal{D}}.$$

Proof. From Lemma 4.2, we have

$$|u(x,t)| \le C_1 t, \quad (x,t) \in \overline{\mathcal{D}},$$

since $t \in (0,2]$ and it is bounded, we obtained

$$|u(x,t)| \le C, \quad (x,t) \in \overline{\mathcal{D}}.$$

□

Lemma 4.4 (**Stability Estimate**). *Let $u(x,t)$ be the solution of the continuous problem* (4.1) *Then,*

$$|u(x,t)| \le \frac{T}{\beta} \parallel \mathcal{L}_\varepsilon u \parallel_{\overline{\mathcal{D}}} + \max\{|\psi_l(t)|, |\psi_r(t)|, |\psi_b(x,t)|\}, \forall (x,t) \in \mathcal{D}.$$

Proof. Let the two barrier functions $\phi^{\pm}$ be defined as

$$\phi^{\pm} = \frac{T}{\beta} \parallel \mathcal{L}_\varepsilon u \parallel_{\overline{\mathcal{D}}} + \max\{|\psi_l(t)|, |\psi_r(t)|, |\psi_b(x,t)|\} \pm u(x,t).$$

The barrier function at the initial condition, given as:

$$\begin{aligned}\phi^{\pm}(x,0) &= \frac{T}{\beta} \parallel \mathcal{L}_\varepsilon u \parallel_{\overline{\mathcal{D}}} + \max\{|\psi_l(0)|, |\psi_r(0)|, |\psi_b(x,0)|\} \pm u(x,0)\\ &\ge \max\{|\psi_l(0)|, |\psi_r(0)|, |\psi_b(x,0)|\} \pm \psi_b(x,0) \ge 0 \quad \forall x \in (0,1).\end{aligned}$$

The barrier function at the boundary conditions, given as:

$$\begin{aligned}\phi^{\pm}(0,t) &= \frac{T}{\beta} \parallel \mathcal{L}_\varepsilon u \parallel_{\overline{\mathcal{D}}} + \max\{|\psi_l(t)|, |\psi_r(t)|, |\psi_b(0,t)|\} \pm u(0,t)\\ &\ge \max\{|\psi_l(t)|, |\psi_r(t)|, |\psi_b(0,t)|\} \pm \psi_l(t) \ge 0\end{aligned}$$

and

$$\begin{aligned}\phi^{\pm}(1,t) &= \frac{T}{\beta} \parallel \mathcal{L}_\varepsilon u \parallel_{\overline{\mathcal{D}}} + \max\{|\psi_l(t)|, |\psi_r(t)|, |\psi_b(1,t)|\} \pm u(0,t)\\ &\ge \max\{|\psi_l(t)|, |\psi_r(t)|, |\psi_b(1,t)|\} \pm \psi_r(t) \ge\end{aligned}$$

Furthermore, we have

$$\begin{aligned}
\mathcal{L}_\varepsilon \phi^{\pm}(x,t) &= \varepsilon \phi^{\pm}_{xx}(x,t) + a(x,t)\phi^{\pm}_x(x,t) - b(x,t)\phi^{\pm}(x,t) - \phi^{\pm}_t(x,t) \\
&= -b(x,t)\big(\frac{T}{\beta} \parallel \mathcal{L}_\varepsilon u \parallel_{\overline{\mathcal{D}}} + \max\{|\psi_l(t)|, |\psi_r(t)|, |\psi_b(x,t)|\}\big) \pm \mathcal{L}_\varepsilon u(x,t) \\
&= -b(x,t)\big(\frac{T}{\beta} \parallel \mathcal{L}_\varepsilon u \parallel_{\overline{\mathcal{D}}} + \max\{|\psi_l(t)|, |\psi_r(t)|, |\psi_b(x,t)|\}\big) \pm f(x,t) + c(x,t)u(x,t-\tau) \\
&\leq -\beta\big(\frac{T}{\beta} \parallel \mathcal{L}_\varepsilon u \parallel + \max\{|\psi_l(t)|, |\psi_r(t)|, |\psi_b(x,t)|\}\big) \pm f(x,t) + \gamma u(x,t-\tau) \\
&\leq -T \parallel \mathcal{L}_\varepsilon u \parallel \mp f(x,t) + \gamma u(x,t-\tau) \leq 0
\end{aligned}$$

Therefore, using Lemma 4.1, we obtain $\phi^{\pm}(x,t) \geq 0$, $\forall (x,t) \in \overline{\mathcal{D}}$. This confirms the desired result. $\square$

Theorem 4.1. *The solution $u(x,t)$ of the problem in (4.1) satisfies the following derivative bounds for all $0 \leq i + 3j \leq 4$:*

$$\left| \frac{\partial^{i+j} u(x,t)}{\partial x^i \partial t^j} \right| \leq C \left(1 + \varepsilon^{-i/2} \exp\left(-x\sqrt{\frac{\alpha}{\varepsilon}} \right) \right), \quad (x,t) \in \overline{\mathcal{D}},$$

where C is a positive constant independent of ε.

Proof. For a fixed $i = 0$ and on the boundaries $x = 0$ and $x = 1$ of $\overline{\Omega}$, we have $u = 0$ and consequently $u_t = 0$. On the boundary $t = 0$, the condition $u = 0$ implies that $u_x = 0$ and $u_{xx} = 0$. It then follows from (4.1) that

$$u_t(x,0) = F(x,0).$$

For $t \in (-\tau, 0)$, we have

$$u_t = \lim_{l \to 0} \frac{u(x, t-\tau+l) - u(x,t-\tau)}{l} = 0.$$

Thus, by choosing K_1 sufficiently large, we ensure that $|u_t(x,t)| \leq K_1$ on $\partial\mathcal{D}$.

Using the assumption of Ng-Stynes in [84] for $a(x,t)$ in the domain $\bar{\mathcal{D}}$ and adopting the technique in [97], we express the differential operator $\mathcal{L}_\epsilon$ defined in (4.1) as

$$\mathcal{L}_\epsilon u(x,t) \equiv \varepsilon u_{xx} + (au)_x - (a_x + b)u - u_t.$$

Applying this operator to u_t yields

$$
\begin{aligned}
\mathcal{L}_\epsilon u_t(x,t) &= \big(\varepsilon u_{txx} + (au_t)_x - (a_x+b)u_t - u_{tt}\big) \quad as \quad a=a(x)\\
&= \big(\varepsilon u_{txx} + au_{tx} - bu_t - u_{tt}\big)\\
&= \big(\varepsilon u_{xx} + au_x - bu - u_t\big)_t + b_t u\\
&= f_t(x,t) + c_t(x,t)u(x,t-\tau) + c(x,t)u_t(x,t-\tau) + b_t u.
\end{aligned}
\tag{4.5}
$$

First, consider the case where $u(x,t-\tau)$ is a known function, which occurs when $t\in(0,\tau)$. Substituting the initial condition into (4.5), we obtain

$$
\mathcal{L}_\epsilon u_t(x,t) = f_t + b_t u.
$$

Since f is sufficiently smooth, Lemma 4.1 and Lemma 4.3 yield

$$
|(\mathcal{L}_\epsilon)\, u_t(x,t)| \le K_2, \quad (x,t)\in(0,1)\times(0,\tau),
$$

and thus $|u_t|\le C$.

Next, we extend the analysis to the domain $(x,t)\in(0,1)\times(0,2\tau)$. For $t\in(\tau,2\tau)$, equation (4.5) becomes

$$
\mathcal{L}_\epsilon u_t(x,t) = f_t + c_t u(x,t-\tau) + c u_t(x,t-\tau) + b_t u.
$$

Given that $|u_t|\le C$ on $(x,t)\in(0,1)\times(0,\tau)$, we have

$$
|\mathcal{L}_\epsilon u_t(x,t)| \le C \quad \text{for} \quad (x,t)\in(0,1)\times(\tau,2\tau).
$$

Therefore, applying the minimum principle over the domain $(x,t)\in(0,1)\times(0,2\tau)$, we conclude that $|u_t|\le C$. By repeating this argument, we can establish the required bound over the entire domain $\overline{\mathcal{D}}$.

To bound the derivatives of the solution in the spatial domain, consider the cases for a fixed $j=0$. In the DPDE (4.1), the delay influences only the time variable t and has no impact on the spatial variable x. For $i=0$, from Lemma 4.3 we have $|u|\le C$. For $i=1$, by using arguments in [54], construct the neighbourhood of $I = (0, \sqrt{\varepsilon}),\ \ \forall r \in I$. By the mean value theorem, there exists some $r^* \in I$ such that

$$u_x(r^*) = \frac{u(\sqrt{\varepsilon}) - u(0)}{\sqrt{\varepsilon}}.$$

This implies

$$|u_x(r^*)| = \varepsilon^{-1/2}|u(\sqrt{\varepsilon}) - u(0)| \leq C\varepsilon^{-1/2}\|u\|. \tag{4.6}$$

Rewriting Eq. (4.1) as

$$\mathcal{L}_\varepsilon u(x,t) \equiv \varepsilon u_{xx} + (au)_x - (a_x + b)u - u_t = F,$$

we obtain

$$\varepsilon u_{xx} + (au)_x = F + (a_x + b)u + u_t.$$

Integrating from r^* to r yields

$$\int_{r^*}^{r} (\varepsilon u_{xx} + (au)_x)\, dx = \int_{r^*}^{r} (F + (a_x + b)u + u_t)\, dx,$$

which gives

$$(\varepsilon u_x + au)|_{r^*}^{r} \leq C \int_{r^*}^{r} (\|F\| + \|u\| + \|u_t\|)\, dx \leq C\varepsilon^{1/2}.$$

Thus,

$$\varepsilon u_x(r,t) + a(r,t)u(r,t) \leq \varepsilon u_x(r^*,t) + a(r^*,t)u(r^*,t) + C\varepsilon^{1/2}.$$

For $r \in (0, \sqrt{\varepsilon})$, we have $|a(r,t)| = |a_0(r,t)r^k| \leq C\varepsilon^{k/2}$ $(k = 1, 2, 3, \ldots)$. Using (4.6), we obtain

$$\begin{aligned}
|u_x(r,t)| &\leq |u_x(r^*,t)| + |a(r^*,t)u(r^*,t)|/\varepsilon + |a(r,t)u(r,t)|/\varepsilon + C\varepsilon^{-1/2} \\
&\leq C_1\varepsilon^{-1/2} + C_2\varepsilon^{k/2-1} + C_3\varepsilon^{k/2-1} + C\varepsilon^{-1/2} \\
&\leq C_4\varepsilon^{-1/2} \leq C\left(1 + \varepsilon^{-1/2}\exp\left(-x\sqrt{\alpha/\varepsilon}\right)\right).
\end{aligned}$$

For $i = 1$, the proof is complete. The required bounds for higher-order derivatives ($i = 2, 3, 4$) follow similarly. $\square$

4.4 Derivation of the Numerical Method

In this section, we developed an exponentially fitted operator finite difference method to solve the problem in (4.1) together with the conditions (4.2).

4.4.1 Temporal Discretization

On the time domain $[0, T]$, we used a uniform mesh with time step Δt. Define: $\Lambda^M = \{t_j = j\Delta t,\, j = 0, \ldots, M,\, t_M = T,\, \Delta t = T/M\}$, $\Lambda^s = \{t_j = j\Delta t;\, j = 0, \ldots, s,\, t_s = \tau,\, \Delta t = \tau/s\}$, where M and s are the number of mesh points in the t-direction over the interval $[0, T]$ and $[-\tau, 0]$ respectively. The step size Δt satisfies $s\Delta t = \tau$, where s is a positive integer. The mesh points are denoted by $t_j = j\Delta t$ with $j \geq -s$. To discretize the time variable for (4.1), we used the Crank-Nicolson method, defined by:

$$\begin{cases} \varepsilon U_{xx}^{j+1/2} + a^{j+1/2}(x)U_x^{j+1/2} - b^{j+1/2}(x)U^{j+1/2}(x) - D_t^- U^{j+1}(x) = F^{j+1/2}(x), \\ U^{j+1}(0) = \psi_l(t_{j+1}), U^{j+1}(1) = \psi_r(t_{j+1}), 0 \leq j \leq M, \\ U^{-j}(x) = \psi_b(x, -t_j), x \in \Omega, j = 1, 2, 3..., s, \end{cases} \tag{4.7}$$

where

$$\begin{cases} D_t^- u^{j+1}(x) = \dfrac{U^{j+1}(x) - U^j(x)}{\Delta t}, \\ U^{j+1/2}(x) = \dfrac{U^{j+1}(x) + U^j(x)}{2}, \\ F^{j+1/2}(x) = \dfrac{F^{j+1}(x) + F^j(x)}{2}, \end{cases}$$

and $U^j(x)$ is an approximate solution of $u(x, t_j)$ at j^{th} time level. The time semi-discretized problem (4.7) can be rewritten as:

$$\begin{cases} \hat{\mathcal{L}}_\epsilon U^{j+1}(x) = R^{j+1}(x), \\ U^{j+1}(0) = \psi_l(t_{j+1}), \quad U^{j+1}(1) = \psi_r(t_{j+1}), \quad 0 \leq j \leq M, \\ U^{-j}(x) = \psi_b(x, -t_j), \quad j = 0, 1, 2, \ldots, s, \quad x \in \Omega, \end{cases} \tag{4.8}$$

where

$$\begin{cases} \hat{\mathcal{L}}_\epsilon U^{j+1}(x) = \dfrac{\varepsilon}{2}(U_{xx})^{j+1} + \dfrac{a^{j+1}(x)}{2}(U_x)^{j+1} - \dfrac{q^{j+1}(x)}{2}U^{j+1}(x), \\ R^{j+1}(x) = F^{j+1/2}(x) - \dfrac{\varepsilon}{2}(U_{xx})^j - \dfrac{a^j(x)}{2}(U_x)^j + \dfrac{d^j(x)}{2}U^j(x), \\ q^{j+1}(x) = b^{j+1}(x) + \dfrac{2}{\Delta t}, \\ d^j(x) = b^j(x) - \dfrac{2}{\Delta t}, \end{cases}$$

and

$$F^j(x) = \begin{cases} f^j(x) + c^j(x)\phi_b(x, t_j - \tau), & j = 0, 1, 2, \ldots, s, \quad x \in \Omega, \\ f^j(x) + c^j(x)U^{j-s}(x), & j = s+1, s+2, \ldots, M-1, \quad x \in \Omega. \end{cases}$$

The semi-discrete operator $\hat{\mathcal{L}}_\epsilon$ satisfies the following minimum principle.

Lemma 4.5 (Semi-Discrete Minimum principle). *Let $\theta^{j+1}(x)$ be smooth, satisfying $\theta^{j+1}(0) \geq 0$, $\theta^{j+1}(1) \geq 0$, and $\hat{\mathcal{L}}_\varepsilon \theta^{j+1}(x) \leq 0$ for all $x \in \Omega$. Then $\theta^{j+1}(x) \geq 0$ for all $x \in \overline{\Omega}, \quad j = 0, 1, \ldots, M-1$.*

Proof. Suppose there exists $\ell \in \Omega$ such that $\theta^{j+1}(\ell) = \min_{x\in\Omega} \theta^{j+1}(x) < 0$. Then $\theta_x^{j+1}(\ell) = 0$, $\theta_{xx}^{j+1}(\ell) \geq 0$, and

$$\hat{\mathcal{L}}_\varepsilon \theta^{j+1}(\ell) = \tfrac{\varepsilon}{2}\theta_{xx}^{j+1}(\ell) + \tfrac{a^{j+1}(\ell)}{2}\theta_x^{j+1}(\ell) - \tfrac{q^{j+1}(\ell)}{2}\theta^{j+1}(\ell) > 0.$$

But $q^{j+1}(\ell) = b^{j+1}(\ell) + \frac{2}{\Delta t} \geq \beta + \frac{2}{\Delta t} > 0$, which contradicts $\hat{\mathcal{L}}_\varepsilon \theta^{j+1}(x) \leq 0$. Hence, $\theta^{j+1}(x) \geq 0$ $\forall x \in \bar{\Omega}$. $\square$

Lemma 4.6 (Semi-Discrete stability estimate). *Let $u^{j+1}(x)$ be the solution of Eq. (4.8). Then, we get the bound*

$$| u^{j+1}(x) | \leq T \frac{\| \hat{\mathcal{L}}_\varepsilon u \|}{\bar{\beta}} + \max\{|\varphi_l^{j+1}(x)|, |\varphi_b(x)|, |\varphi_r^{j+1}(x)|\}, \forall x \in \Omega.$$

Proof. The proof follows a similar approach that presented in Lemma 2.5. $\square$

The local truncation error at time level t_{j+1} is given by,

$$e_{j+1}(x) = \hat{\mathcal{L}}_\varepsilon\, \nu^{j+1}(x) - g^{j+1}(x),$$

where $\nu^{j+1}(x)$ denotes the exact solution of (4.8).

Lemma 4.7. *Suppose that*

$$\left|\frac{\partial^i u}{\partial t^i}\right| \leq C, \quad (x,t) \in \bar{\mathcal{W}} \ \ for \ \ 0 \leq i \leq 2.$$

The local truncation error at $(j+1)^{th}$ *time step is given by*

$$||e_{j+1}|| \leq C(\Delta t)^3$$

Proof. Using Taylor series expansions around $t_{j+1/2} = t_j + \Delta t/2$, we have:

$$u(x,t_{j+1}) = u(x,t_{j+1/2}) + \frac{\Delta t}{2}u_t(x,t_{j+1/2}) + \frac{1}{2!}(\frac{\Delta t}{2})^2 u_{tt} + O((\Delta t)^3). \tag{4.9}$$

$$u(x,t_j) = u(x,t_{j+1/2}) - \frac{\Delta t}{2}u_t(x,t_{j+1/2}) + \frac{1}{2!}(\frac{\Delta t}{2})^2 u_{tt} + O((\Delta t)^3). \tag{4.10}$$

Subtracting (4.10) from (4.9) we get

$$\frac{u(x,t_{j+1}) - u(x,t_j)}{\Delta t} = u_t(x,t_{j+1/2}) + O((\Delta t)^2).$$

$$= \varepsilon u_{xx}(x,t_{j+1/2}) + a(x,t_{j+1/2})u_x(x,t_{j+1/2}) - b(x,t_{j+1/2})u(x,t_{j+1/2}) - F(x,t_{j+1/2}) + O((\Delta t)^2),$$

where $u(x,t_{j+1/2}) = \frac{u(x,t_{j+1})+u(x,t_j)}{2} + O((\Delta t)^2)$.

Further simplification yields

$$\hat{\mathcal{L}}_\epsilon u(x,t_{j+1}) \equiv \frac{\varepsilon}{2}u_{xx}(x,t_{j+1}) + \frac{a(x,t_{j+1})}{2}u_x(x,t_{j+1}) - \frac{q(x,t_{j+1})}{2}u(x,t_{j+1}) = R(x,t_{j+1}) + O((\Delta t)^3). \tag{4.11}$$

From Eq.(4.8) and Eq. (4.11) the local truncation error satisfies

$$\begin{aligned} \hat{\mathcal{L}}_\epsilon e_{j+1} &= O((\Delta t)^3), \\ e_{j+1}(0) &= e_{j+1}(1) = 0. \end{aligned} \tag{4.12}$$

It can be seen that

$$||e_{j+1}|| \leq C(\Delta t)^3.$$

□

The local error estimate of each time step contributes to the global error in the temporal semi-discretization which is denoted by, E_j.

Theorem 4.2. *The global truncation error for temporal discretization up to j^{th} time level is given by*

$$||E_j|| \leq C(\Delta t)^2, \quad \forall j \leq \frac{T}{\Delta t}.$$

Proof. Using the local error estimate up to j^{th} time step, we obtain the global error estimate at j^{th} time step.

$$\begin{aligned} ||E_j|| &= ||\sum_{i=1}^{j} e_i||, \;\; j \leq \frac{T}{\Delta t} \\ &\leq ||e_1|| + ||e_2|| + ||e_3|| + ... + ||e_j|| \\ &\leq C_1(j)(\Delta t)^3 \text{using Lemma 4.7} \\ &\leq C_1 T(\Delta t)^2 \text{ as } \; j.\Delta t \leq T \\ &\leq C(\Delta t)^2, \;\; C = C_1 T. \end{aligned}$$

□

The above results conclude that the semi-discrete scheme (4.8) is second-order convergent in time.

Theorem 4.3. *The solution $u^{j+1}(x)$ and its derivatives satisfy the bound*

$$\left|\frac{d^k u^{j+1}(x)}{dx^k}\right| \leq C\Big(1 + \varepsilon^{-k/2} \exp\big(-x\sqrt{\tfrac{\alpha}{\varepsilon}}\big)\Big), \quad x \in \Omega_x, \quad 0 \leq k \leq 4.$$

Proof. The proof follows directly from Theorem 4.1. □

4.4.2 Spatial Discretization

The spatial domain $\bar{\Omega} = [0, 1]$ is discretized using a uniform mesh of size h as $\bar{\Omega}^N = \left\{x_i = ih, \; i = 0(1)N, h = \frac{1}{N}\right\}$, where N is the number of spatial subintervals. The finite difference operators are defined as follows:

$$\text{Central difference:} \quad \delta_x^2 U_i^j = \frac{U_{i+1}^j - 2U_i^j + U_{i-1}^j}{h^2}, \quad D_x^0 U_i^j = \frac{U_{i+1}^j - U_{i-1}^j}{2h},$$

$$\text{Upwind differences:} \quad D_x^+ U_i^j = \frac{U_{i+1}^j - U_i^j}{h}, \quad D_x^- U_i^j = \frac{U_i^j - U_{i-1}^j}{h}.$$

Applying the central difference scheme to the first and second spatial derivatives in Eq. (4.8), and incorporating a fitting factor σ, we obtain the following discrete system:

$$\begin{cases} \hat{\mathcal{L}}_\varepsilon^N U_i^{j+1} = R_i^{j+1}, \\ U^{j+1}(0) = \phi_l(t_{j+1}), \quad U^{j+1}(1) = \phi_r(t_{j+1}), \quad 0 \le j \le M, \end{cases} \tag{4.13}$$

where

$$\begin{aligned} \hat{\mathcal{L}}_\varepsilon^N U_i^{j+1} &= \frac{\sigma\varepsilon}{2}\delta_x^2 U_i^{j+1} + \frac{a_i^{j+1}}{2} D_x^0 U_i^{j+1} - \frac{q_i^{j+1}}{2} U_i^{j+1}, \\ R_i^{j+1} &= F_i^{j+1/2} - \frac{\sigma\varepsilon}{2}\delta_x^2 U_i^j - \frac{a_i^j}{2} D_x^0 U_i^j + \frac{d_i^j}{2} U_i^j, \\ q_i^{j+1} &= b_i^{j+1} + \frac{2}{\Delta t}, \qquad d_i^j = b_i^j - \frac{2}{\Delta t}. \end{aligned}$$

The source function involving delay is defined as:

$$F_i^j = \begin{cases} f_i^j + c_i^j \phi_b(x_i, t_j - \tau), & j = 0, 1, \ldots, s, \\ f_i^j + c_i^j U_i^{j-s}, & j = s+1, s+2, \ldots, M-1. \end{cases}$$

4.4.3 Fitting Factor Derivation

Using asymptotic analysis from [89], the zeroth-order approximation of the solution to Eq. (4.8) at the time level $j+1$ is given by

$$U^{j+1}(x_i) = U_0^{j+1} + \left(U^{j+1}(0) - U_0^{j+1}\right)\exp\left(-\frac{a(x_i)}{\varepsilon}x_i\right), \tag{4.14}$$

where U_0^{j+1} denotes the solution of the reduced problem obtained by setting $\varepsilon = 0$. Introducing the parameter $\rho = \frac{h}{\varepsilon}$, we rewrite the solution at the mesh points $x_i = ih$ as

$$\lim_{h\to 0} U^{j+1}(ih) = U_0^{j+1} + \left(U^{j+1}(0) - U_0^{j+1}\right) e^{-a(x_i)i\rho}. \tag{4.15}$$

Since the essential features governing the layer structure are captured solely by the homogeneous component, we multiply the homogeneous part of equation (4.13) by h and take the limit as $h \to 0$, to obtain

$$\lim_{h\to 0}\left\{\frac{\sigma(\rho)}{\rho}\left(U_{i+1}^{j+1} - 2U_i^{j+1} + U_{i-1}^{j+1}\right) + a(x_i)\frac{U_{i+1}^{j+1} - U_{i-1}^{j+1}}{2}\right\} = 0. \tag{4.16}$$

Substituting the asymptotic form (4.15) into (4.16) and simplifying, the fitting factor $\sigma(\rho)$ is derived as

$$\sigma(\rho) = \frac{\rho a(x_i)}{2} \coth\left(\frac{\rho a(x_i)}{2}\right). \tag{4.17}$$

This expression for the fitting factor ensures that the finite difference operator accommodates the boundary layer behavior, thereby improving the parameter uniform convergence of the numerical scheme.

4.4.4 Full Discrete Scheme

Using the fitting factor Eq. (4.17) into Eq.(4.13) the full scheme is written as follows:

$$r_i^- U_{i-1}^{j+1} + r_i^c U_i^{j+1} + r_i^+ U_{i+1}^{j+1} = s_i^- U_{i-1}^j + s_i^c U_i^j + s_i^+ U_{i+1}^j + F_i^{j+1/2}, \tag{4.18}$$

where the coefficients are:

$$\begin{aligned} r_i^- &= \frac{\sigma\varepsilon}{2h^2} - \frac{a_i^{j+1}}{4h}, \quad r_i^c = -\left(\frac{\sigma\varepsilon}{h^2} + \frac{b_i^{j+1} + \frac{2}{\Delta t}}{4h}\right), \quad r_i^+ = \frac{\sigma\varepsilon}{2h^2} + \frac{a_i^{j+1}}{4h}, \\ s_i^- &= -\left(\frac{\sigma\varepsilon}{2h^2} - \frac{a_i^j}{4h}\right), \quad s_i^c = \frac{\sigma\varepsilon}{h^2} + \frac{d_i^j}{4h}, \quad s_i^+ = -\left(\frac{\sigma\varepsilon}{2h^2} + \frac{a_i^j}{4h}\right). \end{aligned}$$

The right-hand side function is:

$$F_i^{j+1/2} = \begin{cases} f_i^{j+1/2} + c_i^{j+1/2}\psi_b(x_i, t_{j+1/2} - \tau), & j = 0, 1, \ldots, s, \\ f_i^{j+1/2} + c_i^{j+1/2} U_i^{j+1/2-s}, & j = s+1, \ldots, M-1. \end{cases}$$

Since $|r_i^c| > |r_i^-| + |r_i^+|$, system (4.18) is strictly diagonally dominant and admits a unique solution. Thus, matrix inverse method can be employed to solve it.

4.5 Uniform Convergence Analysis

In this section, we study the discrete minimum principle, stability and parameter uniform convergence for the scheme (4.18).

Lemma 4.8 (**Discrete Minimum Principle**). *The operator defined by the discrete scheme in* (4.13) *satisfies* *the discrete minimum principle. Let U_i^{j+1} be any mesh function such that $U_0^{j+1} \geq 0$, $U_N^{j+1} \geq 0$, and $\hat{\mathcal{L}}_\epsilon^N U_i^{j+1} \leq 0$ for all $i = 1, 2, \ldots, N-1$. Then $U_i^{j+1} \geq 0$ for all $i = 0, 1, 2, \ldots, N$.*

Proof. Suppose there exists an index $s \in \{0, 1, \ldots, N\}$ such that $U_s^{j+1} = \min_{0 \leq i \leq N} U_i^{j+1} < 0$. Then it must be that $s \neq 0$ and $s \neq N$, as the boundary values are non-negative. Hence, $U_{s+1}^{j+1} - U_s^{j+1} > 0$ and $U_{s-1}^{j+1} - U_s^{j+1} > 0$. Substituting into the operator:

$$\begin{aligned}
\hat{\mathcal{L}}_\epsilon^N U_s^{j+1} &= \frac{\sigma\varepsilon}{2} \cdot \frac{U_{s+1}^{j+1} - 2U_s^{j+1} + U_{s-1}^{j+1}}{h^2} + \frac{a_s^{j+1}}{2} \cdot \frac{U_{s+1}^{j+1} - U_{s-1}^{j+1}}{2h} - \left(\frac{b_s^{j+1}}{2} + \frac{1}{\Delta t}\right) U_s^{j+1} \\
&= \left(\frac{\sigma\varepsilon}{h^2} + \frac{a_s^{j+1}}{2h}\right)(U_{s+1}^{j+1} - U_s^{j+1}) + \left(\frac{\sigma\varepsilon}{h^2} - \frac{a_s^{j+1}}{4h}\right)(U_{s-1}^{j+1} - U_s^{j+1}) - \left(\frac{b_s^{j+1}}{2} + \frac{1}{\Delta t}\right) U_s^{j+1}.
\end{aligned}$$

Since $U_{s+1}^{j+1} - U_s^{j+1} > 0$, $U_{s-1}^{j+1} - U_s^{j+1} > 0$, and $U_s^{j+1} < 0$, all three terms above are positive if the coefficients are positive.

Note that $\left(\frac{b_s^{j+1}}{2} + \frac{1}{\Delta t}\right) > \beta > 0$, $\frac{\sigma\varepsilon}{h^2} - \frac{a_s^{j+1}}{4h} = \frac{a_s^{j+1}}{h}\left(\frac{1}{4} + \frac{1}{e^{\rho a_s^{j+1}} - 1}\right) > 0$. Thus, $\hat{\mathcal{L}}_\epsilon^N U_s^{j+1} > 0$, which is a contradiction. Therefore, $U_i^{j+1} \geq 0$, for all $i = 0, 1, 2, \ldots, N$

□

Lemma 4.9 (Stability Estimate). *The solution U_i^{j+1} of the discrete problem (4.18) satisfies the bound*

$$\left|U_i^{j+1}\right| \leq \frac{T}{\beta}\left|\left|\hat{\mathcal{L}}_\epsilon^N U_i^{j+1}\right|\right| + \max\left(|\phi_l(t_{j+1})|, |\phi_r(t_{j+1})|, |\psi_b(x_i, t_{j+1})|\right).$$

Proof. Consider the barrier functions

$$\daleth_{i,j+1}^{\pm} = \frac{T}{\beta}\left|\left|\hat{\mathcal{L}}_\epsilon^N U_i^{j+1}\right|\right| + \max\left(|\phi_l(t_{j+1})|, |\phi_r(t_{j+1})|, |\psi_b(x_i, t_{j+1})|\right) \pm U_i^{j+1}.$$

At the boundary points:

$$\begin{aligned}
\daleth_{j+1}^{\pm}(0) &= \frac{T}{\beta}\left|\left|\hat{\mathcal{L}}_\epsilon^N U_0^{j+1}\right|\right| + \max\left(|\phi_l(t_{j+1})|, |\phi_r(t_{j+1})|, |\psi_b(x_0, t_{j+1})|\right) \pm \phi_l(t_{j+1}) \geq 0, \\
\daleth_{j+1}^{\pm}(1) &= \frac{T}{\beta}\left|\left|\hat{\mathcal{L}}_\epsilon^N U_N^{j+1}\right|\right| + \max\left(|\phi_l(t_{j+1})|, |\phi_r(t_{j+1})|, |\psi_b(x_N, t_{j+1})|\right) \pm \phi_r(t_{j+1}) \geq 0.
\end{aligned}$$

For interior points:

$$
\begin{aligned}
\hat{\mathcal{L}}_{\epsilon}^{N}\beth_{i,j+1}^{\pm} &= \frac{\varepsilon}{2}\delta_x^2\beth_{i,j+1}^{\pm} + \frac{a_i^{j+1}}{2}D_x^{+}\beth_{i,j+1}^{\pm} - \left(\frac{b_i^{j+1}}{2} + \frac{1}{\Delta t}\right)\beth_{i,j+1}^{\pm} \\
&= -\left(\frac{b_i^{j+1}}{2} + \frac{1}{\Delta t}\right)\left(\frac{T}{\beta}\left|\left|\hat{\mathcal{L}}_{\epsilon}^{N}U_i^{j+1}\right|\right| + \max\left(|\phi_l(t_{j+1})|, |\phi_r(t_{j+1})|, |\psi_b(x_i, t_{j+1})|\right)\right) \pm \hat{\mathcal{L}}_{\varepsilon}^{N}U_i^{j+1} \\
&\leq \pm\hat{\mathcal{L}}_{\epsilon}^{N}U_i^{j+1} - \beta\left(\frac{T}{\beta}\left|\left|\hat{\mathcal{L}}_{\epsilon}^{N}U_i^{j+1}\right|\right| + \max\left(|\phi_l(t_{j+1})|, |\phi_r(t_{j+1})|, |\psi_b(x_i, t_{j+1})|\right)\right), \text{ since}(b_i^{j+1} + \frac{1}{\Delta t}) > \beta \\
&= \pm\hat{\mathcal{L}}_{\epsilon}^{N}U_i^{j+1} - \left(T\left|\left|\hat{\mathcal{L}}_{\epsilon}^{N}U_i^{j+1}\right|\right| + \max\left(|\phi_l(t_{j+1})|, |\phi_r(t_{j+1})|, |\psi_b(x_i, t_{j+1})|\right)\right) \leq 0.
\end{aligned}
$$

By Lemma 4.8, $\beth_{i,j+1}^{\pm} \geq 0$, which implies

$$
\left|U_i^{j+1}\right| \leq \frac{T}{\beta}\left|\left|\hat{\mathcal{L}}_{\epsilon}^{N}U_i^{j+1}\right|\right| + \max\left(|\phi_l(t_{j+1})|, |\phi_r(t_{j+1})|, |\psi_b(x_i, t_{j+1})|\right).
$$

□

Lemma 4.10. *For a fixed mesh,*

$$
|\varepsilon(1-\sigma)| \leq Ch \quad \text{and} \quad \lim_{\varepsilon\to 0}\frac{\exp\left(-x_i\sqrt{\beta/\varepsilon}\right)}{(\sqrt{\varepsilon})^{s}} = 0, \quad s \in \mathbb{Z}^{+}.
$$

Proof. We have

$$
\sigma = \frac{\rho a}{2}\coth\left(\frac{\rho a}{2}\right) = \frac{\rho a}{2}\left(1 + \frac{2}{e^{\rho a} - 1}\right) = \frac{\rho a}{2}\left(1 + \frac{2}{1 + \rho a + \frac{(\rho a)^2}{2!} + \cdots - 1}\right).
$$

Using the series expansion and neglecting higher-order terms, we obtain

$$
\sigma \approx 1 + \frac{\rho a}{2}.
$$

Therefore,

$$
|\varepsilon(1-\sigma)| = \left|\varepsilon \cdot \frac{\rho a}{2}\right| = \frac{ha}{2} \leq Ch.
$$

The first part of the lemma follows from the above, and the second part can be proved using Lemma 2.9. □

Theorem 4.4. *Let $U^{j+1}(x_i)$ and U_i^{j+1} are the solutions of* (4.8) *and* (4.18) *respectively. Then the error* *bounds at $(j+1)^{th}$ time level is given by;*

$$\sup_{0<\varepsilon\leq 1}\left|\left|U^{j+1}(x_i)-U_i^{j+1}\right|\right|\leq CN^{-1},\ \ i=0,1,2...,N.$$

Proof. The truncation error in the spatial discretization is given by

$$\begin{aligned}\left\|\hat{\mathcal{L}}_\epsilon^N\left(U^{j+1}(x_i)-U_i^{j+1}\right)\right\| &= \left\|\hat{\mathcal{L}}_\epsilon U^{j+1}(x_i)-\hat{\mathcal{K}}_\epsilon^N U_i^{j+1}\right\| \\ &\leq \left\|\frac{\varepsilon}{2}\left(\frac{d^2}{dx^2}-\sigma\delta_x^2\right)U_i^{j+1}+\frac{a_i^{j+1}}{2}\left(\frac{d}{dx}-D_x^0\right)U_i^{j+1}\right\|,\end{aligned}$$

where

$$\delta_x^2 U_i^{j+1}=\frac{U_{i+1}^{j+1}-2U_i^{j+1}+U_{i-1}^{j+1}}{h^2},\quad D_x^0 U_i^{j+1}=\frac{U_{i+1}^{j+1}-U_{i-1}^{j+1}}{2h}.$$

Using Taylor expansion and Theorem 4.3, we obtain

$$\begin{aligned}\left\|\hat{\mathcal{L}}_\epsilon U^{j+1}(x_i)-\hat{\mathcal{L}}_\epsilon^N U_i^{j+1}\right\| &\leq \left\|\frac{\varepsilon}{2}(1-\sigma)\frac{d^2U^{j+1}(x_i)}{dx^2}-a^{j+1}(x_i)\frac{h^2}{12}\frac{d^3U^{j+1}(x_i)}{dx^3}\right. \\ &\quad \left. -a^{j+1}(x_i)\frac{\sigma\varepsilon h^2}{24}\frac{d^4U^{j+1}(x_i)}{dx^4}\right\| \\ &\leq C\left(h+\frac{e^{-x_i\sqrt{\beta/\varepsilon}}}{\varepsilon}h+\frac{e^{-x_i\sqrt{\beta/\varepsilon}}}{\varepsilon^{3/2}}h^2\right) \\ &\leq Ch\left(1+\frac{e^{-x_i\sqrt{\beta/\varepsilon}}}{\varepsilon}+h\cdot\frac{e^{-x_i\sqrt{\beta/\varepsilon}}}{\varepsilon^{3/2}}\right).\end{aligned}$$

Finally, applying Lemmas 4.9 and 4.10, we conclude that

$$\sup_{0<\varepsilon\leq 1}\left\|U^{j+1}(x_i)-U_i^{j+1}\right\|\leq CN^{-1}.$$

□

Theorem 4.5. *The solution U_i^{j+1} of the fully discrete scheme (4.18) converges uniformly to the solution $u(x_i,t_{j+1})$ of (4.1) and the error estimate is given by*

$$\sup_{0<\varepsilon\leq 1}\left|u(x_i,t_{j+1})-U_i^{j+1}\right|\leq C(N^{-1}+(\Delta t)^2), i=0,1,2,...,N,\ \ j=0,1,2,...,M-1.$$

Proof: The uniform convergence of the scheme follows from the Theorem 4.2 and 4.4. We justify the error estimate as follows.

$$\sup_{0<\varepsilon\le 1}\left|u(x_i,t_{j+1})-U_i^{j+1}\right| \le \sup_{0<\varepsilon\le 1}\left|u(x_i,t_{j+1})-U^{j+1}(x_i)\right| + \sup_{0<\varepsilon\le 1}\left|U^{j+1}(x_i)-U_i^{j+1}\right| \le C((\Delta t)^2+N^{-1}), i=0,1,2,...,N,\ \ j=0,1,2,...,M-1$$

4.6 Numerical Results and Discussion

Two model examples are used to test the accuracy of the proposed scheme for various mesh sizes and perturbation parameter values ε. The maximum absolute error $e_\varepsilon^{M,N}$ and the rate of convergence $R_\varepsilon^{M,N}$ are computed using the double mesh principle, as described in Section 2.6 of Chapter 2.

Example 4.1. *Consider the time delay singularly perturbed boundary turning point problem in [100]*

$$\varepsilon u_{xx}(x,t)+x^p u_x(x,t)-u(x,t)-u_t(x,t)=x^2-1+u(x,t-1)/2,\ \ (x,t)\in\mathcal{D}.$$
$$u(0,t)=1+t^2,\ \ u(1,t)=0,\ \ 0\le t\le 2.$$
$$u(x,t)=(1-x)^2,\ \ on\ \ [0,1]\times[-1,0]$$

Table 4.1: Maximum absolute error and rate of convergence for Example 4.1 for $p=1$

$\varepsilon\downarrow M=N\rightarrow$	32	64	128	256	512	1024
10^{-1}	9.5224e-04	5.0474e-04	2.7431e-04	1.3963e-04	7.0855e-05	3.5932e-05
	0.9158	0.8797	0.9742	0.9786	0.9796	
10^{-3}	2.1214e-03	5.8854e-04	3.0749e-04	2.0497e-04	1.0697e-04	5.5905e-05
	1.8498	0.9366	0.5851	0.9383	0.9383	
10^{-5}	4.0290e-03	2.0649e-03	1.0440e-03	5.2478e-04	2.6309e-04	1.3190e-04
	0.9644	0.9839	0.9923	0.9961	0.9961	
$\vdots$	$\vdots$	$\vdots$	$\vdots$	$\vdots$	$\vdots$	$\vdots$
10^{-9}	4.0290e-03	2.0649e-03	1.0440e-03	5.2478e-04	2.6309e-04	1.3190e-04
	0.9644	0.9839	0.9923	0.9961	0.9961	
PM: $e^{M,N}$	4.0290e-03	2.0649e-03	1.0440e-03	5.2478e-04	2.6309e-04	1.3190e-04
	0.9644	0.9839	0.9923	0.9961	0.9961	
In [100]: $e^{M,N}$	4.308e-03	2.099e-03	1.055e-03	5.304e-04	2.741e-04	1.4138e-04
	1.0373	0.9922	0.9923	0.9521	0.9521	

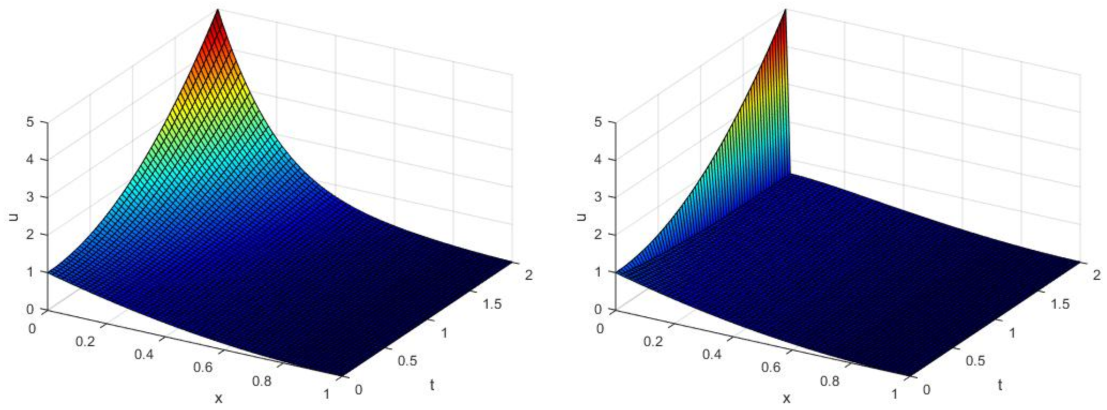

(a) $\varepsilon = 10^{-1}$ (b) $\varepsilon = 10^{-7}$

Figure 4.1: Surface plots of the numerical solution for Example 4.1 for different values of ε with $M = N = 64$ and $p = 1$.

Example 4.2. *Consider the time delay singularly perturbed boundary turning point problem in [100]*

$$\varepsilon u_{xx}(x,t) + x^p(1+te^{-2t})u_x(x,t) - (e^x+1)u(x,t) - u_t(x,t) = p(x^2-1)e^{-t} - tu(x,t-1), \;\; (x,t) \in \mathcal{D},$$

$$u(0,t) = 1+t^2, \;\; u(1,t) = 0, \;\; 0 \le t \le 2.$$

$$u(x,t) = (1-x)^2, \;\; on[0,1] \times [-1,0]$$

Table 4.2: Maximum absolute error and rate of convergence for Example 4.2 for $p = 1$

$\varepsilon \downarrow M = N \rightarrow$	32	64	128	256	512	1024
10^{-1}	2.7819e-03	1.3915e-03	7.4634e-04	3.7620e-04	1.8987e-04	9.5902e-05
	0.9995	0.8987	0.9883	0.9865	0.9865	
10^{-2}	1.4187e-03	5.6769e-04	6.4292e-04	4.2132e-04	2.1890e-04	1.1358e-04
	1.3214	0.7950	0.6097	0.9446	0.9446	
$\vdots$	$\vdots$	$\vdots$	$\vdots$	$\vdots$	$\vdots$	$\vdots$
10^{-6}	4.3654e-03	2.3158e-03	1.1948e-03	6.0704e-04	3.0597e-04	1.5422e-04
	0.9146	0.9547	0.9769	0.9884	0.9884	
10^{-7}	4.3654e-03	2.3158e-03	1.1948e-03	6.0704e-04	3.0597e-04	1.5422e-04
	0.9146	0.9547	0.9769	0.9884	0.9884	
PM: $e^{M,N}$	4.3654e-03	2.3158e-03	1.1948e-03	6.0704e-04	3.0597e-04	1.5422e-04
	0.9146	0.9547	0.9769	0.9884	0.9884	
In [100]: $e^{M,N}$	1.965e-02	5.588e-03	1.950e-03	9.246e-04	4.475e-04	2.1673e-04
	1.814	1.519	1.077	1.047	0.9998	

We computed $e^{M,N}$, $e_\varepsilon^{M,N}$ and $R^{M,N}$ using the scheme (4.18) for each model examples. The computed results are displayed using Tables and Figures. The maximum absolute errors and their corresponding rate

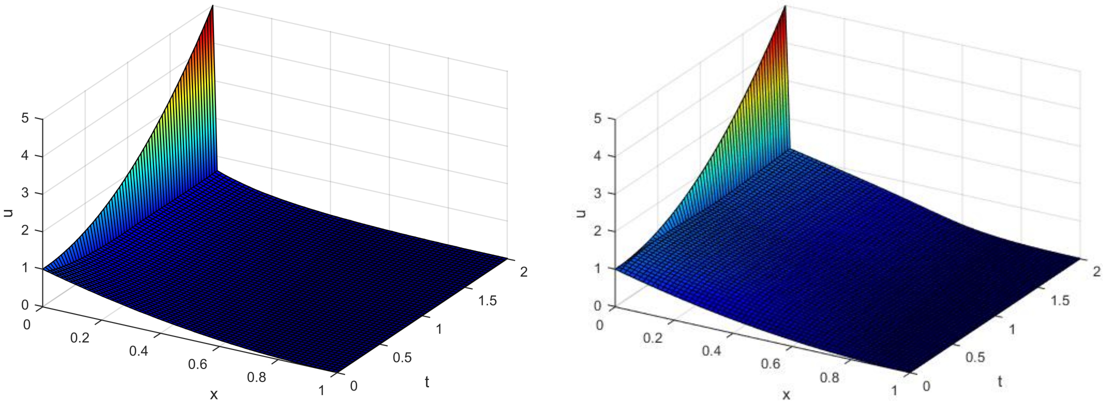

(a) $\varepsilon = 10^{-7}$, $p = 1$

(b) $\varepsilon = 10^{-7}$, $p = 3$

Figure 4.2: Surface plots of the numerical solution for Example 4.2 for different values of p with $M = N = 64$.

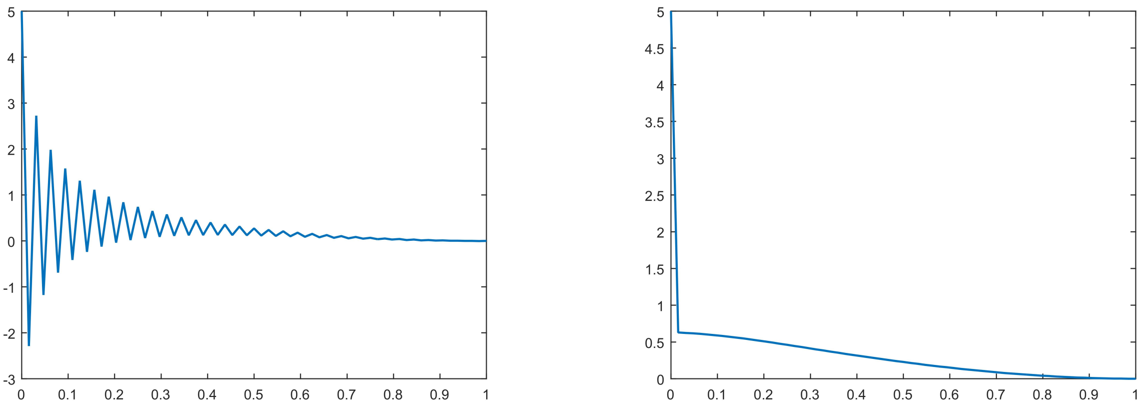

(a) Without fitting factor

(b) With fitting factor

Figure 4.3: Solution profiles for Example 4.1 with and without the fitting factor at $\varepsilon = 2^{-20}$ and $p = 1$.

Table 4.3: $e^{N,M}$ and $r^{N,M}$ for different values of p

$p \downarrow M = N \rightarrow$	32	64	128	256	512	1024
Example 4.1						
2	5.3868e-03	2.7967e-03	1.4250e-03	7.1895e-04	3.6096e-04	1.8121e-04
	0.9457	0.9728	0.9870	0.9941	0.9942	
3	6.3907e-03	3.3561e-03	1.7177e-03	8.6936e-04	4.3728e-04	2.1994e-04
	0.9292	0.9663	0.9824	0.9914	0.9914	
Example 4.2						
2	4.6914e-03	2.5700e-03	1.3734e-03	7.2080e-04	3.7347e-04	1.9350e-04
	0.8683	0.9040	0.9301	0.9486	0.9486	
3	6.6008e-03	3.6580e-03	1.9741e-03	1.0403e-03	5.4047e-04	2.8080e-04
	0.8516	0.8898	0.9242	0.9447	0.9447	

of convergences of the proposed method for Examples 4.1 and 4.2 at $p = 1$ are displayed in Tables 4.1 and 4.2 respectively. From each Table, it can be observed that for fixed mesh as the singular perturbation parameter ε decreases to zero, the maximum absolute error is constant, and as the mesh parameter increases the maximum absolute error decreases. This indicates that the proposed method is $\varepsilon-$ uniform convergence. Moreover, parameter uniform error and its corresponding rate of convergence for Examples 4.1 and 4.2 using different values of p are displayed in Table 4.3 for $M = N$. From the results in this Table, it can be shown that the error bound is also independent of p, and its order of convergence is first order.

Surface plots for the Examples 4.1 and 4.2 are shown in Figures 4.1 and 4.2 for different values of ε and p respectively. In Figure 4.1, as the singular perturbation parameter ε decreases toward zero, the surface plot exhibits a steep change near the left boundary of the domain. In Figure 4.2, the layer appears at the same location as in Figure 4.1; however, as p increases, the peak (hump) becomes higher and shifts away from the boundary layer region. This indicates that the dominant balance between the convection and diffusion terms changes slightly, pushing the layer region toward the interior of the domain. In Figure 4.3, a comparison of the computed solution with and without the exponential fitting factor for Example 4.1 is presented. In Figure 4.3a, it is evident that the computed solution oscillates when the scheme without the exponential fitting factor is employed.

Overall, the figures demonstrate that the solution exhibits a left boundary layer in the spatial domain, and as $\varepsilon \rightarrow 0$, the boundary layer becomes thinner. A comparison with the method in [100] is given in Tables 4.1 and 4.2. The proposed method achieves comparable accuracy and order of convergence, while showing improved performance as the mesh sizes N and M increase.

4.7 Conclusion

In this Chapter, time delay SPPDEs with boundary turning points are considered. The solution of this problem exhibits a left boundary layer on the spatial domain as perturbation parameter approaches zero. The developed scheme is based on Crank-Nicolson finite difference for temporal discretization and exponentially fitted operator finite difference method for spatial discretization on uniform meshes. The solution behaviour on the perturbation parameter is displayed using Figures and Tables. These results proved that the proposed scheme is stable and parameter uniform convergence with second-order accuracy in time and first-order accuracy in space. The error bound is also independent of p. The numerical solution of the considered model examples agreed with the theoretical findings.

Chapter 5

Hybrid Numerical Scheme for Singularly Perturbed Delay Parabolic Convection-Diffusion Problems with Boundary Turning Point

In this chapter, we reconsidered the problem stated in chapter 4 having boundary turning point and time lag. The solution of the problem exhibits a left boundary layer. The developed scheme is a higher order convergence layer-resolving numerical scheme. The discretization of the problem is based on Crank-Nicolson method for temporal direction on a uniform mesh and the hybrid finite difference scheme, which is a combination of the central finite difference method and midpoint upwind scheme on Shishkin mesh for the spatial variable. The stability and parameter-uniform convergence analysis of the scheme is investigated well. Numerical examples are presented to validate the theoretical findings of the scheme.

5.1 Introduction

The midpoint upwind scheme, first introduced in [2], was rigorously analyzed on an equidistant grid. Their analysis demonstrated that this scheme achieves second-order convergence outside the boundary layer regions. Due to its superior accuracy compared to classical first-order upwinding methods [120], the midpoint upwind scheme has been widely adopted, often in combination with central difference schemes, for solving singularly perturbed boundary value problems (SPBVPs) in order to achieve higher accuracy and improved convergence rates.

In this work, we developed a uniformly convergent hybrid numerical scheme for solving the considered singularly perturbed parabolic delay differential equations (SPPDDEs) with boundary turning point. The proposed method employs the Crank–Nicolson method for temporal discretization on a uniform mesh, and a hybrid finite difference scheme in the spatial direction. The spatial discretization combines the central finite difference method within the layer region and the midpoint upwind scheme outside the layer region, implemented on a piecewise Shishkin mesh. This approach yields improved accuracy and robustness, particularly in resolving sharp gradients near the boundary turning points.

5.2 Description of the Problem

Consider the governing problem discussed in Chapter 4.

5.3 Bounds on the Solution and its Derivatives

To avoid redundancy, the analytical properties of the continuous solution established in Chapter 4 remain valid. The corresponding results are omitted here and will be invoked as needed in the subsequent analysis.

5.4 Derivation of the Numerical Method

5.4.1 Temporal Discretization

The temporal discretization is carried out similarly to the procedure presented in Chapter 4. Applying the chosen time discretization technique to problem (4.8) yields a sequence of semi-discrete boundary value problems at each time level. To facilitate the analysis of the numerical method and the construction of parameter-uniform schemes, the solution of the resulting semi-discrete problem is decomposed into regular and singular (layer) components. Thus, the solution $u^{j+1}(x)$ of problem (4.8) can be expressed as

$$u^{j+1}(x) = v^{j+1}(x) + w^{j+1}(x),$$

where $v^{j+1}(x)$ denotes the regular component and $w^{j+1}(x)$ represents the singular (boundary layer) component. Such a decomposition is useful for analyzing the layer behavior of the solution and establishing parameter-uniform error estimates.

The solution and its components satisfy certain bounds, which play an important role in the subsequent stability and convergence analysis. These bounds are stated in the following theorem (see [20]).

Theorem 5.1. *The solution $u^{j+1}(x)$ and its derivatives satisfy the bound*

$$\left|\frac{d^k u^{j+1}(x)}{dx^k}\right| \le C\Big(1 + \varepsilon^{-k/2} \exp\big(-x\sqrt{\tfrac{\alpha}{\varepsilon}}\big)\Big), \quad x \in \Omega_x, \quad 0 \le k \le 4.$$

Moreover, the regular and singular components satisfy

$$\left|\frac{d^k v^{j+1}(x)}{dx^k}\right| \le C\left(1 + \varepsilon^{3-k/2}\right), \quad x \in \Omega_x, \quad 0 \le k \le 4,$$

and

$$\left|\frac{d^k w^{j+1}(x)}{dx^k}\right| \le C\varepsilon^{-k/2} \exp\big(-x\sqrt{\tfrac{\alpha}{\varepsilon}}\big), \quad x \in \Omega_x, \quad 0 \le k \le 4.$$

Proof. The proof proceeds in the same manner as that of Theorem 3.1 in Chapter 3. □

5.4.2 Spatial Discretization.

In this section, we describe the construction of the piecewise-uniform Shishkin mesh for discretizing the spatial domain, and analyze the behavior of the difference scheme applied to semi-discrete problem (4.8). Due to the presence of a boundary layer and turning point near $x = 0$ in problem (4.1), the mesh must be refined in the neighborhood of $x = 0$. To construct the piecewise-uniform mesh, we divide the domain $[0, 1]$ into two subintervals:

$$[0, 1] = [0, \omega] \cup (\omega, 1],$$

where $\omega \in (0, 1)$ is a suitably chosen mesh transition parameter, typically depending on the perturbation parameter ε and the number of mesh intervals N. Each subinterval is partitioned uniformly into $N/2$ mesh intervals.

The mesh points are given by $\overline{\Omega}^N = \{0 = x_0, x_1, \ldots, x_{N/2} = \omega, x_{N/2+1}, \ldots, x_N = 1\}$, where

$$x_i = \begin{cases} i\dfrac{2\omega}{N}, & \text{for } i = 0, 1, \ldots, \dfrac{N}{2}, \\ \omega + \left(i - \dfrac{N}{2}\right)\dfrac{2(1-\omega)}{N}, & \text{for } i = \dfrac{N}{2} + 1, \ldots, N, \end{cases}$$

and $N \geq 4$ is a positive even integer. The transition point ω, is defined in(3.1) in Chapter 3. Based on the definition of x_i, the spatial step sizes for $i = 0, 1, 2, \ldots, N$ are given by:

$$h_i = x_{i+1} - x_i = \begin{cases} h = \dfrac{2\omega}{N}, & \text{for } i = 0, 1, \ldots, \dfrac{N}{2} - 1, \\ H = \dfrac{2(1-\omega)}{N}, & \text{for } i = \dfrac{N}{2}, \ldots, N - 1, \end{cases}$$

where h and H denote the mesh widths in the intervals $[0, \omega]$ and $(\omega, 1]$, respectively. From these expressions, it follows that

$$N^{-1} \leq H \leq 2N^{-1}, \qquad h = \frac{2\sqrt{\varepsilon}}{\sqrt{\alpha}} \ln N.$$

A uniform mesh can be obtained by choosing $\omega = \dfrac{1}{2}$. In analysing the error, we use $\sqrt{\varepsilon} \leq CN^{-1}$ and $\omega = \frac{2\sqrt{\varepsilon}}{\sqrt{\alpha}} \ln N$, otherwise one can proceed with classical way.

We propose a numerical scheme to solve (4.1), which consists of Crank-Nicolson for time derivative, and hybrid scheme for spatial derivatives. The hybrid scheme is a combination of central difference scheme in the inner region $[0, \omega]$ and the midpoint upwind scheme in the outer region $(\omega, 1]$. The proposed scheme is:

$$\frac{1}{2}\left(\hat{\mathcal{L}}^N_{\epsilon,\text{hy}} U_i^{j+1} + \hat{\mathcal{L}}^N_{\epsilon,\text{hy}} U_i^{j}\right) = \begin{cases} \frac{1}{2}\left(c_i^{j+1} U_i^{j+1-s} + c_i^j U_i^{j+1-s} + f_i^{j+1} + f_i^j\right), & 1 \leq i \leq N/2, \\ \frac{1}{2}\left(c_{i+\frac{1}{2}}^{j+1} U_{i+\frac{1}{2}}^{j+1-s} + c_{i+\frac{1}{2}}^{j} U_{i+\frac{1}{2}}^{j-s} + f_{i+\frac{1}{2}}^{j+1} + f_{i+\frac{1}{2}}^{j}\right), & N/2 < i \leq N - 1, \end{cases} \tag{5.1}$$

$$\begin{aligned} &U_0^{j+1} = \psi_l(t_{j+1}), U_N^{j+1} = \psi_r(t_{j+1}), j \in \{0, 1, 2, ..., M-1\}, \\ &U_i^{-j} = \psi_b(x_i, -t_j), j = 0, 1, 2, ..., s, i \in \{1, 2, ..., N-1\}, \end{aligned}$$

where

$$\hat{\mathcal{L}}^N_{\epsilon,\text{hy}} U_i^{j+1} = \begin{cases} \hat{\mathcal{L}}^N_{\epsilon,\text{cen}} U_i^{j+1} = \varepsilon D_x^+ D_x^- U_i^{j+1} + a_i^{j+1} D_x^0 U_i^{j+1} - q_i^{j+1} U_i^{j+1}, & \text{for } 1 \leq i \leq N/2, \\ \hat{\mathcal{L}}^N_{\epsilon,\text{mu}} U_i^{j+1} = \varepsilon D_x^+ D_x^- U_i^{j+1} + a_{i+\frac{1}{2}}^{j+1} D_x^- U_i^{j+1} - q_{i+\frac{1}{2}}^{j+1} U_{i+\frac{1}{2}}^{j+1}, & \text{for } N/2 < i \leq N - 1, \end{cases}$$

where $\hat{\mathcal{L}}^N_{\epsilon,\text{up}}$ is the midpoint upwind scheme and $\hat{\mathcal{L}}^N_{\epsilon,\text{cen}}$ is the central difference scheme.

The difference operators are defined by;

$$\begin{cases} D_x^+D_x^-U_i^{j+1} = \dfrac{2(D^+ - D^-)}{\hat{h}}U_i^{j+1}, \\ D_x^0U_i^{j+1} = \dfrac{U_{i+1}^{j+1} - U_{i-1}^{j+1}}{\hat{h}}, \end{cases} \text{and} \quad \begin{cases} D_x^+U_i^{j+1} = \dfrac{U_{i+1}^{j+1} - U_i^{j+1}}{h_{i+1}}, \\ D_x^-U_i^{j+1} = \dfrac{U_i^{j+1} - U_{i-1}^{j+1}}{h_i}, \quad \hat{h}_i = h_i + h_{i+1}. \end{cases}$$

In the above equations, the mid-point values are given by $a_{i+\frac{1}{2}}^{j+1} = \frac{a_{i+1}^{j+1}+a_i^{j+1}}{2}$, $q_{i+\frac{1}{2}}^{j+1} = \frac{q_{i+1}^{j+1}+q_i^{j+1}}{2}$, $c_{i+\frac{1}{2}}^{j+1} = \frac{c_{i+1}^{j+1}+c_i^{j+1}}{2}$, $f_{i+\frac{1}{2}}^{j+1} = \frac{f_{i+1}^{j+1}+f_i^{j+1}}{2}$, and $U_{i+\frac{1}{2}}^{j+1} = \frac{U_{i+1}^{j+1}+U_i^{j+1}}{2}$.

5.4.3 Full Discrete Scheme

After rearranging the terms in (5.1), we obtained the following discrete scheme.

$$\begin{cases} y_i^-U_{i-1}^{j+1} + y_i^cU_i^{j+1} + y_i^+U_{i+1}^{j+1} = H_i^j, & i \in \{1,2,...,N-1\}, \quad j \in \{0,1,2,...,M-1\}, \\ U_0^{j+1} = \psi_l(t_{j+1}), U_N^{j+1} = \psi_r(t_{j+1}), & j \in \{0,1,2,...,M-1\}, \\ U_i^{-j} = \psi_b(x_i, -t_j), & j = 0,1,2,...,s, i \in \{1,2,...,N-1\}, \end{cases} \tag{5.2}$$

where the coefficients are given by;

$$\begin{cases} y_i^- = \dfrac{2\varepsilon}{\hat{h}_ih_i} - \dfrac{a_i^{j+1}}{\hat{h}_i}, \\ y_i^c = -\dfrac{2\varepsilon}{h_ih_{i+1}} - (b_i^{j+1} + \frac{2}{\Delta t}), \\ y_i^+ = \dfrac{2\varepsilon}{\hat{h}_ih_{i+1}} + \dfrac{a_i^{j+1}}{\hat{h}_i}, \quad i = 1,2,...,\frac{N}{2}, \end{cases} \quad \begin{cases} y_i^- = \dfrac{2\varepsilon}{\hat{h}h_i}, \\ y_i^c = -\dfrac{2\varepsilon}{h_ih_{i+1}} - \dfrac{a_{i+\frac{1}{2}}^{j+1}}{h_{i+1}} - \frac{1}{2}\left(b_{i+\frac{1}{2}}^{j+1} + \dfrac{1}{\Delta t}\right), \\ y_i^+ = \dfrac{2\varepsilon}{\hat{h}h_{i+1}} + \dfrac{a_{i+\frac{1}{2}}^{j+1}}{h_{i+1}} - \frac{1}{2}\left(b_{i+\frac{1}{2}}^{j+1} + \dfrac{1}{\Delta t}\right), \quad i = \frac{N}{2}+1,...,N-1, \end{cases} \tag{5.3}$$

and

$$H_i^j = \begin{cases} \left(c_i^{j+1}U_i^{j+1-s} + c_i^jU_i^{j+1-s} + f_i^{j+1} + f_i^j\right) - \varepsilon D_x^+D_x^-U_i^j + a_i^jD_x^0U_i^j - d_i^jU_i^j, & 1 \le i \le N/2, \\ \left(c_{i+\frac{1}{2}}^{j+1}U_{i+\frac{1}{2}}^{j+1-s} + c_{i+\frac{1}{2}}^jU_{i+\frac{1}{2}}^{j-s} + f_{i+\frac{1}{2}}^{j+1} + f_{i+\frac{1}{2}}^j\right) - \varepsilon D_x^+D_x^-U_i^j + a_{i+\frac{1}{2}}^jD_x^-U_i^j - q_{i+\frac{1}{2}}^jU_{i+\frac{1}{2}}^j, & N/2 < i \le N-1, \end{cases}$$

The coefficient matrix in Eq.(5.2) gives $(N-1)\times(N-1)$ tri-diagonal system of equations with unknowns $U_1, U_2, ..., U_{N-1}$. The system is strictly diagonally dominant and hence invertible. Thus, the solution can be obtained using the matrix inverse method.

5.5 Uniform Convergence Analysis

Lemma 5.1. *For $N \geq N_0 \geq 8$, there exists $\alpha > 0$ such that*

$$(\|b\|_\infty + (\Delta t)^{-1}) \leq \alpha N_0, \quad \textit{and} \quad \frac{N_0}{(\ln N_0)^2} \geq 4\omega_0^2 \|a\|_\infty.$$

Then, we have

$$y_i^- > 0, \quad y_i^+ > 0, \quad \textit{for } 1 \leq i \leq N-1,$$

$$|y_i^-| + |y_i^+| < |y_i^c|, \quad \textit{for } 1 < i < N-1,$$

$$|y_1^+| < |y_1^c|, \quad \textit{and} \quad |y_{N-1}^-| < |y_{N-1}^c|.$$

Proof. From Equations (5.3), it is clear that

$$y_i^- > 0, \quad \text{for } \frac{N}{2} \leq i < N-1,$$

$$y_i^+ > 0, \quad \text{for } 1 \leq i \leq \frac{N}{2}.$$

Now, we have to prove

$$y_i^- > 0, \quad \text{for } 1 \leq i \leq \frac{N}{2}, \quad \text{and} \quad y_i^+ > 0, \quad \text{for } \frac{N}{2} < i < N-1.$$

From Equation (5.3), one can write

$$\begin{aligned} r_i^- &= \left(\frac{2\varepsilon}{\hat{h}_i h_i} - \frac{a_i^{j+1}}{\hat{h}_i} \right) \geq \left(\frac{2\varepsilon}{\hat{h}_i h_i} - \frac{\|a\|_\infty}{\hat{h}_i} \right) = \frac{1}{\hat{h}_i} \left(\frac{2\varepsilon}{h_i} - \|a\|_\infty \right) \\ &\geq \frac{N}{4\omega_0^2} \left(\frac{N}{\ln^2 N} - \|a\|_\infty 4\omega_0^2 \right). \end{aligned}$$

Since for $N \geq N_0 \geq 8$,

$$\frac{N}{\ln^2 N} - \frac{N_0}{\ln^2 N_0} \geq 0,$$

it follows that $y_i^- > 0 \quad$ for $1 \leq i \leq \frac{N}{2}, \quad$ when $\frac{N_0}{\ln^2 N_0} \geq 4\omega_0^2 \|a\|_\infty$.

Here, we consider the domain $(\omega, 1]$, and using $H \le 2N^{-1}$ in Equation ((5.3), we have

$$y_i^+ = \frac{2\varepsilon}{\hat{h}h_{i+1}} + \frac{a_{i+\frac{1}{2}}^{j+1}}{h_{i+1}} - \frac{1}{2}\left(b_{i+\frac{1}{2}}^{j+1} + \frac{1}{\Delta t}\right) > \frac{\alpha}{H} - \frac{1}{2}\left(\|b\|_\infty + \frac{1}{\Delta t}\right) \ge \frac{1}{2}\left(\alpha N - (\|b\|_\infty + (\Delta t)^{-1})\right), \quad \text{for } \frac{N}{2} \le i < N- \tag{46}$$

Therefore, for $N \ge N_0$, we have

$$y_i^+ > 0, \quad \text{for } \frac{N}{2} < i < N-1, \quad \text{when } \alpha N_0 \ge \|b\|_\infty + (\Delta t)^{-1}.$$

From Equations (5.3), one can easily show that

$$|y_1^+| < |y_1^c| \quad \text{and} \quad |y_{N-1}^-| < |y_{N-1}^c|.$$

Now, for $1 < i \le \frac{N}{2}$, we have

$$\begin{aligned} |r_i^-| + |r_i^+| &= \left|\frac{2\varepsilon}{h_i\hat{h}_i} - \frac{a_i^{j+1}}{\hat{h}_i}\right| + \left|\frac{2\varepsilon}{h_{i+1}\hat{h}_i} + \frac{a_i^{j+1}}{\hat{h}_i}\right| \\ &= \frac{2\varepsilon}{h_i\hat{h}_i} - \frac{a_i^{j+1}}{\hat{h}_i} + \frac{2\varepsilon}{h_{i+1}\hat{h}_i} + \frac{a_i^{j+1}}{\hat{h}_i} \quad (\text{since } r_i^-, r_i^+ > 0) \\ &= \frac{2\varepsilon}{h_i h_{i+1}} \quad (\text{using } \hat{h}_i = h_i + h_{i+1}). \end{aligned}$$

However, we also have:

$$|y_i^c| = \left|-\frac{2\varepsilon}{h_i h_{i+1}} - \left(b_i^{j+1} + \frac{2}{\Delta t}\right)\right| = \frac{2\varepsilon}{h_i h_{i+1}} + b_i^{j+1} + \frac{2}{\Delta t}.$$

Hence, $|y_i^-| + |y_i^+| < |y_i^c|$, and for $\frac{N}{2} < i < N-1$, we get

$$|y_i^-| + |y_i^+| = \frac{2\varepsilon}{\hat{h}h_i} + \frac{2\varepsilon}{\hat{h}h_{i+1}} + \frac{a_{i+\frac{1}{2}}^{j+1}}{h_{i+1}} - \frac{1}{2}\left(b_{i+\frac{1}{2}}^{j+1} + \frac{1}{\Delta t}\right) < |y_i^c|,$$

□

Lemma 5.2 (**Discrete minimum Principle**). *Assume that* $U_0^{j+1} \ge 0, U_N^{j+1} \ge 0$ *and* $\hat{\mathcal{L}}_{\epsilon,hy}^N U_i^{j+1} \le 0$, *for* $1 \le i \le N-1$. *Then* $U_i^{j+1} \ge 0$ *for* $1 \le i \le N$ *and* $1 \le j < M$.

Lemma 5.3. *(**Discrete Stability estimate**) The solution U_i^{j+1} of the discrete problem (5.2) satisfies the bound*

$$\left|U_i^{j+1}\right| \leq \frac{T}{\beta}\left|\left|\hat{\mathcal{L}}_{\epsilon,hy}^{N} U_i^{j+1}\right|\right| + \max_{\partial\mathcal{D}^{M,N}}\left|U(x_i,t_{j+1})\right|$$

Proof. The proof follows a similar approach to that of Lemma 4.9. □

To prove $\varepsilon-$uniform error estimates on singular components, the following barrier function are constructed;

$$\varphi_i^n = \begin{cases} \prod_{k=1}^{i}\left(1+\frac{\mu h_k}{\sqrt{\varepsilon}}\right)^{-1}, & 1 \leq i \leq N; \\ 1, & i = 0; \end{cases}$$

where $\mu = \sqrt{\alpha}$ is a constant. Also,

$$\begin{cases} \varphi_{i-1}^n = \left(1+\frac{\mu h_i}{\sqrt{\varepsilon}}\right)^{-1}\varphi_i^n, & 1 \leq i \leq N; \\ \varphi_{i+1}^n = \left(1+\frac{\mu h_{i+1}}{\sqrt{\varepsilon}}\right)^{-1}\varphi_i^n, & 1 \leq i \leq N-1. \end{cases}$$

Lemma 5.4. *The barrier function $\varphi_i^n(\mu)$ satisfies the following inequalities:*

$$\mathcal{L}_{\varepsilon,hy}^{\hat{N}}\varphi_i^n \leq -\frac{C}{\sqrt{\varepsilon}}\varphi_i^n \quad \textit{for} \quad 1 \leq i \leq N$$

Proof. One can refer the proof in [100] □

Lemma 5.5. *The mesh function φ_i^n satisfies the following inequality:*

$$e^{-\mu x_i/\sqrt{\varepsilon}} \leq \prod_{k=1}^{i}\left(1+\frac{\mu h_k}{\sqrt{\varepsilon}}\right)^{-1} = \varphi_i^n, \quad \textit{for all} \quad 0 \leq i \leq N,$$

and on Shishkin mesh, mesh function also satisfies the following inequality:

$$\prod_{k=1}^{i}\left(1+\frac{\mu h_k}{\sqrt{\varepsilon}}\right)^{-1} \leq \begin{cases} CN^{-4i/N}, & 0 < i \leq \frac{N}{2}; \\ CN^{-2}, & \frac{N}{2} \leq i < N. \end{cases}$$

Proof. We are given the mesh function

$$\varphi_i^n = \prod_{k=1}^{i}\left(1+\frac{\mu h_k}{\sqrt{\varepsilon}}\right)^{-1},$$

and aim to establish two inequalities.

1. Lower Bound:

We aim to prove:

$$\prod_{k=1}^{i}\left(1+\frac{\mu h_k}{\sqrt{\varepsilon}}\right)^{-1} \geq e^{-\mu x_i/\sqrt{\varepsilon}}, \quad \text{for all } 0 \leq i \leq N.$$

Taking the logarithm of both sides:

$$\ln\left(\prod_{k=1}^{i}\left(1+\frac{\mu h_k}{\sqrt{\varepsilon}}\right)^{-1}\right) = -\sum_{k=1}^{i}\ln\left(1+\frac{\mu h_k}{\sqrt{\varepsilon}}\right).$$

Using the inequality $\ln(1+z) \leq z$ for $z > -1$, which holds since $\mu, h_k > 0$, we get:

$$-\sum_{k=1}^{i}\ln\left(1+\frac{\mu h_k}{\sqrt{\varepsilon}}\right) \geq -\sum_{k=1}^{i}\frac{\mu h_k}{\sqrt{\varepsilon}} = -\frac{\mu}{\sqrt{\varepsilon}}\sum_{k=1}^{i}h_k = -\frac{\mu x_i}{\sqrt{\varepsilon}}.$$

Taking exponential both sides:

$$\prod_{k=1}^{i}\left(1+\frac{\mu h_k}{\sqrt{\varepsilon}}\right)^{-1} \geq e^{-\mu x_i/\sqrt{\varepsilon}}.$$

2. Upper Bound on Shishkin Mesh:

We now prove:

$$\prod_{k=1}^{i}\left(1+\frac{\mu h_k}{\sqrt{\varepsilon}}\right)^{-1} \leq \begin{cases} CN^{-4i/N}, & 0 < i \leq \frac{N}{2}; \\ CN^{-2}, & \frac{N}{2} \leq i < N. \end{cases}$$

In $[0,\omega]$, the fine mesh size: $h_k \approx \frac{2\omega}{N} = \mathcal{O}(N^{-1}\ln N)$, In $[\omega, 1]$, the coarse mesh size: $h_k \approx \mathcal{O}(N^{-1})$.

Case 1: $0 < i \leq \frac{N}{2}$ (fine mesh)

Here, $h_k \approx \frac{2\omega}{N}$, and $\omega = \mathcal{O}\left(\frac{\sqrt{\varepsilon}}{\mu}\ln N\right)$, so

$$\frac{\mu h_k}{\sqrt{\varepsilon}} \approx \frac{2\omega\mu}{N\sqrt{\varepsilon}} \approx \frac{4\ln N}{N}.$$

Thus,

$$\prod_{k=1}^{i}\left(1+\frac{\mu h_k}{\sqrt{\varepsilon}}\right)^{-1} \le \left(1+\frac{4\ln N}{N}\right)^{-i}.$$

Using the inequality $\left(1+\frac{a}{N}\right)^{-N} \le e^{-a}$, we get:

$$\left(1+\frac{4\ln N}{N}\right)^{-i} = \left[\left(1+\frac{4\ln N}{N}\right)^{-N}\right]^{i/N} \le e^{-4\ln N\cdot i/N} = N^{-4i/N}.$$

Therefore,

$$\prod_{k=1}^{i}\left(1+\frac{\mu h_k}{\sqrt{\varepsilon}}\right)^{-1} \le CN^{-4i/N}.$$

Case 2: $\frac{N}{2} \le i < N$ (coarse mesh)

Here, $h_k \approx \mathcal{O}(1/N)$, and the number of terms is at most N. Thus:

$$1+\frac{\mu h_k}{\sqrt{\varepsilon}} \ge 1+\frac{c}{N}, \quad \text{for some constant } c > 0.$$

So,

$$\prod_{k=1}^{i}\left(1+\frac{\mu h_k}{\sqrt{\varepsilon}}\right)^{-1} \le \left(1+\frac{c}{N}\right)^{-N/2} \le e^{-c/2} \le CN^{-2}.$$

□

Theorem 5.2. *Let $u_i(t)$ and $U_i(t)$ be the solutions of the continuous and discrete problem respectively. Then, the truncation error of the proposed scheme satisfy the following bounds;*

$$\sup_{0<\varepsilon\le 1} |u_i(t) - U_i(t)| \le \begin{cases} CN^{-2}\ln^2 N \quad \textit{for} \quad i = 0, 1, ..., N/2, \\ CN^{-1}(\varepsilon + N^{-1}), \quad \textit{for} \quad i = N/2+1, ..., N \end{cases}$$

where C is a constant independent of ε and the mesh parameter N.

Proof. We prove this theorem by decomposing the numerical solution U_i^N in (5.2) into regular and singular components, similar to the continuous problem, as:

$$U_i^j = V_i^j + W_i^j \quad \text{on the domain } \mathcal{D}^{N,M}.$$

Therefore, the pointwise error of the discrete solution at each mesh point (x_i, t_j) is decomposed as:

$$u_i^j - U_i^j = v_i^j - V_i^j + w_i^j - W_i^j. \tag{5.4}$$

We now estimate the truncation error separately for the regular and singular components.

First, for the regular component:

$$\hat{\mathcal{L}}_{\varepsilon,\text{hy}}^N (v - V)_i^j = \begin{cases} \left| \varepsilon \left(D_x^+ D_x^- - \dfrac{\partial^2}{\partial x^2} \right) v_i^j + a_i^j \left(D_x^0 - \dfrac{\partial}{\partial x} \right) v_i^j \right|, & i \le N/2, \\ \left| \varepsilon \left(D_x^+ D_x^- - \dfrac{\partial^2}{\partial x^2} \right) v_i^j + a_{i+\frac{1}{2}}^j \left(D_x^+ - \dfrac{\partial}{\partial x} \right) v_i^j \right. & \\ \quad \left. - q_{i+\frac{1}{2}}^j \left(\dfrac{v_i^j + v_{i+1}^j}{2} - v_{i+\frac{1}{2}}^j \right) \right|, & i > N/2, \end{cases}$$

This satisfies the inequality:

$$\hat{\mathcal{L}}_{\varepsilon,\text{hy}}^N (v - V)_i^j \le \begin{cases} C h_i \left(\varepsilon \displaystyle\int_{x_{i-1}}^{x_{i+1}} |v_{xxxx}| \, dx + h_i \int_{x_{i-1}}^{x_{i+1}} |v_{xxx}| \, dx \right), & \text{for } i \le N/2, \\ C \left(\varepsilon \displaystyle\int_{x_{i-1}}^{x_{i+1}} |v_{xxx}| \, dx + h_{i+1} \int_{x_i}^{x_{i+1}} (|v_{xxx}| + |v_{xx}| + |v_x|) \, dx \right), & \text{for } i > N/2. \end{cases}$$

Alternatively, the inequality can be expressed as:

$$\hat{\mathcal{L}}_{\varepsilon,\text{hy}}^N (v - V)_i^j \le \begin{cases} C \left[h_i (h_i + h_{i+1}) (\varepsilon |v_{xxxx}| + |v_{xxx}|) \right], & i \le N/2, \\ C \left[\varepsilon (h_i + h_{i+1}) |v_{xxx}| + h_{i+1}^2 (|v_{xxx}| + |v_{xx}| + |v_x|) \right], & i > N/2. \end{cases}$$

Using the derivative bounds of the regular component (Theorem 5.1), we obtain

$$\hat{\mathcal{L}}_{\varepsilon,\text{hy}}^N (v - V)_i^j \le \begin{cases} C N^{-2} \quad \text{for} \quad i = 0, 1, ..., N/2, \\ C N^{-1} (\varepsilon + N^{-1}), \quad \text{for} \quad i = N/2 + 1, ..., N. \end{cases} \tag{5.5}$$

Applying Lemma 5.3, we get

$$|(v - V)_i^j| \le \begin{cases} C N^{-2} \quad \text{for} \quad i = 0, 1, ..., N/2, \\ C N^{-1} (\varepsilon + N^{-1}), \quad \text{for} \quad i = N/2 + 1, ..., N. \end{cases} \tag{5.6}$$

Next, we estimate the truncation error for the singular component. First, consider the outer layer region $[\omega, 1]$. In this region, both w and W are small. Consider the following barrier functions:

$$\Psi^{\pm}(x_i, t_j) = C\varphi_i^j \pm W(x_i, t_j) \quad \forall (x_i, t_j) \in \mathcal{D}^{N,M};$$

where $C = |W(x_0, t_j)|$. We observe that

$$\begin{aligned}
\Psi^{\pm}(x_0, t_j) &= C\varphi_0^j \pm W(x_0, t_j) = C \pm W(x_0, t_j) \geq 0, \\
\Psi^{\pm}(x_N, t_j) &= C\varphi_N^j \geq 0, \\
\hat{\mathcal{L}}^N_{\varepsilon,\text{hy}} \Psi^{\pm}(x_i, t_j) &= C\hat{\mathcal{L}}^N_{\varepsilon,\text{hy}}\varphi_i^j \pm \hat{\mathcal{L}}^N_{\varepsilon,\text{hy}} W(x_i, t_j) = -\frac{C}{\sqrt{\varepsilon}}\varphi_i^j \leq 0.
\end{aligned}$$

Using Lemma 5.2, the following estimate is obtained:

$$|W(x_i, t_j)| \leq C\varphi_i^j = C\prod_{j=1}^{i}\left(1 + \frac{\mu h_j}{\sqrt{\varepsilon}}\right)^{-1}.$$

Using the triangle inequality and Theorem 5.1, we have

$$\begin{aligned}
|\left(w - W\right)(x_i, t_j)| &\leq |w(x_i, t_j)| + |W(x_i, t_j)| \leq C\exp\left(-\frac{\sqrt{\alpha}}{\sqrt{\varepsilon}}x_i\right) + C\prod_{k=i}^{i}\left(1 + \frac{\sqrt{\alpha}h_k}{\sqrt{\varepsilon}}\right)^{-1} \\
&\leq C\prod_{k=1}^{i}\left(1 + \frac{\sqrt{\alpha}h_k}{\sqrt{\varepsilon}}\right)^{-1} + C\prod_{k=i}^{i}\left(1 + \frac{\sqrt{\alpha}h_k}{\sqrt{\varepsilon}}\right)^{-1} = C\prod_{k=1}^{i}\left(1 + \frac{\sqrt{\alpha}h_k}{\sqrt{\varepsilon}}\right)^{-1}.
\end{aligned}$$

Using Lemma 5.5, the error bound in the outer region is given by

$$|\left(w - W\right)(x_i, t_j)| \leq CN^{-2}, \quad (x_i, t_j) \in [\sigma, 1] \times (0, T].$$

For the inner layer region $(x_i, t_j) \in [0, \omega] \times (0, T]$, the truncation error becomes

$$\begin{aligned}
\hat{\mathcal{L}}^N_{\varepsilon,\text{hy}}(w - W)(x_i, t_j) &\leq Ch_i\left[\int_{x_{i-1}}^{x_{i+1}}(\varepsilon|w_{xxxx}| + |w_{xxx}|)\,dx\right] \leq C\frac{h_i}{\varepsilon^{3/2}}\left[\int_{x_{i-1}}^{x_{i+1}}\exp\left(-\sqrt{\frac{\alpha}{\varepsilon}}x\right)\,dx\right] \\
&\leq C\frac{h_i}{\sqrt{\alpha\varepsilon}}\left[\exp\left(-\sqrt{\frac{\alpha}{\varepsilon}}x_{i+1}\right) - \exp\left(-\sqrt{\frac{\alpha}{\varepsilon}}x_{i-1}\right)\right] \\
&= C\frac{h_i}{\sqrt{\alpha\varepsilon}}\left[\exp\left(-\sqrt{\frac{\alpha}{\varepsilon}}x_i\right)\left\{\exp\left(\sqrt{\frac{\alpha}{\varepsilon}}h\right) - \exp\left(-\sqrt{\frac{\alpha}{\varepsilon}}h\right)\right\}\right] \\
&= C\frac{h_i}{\sqrt{\alpha\varepsilon}}\left[\exp\left(-\sqrt{\frac{\alpha}{\varepsilon}}x_i\right)\sinh\left(\sqrt{\frac{\alpha}{\varepsilon}}h\right)\right].
\end{aligned}$$

Using the assumption in Lemma 5.1, we have $\sqrt{\frac{\alpha}{\varepsilon}}h \leq 2$. Since $\sinh \nu \leq C\nu$ for $0 \leq \nu \leq 2$, it follows that

$$\sinh\left(\sqrt{\frac{\alpha}{\varepsilon}}h\right) \leq \sqrt{\frac{\alpha}{\varepsilon}}h.$$

Therefore, the above expression becomes

$$\hat{\mathcal{L}}^N_{\varepsilon,\text{hy}}(w-W)^j_i \leq C\frac{h^2}{\varepsilon^{3/2}}\exp\left(-\sqrt{\frac{\alpha}{\varepsilon}}x_i\right) \leq C\frac{N^{-2}\ln^2 N}{\sqrt{\varepsilon}}\varphi^n_i \quad \text{(by Lemma 5.5).} \tag{5.7}$$

Considering the barrier functions

$$\psi^{\pm}_j(x_i) = C\left[N^{-2} + (N^{-2}\ln^2 N)\prod_{k=1}^{N}\left(1 + h_k\sqrt{\frac{\alpha}{\varepsilon}}\right)^{-1}\right]\varphi^j_i \pm (w-W)(x_i,t_j),$$

we observe that

$$\psi^{\pm}_j(x_0) \geq 0, \quad \psi^{\pm}_j(x_N) \geq 0,$$

and by Lemma 5.4,

$$\hat{\mathcal{L}}^N_{\varepsilon,\text{hy}}\psi^{\pm}_j(x_i) \leq 0.$$

Applying the discrete minimum principle, the barrier functions satisfy $\psi^{\pm}_j(x_i) \geq 0$. Using the discrete barrier functions above and Lemma 5.2, we obtain

$$|(w-W)(x_i,t_j)| \leq CN^{-2}\ln^2 N.$$

Combining the errors for the regular and singular components yields the required result. □

Theorem 5.3. *The solution U^j_i of the fully discrete scheme* (5.1) *converges uniformly to the solution $u(x,t)$ of* (4.1) *and the error estimate is given by*

$$\sup_{0<\varepsilon\leq 1}\left|u(x_i,t_j) - U^j_i\right| \leq C(N^{-2}\ln^2 N + (\Delta t)^2), i = 0,1,2,...,N, \ \ j = 0,1,2,...,M,$$

where C is constant independent of ε and the parameters N and Δt.

Proof. The proof is derived from the bounds established in Theorems 4.2 and 5.2. □

5.6 Numerical Results and Discussion

To assess the accuracy of the proposed scheme, we solved two model problems for different mesh sizes (N, M) and perturbation values ε. We report the maximum absolute error $e_\varepsilon^{M,N}$ and the corresponding rate of convergence $R_\varepsilon^{M,N}$. When the exact solution is unavailable, we estimate these via the double–mesh principle (see Chapter 2, Section 2.6). Let $U^{M,N}$ denote the numerical solution on the coarse grid $\mathcal{D}^{M,N}$ and $U^{2M,2N}$ the solution on the refined grid $\mathcal{D}^{2M,2N}$. we define

$$e_\varepsilon^{M,N} = \max_{(x_i,t_j)\in\mathcal{D}^{M,N}} \left| U_{i,j}^{M,N} - U^{2M,2N}(x_{2i}, t_{2j}) \right|, \qquad R_\varepsilon^{M,N} = \log_2\left(\frac{e_\varepsilon^{M,N}}{e_\varepsilon^{2M,2N}}\right).$$

These quantities serve as proxies for $e_\varepsilon^{M,N}$ and $R_\varepsilon^{M,N}$ in the absence of an exact solution.

Example 5.1. *Consider the following singularly perturbed convection-diffusion boundary turning point problem with time delay [100]:*

$$\begin{aligned}
&\varepsilon u_{xx}(x,t) + x^p u_x(x,t) - u(x,t) - u_t(x,t) = x^2 - 1 + \frac{u(x,t-1)}{2}, \quad (x,t) \in \mathcal{D},\\
&u(0,t) = 1 + t^2, \quad u(1,t) = 0, \quad 0 \le t \le 2,\\
&u(x,t) = (1-x)^2, \quad \textit{on} \quad [0,1]\times[-1,0].
\end{aligned}$$

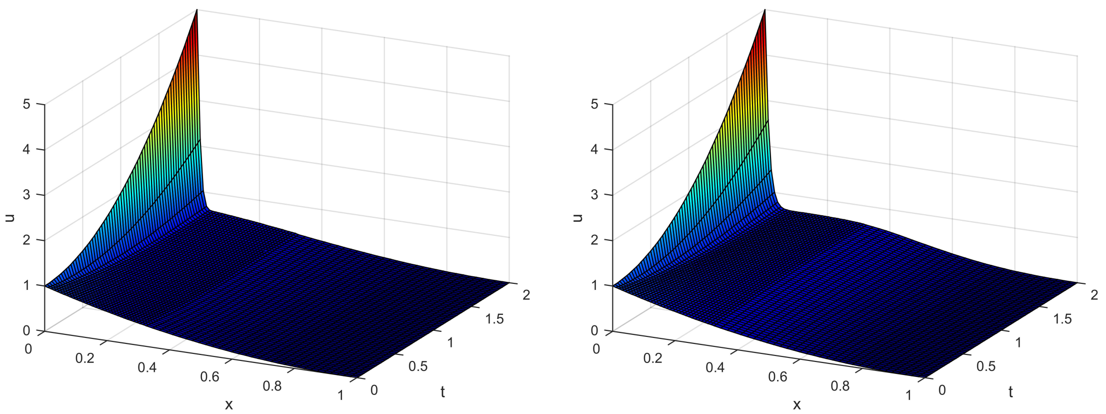

(a) $p = 1$ (b) $p = 3$,

Figure 5.1: Surface plots of the numerical solution for Example 5.1 with $\varepsilon = 10^{-4}$ for varying values of p.

Example 5.2. *Consider the following singularly perturbed convection-diffusion boundary turning point*

Table 5.1: Maximum absolute error and rate of convergence for Example 5.1 for $p = 1$

$\varepsilon \downarrow M = N \rightarrow$	32	64	128	256	512	1024
10^{-1}	5.8011e-03	1.7372e-03	4.0391e-04	9.5349e-05	2.3609e-05	5.8902e-06
	1.7395	2.1047	2.0827	2.0139	2.0029	
10^{-3}	5.5722e-03	1.8242e-03	5.8253e-04	1.8258e-04	3.7280e-05	9.9410e-06
	1.6110	1.6469	1.6738	1.6849	1.9861	
10^{-5}	5.5849e-03	1.8295e-03	5.8303e-04	1.8341e-04	5.7286e-05	1.4510e-05
	1.6100	1.6498	1.6689	1.6788	1.9811	
10^{-7}	5.5867e-03	1.8304e-03	5.8321e-04	1.8428e-04	5.8120e-05	1.4728e-05
	1.6098	1.6501	1.6621	1.6647	1.9804	
10^{-9}	5.5869e-03	1.8305e-03	5.8323e-04	1.8429e-04	5.8123e-05	1.4731e-05
	1.6098	1.6501	1.6621	1.6647	1.9802	
10^{-10}	5.5869e-03	1.8305e-03	5.8323e-04	1.8429e-04	5.8123e-05	1.4731e-05
	1.6098	1.6501	1.6621	1.6647	1.9802	
$e^{M,N}$	5.5869e-03	1.8305e-03	5.8323e-04	1.8429e-04	5.8123e-05	1.4731e-05
$R^{M,N}$	1.6098	1.6501	1.6621	1.6647	1.9802	
In [100]: $e^{M,N}$	4.308e-03	2.099e-03	1.055e-03	5.304e-03	2.741e-04	
$R^{M,N}$	1.0373	0.9922	0.9923	0.9521		
Chap 4: $e^{M,N}$	4.0290e-03	2.0649e-03	1.0440e-03	5.2478e-04	2.6309e-04	1.3190e-04
$R^{M,N}$	0.9644	0.9839	0.9923	0.9961	0.9961	

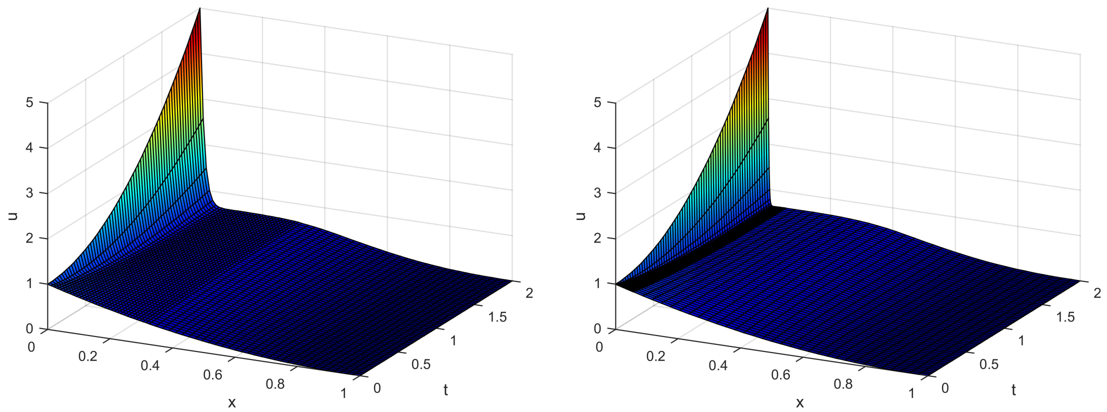

(a) $\varepsilon = 10^{-4}$ (b) $\varepsilon = 10^{-6}$

Figure 5.2: Surface plots of the numerical solution for Example 5.1 with $p = 3$ for varying values of ε.

problem with time delay [100]:

$$\varepsilon u_{xx}(x,t) + x^p(1 + te^{-2t})u_x(x,t) - (e^x + 1)u(x,t) - u_t(x,t) = p(x^2 - 1)e^{-t} - tu(x,t-1), \quad (x,t) \in \mathcal{D},$$

$$u(0,t) = 1 + t^2, \quad u(1,t) = 0, \quad 0 \leq t \leq 2,$$

$$u(x,t) = (1-x)^2, \quad on \quad [0,1] \times [-1,0].$$

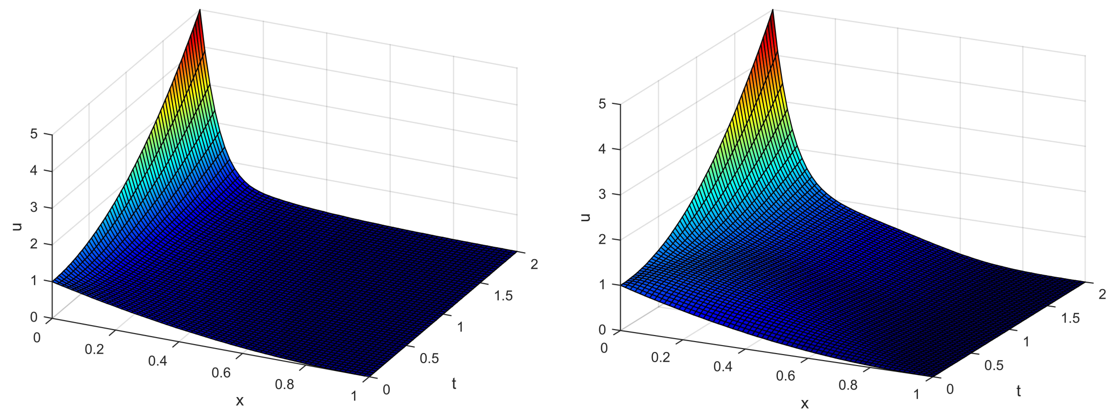

(a) $p = 1$ (b) $p = 3$

Figure 5.3: Surface plots of the numerical solution for Example 5.2 with $\varepsilon = 10^{-2}$ for varying values of p.

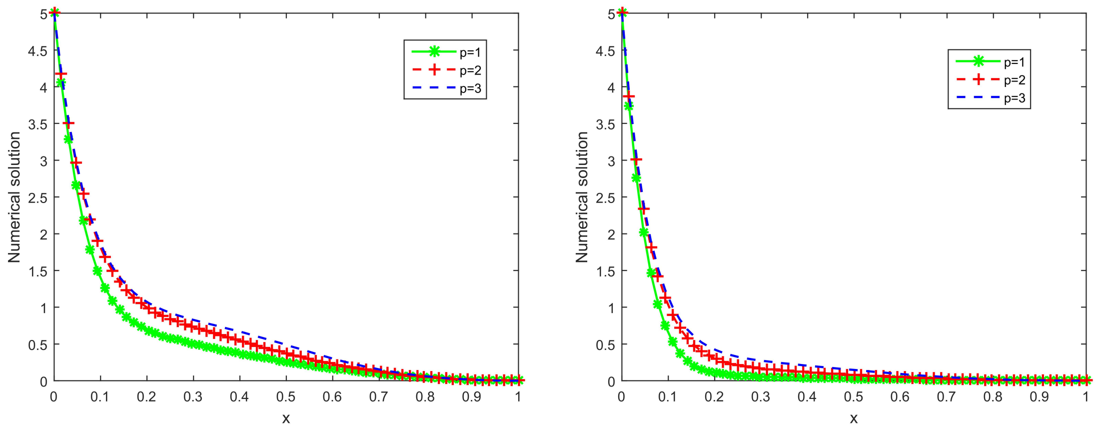

(a) Example 5.1 (b) Example 5.2

Figure 5.4: Profile of numerical Solution for $\varepsilon = 10^{-2}$ with different values of p values.

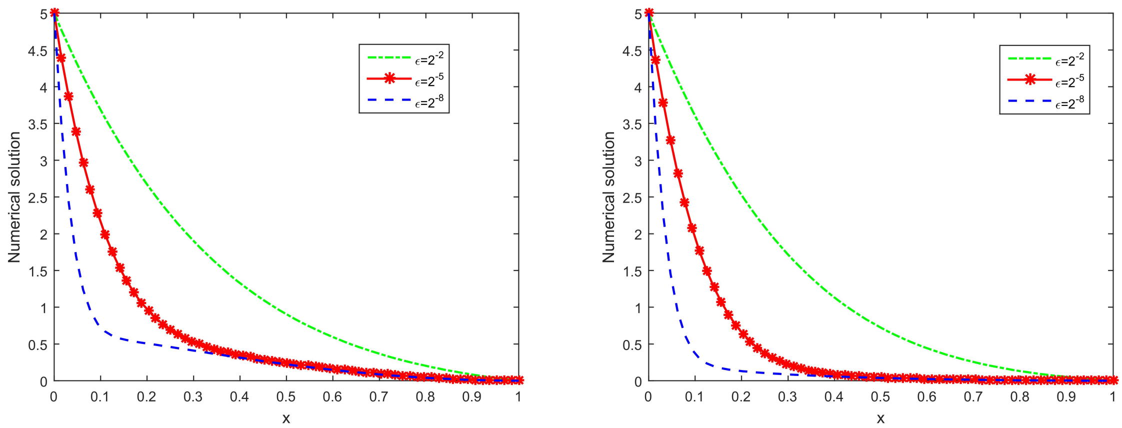

(a) Example 5.1 (b) Example 5.2

Figure 5.5: Profile of numerical solution for $p = 1$ with different values of ε.

Table 5.2: Maximum absolute error and rate of convergence for Example 5.2 for $p = 1$

$\varepsilon \downarrow M = N \rightarrow$	32	64	128	256	512	1024
10^{-1}	9.8283e-04	2.5980e-04	6.8670e-05	1.8140e-05	4.7870e-06	1.2630e-06
	1.9195	1.9196	1.9205	1.9219	1.9223	
10^{-3}	8.2834e-03	2.8305e-03	8.7580e-04	2.5140e-04	6.7220e-05	1.7885e-05
	1.5491	1.6923	1.8006	1.9030	1.9101	
10^{-5}	8.4488e-03	2.8860e-03	8.9330e-04	2.5670e-04	6.8860e-05	1.8385e-05
	1.5497	1.6919	1.7997	1.8983	1.9059	
10^{-7}	8.4504e-03	2.8870e-03	8.9370e-04	2.5680e-04	6.8750e-05	1.8360e-05
	1.5494	1.6919	1.7995	1.9015	1.9050	
10^{-9}	8.4504e-03	2.8870e-03	8.9370e-04	2.5680e-04	6.8750e-05	1.8360e-05
	1.5494	1.6919	1.7995	1.9015	1.9050	
10^{-10}	8.4504e-03	2.8870e-03	8.9370e-04	2.5680e-04	6.8750e-05	1.8360e-05
	1.5494	1.6919	1.7995	1.9015	1.9050	
$e^{M,N}$	8.4504e-03	2.8870e-03	8.9370e-04	2.5680e-04	6.8750e-05	1.8360e-05
$R^{M,N}$	1.5494	1.6919	1.7995	1.9015	1.9050	
In [100] $e^{M,N}$	1.965e-02	5.588e-03	1.950e-03	9.246e-04	4.475e-04	
	1.8140	1.5190	1.0770	1.0470		
In Chap 4 $e^{M,N}$	4.3654e-03	2.3158e-03	1.1948e-03	6.0704e-04	3.0597e-04	1.5422e-04
	0.9146	0.9547	0.9769	0.9884	0.9884	

Table 5.3: $e^{M,N}$ and $R^{M,N}$ with different values of p.

$p \downarrow M = N \rightarrow$	32	64	128	256	512	1024
	Example 5.1					
2	6.5930e-03	2.1934e-03	6.9896e-04	2.0378e-04	5.7192e-05	1.5675e-05
	1.5878	1.6499	1.7782	1.8331	1.8673	
3	6.5931e-03	2.1935e-03	6.9900e-04	2.0386e-04	5.7287e-05	1.5703e-05
	1.5877	1.6499	1.7777	1.8313	1.8672	
	Example 5.2					
2	9.9992e-03	3.3178e-03	1.0421e-03	3.0266e-04	8.4021e-05	2.2556e-05
	1.5916	1.6707	1.7837	1.8489	1.8972	
3	9.7879e-03	3.4012e-03	1.0651e-03	3.1260e-04	8.6285e-05	2.3164e-05
	1.5250	1.6751	1.7686	1.8571	1.8972	

From Tables 5.1 and 5.2, it can be observed that the mesh parameters and maximum absolute errors are inversely related. As the mesh parameters M and N increases, the maximum absolute error decreases. Furthermore, for a fixed mesh parameter, as the perturbation parameter decreases, the maximum absolute error remains stable. This indicates that the proposed method exhibits parameter-uniform convergence. Additionally, Table 5.3 presents the values of $e^{M,N}$ and $R^{M,N}$ for different values of p. The results show that variations in p do not affect the stability or convergence of the proposed method, confirming its robustness. Although increasing p strengthens the turning point effect and slightly increases the maximum absolute error, the method remains almost second-order ε-uniformly convergent. Comparisons with other methods, as shown in Tables 5.1 and 5.2, demonstrate that the proposed method outperforms existing methods, such as the one in [100], in terms of both accuracy and order of convergence.

Surface plots in Figures 5.1 and 5.3 for Examples 5.1 and 5.2, respectively, are displayed for a fixed ε and different values of p. These figures demonstrate that as p increases, the peak of the solution becomes more pronounced and shifts away from the boundary layer region. Furthermore, Figure 5.2 presents a surface plot for Example 5.1 with varying values of ε. From this figure, it can be observed that as the perturbation parameter ε becomes smaller, the mesh condenses toward the left side of the spatial domain in order to resolve the boundary layer effectively. Additionally, Figure 5.4 shows the solution profiles for Examples 5.1 and 5.2 with a fixed ε and different p values, illustrating its the effect on the solution. Finally, in Figure 5.5, numerical solution profiles for Examples 5.1 and 5.2 are displayed for $p = 1$ and varying ε values. As $\varepsilon \to 0$, formation of boundary layer becomes visible on the left side of the spatial domain.

5.7 Conclusion

In this chapter, we studied singularly perturbed partial differential equations (SPPDEs) with multiple boundary turning points and a large time lag. The solution to this class of problems exhibits a left boundary layer in the spatial domain as the perturbation parameter ε approaches zero. The combined effect of the perturbation parameter and turning points significantly increases the complexity of the problem, making it challenging to obtain an oscillation-free numerical solution. To overcome these challenges, a robust numerical scheme was developed. The method employs Crank–Nicolson time discretization on a uniform mesh, while spatial discretization is performed using a hybrid approach: central finite difference within the layer region and a midpoint upwind scheme outside the layer region, all constructed on a Shishkin mesh. Figures and tables illustrate the behaviour of the solution with respect to the perturbation parameter and confirm that the proposed scheme is stable and achieves parameter-uniform convergence with nearly second-order accuracy. Comparative results show that the proposed method performs better than existing techniques reported in the literature and the results presented in Chapter 4, particularly in terms of accuracy and order of convergence. Numerical experiments on model problems validate the theoretical analysis. The stability and convergence results demonstrate that the global error decreases quadratically with mesh refinement in both time and space, independent of the perturbation parameter. Overall, the proposed method provides an efficient, accurate, and parameter-uniform approach for solving this class of problems.

Chapter 6

Nonstandard Finite Difference Method for Singularly Perturbed Parabolic Convection–Diffusion Turning-Point Problems with General Shifts

In this chapter, we considered a Singularly Perturbed Parabolic Convection–Diffusion Turning-Point Problems with General Shifts. The problem involves both delay and advance parameters in the spatial variable of the reaction terms. The solution exhibits boundary layer on either the left or right side of the domain, depending on the sign of the coefficient of the convection term. We developed a scheme in order to solve such problems. The scheme is formulated using the Crank–Nicolson method for temporal discretization, combined with a non-standard finite difference method for spatial discretization. The stability and uniform convergence of the proposed scheme are also discussed. A numerical example is incorporated to show the scheme's applicability and to reinforce the theoretical analysis.

6.1 Introduction

Singularly perturbed parabolic differential-difference equations (SPPDDEs), which incorporate both sharp spatial gradients and memory effects through delay or advance terms, frequently arise in biological modeling, control theory, and other applied sciences [16]. When these equations include boundary turning points locations where the convection coefficient vanishes and changes sign the solution exhibits complex multiscale behavior, such as interior or boundary layers, making their numerical treatment particularly challenging. Classical methods often fail to resolve such layers unless excessively fine meshes are used. Although significant progress has been made in designing parameter-uniform methods for singularly perturbed differential-difference problems [14, 15, 13, 57, 101, 103, 122], robust and uniformly convergent schemes for SPDDEs with multiple turning points remain scarce [98]. To address this gap, we proposed a Crank–Nicolson-based temporal discretization combined with a nonstandard finite difference method (NSFDM) on a uniform spatial mesh to solve SPPDDEs with multiple boundary turning points. NSFDMs, built upon exact finite difference principles using problem-adapted denominator functions, offer flexibility and improved accuracy in resolving boundary layers without excessive mesh refinement. This approach aims to deliver enhanced stability and uniform convergence across a wide range of perturbation parameters.

6.2 Description of the Problem

Consider a class of singularly perturbed parabolic convection–diffusion turning-Point problems with general shifts on the reaction terms, given by

$$\begin{cases} \varepsilon u_{xx} + a(x,t)u_x(x,t) - b(x,t)u(x-\delta,t) - c(x,t)u(x,t) - d(x,t)u(x+\mu,t) - u_t(x,t) = f(x,t), (x,t) \in \mathcal{D}, \\ u(x,0) = u_0(x), x \in \mathcal{D}_b = \{(x,0) : x \in \overline{\Omega}\}, \\ u(x,t) = \phi_1(x,t), \quad (x,t) \in \mathcal{D}_l = \{(x,t) : (x,t) \in [-\delta,0] \times \Lambda\}, \\ u(x,t) = \phi_2(x,t), (x,t) \in \mathcal{D}_r = \{(x,t) : (x,t) \in [1,1+\mu] \times \Lambda\}, \end{cases} \tag{6.1}$$

where $\mathcal{D} = \Omega \times \Lambda = (0,1) \times (0,T]$ for some fixed $T > 0$, and $0 < \varepsilon \ll 1$ is the singular perturbation parameter. The constants δ and μ are the delay and advance parameters, respectively, satisfying $\delta, \mu \leq C\varepsilon$ for some constant $C > 0$.

The coefficients in (6.1) are defined as

$$\begin{cases} a(x,t) = a_0(x,t)x^p, \quad p \geq 1, \\ a_0(x,t) \geq \alpha > 0, \quad b(x,t) \geq \beta > 0, \quad c(x,t) \geq \gamma > 0, \quad d(x,t) \geq \eta > 0, \quad \text{for all } (x,t) \in \overline{\mathcal{D}}. \end{cases}$$

We assume that the coefficient functions $a(x,t), b(x,t), c(x,t), d(x,t), f(x,t)$ are defined on the closure $\bar{\mathcal{D}}$, and possess sufficient smoothness: $a, b, c, d, f \in C^{2,1}(\overline{\mathcal{D}})$. The boundary conditions $\phi_1, \phi_2 \in C^{2,1}(\partial\mathcal{D})$ are also smooth on their respective domains, and the initial condition $u_0 \in C^2(\overline{\mathcal{D}} \cap \{t = 0\})$. Moreover, all data are assumed to be uniformly bounded and independent of ε, ensuring the well-posedness of the problem and guaranteeing the existence and uniqueness of the solution. The parameter p in the convection term coefficient determines the order of the boundary turning point: The coefficient function $b(x,t), c(x,t)$ and $d(x,t)$ are assumed to satisfy $b(x,t) + c(x,t) + d(x,t) \geq q^* > 0$, $\forall (x,t) \in \mathcal{D}$, for some constant q^*.

6.3 Properties of the Continuous Solution

Using Taylor series expansions around x, for small δ and μ, we have:

$$
\begin{aligned}
u(x-\delta,t) &\approx u(x,t) - \delta u_x(x,t) + \frac{\delta^2}{2} u_{xx}(x,t) + \mathcal{O}(\delta^3), \\
u(x+\mu,t) &\approx u(x,t) + \mu u_x(x,t) + \frac{\mu^2}{2} u_{xx}(x,t) + \mathcal{O}(\mu^3).
\end{aligned} \tag{6.2}
$$

Substituting (6.2) into (6.1), we obtain the asymptotically equivalent problem:

$$
\begin{cases}
\mathcal{K}_{c_\varepsilon} u(x,t) \equiv c_\varepsilon(x,t)\, u_{xx}(x,t) + p(x,t)\, u_x(x,t) - q(x,t)\, u(x,t) - u_t(x,t) = f(x,t), (x,t) \in \mathcal{D}, \\
u(x,0) = u_0(x), \quad x \in \overline{\Omega}, \\
u(0,t) = \phi_1(0,t), \quad u(1,t) = \phi_2(1,t), \quad t \in \overline{\Lambda},
\end{cases} \tag{6.3}
$$

where the modified coefficients are given by

$$
\begin{aligned}
c_\varepsilon(x,t) &= \varepsilon - \frac{\delta^2}{2} b(x,t) - \frac{\mu^2}{2} d(x,t), \\
p(x,t) &= a(x,t) + \delta b(x,t) - \mu d(x,t), \\
q(x,t) &= b(x,t) + c(x,t) + d(x,t).
\end{aligned}
$$

For sufficiently small delay δ and advance μ parameters, the approximation from the original system (6.1) to the reduced system (6.3) is valid because the difference between the two models is bounded by $\mathcal{O}(\delta^3 + \mu^3)$. This bound arises from the Taylor expansion of the deviating arguments, where the linear and quadratic terms are retained, and only the cubic and higher-order terms are neglected. Since $\delta, \mu < \varepsilon$, the effect of discarding the higher-order terms does not influence either the stability or the convergence of the scheme. In this sense, the two systems are said to be asymptotically equivalent, meaning that they yield numerically indistinguishable solutions within the prescribed accuracy of the discretization.

Moreover, we assume that the modified coefficients satisfy the following bounds: $0 < c_\varepsilon(x,t) \leq \varepsilon - \frac{\delta^2}{2}\beta - \frac{\mu^2}{2}\eta, \quad p(x,t) = a(x,t) + \delta b(x,t) - \mu d(x,t) \geq p^* > 0$ and $q(x,t) = b(x,t) + c(x,t) + d(x,t) \geq q^* > 0$, ensuring the presence of a boundary layer near $x = 0$.

The existence and uniqueness of the solution are guaranteed by the smoothness and boundedness assumptions together with the following compatibility conditions:

$$u_0(0) = \phi_1(0,0), \quad u_0(1) = \phi_2(1,0), \tag{6.4}$$

and

$$\begin{cases} c_\varepsilon \frac{\partial^2 u_0(0)}{\partial x^2} + p(0,0)\frac{\partial u_0(0)}{\partial x} - q(0,0)u_0(0) - \frac{\partial \phi_1(0,0)}{\partial t} = f(0,0), \\ c_\varepsilon \frac{\partial^2 u_0(1)}{\partial x^2} + p(1,0)\frac{\partial u_0(1)}{\partial x} - q(1,0)u_0(1) - \frac{\partial \phi_2(1,0)}{\partial t} = f(1,0), \end{cases} \tag{6.5}$$

The comparability condition at the corner points also ensure that there exists a constant C independent of c_ε such that $\forall (x,t) \in \overline{\mathcal{D}}$,

$$|u(x,t) - u(x,0)| \leq Ct,$$
$$|u(x,t) - u(0,t)| \leq C(1-x).$$

Lemma 6.1. ***(The continuous minimum principle):*** *Let $\theta(x,t)$ be a sufficiently smooth function defined on $\mathcal{D}$ which satisfies $\theta(x,t) \geq 0, \forall (x,t) \in \partial\mathcal{D}$ and $\mathcal{K}_{c_\varepsilon}\vartheta(x,t) \leq 0, \ \forall (x,t) \in \mathcal{D}$. Then $\vartheta(x,t) \geq 0, \ \forall (x,t) \in \bar{\mathcal{D}}$.*

Proof. Let the point $(y,z) \in \bar{\mathcal{D}}$ and $\digamma(y,z) = \min_{(x,t)\in\bar{\mathcal{D}}} \vartheta(x,t) < 0$. Since $\vartheta(x,t) \geq 0, \ \forall (x,t) \in \partial\mathcal{D}$, we have $(y,z) \notin \partial\mathcal{D}$. The inequality $\vartheta(y,z) = \min_{(x,t)\in\bar{\mathcal{D}}} \vartheta(x,t) < 0$ implies that $\frac{\partial \digamma(y,z)}{\partial t} = 0$,$\frac{\partial \digamma(y,z)}{\partial x} = 0$ and $\frac{\partial \digamma(y,z)}{\partial x} \geq 0$.
This gives that

$$\mathcal{K}_{c_\varepsilon}\vartheta(y,z) = (c_\varepsilon \frac{\partial^2 \vartheta}{\partial x^2} + p\frac{\partial \vartheta}{\partial x} - q\vartheta - \frac{\partial \vartheta}{\partial t})(y,z) > 0$$

which is a contradict as $\mathcal{K}_{c_\varepsilon}\vartheta(x,t) \leq 0, \forall (x,t) \in \mathcal{D}$. Hence $\vartheta(x,t) \geq 0 \ \forall (x,t) \in \bar{\mathcal{D}}$. □

Lemma 6.2 (Stability Estimate). *Suppose $u(x,t)$ be the solution of (6.3). Then it satisfies*

$$||u(x,t)||_{\bar{\mathcal{D}}} \leq ||u(x,t)||_{\partial\mathcal{D}} + \frac{T}{p^*}||f(x,t)||_{\bar{\mathcal{D}}}.$$

Proof. Consider the barrier functions

$$\varpi^{\pm}(x,t) = ||u(x,t)||_{\partial\mathcal{D}} + \frac{T}{p^*}||f(x,t)||_{\bar{\mathcal{D}}} \pm u(x,t).$$

$$\begin{aligned}
&On\ the\ boundary\ points, \\
&\varpi^{\pm}(0,t) = ||u(0,t)||_{\partial\mathcal{D}} + \frac{T}{p^*}||f(x,t)||_{\bar{\mathcal{D}}} \pm u(0,t) \geq 0. \\
&\varpi^{\pm}(1,t) = ||u(1,t)||_{\partial\mathcal{D}} + \frac{T}{p^*}||f(x,t)||_{\bar{\mathcal{D}}} \pm u(1,t) \geq 0.
\end{aligned}$$

$$\begin{aligned}
&And\ in\ the\ interior\ points, \\
\mathcal{K}_{c_\varepsilon}\varpi^{\pm}(x,t) =& -q(x,t)[||u(x,t)||_{\partial\mathcal{D}} + \frac{T}{p^*}||f(x,t)||_{\bar{\mathcal{D}}}] \pm \mathcal{K}_{c_\varepsilon}u(x,t) \\
\leq& -p^*[||u(x,t)||_{\partial\mathcal{D}} + \frac{T}{p^*}||f(x,t)||_{\bar{\mathcal{D}}}] \pm f(x,t) \leq 0.
\end{aligned}$$

Using Lemma 6.1 , $\varpi^{\pm}(x,t) \geq 0,\ \forall (x,t) \in \bar{\mathcal{D}}$. This implies that $||u(x,t)||_{\bar{\mathcal{D}}} \leq ||u(x,t)||_{\partial\mathcal{D}} + \frac{T}{p^*}||f(x,t)||_{\overline{\mathcal{D}}}$. □

Lemma 6.3. *Let $u(x,t)$ be the solution of continuous problem (6.3), then it satisfies the following inequality with some constant C.*

$$\begin{aligned}
|u(x,t) - s_0(x)| &\leq Ct, \quad \text{and} \\
|u(x,t) - s_0(x)| &\leq C(1-x), \quad \forall (x,t) \in \overline{\mathcal{D}}, \\
|u(x,t)| &\leq C.
\end{aligned}$$

Proof. One can refer the detail proof in [105]. □

Theorem 6.1. *The solution $u(x,t)$ of the problem (6.3) satisfies the following bound on its derivatives:*

$$\left|\frac{\partial^{(i+j)}}{\partial x^i \partial t^j}u(x,t)\right| \leq C\left(1 + c_\varepsilon^{-i/2}\exp\left(-x\sqrt{\frac{p^*}{c_\varepsilon}}\right)\right),$$

where i and j are non-negative integers such that $0 \leq i + 3j \leq 4$.

Proof. The proof of this is similar to the proof in Chapter 2 of Theorem 2.1 ☐

To obtain stronger estimates for the bounds on the solution u and its derivatives, we decompose the solution of (6.3) into regular and singular components as

$$u(x,t) = v(x,t) + w(x,t), \quad (x,t) \in \bar{\mathcal{D}},$$

where the regular part $v(x,t)$ is the solution of the inhomogeneous problem

$$\begin{cases} \mathcal{K}_\varepsilon v(x,t) = f(x,t), & (x,t) \in \mathcal{D}, \\ v(x,0) = u_0(x), & \text{on } x \in \overline{\Omega}, \\ v(1,t) = \phi_2(1,t), & \text{for} \quad t \in \bar{\Lambda}, \end{cases}$$

and the singular part $w(x,t)$ is the solution of the homogeneous problem

$$\begin{cases} \mathcal{K}_\varepsilon w(x,t) = 0, & (x,t) \in \mathcal{D}, \\ w(x,0) = 0, x \in \overline{\Omega} & \\ w(1,t) = 0, & \\ w(0,t_{j+1}) = \phi_1(0,t) - v(0,t), \quad t \in \bar{\Lambda}. & \end{cases}$$

In the next theorem, we set the bound for the derivatives of solution.

Theorem 6.2. *The regular and singular components, along with their derivatives, satisfy the following bounds.*

$$\left| \frac{\partial^{i+j}}{\partial x^i \partial t^j} v(x,t) \right| \leq C(1 + c_\varepsilon^{2-i/2}), \left| \frac{\partial^{i+j}}{\partial x^i \partial t^j} w(x,t) \right| \leq C(c_\varepsilon^{-i/2} \exp\left(-x\sqrt{\frac{p^*}{c_\varepsilon}}\right)), \ (x,t) \in \bar{\mathcal{D}},$$

where i and j are non-negative integers such that $0 \leq i + 3j \leq 4$.

Proof. The proof follows a similar approach to that in Chapter 3 of Theorem 3.1. ☐

6.4 Derivation of the Numerical Method

In this section, we looked at how the suggested numerical method was derived in order to obtain a better approximation solution of the equation (6.1).

6.4.1 Temporal Discretization

We discretize the time domain $[0, T]$ using uniform mesh as: $\Lambda^M = \left\{ t_j = j\Delta t, j = 0, 1, ..., M, \Delta t = \frac{T}{M} \right\}$,

where M is the number of mesh elements in $[0, T]$ with step size $k = \Delta t = t_{j+1} - t_j$, for $j = 0, 1, ..., M - 1$.

The temporal variable in problem (6.3) is discretized at the point $(x, t_{j+1/2})$ we have

$$\begin{cases} U^0(x) = u_0(x), \quad x \in \overline{\Omega}, \\ c_\varepsilon U_{xx}^{j+1/2} + p^{j+1/2}(x) U_x^{j+1/2} - q^{j+1/2}(x) U^{j+1/2}(x) - D_t^- U^{j+1}(x) = f^{j+1/2}(x), \\ U^{j+1}(0) = \phi_1(0, t_{j+1}), U^{j+1}(1) = \phi_2(1, t_{j+1}), 0 \le j \le M, \end{cases} \tag{6.6}$$

where

$$\begin{cases} D_t^- u^{j+1}(x) = \dfrac{U^{j+1}(x) - U^j(x)}{\Delta t}, \\ U^{j+1/2}(x) = \dfrac{U^{j+1}(x) + U^j(x)}{2}, \\ f^{j+1/2}(x) = \dfrac{f^{j+1}(x) + f^j(x)}{2}, \end{cases}$$

and $U^j(x)$ is an approximate solution of $u(x, t_j)$ at j^{th} time level.

The time semi-discretized problem (6.6) can be rewritten as

$$\begin{cases} U^0(x) = u_0(x), \quad x \in \overline{\Omega}, \\ \hat{\mathcal{K}}_{c_\varepsilon} U^{j+1}(x) = R^{j+1}(x), \\ U^{j+1}(0) = \phi_1(0, t_{j+1}), U^{j+1}(1) = \phi_2(1, t_{j+1}), 0 \le j < M, \end{cases} \tag{6.7}$$

where

$$\begin{cases} \hat{\mathcal{K}}_{c_\varepsilon} U^{j+1}(x) = \frac{c_\varepsilon}{2}(U_{xx})^{j+1} + \frac{p^{j+1}(x)}{2}(U_x)^{j+1} - \frac{Q^{j+1}(x)}{2}(U(x))^{j+1}, \\ R^{j+1}(x) = f^{j+1/2}(x) - \frac{c_\varepsilon}{2}(U_{xx})^j - \frac{p^j(x)}{2}(U_x)^j + \frac{d^j(x)}{2}(U(x))^j, \\ Q^{j+1}(x) = q^{j+1}(x) + \frac{2}{\Delta t}, \\ d^j(x) = q^j(x) - \frac{2}{\Delta t}. \end{cases}$$

The semi-discrete operator $\hat{\mathcal{K}}_{c_\varepsilon}$ satisfies the following minimum principle.

Lemma 6.4 (Semi-Discrete Minimum principle). *Suppose $\theta^{j+1}(x)$ be smooth function satisfying $\theta^{j+1}(0) \geq 0, \theta^{j+1}(1) \geq 0$ and $\hat{\mathcal{K}}_{c_\varepsilon}\theta^{j+1}(x) \leq 0, \ \ \forall x \in \Omega$. Then $\theta^{j+1}(x) \geq 0, \ \ \forall x \in \overline{\Omega}$ and $j = 0, 1, 2, ...M-1$.*

Proof. Let $\ell \in \Omega$ such that $\theta^{j+1}(\ell) = \min \theta^{j+1}(x) < 0, \ \ \forall x \in \Omega$. This implies that $\left(\theta^{j+1}(\ell)\right)' = 0$ and $\left(\theta^{j+1}(\ell)\right)'' \geq 0$. Then, we have

$$\hat{\mathcal{K}}_{c_\varepsilon}\theta^{j+1}(\ell) = \frac{c_\varepsilon}{2}\left(\theta^{j+1}(\ell)\right)'' + \frac{p^{j+1}(x)}{2}\left(\theta^{j+1}(\ell)\right)' - \frac{Q^{j+1}(x)}{2}(\theta^{j+1}(\ell)) > 0.$$

Since $Q^{j+1}(\ell) = b^{j+1}(\ell) + \frac{2}{\Delta t} \geq \beta + \frac{2}{\Delta t} > 0$, this contradict the assumption that $\hat{\mathcal{K}}_{c_\varepsilon}\theta^{j+1}(x) \leq 0$. Therefore, we conclude that $\theta^{j+1}(x) \geq 0 \ \ \text{on} \ \overline{\Omega}$. □

Lemma 6.5 (Stability Estimate). *Let U^{j+1} be the discrete solution at time level t_{j+1}. If $U^{j+1}(0) \geq 0$ and $U^{j+1}(1) \geq 0$, then for all nodal points $x \in \bar{\Omega}$,*

$$\left|U^{j+1}(x)\right| \leq \max_{\partial\mathcal{D}^M}\left|U^{j+1}(x)\right| + \frac{T}{p^*}\max_{x\in\Omega}\left|\hat{\mathcal{K}}_{c_\varepsilon}U^{j+1}(x)\right|.$$

Proof. The proof follows a similar approach that presented in Lemma 2.5. □

The local truncation error of the time semi-discretization is given by $e_{j+1}(x) = \hat{\mathcal{K}}_\epsilon\, u^{j+1}(x) - g^{j+1}(x)$, where $u^{j+1}(x)$ is the solution of Eq. (6.7).

Theorem 6.3. *Suppose that*

$$\left|\frac{\partial^i u}{\partial t^i}\right| \leq C, \ \ (x,t) \in \bar{\mathcal{D}} \ \ for \ \ 0 \leq i \leq 3.$$

The local truncation error at $(j+1)^{th}$ time step is given by

$$||e_{j+1}|| \leq C(\Delta t)^3.$$

Proof. Using Taylor series expansion we have

$$u(x,t_{j+1}) = u(x,t_{j+1/2}) + \frac{\Delta t}{2}u_t(x,t_{j+1/2}) + \frac{1}{2!}(\frac{\Delta t}{2})^2 u_{tt} + O((\Delta t)^3). \tag{6.8}$$

$$u(x,t_j) = u(x,t_{j+1/2}) - \frac{\Delta t}{2}u_t(x,t_{j+1/2}) + \frac{1}{2!}(\frac{\Delta t}{2})^2 u_{tt} + O((\Delta t)^3). \tag{6.9}$$

Subtracting (6.9) from (6.8) we get

$$\frac{u(x,t_{j+1}) - u(x,t_j)}{\Delta t} = u_t(x,t_{j+1/2}) + O(\Delta t)^2).$$

$$= c_\varepsilon u_{xx}(x,t_{j+1/2}) + p(x,t_{j+1/2})u_x(x,t_{j+1/2}) - q(x,t_{j+1/2})u(x,t_{j+1/2}) - f(x,t_{j+1/2}) + O((\Delta t)^2),$$

where $u(x,t_{j+1/2}) = \frac{u(x,t_{j+1})+u(x,t_j)}{2} + O((\Delta t)^2))$.

Further simplification yields

$$\hat{\mathcal{K}}_{c_\varepsilon}u(x,t_{j+1}) \equiv \frac{c_\varepsilon}{2}u_{xx}(x,t_{j+1}) + \frac{p(x,t_{j+1})}{2}u_x(x,t_{j+1}) - \frac{q(x,t_{j+1})}{2}u(x,t_{j+1}) = R(x,t_{j+1}) + O((\Delta t)^3). \tag{6.10}$$

From Eq.(6.7) and Eq. (6.10) the local truncation error satisfies

$$\begin{aligned} \hat{\mathcal{K}}_{c_\varepsilon}e_{j+1} &= O(\Delta t)^3, \\ e_{j+1}(0) = e_{j+1}(1) &= 0. \end{aligned} \tag{6.11}$$

It can be seen that

$$||e_{j+1}|| \le C(\Delta t)^3.$$

□

The local error estimate of each time step contributes to the global error in the temporal semi-discretization which is denoted by, E_j.

Theorem 6.4. *The global truncation error for temporal discretization up to j^{th} time level is given by*

$$||E_j|| \le C(\Delta t)^2, \quad \forall j \le \frac{T}{\Delta t}.$$

Proof. Using the local error estimate up to j^{th} time step, we obtain the global error estimate at j^{th} time step.

$$\begin{aligned}
||E_j|| =&|| \sum_{i=1}^{j} e_i||, \;\; j \leq \frac{T}{\Delta t} \\
&\leq ||e_1|| + ||e_2|| + ||e_3|| + ... + ||e_j|| \\
&\leq C_1(j)(\Delta t)^3 \quad \text{(using Lemma 6.3)} \\
&\leq C_1 T(\Delta t)^2 \text{ as } \; j.\Delta t \leq T \\
&\leq C(\Delta t)^2, \;\; C = C_1 T.
\end{aligned}$$

□

Theorem 6.5. *The solution $u^{j+1}(x)$ of the problem (6.3) satisfies the following bound on its derivatives:*

$$\left|\frac{d^k u^{j+1}(x)}{dx^k}\right| \leq C\left(1 + c_\varepsilon^{-k/2} \exp\left(-x\sqrt{\frac{p^*}{c_\varepsilon}}\right)\right), k = 0, 1, 2, 3, 4.$$

Proof. The proof follows a similar approach to that used in Theorem 2.3 of Chapter 2. □

6.4.2 Spatial Discretization

For the spatial derivative approximations, we employ the Nonstandard Finite Difference Method (NSFDM) as described in [75]. In this approach, the standard finite difference formulas are modified by introducing a problem-dependent denominator function ξ^2, which depends on both the step size (h) and c_ε. This denominator function is derived from the exact solution of the corresponding local differential equation, ensuring that the scheme captures the exponential behavior of the layer solutions while preserving essential qualitative properties such as stability, positivity, and correct asymptotic behavior even on a coarse mesh.

The spatial domain $\bar{\Omega} = [0, 1]$ is discretized using uniform space length h as

$$\overline{\Omega}^N = \left\{x_i = ih, i = 1, ..., N-1, x_0 = 0, x_N = 1, h = \frac{1}{N}\right\},$$

where N is the number of mesh intervals in the spatial discretization. Now, consider (6.5) using the lower bounds of the coefficients and the homogeneous part

$$c_\varepsilon u_{xx} + p^* u_x - \gamma u = 0. \tag{6.12}$$

$$c_\varepsilon u_{xx} + p^* u_x = 0. \tag{6.13}$$

Since the layer behaviour of (6.12) and (6.13) are the same. The finite difference scheme that replaced h^2 by a non-negative denominator function ξ^2 is

$$c_\varepsilon \frac{U_{i+1} - 2U_i + U_{i-1}}{\xi_i^2} + p^* \frac{U_{i+1} - U_i}{h} = 0. \tag{6.14}$$

We can find ξ_i^2 using the following procedures. First, we rewrite equation (6.13) equivalently as a first-order coupled system of differential equations

$$\frac{du}{dx} = v, \tag{6.15}$$

$$\frac{dv}{dx} = \frac{-p^*}{c_\varepsilon} v. \tag{6.16}$$

From (6.16) we have $v(x) = exp(-\frac{p^*}{c_\varepsilon} x)$. By applying first order difference scheme for (6.15) as:

$$v_i = \frac{U_{i+1} - U_i}{h} = \exp\left(-\frac{p^*}{c_\varepsilon} x_i\right), \tag{6.17}$$

then substituting (6.17) into (6.14) we obtain the denominator function $\xi_i^2 = \frac{hc_\varepsilon}{p^*}(exp(\frac{hp^*}{c_\varepsilon}) - 1) \equiv h^2 + O(\frac{h^3}{c_\varepsilon})$. So equation (6.14) becomes

$$c_\varepsilon \frac{(U_{i+1} - 2U_i + U_{i-1})}{\frac{hc_\varepsilon}{p^*}(\exp\left(\frac{hp^*}{c_\varepsilon}\right) - 1)} + p^* \frac{(U_{i+1} - U_i)}{h} = 0.$$

Therefore, the denominator function $\xi^2 = \frac{hc_\varepsilon}{p^*}(\exp\left(\frac{hp^*}{c_\varepsilon}\right) - 1)$ can replace h^2. Adopting this denominator function to the variable coefficient problem written as

$$\xi^2(c_\varepsilon, h) = \frac{hc_\varepsilon}{p_i^{j+1}}(\exp\left(\frac{hp_i^{j+1}}{c_\varepsilon}\right) - 1), \tag{6.18}$$

6.4.3 Full Discrete Scheme

Using (6.18) and (6.5) the full discrete scheme becomes

$$\begin{gathered}\hat{\mathcal{K}_{c_\varepsilon}}^N U^{j+1}(x_i) \equiv \frac{c_\varepsilon}{2} \frac{(U_{i+1}^{j+1} - 2U_i^{j+1} + U_{i-1}^{j+1})}{\xi_{i,j+1}^2} + \frac{p_i^{j+1}}{2} \frac{(U_{i+1}^{j+1} - U_i^{j+1})}{h} - (\frac{q_i^{j+1}}{2} + \frac{1}{\Delta t})U_i^{j+1} = H_i^{j+1}, \\ u_0^{j+1} = \phi(t_{j+1}), u_N^{j+1} = \psi(t_{j+1}), u_i^0 = u_0(x_i),\end{gathered} \tag{6.19}$$

$$i = 1, 2, 3, ..., N-1, \;\; j = 0, 1, 2, ..., M-1,$$

where

$$H_i^{j+1} = -\frac{c_\varepsilon}{2}\frac{(U_{i+1}^j - 2U_i^j + U_{i-1}^j)}{\xi_{i,j}^2} - \frac{p_i^j}{2}\frac{(U_{i+1}^j - U_i^j)}{h} + (\frac{q_i^j}{2} - \frac{1}{\Delta t})U_i^j + \frac{f_i^{j+1} + f_i^j}{2}.$$

After rearrange the terms in (6.19), we arrive the following recurrence relation of the form

$$r_i^- U_{i-1}^{j+1} + r_i^c U_i^{j+1} + r_i^+ U_{i+1}^{j+1} = s_i^- U_{i-1}^j + s_i^c U_i^j + s_i^+ U_{i+1}^j + \frac{f_i^{j+1} + f_i^j}{2}, \tag{6.20}$$

where the coefficients are given by

$$\begin{cases} r_i^- = \dfrac{c_\varepsilon}{2\xi_{i,j+1}^2}, \\ r_i^c = -(\dfrac{c_\varepsilon}{\xi_{i,j+1}^2} + \dfrac{p_i^{j+1}}{2h} + \dfrac{q_i^{j+1}}{2} + \dfrac{1}{\Delta t}), \\ r_i^+ = \dfrac{c_\varepsilon}{2\xi_{i,j+1}^2} + \dfrac{p_i^{j+1}}{2h}, \end{cases} \qquad \begin{cases} s_i^- = -\dfrac{c_\varepsilon}{2\xi_{i,j}^2}, \\ s_i^c = \dfrac{c_\varepsilon}{\xi_{i,j}^2} + \dfrac{p_i^j}{2h} + \dfrac{q_i^j}{2} - \dfrac{1}{\Delta t}, \\ s_i^+ = -(\dfrac{c_\varepsilon}{2\xi_{i,j}^2} + \dfrac{p_i^j}{2h}). \end{cases}$$

Since $|r_i^c| \geq |r_i^-| + |r_i^+|$, the tri-diagonal system (6.20) is diagonally dominant system of equations. So it has a unique solution. Thus, we can use any tri-diagonal solver, such as Thomas algorithm, to solve this system of equations.

6.5 Convergence Analysis

In this section, we study the discrete minimum principle, stability and $\varepsilon-$uniform convergence for the scheme (6.20) .

Lemma 6.6. *(**The discrete minimum principle**) Assume that* $U_0^{j+1} \geq 0, U_N^{j+1} \geq 0$ *and* $\hat{\mathcal{K}}_{c_\varepsilon}^N U_i^{j+1} \leq 0$ for $0 < i < N, 0 \leq j < M$ *Then,* $U_i^{j+1} \geq 0$ $\; for \;$ $0 < i < N, 0 \leq j < M.$

Proof. Suppose there exist $s \in \{0, 1, 2, ..., N\}$ such that $U_s^{j+1} = \min\limits_{0 \leq i \leq N} U_i^{j+1} < 0$ which implies $k \neq 0$ and

$k \neq N$. Also we have $(U_{s+1}^{j+1} - U_s^{j+1}) > 0$ and $(U_{s-1}^{j+1} - U_s^{j+1}) > 0$. Then,

$$\begin{aligned}
\hat{\mathcal{K}}_{c_\varepsilon}^N u_s^{j+1} &= c_\varepsilon \frac{(U_{s+1}^{j+1} - 2U_s^{j+1} + U_{s-1}^{j+1})}{\xi^2} + p_s^{j+1} \frac{(U_{s+1}^{j+1} - U_s^{j+1})}{h} - (q_s^{j+1} + \frac{1}{\Delta t})U_s^{j+1} \\
&= c_\varepsilon \frac{(U_{s+1}^{j+1} - U_s^{j+1}) + (U_{s-1}^{j+1} - U_s^{j+1})}{\xi^2} + p_s^{j+1} \frac{(U_{s+1}^{j+1} - U_s^{j+1})}{h} - (q_s^{j+1} + \frac{1}{\Delta t})U_s^{j+1} > 0,
\end{aligned}$$

since $(q_s^{j+1} + \frac{1}{\Delta t}) > \beta > 0$. It contradict the assumption that $\hat{\mathcal{K}}_{c_\varepsilon}^N U_i^{j+1} \leq 0 \; for \; 0 < i < N, 0 \leq j < M$. Therefore, the operator $\hat{\mathcal{K}}_{c_\varepsilon}^N$ satisfy the discrete minimum principle. □

Lemma 6.7 (**Stability Estimate**). *The solution of the discrete problem* (6.20) *satisfies the bound*

$$\left|u_i^{j+1}\right| \leq \left|\left|\hat{\mathcal{K}}_{c_\varepsilon}^N u_i^{j+1}\right|\right| + \max(|\psi(t_{j+1})|, |\phi(t_j+1)|).$$

Proof. Consider the barrier functions

$$\psi^{\pm}(x_i, t_{j+1}) = \left|\left|\hat{\mathcal{K}}_{c_\varepsilon}^N u_i^{j+1}\right|\right| + \max(|\psi(t_{j+1})|, |\phi(t_{j+1})|) \pm u_i^{j+1}$$

At the boundary points we have

$$\psi^{\pm}(0, t_{j+1}) = \left|\left|\hat{\mathcal{K}}_{c_\varepsilon}^N u_0^{j+1}\right|\right| + \max(|\psi(t_{j+1})|, |\phi(t_{j+1})|) \pm u_0^{j+1} \geq 0$$

$$\psi^{\pm}(1, t_{j+1}) = \left|\left|\hat{\mathcal{K}}_{c_\varepsilon}^N u_N^{j+1}\right|\right| + \max(|\psi(t_{j+1})|, |\phi(t_{j+1})|) \pm u_N^{j+1} \geq 0$$

For the interior points we have

$$\begin{aligned}
\hat{\mathcal{K}}_{c_\varepsilon}^N \psi_{i,j+1}^{\pm} =& \varepsilon \delta_x^2 \psi_{i,j+1}^{\pm} + p_i^{j+1} D_x^+ \psi_{i,j+1}^{\pm} - (q_i^{j+1} + \frac{1}{\Delta t})\psi_{i,j+1}^{\pm} \\
=& c_\varepsilon \delta_x^2 \psi_{i,j+1}^{\pm} + p_i^{j+1} D_x^+ \psi_{i,j+1}^{\pm} - (q_i^{j+1} + \frac{1}{\Delta t})(\left|\left|\hat{\mathcal{K}}_{c_\varepsilon}^N u_i^{j+1}\right|\right| + \max(|\psi(t_{j+1})|, |\phi(t_{j+1})|) \pm u_i^{j+1}) \\
=& -(b_i^{j+1} + \frac{1}{\Delta t})(\left|\left|\hat{\mathcal{K}}_{c_\varepsilon}^N u_i^{j+1}\right|\right| + \max(|\psi(t_{j+1})|, |\phi(t_{j+1})|)) \pm \hat{\mathcal{K}}_{c_\varepsilon}^N u_i^{j+1} \\
\leq& 0.
\end{aligned}$$

Now, using Lemma 6.6 we get the desired result. □

Lemma 6.8. *For $c_\varepsilon \to 0$ and for fixed mesh , it holds*

$$\lim_{c_\varepsilon \to 0} \frac{\exp\Big(-x_i\sqrt{(p^*/c_\varepsilon)}\Big)}{(\sqrt{c_\varepsilon})^s} = 0, \;\; s \in Z^+ \quad \textit{and} \quad c_\varepsilon \left|1 - \frac{h^2}{\xi^2}\right| \leq Ch.$$

Proof.

$$\frac{\exp\Big(-x_i\sqrt{(p^*/c_\varepsilon)}\Big)}{(\sqrt{c_\varepsilon})^s} \leq \frac{\exp\Big(-x_1\sqrt{(p^*/c_\varepsilon)}\Big)}{(\sqrt{c_\varepsilon})^s} = \frac{\exp\Big(-h\sqrt{(p^*/\varepsilon)}\Big)}{(\sqrt{c_\varepsilon})^s} \quad for \;\; i = 1, 2, ..., N.$$

Let $\eta = 1/\sqrt{c_\varepsilon}$, then

$$\lim_{c_\varepsilon \to 0} \frac{\exp\Big(-h\sqrt{(p^*/c_\varepsilon)}\Big)}{(\sqrt{c_\varepsilon})^s} = \lim_{\eta \to \infty} \frac{\eta^s}{\exp(h\sqrt{p^*}\eta)}.$$

Applying L'Hospitals rule repeatedly we have

$$\lim_{c_\varepsilon \to 0} \frac{\exp\Big(-h\sqrt{(\alpha/c_\varepsilon)}\Big)}{(\sqrt{c_\varepsilon})^s} = \lim_{\eta \to \infty} \frac{\eta^s}{\exp(h\sqrt{p^*}\eta)} = \lim_{\eta \to \infty} \frac{s!}{(h\sqrt{p^*})^s \exp(h\sqrt{p^*}\eta)} = 0.$$

And

$$c_\varepsilon \left|1 - \frac{h^2}{\xi^2}\right| = c_\varepsilon \left|1 - \frac{h^2}{\frac{c_\varepsilon h}{\alpha}(\exp\Big(\frac{p^*h}{c_\varepsilon}\Big) - 1)}\right| = c_\varepsilon \left|1 - \frac{p^*h}{\varepsilon(\exp\Big(\frac{p^*h}{c_\varepsilon}\Big) - 1)}\right| = p^*h\left|\frac{c_\varepsilon}{p^*h} - \frac{1}{\exp\Big(\frac{p^*h}{c_\varepsilon}\Big) - 1}\right|.$$

Let $\sigma = \frac{p^*h}{c_\varepsilon}$, then using L'Hospital's rule repeatedly we have the following

$$\lim_{\sigma \to 0} p^*h(\frac{1}{\sigma} - \frac{1}{\exp(\sigma) - 1}) = \frac{1}{2}p^*h \;, \;\; \lim_{\sigma \to \infty} p^*h(\frac{1}{\sigma} - \frac{1}{\exp(\sigma) - 1}) = 0.$$

Therefore, $c_\varepsilon \left|1 - \frac{h^2}{\xi^2}\right| = p^*h(\frac{1}{\sigma} - \frac{1}{\exp(\sigma)-1}) \leq Ch$ for $\sigma \in (0, \infty)$. ☐

Theorem 6.6. *Let $U^{j+1}(x_i)$ and U_i^{j+1} are the exact solution of (6.5) and the numerical solution of (6.20) respectively. Then, the proposed scheme satisfies the following error bound at $(j+1)^{th}$ time level;*

$$\sup_{0 < c_\varepsilon \leq 1} \left|u^{j+1}(x_i) - U_i^{j+1}\right| \leq CN^{-1}.$$

Proof. The truncation error in the spatial discretization is

$$\begin{aligned}\left|\hat{\mathcal{K}_{c_\varepsilon}}^N(U^{j+1}(x_i)-U_i^{j+1})\right| &= \left|(\hat{\mathcal{K}_{c_\varepsilon}}U^{j+1}(x_i)-\hat{\mathcal{K}_{c_\varepsilon}}^N U_i^{j+1})\right| \\ &\le \left|c_\varepsilon(\frac{d^2}{dx^2}-\delta_x^2)U_i^{j+1}+p_i^{j+1}(\frac{d}{dx}-D^+)U_i^{j+1}\right|,\end{aligned}$$

where

$$\delta_x^2 U_i^{j+1}=\frac{U_{i+1}^{j+1}-2U_i^{j+1}+U_{i-1}^{j+1}}{\xi^2} \ \ and \ \ D_x^+U_i^{j+1}=\frac{(U_{i+1}^{j+1}-U_i^{j+1})}{h}.$$

Now, using Taylor series expansion of $U_{i+1},\ \ U_{i-1},\ \ \xi^2$ and bounds on the derivatives of U Theorem 6.5 we have the following,

$$\begin{aligned}\left|\hat{\mathcal{K}}_{c_\varepsilon}U^{j+1}(x_i)-\hat{\mathcal{K}}_{c_\varepsilon}^N U_i^{j+1}\right| &\le \left|\left(c_\varepsilon\left(1-\frac{h^2}{\xi^2}\right)-\frac{hp_i^{j+1}}{2}\right)\frac{d^2U^{j+1}(x_i)}{dx^2}-p_i^{j+1}\frac{h^2}{6}\frac{d^3U^{j+1}(x_i)}{dx^3}-p_i^{j+1}\frac{c_\varepsilon h^4}{12\xi^2}\frac{d^4U^{j+1}(x_i)}{dx^4}\right| \\ &\le C\left(h\left(1+c_\varepsilon^{-1}e^{-x_i\sqrt{\alpha/c_\varepsilon}}\right)+h^2\left(1+c_\varepsilon^{-3/2}e^{-x_i\sqrt{\alpha/c_\varepsilon}}\right)+\frac{c_\varepsilon h^4}{\xi^2}\left(1+c_\varepsilon^{-2}e^{-x_i\sqrt{\alpha/c_\varepsilon}}\right)\right) \\ &\le C\left(h\left(1+c_\varepsilon^{-1}e^{-x_i\sqrt{\alpha/c_\varepsilon}}\right)+h^2\left(1+c_\varepsilon^{-3/2}e^{-x_i\sqrt{\alpha/c_\varepsilon}}\right)+h^3\left(1+c_\varepsilon^{-2}e^{-x_i\sqrt{\alpha/c_\varepsilon}}\right)\right).\end{aligned}$$

Since $h^3<h^2<h$ and using Lemma 6.7 and 6.8 , we have $\left|(U^{j+1}(x_i)-U_i^{j+1})\right|\le CN^{-1}$. □

Theorem 6.7. *The solution U_i^{j+1} of the fully discrete scheme (6.20) converges uniformly to the solution $u(x,t)$ of (6.3) and the error estimate is given by*

$$\sup_{0<c_\varepsilon\le 1}\left|u(x_i,t_j)-U_i^{j+1}\right|\le C(N^{-1}+(\Delta t)^2), \qquad i=0,1,2,...,N,\ \ j=0,1,2,...,M.$$

Proof. The uniform convergence of the scheme follows from the Theorem 6.4 and 6.6. We justify it as follows

$$\begin{aligned}\sup_{0<c_\varepsilon\le 1}\left|u(x_i,t_{j+1})-U_i^{j+1}\right| &\le \sup_{0<c_\varepsilon\le 1}\left|u(x_i,t_{j+1})-U^{j+1}(x_i)\right| \\ &+\sup_{0<c_\varepsilon\le 1}\left|U^{j+1}(x_i)-U_i^{j+1}\right|\le C(N^{-1}+(\Delta t)^2), \quad i=0,1,2,...,N,\ \ j=0,1,2,...,M.\end{aligned}$$

□

6.6 Numerical Examples and Results

In order to check the performance of the proposed method, we used model examples on the underlying interval for different values of mesh size(h,k), shift parameters μ,δ and perturbation parameter ε. Since the exact solutions for these problems are not known, the maximum absolute errors are computed using double - mesh principles given by:

$$e_{c_\varepsilon}^{M,N} = \max_{(x_i,t_j)\in D} \left| \left(U_i^j\right)^{M,N} - \left(U_i^j\right)^{2M,2N} \right|$$

where $\left(U_i^j\right)^{M,N}$ is the numerical solution obtained using mesh sizes (h,k) and $\left(U_i^j\right)^{2M,2N}$ is the numerical solution obtained by halving the original mesh (h,k). The corresponding parameter uniform error is given by

$$e^{M,N} = \max e_{c_\varepsilon}^{M,N}$$

Additionally, we assessed the corresponding rate of convergence using the following formulas:

$$R_{c_\varepsilon}^{M,N} = \frac{\log e_{c_\varepsilon}^{M,N} - \log e_{c_\varepsilon}^{2M,2N}}{\log 2}, R^{M,N} = \frac{\log e^{M,N} - \log e^{2M,2N}}{\log 2}.$$

Example 6.1. *Consider the singularly perturbed parabolic convection–diffusion turning-point problem with general shifts [98]*

$$\begin{cases} \varepsilon u_{xx} + x^p u_x(x,t) - 2u(x-\delta,t) - u(x,t) - u(x+\mu,t) - u_t(x,t) = x^2 - 1, \quad (x,t) \in \mathcal{D}, \\ u(x,0) = (1-x)^2, \quad x \in \overline{\Omega}, \\ u(x,t) = 1 + t^2, \quad (x,t) \in [-\delta,0] \times (0,1], \\ u(x,t) = 0, \quad (x,t) \in [1,1+\mu] \times (0,1]. \end{cases}$$

Example 6.2. *Consider the singularly perturbed parabolic convection–diffusion turning-point problem with general shifts*

$$\begin{cases} \varepsilon u_{xx} + (1+te^{-2t}) x^p u_x(x,t) - 2u(x-\delta,t) - u(x,t) - u(x+\mu,t) - u_t(x,t) = (x^2 - 1)e^{-t}, \quad (x,t) \in \mathcal{D}, \\ u(x,0) = (1-x)^2, \quad x \in \overline{\Omega}, \\ u(x,t) = 1 + t^2, \quad (x,t) \in [-\delta,0] \times (0,1], \\ u(x,t) = 0, \quad (x,t) \in [1,1+\mu] \times (0,1]. \end{cases}$$

The numerical results in Tables 6.1 and 6.4 for Examples 6.1 and 6.2, respectively, present the maximum absolute error and the convergence rate of the scheme for fixed delay and advance parameters. These results

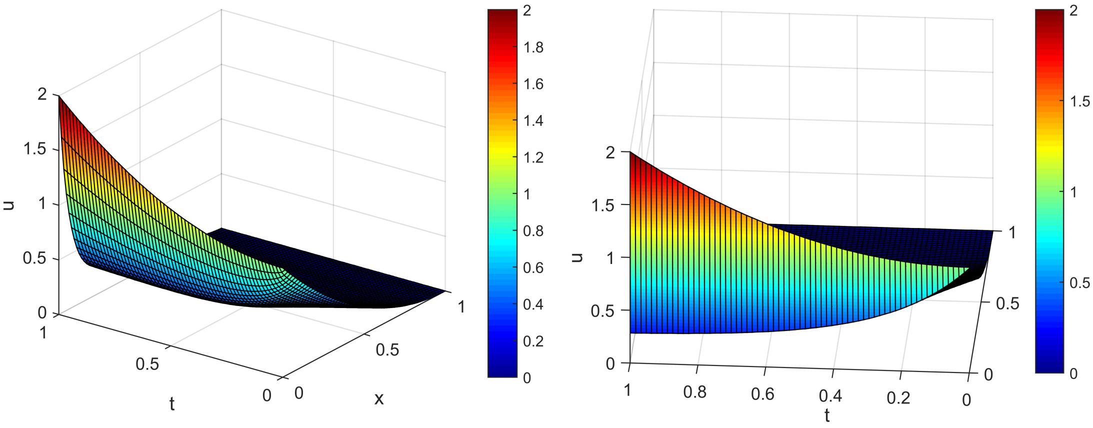

(a) $\varepsilon = 2^{-2}$ (b) $\varepsilon = 2^{-12}$

Figure 6.1: Surface plots of the numerical solution for Example 6.2 with $M = N = 64$, $p = 1$, and parameters $\delta = 0.6\varepsilon$, $\mu = 0.5\varepsilon$.

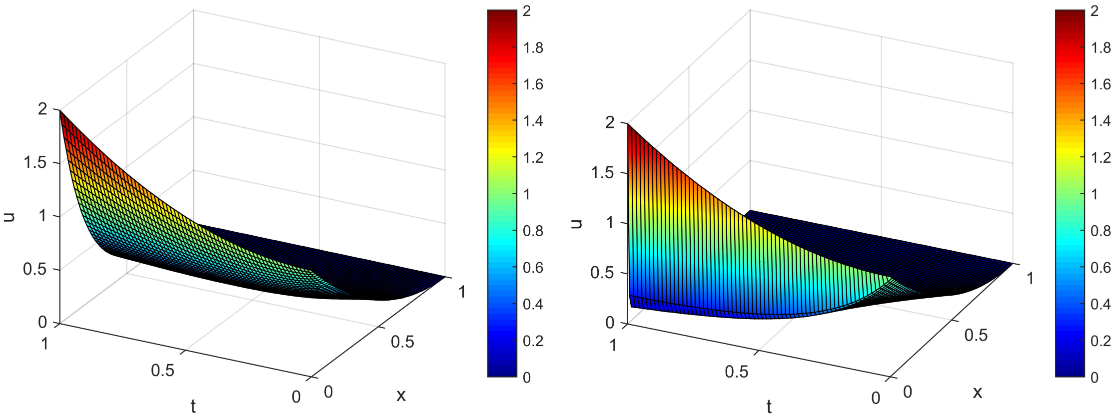

(a) $\varepsilon = 2^{-2}$ (b) $\varepsilon = 2^{-12}$

Figure 6.2: Surface plots of the numerical solution for Example 6.1 with $M = N = 64$, $p = 1$, and parameters $\delta = 0.4\varepsilon$, $\mu = 0.8\varepsilon$.

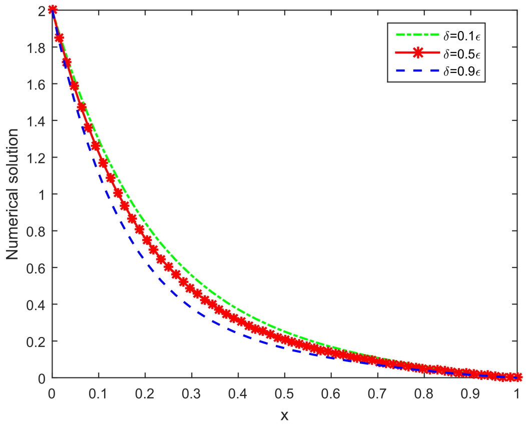

(a) $\varepsilon = 2^{-2}, p = 1, \mu = 0$

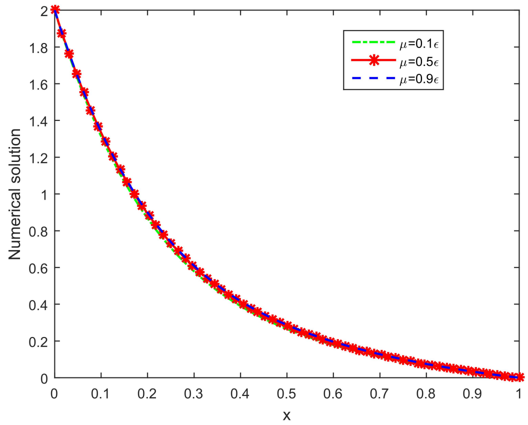

(b) $\varepsilon = 2^{-2}, p = 1, \delta = 0$

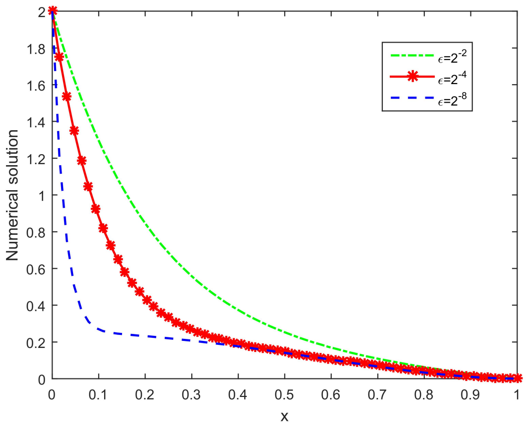

(c) $\delta = 0.2\epsilon, \mu = 0.3\varepsilon, p = 1$

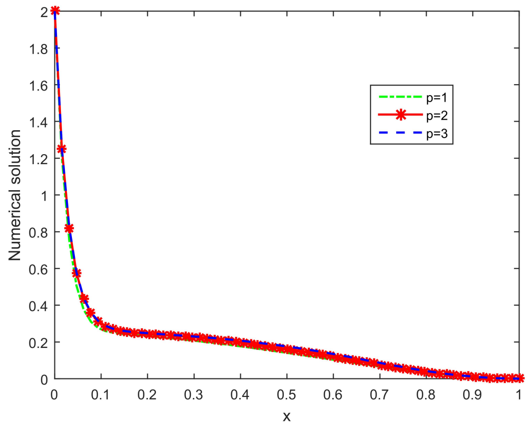

(d) $\delta = 0.4\varepsilon, \mu = 0.8\varepsilon, \varepsilon = 2^{-8}$

Figure 6.3: Example 6.1 on (a)effect of δ , (b) effect of μ, (c) influence of ε (d) effect of p on the solution, for $M = N = 64$.

Table 6.1: Maximum absolute error and rate of convergence for Example 5.1 for $p = 1$ and $\delta = 0.9\varepsilon, \mu = 0.5\varepsilon$

$\varepsilon \downarrow M = N \rightarrow$	32	64	128	256	512	1024
2^{-6}	1.2570e-03	6.5744e-04	3.3678e-04	1.7085e-04	5.5905e-05	2.8024e-05
	0.9350	0.9651	0.9792	0.9926	0.9963	
2^{-10}	1.2582e-03	6.5936e-04	3.3763e-04	1.7089e-04	8.5965e-05	4.3181e-05
	0.9323	0.9656	0.9823	0.9913	0.9934	
2^{-14}	1.2583e-03	6.5948e-04	3.3769e-04	1.7092e-04	8.5980e-05	4.3252e-05
	0.9321	0.9656	0.9824	0.9913	0.9912	
2^{-16}	1.2583e-03	6.5948e-04	3.3769e-04	1.7092e-04	8.5980e-05	4.3292e-05
	0.9321	0.9656	0.9824	0.9913	0.9899	
2^{-18}	1.2583e-03	6.5948e-04	3.3769e-04	1.7092e-04	8.5980e-05	4.3292e-05
	0.9321	0.9656	0.9824	0.9913	0.9899	
$e^{M,N}$	1.2583e-03	6.5948e-04	3.3769e-04	1.7092e-04	8.5980e-05	4.3292e-05
$R^{M,N}$	0.9321	0.9656	0.9824	0.9913	0.9899	
In [98]: $e_\varepsilon^{M,N}$	2.044e-02	1.303e-02	7.866e-03	4.607e-03		
$R_\varepsilon^{M,N}$	0.7	0.77	0.85	0.93		

Table 6.2: Maximum absolute error and rate of convergence for Example 5.1 with $p = 1$ and different values of δ and μ for $\varepsilon = 2^{-10}$

$M = N \rightarrow$	32	64	128	256	512	1024
$\delta \downarrow, \mu = 0.5\varepsilon$						
0	1.2583e-03	6.5954e-04	3.3772e-04	1.7094e-04	8.5968e-05	4.3281e-05
	0.9319	0.9656	0.9824	0.9916	0.9901	
0.3ε	1.2583e-03	6.5948e-04	3.3769e-04	1.7092e-04	8.5970e-05	4.3282e-05
	0.9321	0.9656	0.9824	0.9914	0.9901	
0.6ε	1.2583e-03	6.5942e-04	3.3766e-04	1.7091e-04	8.5972e-05	4.3283e-05
	0.9322	0.9656	0.9823	0.9913	0.9901	
$\mu \downarrow, \delta = 0.5\varepsilon$						
0	1.2583e-03	6.5939e-04	3.3764e-04	1.7090e-04	8.5971e-05	4.3282e-05
	0.9322	0.9656	0.9823	0.9913	0.9901	
0.3ε	1.2583e-03	6.5942e-04	3.3766e-04	1.7091e-04	8.5974e-05	4.3283e-05
	0.9322	0.9656	0.9823	0.9913	0.9901	
0.6ε	1.2583e-03	6.5945e-04	3.3768e-04	1.7092e-04	8.5976e-05	4.3284e-05
	0.9321	0.9656	0.9823	0.9913	0.9901	

demonstrate the uniform convergence of the proposed scheme. As shown in the tables, when the perturbation parameter ε decreases, the maximum absolute error stabilizes and becomes constant, indicating convergence independent of ε. Additionally, Table 6.1 compares the $\varepsilon-$uniform errors and convergence rates of the proposed scheme with that reported in the literature. The results demonstrate that our scheme achieves higher accuracy than the method presented in [98]. Tables 6.2 and 6.5 present the maximum absolute errors for various values of the delay and advance parameters. The results indicate that the shift parameters do not affect

Table 6.3: Maximum absolute error and its corresponding rate of convergence for $\varepsilon = 2^{-5}$ with different values of p.

$p \downarrow,\ M = N \rightarrow$	32	64	128	256	512	1024
$\delta = 0.4\varepsilon,\ \mu = 0.8\varepsilon$						
2	5.6269e-03	2.7727e-03	1.4847e-03	7.4793e-04	3.7731e-04	1.8962e-04
	1.0211	0.9011	0.9892	0.9871	0.9926	
3	5.6397e-03	2.7751e-03	1.4855e-03	7.4812e-04	3.7736e-04	1.8964e-04
	1.0231	0.9016	0.9893	0.9873	0.9927	
$\delta = 0.2\varepsilon,\ \mu = 0.4\varepsilon$						
2	5.1552e-03	2.5150e-03	1.3505e-03	6.8171e-04	3.4201e-04	1.7132e-04
	1.0355	0.8971	0.9862	0.9951	0.9975	
3	5.1682e-03	2.5191e-03	1.3513e-03	6.8191e-04	3.4206e-04	1.7134e-04
	1.0367	0.8986	0.9866	0.9954	0.9975	

Table 6.4: Maximum absolute error and rate of convergence for Example 6.2 for $p = 1$ and $\delta = 0.3\varepsilon, \mu = 0.0\varepsilon$

$\varepsilon \downarrow M = N \rightarrow$	32	64	128	256	512	1024
2^{-1}	2.8347e-03	1.4723e-03	7.5289e-04	3.9214e-04	2.0158e-04	1.0246e-04
	0.9451	0.9676	0.9411	0.9600	0.9763	
2^{-2}	3.6248e-03	1.8935e-03	9.8276e-04	5.1182e-04	2.6617e-04	1.3742e-04
	0.9368	0.9461	0.9412	0.9435	0.9538	
2^{-4}	5.2316e-03	2.7358e-03	1.4284e-03	7.4253e-04	3.8621e-04	1.9945e-04
	0.9353	0.9378	0.9438	0.9431	0.9533	
2^{-6}	6.8342e-03	3.6175e-03	1.9087e-03	1.0036e-03	5.3142e-04	2.8068e-04
	0.9177	0.9225	0.9274	0.9175	0.9208	
2^{-8}	8.1246e-03	4.2138e-03	2.2065e-03	1.1537e-03	6.0148e-04	3.1582e-04
	0.9472	0.9332	0.9357	0.9397	0.9294	
2^{-9}	8.3152e-03	4.3617e-03	2.3074e-03	1.2032e-03	6.3125e-04	3.3173e-04
	0.9309	0.9186	0.9394	0.9308	0.9282	
2^{-10}	8.4268e-03	4.4329e-03	2.3458e-03	1.2336e-03	6.5147e-04	3.4268e-04
	0.9268	0.9181	0.9273	0.9213	0.9268	
2^{-12}	8.7526e-03	4.6135e-03	2.4529e-03	1.2917e-03	6.8042e-04	3.5826e-04
	0.9238	0.9116	0.9252	0.9249	0.9254	
2^{-14}	8.7526e-03	4.6135e-03	2.4529e-03	1.2917e-03	6.8042e-04	3.5826e-04
	0.9238	0.9116	0.9252	0.9249	0.9254	
$e^{M,N}$	8.7526e-03	4.6135e-03	2.4529e-03	1.2917e-03	6.8042e-04	3.5826e-04
$R^{M,N}$	0.9238	0.9116	0.9252	0.9249	0.9254	

the uniform convergence of the proposed scheme. In Table 6.3, we present the maximum absolute errors for a fixed ε across different values of p. The results demonstrate that the value of p does not affect the uniform convergence of the scheme. Overall, from each tables it can be observed that the convergence of the scheme

Table 6.5: Maximum absolute error and rate of convergence for Example 6.2 with $p = 2$ and different values of δ and μ for $\varepsilon = 2^{-7}$

$M = N \rightarrow$	32	64	128	256	512	1024
$\delta \downarrow,\ \mu = 0.5\varepsilon$						
0	6.1853e-03	3.2827e-03	1.7435e-03	9.2687e-04	4.9345e-04	2.6317e-04
	0.9140	0.9129	0.9116	0.9095	0.9069	
0.2ε	6.1984e-03	3.2914e-03	1.7491e-03	9.3070e-04	4.9616e-04	2.6507e-04
	0.9132	0.9121	0.9102	0.9075	0.9044	
0.4ε	6.2086e-03	3.3002e-03	1.7547e-03	9.3454e-04	4.9887e-04	2.6697e-04
	0.9117	0.9113	0.9089	0.9056	0.9020	
0.6ε	6.2194e-03	3.3090e-03	1.7604e-03	9.3839e-04	5.0159e-04	2.6888e-04
	0.9104	0.9105	0.9076	0.9037	0.8996	
$\mu \downarrow,\ \delta = 0.6\varepsilon$						
0	6.2312e-03	3.3179e-03	1.7661e-03	9.4225e-04	5.0432e-04	2.7079e-04
	0.9092	0.9097	0.9064	0.9018	0.8972	
0.2ε	6.2427e-03	3.3268e-03	1.7719e-03	9.4612e-04	5.0705e-04	2.7271e-04
	0.9080	0.9088	0.9052	0.8999	0.8948	
0.4ε	6.2544e-03	3.3357e-03	1.7776e-03	9.5000e-04	5.0979e-04	2.7464e-04
	0.9069	0.9081	0.9039	0.8980	0.8924	
0.6ε	6.2662e-03	3.3447e-03	1.7834e-03	9.5389e-04	5.1254e-04	2.7657e-04
	0.9057	0.9073	0.9027	0.8962	0.8900	

is independent of the parameters.

The solution of the problems in Examples 6.1 and 6.2 exhibit a boundary layer on the left side of the spatial domain. In Figures 6.1 and 6.2 one can observe its formation as the perturbation parameter goes small. Figure 6.3 illustrates the influence of the shift parameters (μ and δ), the perturbation parameter (ε), and the exponent p on the solution profile by varying each parameter individually. As shown in Figure 6.3a, increasing the values of δ increases the steepness of the boundary layer, while the layer thickness remains essentially unchanged. In contrast, Figure 6.3b shows that this effect is less pronounced under the corresponding parameter configuration. Figure 6.3c demonstrates that as $\varepsilon \rightarrow 0$, the solution exhibits a sharper boundary layer, with a noticeable reduction in the layer width. This behavior is consistent with the nature of singularly perturbed problems, where smaller perturbation parameters lead to thinner and steeper boundary layers. Finally, Figure 6.3d shows that as p increases, the convection coefficient becomes more strongly varying near the boundary. This modifies the gradient of the solution and may slightly shift the layer location; however, the boundary layer thickness remains primarily governed by the perturbation parameter ε. Thus, variations in p influence the solution profile but do not significantly alter the asymptotic thickness of the boundary layer. In all cases, the influence of these parameters becomes more visible for relatively large values of ε, where the interaction between convection, diffusion, and shift terms is more apparent in the solution profile.

6.7 Conclusion

This chapter presents a uniformly convergent numerical scheme for solving singularly perturbed parabolic differential-difference equations with both delay and advance terms in the spatial variable, with boundary turning point. As the perturbation parameter tends to zero, the solution develops a left boundary layer in the spatial domain. The proposed scheme combines the Crank-Nicolson method for time discretization with a nonstandard finite difference method in space on a uniform mesh. A detailed analysis is provided to establish the stability and uniform convergence of the method. To validate its applicability, the scheme is tested on model examples, and the effects of the perturbation parameter and shift parameters on the solution are illustrated graphically. The method is shown to converge uniformly with linear order. Furthermore, a comparison with existing method from the literature demonstrates that the proposed scheme delivers higher accuracy and uniform convergence over previous approach.

Chapter 7

Layer-Resolving Mesh Method for Singularly Perturbed Parabolic Convection-Diffusion Turning Point Problems with General Shifts

In this chapter, we devised a uniformly convergent numerical scheme for solving SPP considered in chapter 6. The solutions to such problems typically exhibit a left boundary layer due to the presence of a small perturbation parameter on the diffusion term. To resolve the boundary layer, we employ a piecewise-uniform Shishkin mesh in the spatial direction while maintaining a uniform mesh in the temporal direction. For discretization, we combined the Crank–Nicolson method for temporal derivatives with a hybrid finite difference scheme for spatial derivatives. We established almost second order ε-uniform convergence of the proposed method through rigorous theoretical analysis. Numerical experiments are presented to validate the theoretical error estimates and demonstrate the scheme's efficiency in handling boundary layer and turning point phenomena.

7.1 Introduction

Unlike singularly perturbed differential equations (SPDEs) that relate a function to its derivatives at the same instant, singularly perturbed delay/advance partial differential equations model systems whose behavior depends on both present state and past history. As the perturbation parameter approaches zero, the solution of SPDDEs typically loses smoothness and develops boundary layers [41]. Such type of problems have variety of applications in the study of variational problems in control theory [35], modeling neuronal variability [118] and analysing neural responses to random synaptic inputs [124, 125].

The presence of ε in the highest-order derivative term often leads to the formation of boundary layers or interior layers, where the solution exhibits rapid variations. These layers require advanced numerical techniques to resolve accurately, as standard methods may fail to capture the sharp transitions. Different scholars have developed various numerical methods for solving singularly perturbed parabolic differential-difference equations (SPPDDEs) [14, 15, 13, 57, 101, 102], and singularly perturbed turning point problems (with or without delays) have also been well-studied [72, 73, 66, 29, 59, 4, 108, 111, 67]. However, SPPDDEs with turning points were studied for the first time in [98]. To the best of our knowledge, no further studies have been conducted to solve such problems. Since the previous work achieved only first-order convergence, we developed an almost second-order convergent method. To obtain a more accurate numerical solution than the previously mentioned approaches, this study employs the Crank–Nicolson method for time discretization on a uniform mesh and the central finite difference method in the layer region and midpoint upwind in outer layer region for spatial discretization on a Shishkin mesh.

7.2 Description of the Problem

This chapter investigates a singularly perturbed parabolic convection–diffusion turning-point problem with general shifts discussed in chapter 6.

7.3 Bounds of Continuous Solution

To avoid redundancy, the analytical properties of the continuous solution (continuous minimum principle, stability estimates, and derivative bounds) are established in Chapter 6. These results are omitted here but will be referenced as needed in the subsequent analysis.

7.4 Derivation of the Numerical Method

7.4.1 Time Discretization

In this subsection, a similar semi-discretization and error analysis are used as in chapter 6, Subsection 6.4.1. To avoid redundancy, the details are omitted here, as the model problem is the same as that in chapter 6 and will be referenced whenever necessary.

7.4.2 Spatial Discretization

The spatial domain $\overline{\Omega} = [0, 1]$ is discretized using a piecewise-uniform Shishkin mesh to resolve the boundary layer near $x = 0$. The interval is partitioned as $[0, 1] = [0, \omega] \cup (\omega, 1]$, where the transition point ω separates the fine and coarse regions and is defined by

$$\omega = \min \left\{ \frac{1}{2}, \frac{2\sqrt{c_\varepsilon}}{\sqrt{p^*}} \ln N \right\}. \tag{7.1}$$

Each sub-interval is uniformly subdivided into $N/2$ segments, giving the grid

$$\overline{\Omega}^N = \{x_0, x_1, \ldots, x_N\}, \quad x_0 = 0,\ x_N = 1,$$

with

$$x_i = \begin{cases} i\frac{2\omega}{N}, & 0 \le i \le N/2, \\ \omega + (i - N/2)\frac{2(1-\omega)}{N}, & N/2 < i \le N, \end{cases}$$

and corresponding mesh sizes

$$h_i = x_{i+1} - x_i = \begin{cases} h = 2\omega/N, & 0 \le i \le N/2, \\ H = 2(1-\omega)/N, & N/2 < i \le N-1. \end{cases}$$

From these definitions, it follows that $N^{-1} \le H \le 2N^{-1}$ and $h = 2\sqrt{c_\varepsilon}/\sqrt{p^*} \ln N$. A uniform mesh corresponds to $\omega = 1/2$.

7.4.3 Fully Discrete Hybrid Finite Difference Scheme

Let U_i^j denote the numerical approximation to $U(x_i, t_j)$ at node x_i and time level t_j. The temporal domain is discretized uniformly with step size Δt, and averaging the spatial operator at t_j and t_{j+1}. The discrete spatial operator $\hat{\mathcal{K}}_{c_\varepsilon,\text{hy}}^N$ is defined piecewise to match the layer-adapted mesh:

$$\hat{\mathcal{K}}_{c_\varepsilon,\text{hy}}^N = \begin{cases} \hat{\mathcal{K}}_{c_\varepsilon,\text{cen}}^N, & 1 \le i \le N/2, \\ \hat{\mathcal{L}}_{c_\varepsilon,\text{mu}}^N, & N/2 < i \le N-1, \end{cases}$$

where $\hat{\mathcal{K}}_{c_\varepsilon,\text{cen}}^N$ and $\hat{\mathcal{K}}_{c_\varepsilon,\text{mu}}^N$ denote the central difference and midpoint upwind operators, respectively. This hybrid approach combines second-order accuracy in the layer region with stability in the coarse region. In the fine mesh (layer) region, $1 \le i \le N/2$, the central difference operator is defined by

$$\hat{\mathcal{K}}_{c_\varepsilon,\text{cen}}^N U_i^{j+1} = \varepsilon D_x^+ D_x^- U_i^{j+1} + p_i^{j+1} D_x^0 U_i^{j+1} - \left(q_i^{j+1} + \frac{2}{\Delta t} \right) U_i^{j+1}. \tag{7.2}$$

In the coarse mesh region, $N/2 < i \le N-1$, the midpoint upwind operator is used:

$$\hat{\mathcal{K}}_{c_\varepsilon,\text{mu}}^N U_i^{j+1} = \varepsilon D_x^+ D_x^- U_i^{j+1} + p_{i+\frac{1}{2}}^{j+1} D_x^+ U_i^{j+1} - \left(q_{i+\frac{1}{2}}^{j+1} + \frac{2}{\Delta t} \right) U_{i+\frac{1}{2}}^{j+1}. \tag{7.3}$$

This choice ensures numerical stability in convection-dominated regions. The corresponding operators at the previous time level t_j are defined analogously, with the time-dependent coefficients evaluated at t_j. All spatial derivatives are approximated using finite difference operators on a nonuniform mesh. The forward, backward, and central difference operators are defined in the usual manner, while midpoint values of the coefficients, source term, and numerical solution are introduced through arithmetic averaging. Using Eqs.(7.2) and (7.3), the scheme can be written in the tri-diagonal form as:

$$\begin{cases} \hat{\mathcal{K}}_{c_\varepsilon,\text{hy}}^N U_i^{j+1} := y_i^- U_{i-1}^{j+1} + y_i^c U_i^{j+1} + y_i^+ U_{i+1}^{j+1} = R_i^j, & i = 1, 2, \ldots, N-1, \; j = 0, 1, \ldots, M-1, \\ U_0^{j+1} = \phi_1(t_{j+1}), \quad U_N^{j+1} = \phi_2(t_{j+1}), & j = 0, 1, \ldots, M-1, \\ U_i^0 = u_0(x_i), & i = 1, 2, \ldots, N-1, \end{cases} \tag{7.4}$$

with the coefficients defined by

$$
\begin{cases}
y_i^- = \dfrac{2\varepsilon}{\hat{h}_i h_i} - \dfrac{p_i^{j+1}}{\hat{h}_i}, \\
y_i^c = -\dfrac{2\varepsilon}{h_i h_{i+1}} - \Big(q_i^{j+1} + \dfrac{2}{\Delta t}\Big), \qquad 1 \le i \le \dfrac{N}{2}, \\
y_i^+ = \dfrac{2\varepsilon}{\hat{h}_i h_{i+1}} + \dfrac{p_i^{j+1}}{\hat{h}_i}, \\
y_i^- = \dfrac{2\varepsilon}{\hat{h}\, h_i}, \\
y_i^c = -\dfrac{2\varepsilon}{h_i h_{i+1}} - \dfrac{p_{i+\frac{1}{2}}^{j+1}}{h_{i+1}} - \dfrac{1}{2}\Big(q_{i+\frac{1}{2}}^{j+1} + \dfrac{2}{\Delta t}\Big), \qquad \dfrac{N}{2} < i \le N-1. \\
y_i^+ = \dfrac{2\varepsilon}{\hat{h}\, h_{i+1}} + \dfrac{p_{i+\frac{1}{2}}^{j+1}}{h_{i+1}} - \dfrac{1}{2}\Big(q_{i+\frac{1}{2}}^{j+1} + \dfrac{2}{\Delta t}\Big),
\end{cases}
\tag{7.5}
$$

and the right-hand side is given by

$$
R_i^j = \begin{cases}
R_i^j = (f_i^{j+1} + f_i^j) - \varepsilon D_x^+ D_x^- U_i^j & \\
\qquad + p_i^j D_x^0 U_i^j - \Big(q_i^j - \dfrac{2}{\Delta t}\Big) U_i^j, & 1 \le i \le \dfrac{N}{2}, \\
R_i^j = (f_{i+\frac{1}{2}}^{j+1} + f_{i+\frac{1}{2}}^j) - \varepsilon D_x^+ D_x^- U_i^j & \\
\qquad + p_{i+\frac{1}{2}}^j D_x^+ U_i^j - \Big(q_{i+\frac{1}{2}}^j - \dfrac{2}{\Delta t}\Big) U_{i+\frac{1}{2}}^j, & \dfrac{N}{2} < i \le N-1.
\end{cases}
$$

The resulting linear system consists of $(N-1) \times (N-1)$ algebraic equations with unknowns

$$U_1^{j+1}, U_2^{j+1}, \ldots, U_{N-1}^{j+1}.$$

This fully discrete formulation, together with the hybrid spatial operators, forms the basis for the stability analysis and the proof of uniform convergence presented in the following section.

7.5 Convergence Analysis of the Discrete Scheme

Lemma 7.1. *For $N \ge N_0 \ge 8$, there exists $\alpha > 0$ such that*

$$(\|q\|_\infty + (\Delta t)^{-1}) \le \alpha N_0, \quad \textit{and} \quad \frac{N_0}{(\ln N_0)^2} \ge 4\omega_0^2 \|p\|.$$

Then, we have

$$y_i^- > 0, \quad y_i^+ > 0, \quad \textit{for } 1 \le i \le N-1,$$

$$|y_i^-| + |y_i^+| < |y_i^c|, \quad \textit{for } 1 < i < N-1,$$

$$|y_1^+| < |y_1^c|, \quad \textit{and} \quad |y_{N-1}^-| < |y_{N-1}^c|.$$

Proof. The proof is analogous to the proof of Lemma 3.1 presented in Chapter 3. □

Remark 7.1. *From the lemma 7.1 the matrix associated with the discrete operator $\hat{\mathcal{K}}_{c_\varepsilon,hy}^N$ in Eq. (7.4) is strictly diagonally dominance and so has a unique solution. The operator $\hat{\mathcal{K}}_{c_\varepsilon,hy}^N$ in Eq. (7.4) satisfies the following minimum principle. Hence the scheme (7.4) is uniformly stable in the maximum norm.*

Lemma 7.2 (Discrete minimum Principle). *Let $U^{M,N}$ be any mesh function defined of $\overline{\mathcal{D}}^{M,N}$. Assume that $U_0^{j+1} \ge 0, U_N^{j+1} \ge 0$ and $\hat{\mathcal{K}}_{c_\epsilon,hy}^N U_i^{j+1} \le 0$, for $1 \le i \le N-1$. Then $U_i^{j+1} \ge 0 \quad$ for $\quad 1 \le i \le N$ and $1 \le j < M$.*

Proof. The proof follows using Lemma 7.1 and Remark 7.1. □

Lemma 7.3 (Stability Estimate). *The solution U_i^{j+1} of the discrete problem (7.4) satisfies the bound*

$$\left|U_i^{j+1}\right| \le \frac{T}{p^*}\left|\left|\hat{\mathcal{K}}_{c_\epsilon,hy}^N U_i^{j+1}\right|\right| + \max_{\partial\mathcal{D}^{M,N}} \left|U(x_i, t_{j+1})\right|$$

Next, we derive an estimate of the classical local truncation error arising from the spatial discretization using Taylor series expansions at the j^{th} time level.

Lemma 7.4. *Let $u^j(x)$ and $U^j(x)$ be the solutions of the semi-discrete problem (6.7) and the fully discrete problem (7.4), respectively. Then the local truncation error associated with the spatial discretization is given by*

$$\tau_i^j = \hat{\mathcal{K}}_{c_\epsilon,hy}^N U^j(x_i) - \hat{\mathcal{K}}_{c_\epsilon,hy} u^j(x_i) = \begin{cases} \hat{\mathcal{K}}_{c_\varepsilon,cen}^N U^j(x_i) - \hat{\mathcal{K}}_{c_\epsilon} u^j(x_i), & i = 1, 2, \ldots, \frac{N}{2}, \\ \hat{\mathcal{K}}_{c_\varepsilon,mu}^N U^j(x_i) - \hat{\mathcal{K}}_{c_\epsilon} u^j(x_{i+\frac{1}{2}}), & i = \frac{N}{2}+1, \ldots, N-1. \end{cases}$$

Moreover, the local truncation error satisfies the estimate

$$|\tau_i^j| \leq \begin{cases} C\left[\varepsilon h_i \displaystyle\int_{x_{i-1}}^{x_{i+1}} u_{xxxx}(x)\,dx + h_i \displaystyle\int_{x_{i-1}}^{x_{i+1}} u_{xxx}(x)\,dx\right], & i = 1, 2, \ldots, \frac{N}{2}, \\ C\left[\varepsilon \displaystyle\int_{x_{i-1}}^{x_{i+1}} u_{xxx}(x)\,dx + h_i \displaystyle\int_{x_{i-1}}^{x_i} \big(u_{xxx}(x) + u_{xx}(x) + u_x(x)\big)\,dx\right], & i = \frac{N}{2}+1, \ldots, N-1, \end{cases}$$

where C is a positive constant independent of ε, h_i, and Δt.

Proof. The proof is by using the Taylor series expansion with the integral form of the remainder [67] $\square$

In order to derive a parameter-uniform error estimate for the fully discrete scheme (7.4), the discrete problem is decomposed, in analogy with the continuous problem, into its regular and singular parts as follows:

$$U_i^j = V_i^j + W_i^j, \qquad i = 0, 1, \ldots, N,\ j = 0, 1, \ldots, M,$$

where V_i^j and W_i^j denote the discrete regular and singular components, respectively. The discrete regular component V_i^j is defined as the solution of the inhomogeneous discrete problem

$$\begin{cases} \hat{\mathcal{K}}^N_{c_\varepsilon, hy} V_i^{j+1} = f_i^{j+1}, & 1 \leq i \leq N-1,\ 0 \leq j \leq M-1, \\ V_i^0 = u_0(x_i), & 0 \leq i \leq N, \\ V_N^{j+1} = \phi_2(1, t_{j+1}), & 0 \leq j \leq M-1, \end{cases}$$

while the discrete singular component W_i^j satisfies the homogeneous discrete problem

$$\begin{cases} \hat{\mathcal{K}}^N_{c_\varepsilon, hy} W_i^{j+1} = 0, & 1 \leq i \leq N-1,\ 0 \leq j \leq M-1, \\ W_i^0 = 0, & 0 \leq i \leq N, \\ W_N^{j+1} = 0, & 0 \leq j \leq M-1, \\ W_0^{j+1} = \phi_1(0, t_{j+1}) - V_0^{j+1}, & 0 \leq j \leq M-1. \end{cases}$$

Therefore, the pointwise error of the discrete solution at each mesh point (x_i, t_j) is decomposed as:

$$(U - u)(x_i, t_j) = (V - v)(x_i, t_j) + (W - w)(x_i, t_j). \tag{7.6}$$

We now proceed to establish error estimates for the regular and singular parts separately.

Theorem 7.1 (Error estimate in the regular component)**.** *For each time level $t_j \in \Lambda^M$, the regular component satisfies the following error estimates:*

$$\big|(V-v)(x_i,t_j)\big| \leq \begin{cases} CN^{-2}, & i = 0,1,2,\dots,\dfrac{N}{2}, \\ CN^{-1}\big(c_\varepsilon + N^{-1}\big), & i = \dfrac{N}{2}+1,\dots,N, \end{cases}$$

where C is a positive constant independent of c_ε and N.

Proof. The error in the regular component is estimated in a manner analogous to the classical argument presented in Lemma 7.4. Using the mesh property

$$h_i + h_{i+1} \leq 2N^{-1}, \qquad i = 1,2,\dots,N,$$

we obtain the following bounds:

$$\hat{\mathcal{K}}^N_{c_\varepsilon,hy}(V-v)(x_i,t_j) \leq \begin{cases} C\left[h_i(h_i+h_{i+1})\left(\varepsilon\dfrac{\partial^4 v}{\partial x^4} + \dfrac{\partial^3 v}{\partial x^3}\right)\right], & i = 0,1,2,\dots,\dfrac{N}{2}, \\ C\left[\varepsilon(h_i+h_{i+1})\dfrac{\partial^3 v}{\partial x^3} + h_i^2\left(\dfrac{\partial^3 v}{\partial x^3} + \dfrac{\partial^2 v}{\partial x^2} + \dfrac{\partial v}{\partial x}\right)\right], & i = \dfrac{N}{2}+1,\dots,N. \end{cases}$$

Invoking the derivative bounds for the regular component v established in Theorem 6.5, the above estimates reduce to

$$\hat{\mathcal{K}}^N_{c_\varepsilon,hy}(V-v)(x_i,t_j) \leq \begin{cases} CN^{-2}, & i = 0,1,2,\dots,\dfrac{N}{2}, \\ CN^{-1}\big(c_\varepsilon + N^{-1}\big), & i = \dfrac{N}{2}+1,\dots,N. \end{cases}$$

Next, we define the discrete barrier functions

$$Z^{M,N}(x_i,t_j) = \hat{\mathcal{K}}^N_{c_\varepsilon,hy}(V-v)(x_i,t_j) \pm (V-v)(x_i,t_j).$$

Applying the discrete maximum principle stated in Lemma 7.2 yields the desired error estimate:

$$\big|(V-v)(x_i,t_j)\big| \leq \begin{cases} CN^{-2}, & i = 0,1,\dots,\dfrac{N}{2}, \\ CN^{-1}\big(c_\varepsilon + N^{-1}\big), & i = \dfrac{N}{2}+1,\dots,N. \end{cases}$$

□

Theorem 7.2 (Error estimate in the singular component)**.** *For each time level $t_j \in \Lambda^M$, the singular component satisfies the following error estimates:*

$$\left|(W - w)(x_i, t_j)\right| \leq \begin{cases} CN^{-2}\ln^2 N, & i = 0, 1, 2, \ldots, \dfrac{N}{2}, \\ CN^{-2}, & i = \dfrac{N}{2} + 1, \ldots, N, \end{cases}$$

where C is a positive constant independent of c_ε and N.

Proof. The detail of the proof is in [100] □

By combining the errors in the regular and singular components, we obtain the overall spatial discretization error bound, as stated in the following theorem.

Theorem 7.3 (Error estimate in the space direction)**.** *Let $u^j(x_i)$ and U_i^j be the solutions of the semi-discrete problem* (6.7) *and the fully discrete problem* (7.4)*, respectively. Then, at the jth time level, the following error estimate in the space direction holds:*

$$\|u^j(x_i) - U_i^j\|_{\Omega_N} \leq \begin{cases} CN^{-2}\ln^2 N, & i = 0, 1, 2, \ldots, N/2, \\ CN^{-2}, & i = N/2 + 1, \ldots, N, \end{cases}$$

where C is a positive constant independent of c_ε and N.

Proof. The result follows directly from Theorems 7.1 and 7.2. □

Theorem 7.4 (c_ε-uniform error estimate)**.** *Let u and U denote the exact and numerical solutions of the continuous problem* (6.3) *and the fully discrete scheme* (7.4)*, respectively. Then the following parameter-uniform error estimate holds:*

$$\sup_{0<c_\varepsilon\leq 1} \|U(x_i, t_j) - u(x_i, t_j)\|_{\mathcal{D}_{N,M}} \leq \begin{cases} C\big((\Delta t)^2 + N^{-2}\ln^2 N\big), & i = 0, 1, 2, \ldots, \dfrac{N}{2}, \\ C\big((\Delta t)^2 + N^{-2}\big), & i = \dfrac{N}{2} + 1, \ldots, N, \end{cases}$$

where C is a positive constant independent of c_ε, M, and N.

Proof. The proof is derived from the bounds established in Theorem 7.3 and Theorem 6.4. □

7.6 Numerical Example and Results

To estimate the maximum absolute errors and its corresponding rate of convergence of the current approach, we used the double mesh principle formula stated in chapter 6 section 6.6.

Example 7.1. *Consider the singularly perturbed parabolic convection–diffusion turning-point problem with general Shifts [98]*

$$\begin{cases} \varepsilon u_{xx} + x^p u_x(x,t) - 2u(x-\delta,t) - u(x,t) - u(x+\mu,t) - u_t(x,t) = x^2 - 1, & (x,t) \in \mathcal{D}, \\ u(x,0) = (1-x)^2, \quad x \in \overline{\Omega}, \\ u(x,t) = 1 + t^2, \quad (x,t) \in [-\delta, 0] \times (0,1], \\ u(x,t) = 0, \quad (x,t) \in [1, 1+\mu] \times (0,1]. \end{cases}$$

Table 7.1: Maximum absolute error and rate of convergence for Example 7.1 for $p = 1$ and $\delta = 0.9\varepsilon, \mu = 0.5\varepsilon$

$\varepsilon \downarrow M = N \rightarrow$	32	64	128	256	512	1024
10^{-2}	4.6237e-04	1.5708e-04	5.2396e-05	1.5003e-05	3.8675e-06	9.7073e-07
	1.5575	1.5840	1.8042	1.9556	1.9942	
10^{-4}	4.6295e-04	1.5728e-04	5.2452e-05	1.5022e-05	3.9354e-06	1.0115e-06
	1.5575	1.5842	1.8041	1.9327	1.9600	
10^{-6}	4.6301e-04	1.5730e-04	5.2459e-05	1.5025e-05	3.9362e-06	1.0119e-06
	1.5575	1.5842	1.8041	1.9327	1.9596	
10^{-8}	4.6301e-04	1.5730e-04	5.2460e-05	1.5025e-05	3.9363e-06	1.0120e-06
	1.5575	1.5842	1.8041	1.9327	1.9596	
10^{-10}	4.6301e-04	1.5730e-04	5.2460e-05	1.5025e-05	3.9363e-06	1.0120e-06
	1.5575	1.5842	1.8041	1.9327	1.9596	
$e^{M,N}$	4.6301e-04	1.5730e-04	5.2460e-05	1.5025e-05	3.9363e-06	1.0120e-06
$R^{M,N}$	1.5575	1.5841	1.8042	1.9327	1.9596	
In Chap 6: $e^{M,N}$	1.2583e-03	6.5948e-04	3.3769e-04	1.7092e-04	8.5980e-05	4.3292e-05
	0.9321	0.9656	0.9824	0.9913	0.9961	
In [98] $e_\varepsilon^{M,N}$	2.0440e-02	1.3030e-02	7.8660e-03	4.6070e-03	— — ——	— — ——
	0.7047	0.7718	0.8526	0.9357		

Example 7.2. *Consider the singularly perturbed parabolic convection–diffusion turning-point problem with*

Table 7.2: Maximum absolute error and rate of convergence for Example 7.1 for $p = 2$ and $\delta = 0.2\varepsilon, \mu = 0.4\varepsilon$

$\varepsilon \downarrow M = N \rightarrow$	32	64	128	256	512	1024
10^{-1}	3.9582e-03	1.2337e-03	3.5912e-04	1.0042e-04	2.5460e-05	6.4528e-06
	1.6818	1.7804	1.8386	1.9798	1.98023	
10^{-2}	6.4275e-03	2.1684e-03	6.8247e-04	2.0890e-04	5.7280e-05	1.5703e-05
	1.5679	1.6677	1.7082	1.8678	1.8680	
10^{-4}	6.4284e-03	2.1691e-03	6.8284e-04	2.0913e-04	5.7390e-05	1.5748e-05
	1.5674	1.6674	1.7075	1.8672	1.8674	
10^{-6}	6.4287e-03	2.1694e-03	6.8300e-04	2.0924e-04	5.7438e-05	1.5770e-05
	1.5672	1.6673	1.7072	1.8670	1.8671	
10^{-8}	6.4289e-03	2.1695e-03	6.8306e-04	2.0929e-04	5.7457e-05	1.5778e-05
	1.5672	1.6672	1.7064	1.8648	1.8672	
10^{-9}	6.4290e-03	2.1696e-03	6.8309e-04	2.0931e-04	5.7465e-05	1.5751e-05
	1.5672	1.6672	1.7064	1.8648	1.8672	
10^{-10}	6.4290e-03	2.1696e-03	6.8309e-04	2.0931e-04	5.7465e-05	1.5751e-05
	1.5672	1.6672	1.7064	1.8648	1.8672	
$e^{M,N}$	6.4290e-03	2.1696e-03	6.8309e-04	2.0931e-04	5.7465e-05	1.5751e-05
$R^{M,N}$	1.5672	1.6672	1.7064	1.8648	1.8672	

Table 7.3: Maximum absolute error and rate of convergence for Example 7.1 with $p = 2$ and different values of δ and μ for $\varepsilon = 10^{-3}$

$M = N \rightarrow$	32	64	128	256	512	1024
$\delta \downarrow,\ \mu = 0.5\varepsilon$						
0	6.2348e-03	2.1296e-03	7.1732e-04	2.1504e-04	6.0872e-05	1.6852e-05
	1.5498	1.5698	1.7380	1.8206	1.8528	
0.2ε	6.2347e-03	2.1296e-03	7.1731e-04	2.1504e-04	6.0871e-05	1.6852e-05
	1.5498	1.5698	1.7380	1.8206	1.8528	
0.4ε	6.2347e-03	2.1296e-03	7.1730e-04	2.1504e-04	6.0870e-05	1.6852e-05
	1.5498	1.5698	1.7380	1.8206	1.8528	
0.6ε	6.2346e-03	2.1296e-03	7.1729e-04	2.1504e-04	6.0869e-05	1.6852e-05
	1.5497	1.5698	1.7380	1.8206	1.8527	
$\mu \downarrow,\ \delta = 0.6\varepsilon$						
0	6.2345e-03	2.1295e-03	7.1729e-04	2.1503e-04	6.0868e-05	1.6851e-05
	1.5497	1.5698	1.7380	1.8206	1.8528	
0.2ε	6.2346e-03	2.1296e-03	7.1729e-04	2.1504e-04	6.0869e-05	1.6852e-05
	1.5497	1.5698	1.7380	1.8206	1.8528	
0.4ε	6.2346e-03	2.1296e-03	7.1730e-04	2.1504e-04	6.0869e-05	1.6852e-05
	1.5497	1.5698	1.7380	1.8206	1.8528	
0.6ε	6.2346e-03	2.1296e-03	7.1730e-04	2.1504e-04	6.0870e-05	1.6852e-05
	1.5497	1.5698	1.7380	1.8206	1.8527	

general Shifts

$$
\begin{cases}
\varepsilon u_{xx} + (1 + te^{-2t})x^p u_x(x,t) - 2u(x-\delta,t) - u(x,t) - u(x+\mu,t) - u_t(x,t) = (x^2-1)e^{-t}, \quad (x,t) \in \mathcal{D}, \\
u(x,0) = (1-x)^2, \quad x \in \overline{\Omega}, \\
u(x,t) = 1 + t^2, \quad (x,t) \in [-\delta, 0] \times (0,1], \\
u(x,t) = 0, \quad (x,t) \in [1, 1+\mu] \times (0,1].
\end{cases}
$$

Table 7.4: Maximum absolute error and its corresponding rate of convergence for $\varepsilon = 10^{-5}$ and different values of p.

$p\downarrow,\ M=N\rightarrow$	32	64	128	256	512	1024
Example 7.1, $\delta = 0.4\varepsilon,\ \mu = 0.8\varepsilon$						
3	1.3819e-02	4.8805e-03	1.5603e-03	4.4649e-04	1.1646e-04	2.9718e-05
	1.5015	1.6452	1.8051	1.9387	1.9704	
4	1.3832e-02	4.8863e-03	1.5618e-03	4.4696e-04	1.1674e-04	2.9803e-05
	1.5012	1.6455	1.8045	1.9368	1.9697	
Example 7.2, $\delta = 0.2\varepsilon,\ \mu = 0.4\varepsilon$						
3	1.3816e-02	4.8456e-03	1.5486e-03	4.4283e-04	1.1546e-04	2.9428e-05
	1.5115	1.6457	1.8061	1.9393	1.9721	
4	1.3829e-02	4.8512e-03	1.5501e-03	4.4337e-04	1.1575e-04	2.9515e-05
	1.5113	1.6460	1.8058	1.9374	1.9714	

Table 7.5: Maximum absolute error and rate of convergence for Example 7.2 for $p = 1$ and $\delta = 0.8\varepsilon, \mu = 0.6\varepsilon$

$\varepsilon\downarrow M=N\rightarrow$	32	64	128	256	512	1024
10^{-1}	4.1985e-03	1.3085e-03	3.8085e-04	1.0648e-04	2.6995e-05	6.8422e-06
	1.6820	1.7806	1.8386	1.9798	1.9796	
10^{-2}	6.8165e-03	2.2997e-03	7.2375e-04	2.2155e-04	6.0741e-05	1.6651e-05
	1.5678	1.6678	1.7082	1.8678	1.8680	
10^{-4}	6.8174e-03	2.3004e-03	7.2413e-04	2.2179e-04	6.0853e-05	1.6697e-05
	1.5675	1.6674	1.7075	1.8672	1.8674	
10^{-6}	6.8177e-03	2.3007e-03	7.2429e-04	2.2190e-04	6.0902e-05	1.6719e-05
	1.5674	1.6672	1.7072	1.8670	1.8671	
10^{-8}	6.8179e-03	2.3008e-03	7.2435e-04	2.2195e-04	6.0922e-05	1.6727e-05
	1.5673	1.6672	1.7070	1.8668	1.8669	
10^{-9}	6.8180e-03	2.3009e-03	7.2438e-04	2.2197e-04	6.0930e-05	1.6730e-05
	1.5672	1.6673	1.7064	1.8634	1.8647	
10^{-10}	6.8180e-03	2.3009e-03	7.2438e-04	2.2197e-04	6.0930e-05	1.6730e-05
	1.5672	1.6673	1.7064	1.8634	1.8647	
$e^{M,N}$	6.8180e-03	2.3009e-03	7.2438e-04	2.2197e-04	6.0930e-05	1.6730e-05
$R^{M,N}$	1.5672	1.6673	1.7064	1.8634	1.8647	

The numerical results reported in Tables 7.1 and 7.2 for Example 7.1 present the maximum absolute errors and the corresponding convergence rates of the proposed scheme for various values of the perturbation parameter c_ε with $p = 1, 2$. It is observed from the tables that, as c_ε decreases, the maximum absolute error stabilizes and eventually becomes nearly constant, indicating that the accuracy of the scheme is independent of ε. This behavior clearly confirms the c_ε-uniform convergence of the scheme for different values of p. Furthermore, Table 7.1 compares the c_ε-uniform errors and convergence rates of the proposed scheme for Example 7.1 with a result available in the literature. The comparison shows that the present scheme yields higher accuracy than the method reported in [98]. Table 7.3 presents the maximum absolute errors

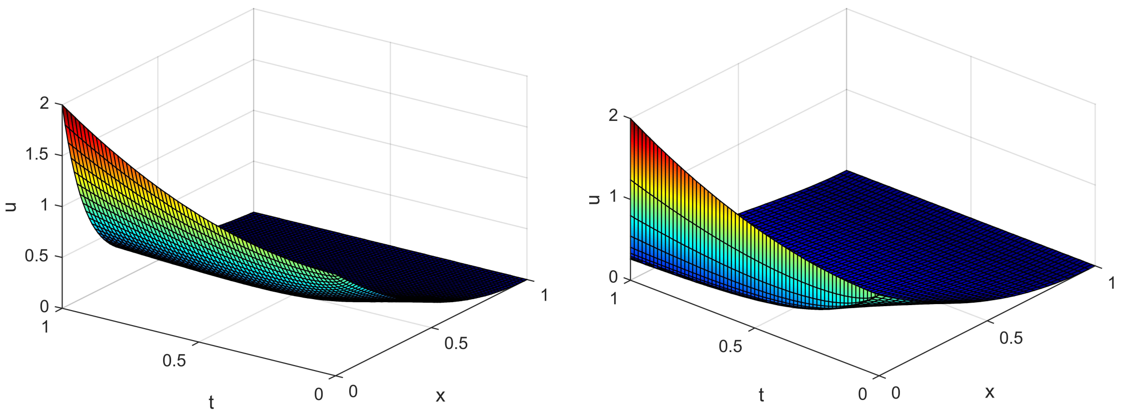

(a) $\varepsilon = 10^{-1}$ (b) $\varepsilon = 10^{-10}$

Figure 7.1: Surface plots of the numerical solution for $M = N = 64$, $p = 1$, and parameters $\delta = 0.6\varepsilon$, $\mu = 0.5\varepsilon$.

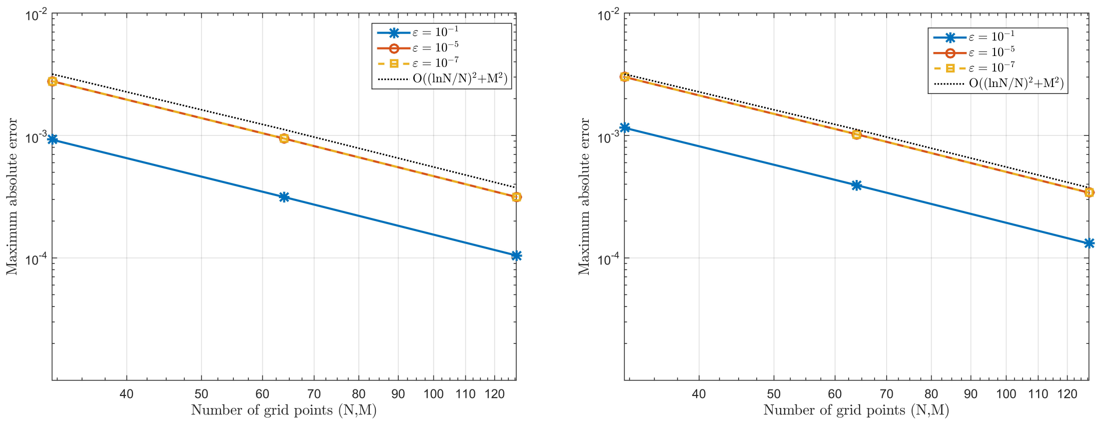

(a) $p = 1$ (b) $p = 3$

Figure 7.2: Log-Log plots of maximum absolute errors for Example 7.1 with parameters $\delta = 0.6\varepsilon$, $\mu = 0.5\varepsilon$ and different values of p.

for different values of the delay and advance parameters for Example 7.1. The results indicate that the shift parameters do not affect the convergence behavior of the scheme. In Table 7.4, the maximum absolute errors are reported for a fixed value of c_ε and different values of p for Examples 7.1 and 7.2. These results demonstrate that the parameter p has no significant influence on the convergence of the scheme. The results presented in Table 7.5 for Example 7.2 exhibit the same behavior as those shown in Table 7.1 for Example 7.1, demonstrating the c_ε-uniform convergence of the scheme. Overall, the proposed scheme exhibits an almost second-order c_ε-uniform convergence.

The solutions of the problems in Examples 7.1 and 7.2 exhibit a boundary layer near the left boundary of

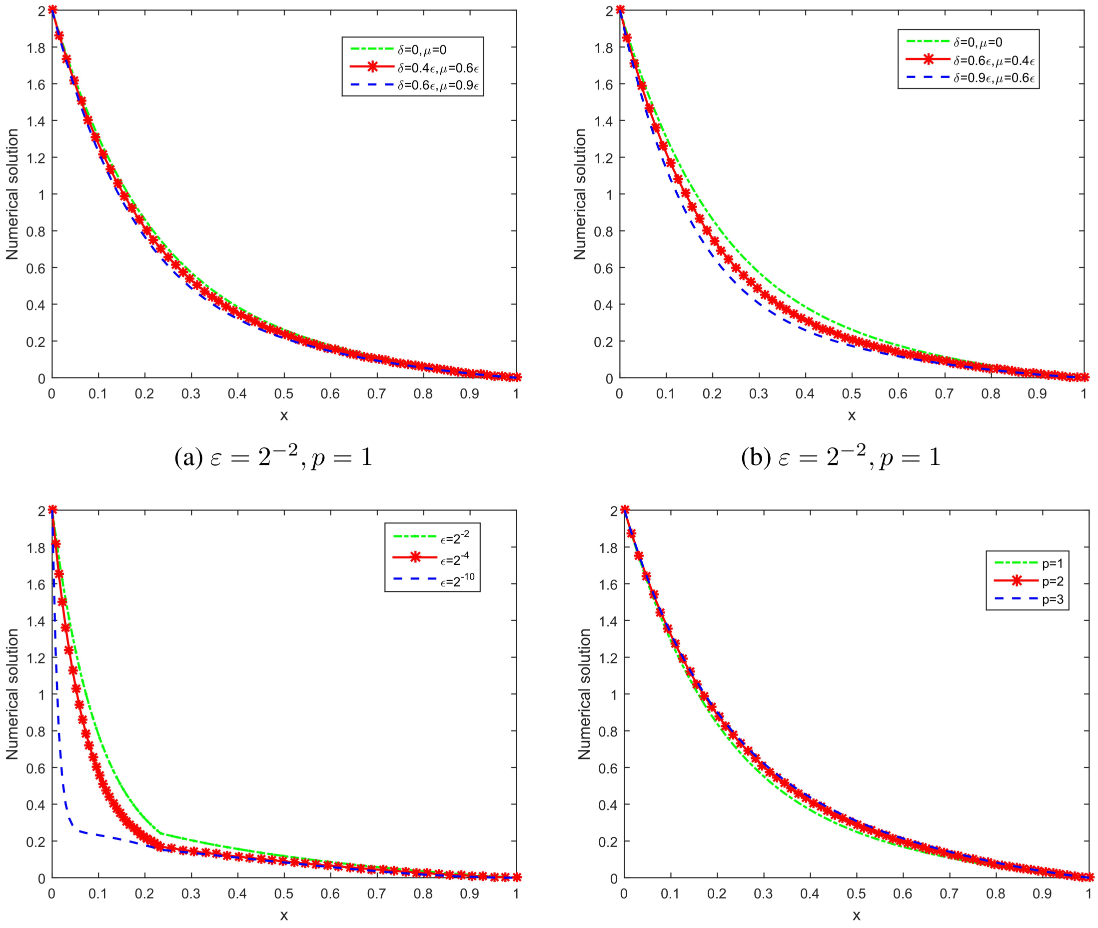

(a) $\varepsilon = 2^{-2}, p = 1$ (b) $\varepsilon = 2^{-2}, p = 1$

(c) $\delta = \mu = 0.3\varepsilon, p = 1$ (d) $\delta = 0.3\varepsilon, \mu = 0.6\varepsilon, \varepsilon = 2^{-2}$

Figure 7.3: Example 7.1 on (a) and (b) effect of both δ and μ, and (c) influence of ε (d) effect of p on the solution.

the spatial domain. In Figure 7.1, corresponding to Example 7.1, the formation of a boundary layer becomes steep gradient as the perturbation parameter c_ε decreases. A similar behavior is observed in Figure 7.4a for Example 7.2. Figure 7.2 presents the log–log plots of the maximum absolute errors of the proposed scheme for Example 7.1, computed for different values of c_ε and p. As observed from the figure, for all considered values of the perturbation parameter and p, the error curves overlap and remain parallel to the reference line $N^{-2}\ln^2 N$ as $c_\varepsilon \to 0$. This behavior indicates that the scheme is almost second-order convergent and that its convergence is independent of the parameters. Figure 7.3 further illustrates the influence of the shift parameters, the perturbation parameter, and the order of the turning point p on the solution profile for example 7.1 by displaying solutions corresponding to different values of these parameters.

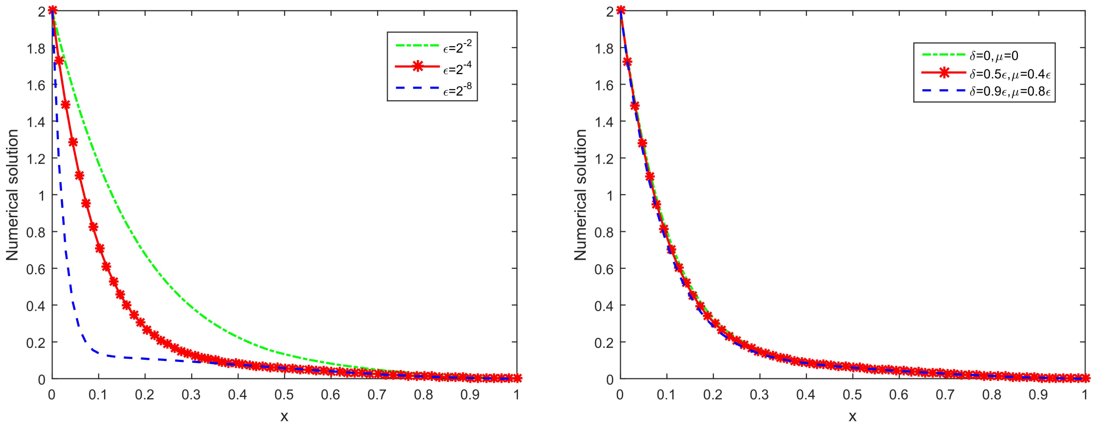

(a) $\delta = 0.4\varepsilon, \mu = 0.3\varepsilon, p = 1$

(b) $\varepsilon = 2^{-4}, p = 1$

Figure 7.4: Solution profiles for Example 7.2 for different values of ε, δ, and μ with $p = 1$.

7.7 Conclusion

Layer resolving mesh numerical scheme is developed for SPPDDEs involving general shift in the spatial variable with boundary turning point. The solution of the considered problem exhibit a left boundary layer in the spatial domain as the perturbation parameter approaches zero. The developed numerical scheme combines the Crank–Nicolson method for time discretization on a uniform time mesh with a hybrid finite difference approach for spatial discretization on a Shishkin mesh, where central differences are applied in the boundary layer region and a midpoint upwind scheme is employed in the outer region. The stability and ε-uniform convergence of the scheme are thoroughly investigated. The applicability of the proposed method is validated through model examples. The effects of the perturbation parameter and shift parameters and p on the solution are demonstrated graphically. The scheme is shown to be c_ε- uniformly convergent with an order of convergence $\mathcal{O}(N^{-2}\ln^2 N + (\Delta t)^2)$. Its performance is evaluated through comparison with some existing method in published literature. Numerical results confirm that the proposed scheme yields more accurate and higher-order ε-uniformly convergent solutions.

Chapter 8

General Discussion, Conclusion and Future Works

This chapter presents the general discussion and summary of the contributed results made in this dissertation, followed by recommendations for possible extensions of the present works.

8.1 General Discussion and Conclusion

The work carried out in this dissertation has achieved many interesting and significant results in solving singularly perturbed time-dependent DEs and DDEs with boundary turning point (BTP) using simple, efficient (easy to use and accurate), and uniformly convergent numerical methods. The developed numerical methods employ techniques such as non-standard finite difference methods (FDMs), exponentially fitted operator FDM, and fitted mesh FDMs.

In Chapters 2 and 3, uniformly convergent numerical methods are developed for solving singularly perturbed parabolic differential equations with BTP. In Chapter 2, the non-standard finite difference method (FDM) is employed for spatial discretization, combined with the Crank–Nicolson method for temporal discretization on uniform meshes. Furthermore, Richardson extrapolation is applied to improve the spatial order of convergence. The computed solutions are presented in tables and figures using the maximum absolute error for various values of the perturbation parameter ε and order of turning point p. The proposed scheme is compared with published results and demonstrates higher order accuracy and parameter uniform convergence.

In Chapter 3, a hybrid fitted mesh finite difference method is introduced. Here, the Crank–Nicolson method is employed for temporal discretization, while the midpoint upwind FDM is applied in the outer layer region and the central finite difference method in the boundary layer region for spatial discretization. The developed scheme in this chapter exhibits nearly second-order convergence. Comparing the rate of convergence and maximum absolute errors, the hybrid FDM scheme provides more accurate and higher-order results than the non-standard FDM of Chapter 2. Furthermore, the hybrid scheme allocates an adequate number of mesh points within the boundary layer region.

In Chapters 4 and 5, singularly perturbed parabolic differential equations with large delay in time are addressed. In Chapter 4, the Crank-Nicolson method is applied for temporal discretization, and an exponentially fitted operator FDM is used for spatial discretization. A uniformly convergent numerical scheme is developed, with the exponential fitting parameter derived from the asymptotic solution of the problem. Stability and uniform convergence of the scheme are thoroughly analyzed. The benefit of using the exponential fitting parameter is illustrated by comparing results with and without its inclusion. The developed scheme achieves first-order uniform convergence as $\varepsilon \to 0$.

In Chapter 5, the Crank–Nicolson method is again employed for temporal discretization, while the hybrid scheme which a combination of central difference with midpoint upwind scheme on shishkin mesh is used for spatial discretization. Numerical results are presented in terms of maximum absolute errors in tables and figures. Stability of the scheme is established using a solution bound. The scheme is shown to be uniformly convergent with almost second-order accuracy. The numerical schemes presented in this chapter produce stable and more accurate results than the exponentially fitted operator method in chapter 4.

In Chapters 6 and 7, singularly perturbed parabolic differential-difference equations with delay and advance terms in the reaction component with BTP are considered. In Chapter 6, the Crank–Nicolson method is employed for temporal discretization, while a non-standard finite difference method (FDM) is used for spatial discretization to handle the problem. The stability and uniform convergence of the scheme are thoroughly investigated. The uniform absolute error and uniform rate of convergence of the scheme are compared with results from schemes in the literature. The developed scheme demonstrates accuracy, stability, and first-order uniform convergence.

In Chapter 7, the problem from Chapter 6 is revisited. The Crank Nicolson method is used for temporal semi-discretization, while a hybrid spatial discretization combining the central finite difference and midpoint upwind schemes is applied on a Shishkin mesh. The stability and uniform convergence of the scheme are analysed in detail. The developed scheme exhibits nearly second-order uniform convergence and improves upon the results obtained in Chapter 6. The maximum absolute error and rate of convergence are compared with some methods from the literature. The proposed scheme provides more accurate results and demonstrates layer-resolving capability.

In all chapters, comprehensive computational experiments have been conducted to validate that the numerical results align closely with the theoretical predictions. Moreover, comparative analyses reveal that the proposed schemes consistently deliver more accurate and higher order convergent rates compared to some existing methods in the literature. To visually support these findings, results are illustrated through maximum error plots on log–log scales and one-dimensional profiles of the numerical solutions.

8.2 Future Work

In this study we considered only a few classes of parabolic convection-diffusion singularly perturbed differential equations (SPDEs) and differential-difference equations (SPDDEs) with boundary turning points (BTP). The turning points were assumed to arise solely from vanishing convection coefficients at the boundary; however, they may also result from discontinuous data, nonlinearity, or incompatibility conditions, which warrant further investigation.

The analysis was limited to small spatial shifts, excluding large delays. Moreover, while boundary layers were the primary focus, problems involving interior layers particularly those arising from turning-point problems with a sign change of the convection coefficient in the interior of the domain remain unexplored.

Future research directions include:

- Extending the proposed schemes to problems with interior layers and discontinuous data, where complex layer structures may occur.
- Developing methods for problems with large spatial delays to account for additional nonlocal effects.
- Implementing graded meshes such as Bakhvalov or equidistributed meshes to achieve higher accuracy and improved convergence compared to Shishkin meshes.
- Extending the proposed schemes to two-dimensional problems with turning points.
- Investigating nonlinear turning point problems, as real-life models are often nonlinear, and extending the proposed techniques to address such cases.

Bibliography

[1] L. R. Abrahamsson. A priori estimates for solutions of singular perturbations with a turning point. *Studies in Applied Mathematics*, 56:51–69, 1977.

[2] L. R. Abrahamsson, H. B. Keller, and H.-O. Kreiss. Difference approximations for singular perturbations of systems of ordinary differential equations. *Numerische Mathematik*, 22(5):367–391, 1974.

[3] R. C. Ackerberg and R. E. O'Malley. Boundary layer problems exhibiting resonance. *Studies in Applied Mathematics*, 49:277–295, 1970.

[4] H.J. Al Salman, F.W. Gelu, and A.A. Al Ghafli. A fitted mesh robust numerical method and analysis for the singularly perturbed parabolic pdes with a degenerate coefficient. *Results in Applied Mathematics*, 24:100519, 2024.

[5] M. V. Alekseevskii. On a difference scheme for singularly perturbed parabolic equations. *Science note, Erevan State University, Natural Sciences, Erevan*, (1):3–13, 1980.

[6] A. Andargie and Y. N. Reddy. An exponentially fitted special second-order finite difference method for solving singular perturbation problems. *Applied Mathematics and Computation*, 190(2):1767–1782, 2007.

[7] A. Andargie and Y. N. Reddy. An asymptotic-fitted method for solving singularly perturbed delay differential equations. 2012.

[8] A. R. Ansari, S. A. Bakr, and G. I. Shishkin. A parameter-robust finite difference method for singularly perturbed delay parabolic partial differential equations. *Journal of computational and applied mathematics*, 205(1):552–566, 2007.

[9] J. Arino and P. Van Den Driessche. Time delays in epidemic models. In *Delay Differential Equations and Applications*, pages 539–578. Springer, 2006.

[10] D. Arslan. A uniformly convergent numerical study on bakhvalov-shishkin mesh for singularly perturbed problem. *Communications in Mathematics and Applications*, 11(1):161–171, 2020.

[11] C. T. H. Baker, G. A. Bocharov, and F. A. Rihan. A report on the use of delay differential equations in numerical modelling in the biosciences. Technical report, Citeseer, 1999.

[12] N. S. Bakhvalov. On the optimization of the methods for solving boundary value problems in the presence of a boundary layer. *Zhurnal Vychislitel'noi Matematiki i Matematicheskoi Fiziki*, 9(4):841–859, 1969.

[13] K. Bansal, P. Rai, and K. K. Sharma. Numerical treatment for the class of time dependent singularly perturbed parabolic problems with general shift arguments. *Differential Equations and Dynamical Systems*, 25(2):327–346, 2017.

[14] K. Bansal and K. K. Sharma. ε-uniform numerical technique for the class of time dependent singularly perturbed parabolic problems with state dependent retarded argument arising from generalised stein's model of neuronal variability. *Differential Equations and Dynamical Systems*, pages 1–28, 2016.

[15] K. Bansal and K. K. Sharma. Parameter uniform numerical scheme for time dependent singularly perturbed convection-diffusion-reaction problems with general shift arguments. *Numerical Algorithms*, 75(1):113–145, 2017.

[16] Alfredo Bellen and Marino Zennaro. *Numerical Methods for Delay Differential Equations*. Numerical Mathematics and Scientific Computation. Oxford University Press, Oxford, 2013.

[17] Richard Bellman and Kenneth L. Cooke. *Differential-difference equations*. Academic Press, 1963.

[18] A. Berger, H. Han, and R. B. Kellogg. A priori estimates and analysis of a numerical method for a turning point problem. *Mathematics of Computation*, 42:465–492, 1984.

[19] A. W. Bush. *Perturbation methods for engineers and scientists*. Routledge, 2018.

[20] C. Clavero and J. L. Gracia. A high order hodie finite difference scheme for 1D parabolic singularly perturbed reaction–diffusion problems. *Applied Mathematics and Computation*, 218:5067–5080, 2012.

[21] C. Clavero, J. L. Gracia, and F. Lisbona. High order methods on shishkin meshes for singular perturbation problems of convection–diffusion type. *Numerical Algorithms*, 22(1):73–97, 1999.

[22] J. D. Cole and L. P. Cook. *Transonic Aerodynamics*, volume 30. Elsevier, 2012.

[23] K. Cooke, P. Van den Driessche, and X. Zou. Interaction of maturation delay and nonlinear birth in population and epidemic models. *Journal of Mathematical Biology*, 39(4):332–352, 1999.

[24] Kenneth L. Cooke and Pauline Van Den Driessche. Stability analysis for a vector disease model. *Rocky Mountain Journal of Mathematics*, 9(1):31–42, 1979.

[25] P. Das. *Robust numerical schemes for singularly perturbed boundary-value problems on adaptive meshes*. Unpublished doctoral dissertation.

[26] G. De, D. N. Allen, and R. V. Southwell. Relaxation methods applied to determine the motion, in two dimensions, of a viscous fluid past a fixed cylinder. *The Quarterly Journal of Mechanics and Applied Mathematics*, 8(2):129–145, 1955.

[27] Pieter P. N. de Groen. A singular perturbation problem with boundary and turning point resonance. *Applied Mathematics Letters*, 1(1):49–51, 1988.

[28] R. P. Dunne and E. O'Riordan. A parameter-uniform numerical method for a singularly perturbed parabolic problem with a turning point. *Computers & Mathematics with Applications*, 56(3):613–626, 2008.

[29] R.K. Dunne, E. O'Riordan, and G.I. Shishkin. A fitted mesh method for a class of singularly perturbed parabolic problems with a boundary turning point. *Computational Methods in Applied Mathematics*, 3(3):361–372, 2003.

[30] Milton Van Dyke. Perturbation methods in fluid mechanics / annotated edition. Technical Report 75-46926, NASA STI/Recon Technical Report A, 1975.

[31] K. V. Emel'yanov. Difference scheme for a three-dimensional elliptic equation with small parameters at highest-order derivatives. kraevye zadachi dlya uravn. mat. fiz. *Boundary Value Problems for Equations of Mathematical physics*, pages 30–42, 1973.

[32] P. A. Farrell. Sufficient condition for the uniform convergence of difference scheme for singularly perturbed turning and non-turning point problems. In *Computational and Asymptotic Methods for Boundary and Interior Layers*, pages 230–235. Boole Press, Dublin, 1982.

[33] P. A. Farrell. Sufficient condition for the uniform convergence of a difference scheme for a singularly perturbed turning point problem. *SIAM Journal on Numerical Analysis*, 25:618–643, 1988.

[34] G. File and Y. N. Reddy. Fitted-modified upwind finite difference method for solving singularly perturbed differential difference equations. *International Journal of Mathematical Models and Methods in Applied Sciences*, 6(7):791–802, 2012.

[35] V. Y. Glizer. Asymptotic analysis and solution of a finite-horizon h^∞ control problem for singularly-perturbed linear systems with small state delay. *Journal of Optimization Theory and Applications*, 117(2):295–325, 2003.

[36] Kandiah Gopalsamy. *Stability and oscillations in delay differential equations of population dynamics*. Kluwer Academic, 1992.

[37] L. Govindarao and J. Mohapatra. Numerical analysis and simulation of delay parabolic partial differential equation involving a small parameter. *Engineering Computations*, 37(1):289–312, 2020.

[38] J. Grassman and B. J. Matkowsky. A variational approach to singularly perturbed boundary value problems for ordinary and partial differential equations with turning points. *SIAM Journal on Applied Mathematics*, 23(3):588–597, 1977.

[39] R. Gupta and M. K. Kadalbajoo. Numerical treatment of a singularly perturbed parabolic convection–diffusion problem with a turning point. *Computers & Mathematics with Applications*, 58(6):1128–1141, 2009.

[40] V. Gupta and M. K. Kadalbajoo. A layer adaptive b-spline collocation method for singularly perturbed one-dimensional parabolic problem with a boundary turning point. *Numerical Methods for Partial Differential Equations*, 27:1143–1164, 2010.

[41] V. Gupta, M. Kumar, and S. Kumar. Higher order numerical approximation for time dependent singularly perturbed differential-difference convection-diffusion equations. *Numerical Methods for Partial Differential Equations*, 34(1):357–380, 2018.

[42] W. S. Hailu and G. F. Duressa. Uniformly convergent numerical scheme for solving singularly perturbed parabolic convection-diffusion equations with integral boundary condition. *Differential Equations and Dynamical Systems*, pages 1–27, 2023.

[43] Jack K. Hale and Sjoerd M. Verduyn Lunel. *Introduction to functional differential equations*, volume 99 of *Applied Mathematical Sciences*. Springer, 1993.

[44] Thomas C. Hanks. Model relating heat-flow values near, and vertical velocities of mass transport beneath, oceanic rises. *Journal of Geophysical Research*, 76(2):537–544, 1971.

[45] M. H. Holmes. The wkb and related methods. In *Introduction to Perturbation Methods*, pages 223–296. Springer, 2013.

[46] F. A. Howes. An asymptotic numerical method for a model system with turning points. *Journal of Computational and Applied Mathematics*, 29:343–356, 1990.

[47] Arlen Mikhailovich Il'in. Differencing scheme for a differential equation with a small parameter affecting the highest derivative. *Mathematical Notes of the Academy of Sciences of the USSR*, 6(2):596–602, 1969.

[48] D. Jindge. Singularly perturbed boundary value problems for linear equations with turning points. *Journal of Mathematical Analysis and Applications*, 155:322–337, 1991.

[49] M. K. Kadalbajoo and V. Gupta. A brief survey on numerical methods for solving singularly perturbed problems. *Applied Mathematics and Computation*, 217(8):3641–3716, 2010.

[50] M. K. Kadalbajoo and K. C. Patidar. A survey of numerical techniques for solving singularly perturbed ordinary differential equations. *Applied Mathematics and Computation*, 130(2-3):457–510, 2002.

[51] M. K. Kadalbajoo and K. C. Patidar. Singularly perturbed problems in partial differential equations: a survey. *Applied Mathematics and Computation*, 134(2-3):371–429, 2003.

[52] Mohan K. Kadalbajoo and YiN Reddy. Asymptotic and numerical analysis of singular perturbation problems: a survey. *Applied Mathematics and Computation*, 30(3):223–259, 1989.

[53] R. B. Kellogg. Difference approximation for a singular perturbation problem with turning point. In *Analytical and Numerical Approaches to Asymptotic Problems in Analysis*, pages 133–139. North-Holland Publishing Company, Amsterdam, 1981.

[54] R. B. Kellogg and A. Tsan. Analysis of some difference approximations for a singular perturbation problem without turning points. *Mathematics of Computation*, 32(144):1025–1039, 1978.

[55] J. Kevorkian and J. D. Cole. *Perturbation Methods in Applied Mathematics*. Springer-Verlag, New York, 1981.

[56] Y. Kuang. *Delay differential equations: with applications in population dynamics*. Academic press, 1993.

[57] D. Kumar and M. K. Kadalbajoo. A parameter-uniform numerical method for time-dependent singularly perturbed differential-difference equations. *Applied Mathematical Modelling*, 35(6):2805–2819, 2011.

[58] S. Kumar, K. K. Sharma, and K. C. Patidar. A first-order parameter-uniform numerical method for singularly perturbed parabolic problems with turning point. *International Journal of Computer Mathematics*, 97(1):131–150, 2020.

[59] P. Kumari, D. Kumar, and H. Ramos Calle. Parameter independent scheme for singularly perturbed problems including a boundary turning point of multiplicity ≥ 1. *Journal of Applied Analysis & Computation*, 13(3):1304–1320, 2023.

[60] S. Kumari, K. K. Sharma, and K. C. Patidar. A parameter uniform finite difference method for a singularly perturbed parabolic convection-diffusion problem with a turning point. *Mathematics*, 11(2):423, 2023.

[61] Petr Lánskỳ, Miroslav Musila, and Charles E. Smith. Effects of afterhyperpolarization on neuronal firing. *Biosystems*, 27(1):25–38, 1992.

[62] T. Linß. *Layer-Resolving Mesh Methods for Convection-Diffusion Problems with Turning Points*. PhD thesis, Technische Universität Chemnitz, 2001.

[63] V. D. Liseikin. On numerical solution of two-dimensional elliptic equation with a small parameter at highest-order derivatives. *Chislennye Metody Mekhanici Sploshnoy Sredy (Numerical Methods of Continuum Mechanics)*, 14:110–115, 1983.

[64] L. Lopez. Stability of a three point scheme for linear second order singularly perturbed bvps with turning points. *Applied Mathematics and Computation*, 52:279–300, 1992.

[65] Michael C. Mackey and Leon Glass. Oscillation and chaos in physiological control systems. *Science*, 197(4300):287–289, 1977.

[66] A. Majumdar and S. Natesan. Second-order uniformly convergent richardson extrapolation method for singularly perturbed degenerate parabolic partial differential equations. *International Journal of Applied and Computational Mathematics*, 3:31–53, 2017.

[67] A. Majumdar and S. Natesan. ε-uniform hybrid numerical scheme for a singularly perturbed degenerate parabolic convection-diffusion problem. *International Journal of Computer Mathematics*, 96:1313–1334, 2019.

[68] M. Majumdar and S. Natesan. A second-order parameter-uniform numerical method for singularly perturbed parabolic problems with turning point. *Applied Mathematics and Computation*, 217(7):3057–3076, 2010.

[69] M. Majumdar and S. Natesan. Parameter-uniform finite difference method for a class of parabolic turning point problems. *Journal of Computational and Applied Mathematics*, 262:96–109, 2014.

[70] R. M. M. Mattheij and P. M. van Loan. A new approach to turning point theory. In *BAIL V*, pages 251–256. Boole, Dun-Laoghaire, 1988. Conference held in Shanghai.

[71] É. Matzinger. Asymptotic behaviour of solutions near a turning point: the example of the brusselator equation. *Journal of Differential Equations*, 220:478–510, 2006.

[72] W.G. Melesse, A.A. Tiruneh, and G.A. Derese. Uniform hybrid difference scheme for singularly perturbed differential-difference turning point problems exhibiting boundary layers. *Abstract and Applied Analysis*, 2020(1):7045756, 2020.

[73] W.G. Melesse, A.A. Tiruneh, and G.A. Getachew. Fitted mesh method for singularly perturbed delay differential turning point problems exhibiting twin boundary layers. *Journal of Applied Mathematics & Informatics*, 38(1–2):113–132, 2020.

[74] Wondimu G. Melesse, Asmamaw A. Tiruneh, and Getachew A. Derese. Uniform hybrid difference scheme for singularly perturbed differential-difference turning point problems exhibiting boundary layers. *Abstract and Applied Analysis*, 2020(1):7045756, 2020.

[75] R. E. Mickens. *Advances in the applications of nonstandard finite difference schemes*. World Scientific, 2005.

[76] Ronald E. Mickens. *Nonstandard Finite Difference Models of Differential Equations*. World Scientific, Singapore, 1994.

[77] J. J. Miller, E. O'riordan, and G. I. Shishkin. *Fitted numerical methods for singular perturbation problems: error estimates in the maximum norm for linear problems in one and two dimensions*. World scientific, 1996.

[78] J. J. Miller, E. O'Riordan, and G. I. Shishkin. *Fitted Numerical Methods For Singular Perturbation Problems*. world scientific, revised edition, 2012.

[79] J. J. H. Miller, E. O'Riordan, and G. I. Shishkin. *Fitted Numerical Methods for Singular Perturbation Problems: Error Estimates in the Maximum Norm for Linear Problems in One and Two Dimensions*. World Scientific, Singapore, 1996.

[80] Peter D. Miller. *Applied Asymptotic Analysis*. American Mathematical Society, Providence, 2006.

[81] W. L. Miranker and J. P. Morreeuw. Semianalytic numerical studies of turning point problems arising in stiff boundary value problems. *Mathematics of Computation*, 28:1017–1034, 1974.

[82] R. S. Muhammad. Numerical derivative using the piecewise uniform mesh. *Kirkuk University Journal-Scientific Studies*, 13(3):135–153, 2018.

[83] M. Musila and P. Lánský. Generalized stein's model for anatomically complex neurons. *BioSystems*, 25(3):179–191, 1991.

[84] M. J. Ng-Stynes, E. O'Riordan, and M. Stynes. Numerical methods for time-dependent convection-diffusion equations. *Journal of Computational and Applied Mathematics*, 21(3):289–310, 1988.

[85] M. J. Ng-Stynes, E. O'Riordan, and M. Stynes. Numerical methods for time-dependent convection-diffusion equations. *Journal of Computational and Applied Mathematics*, 21(3):289–310, 1988.

[86] Frank W. J. Olver. *Asymptotics and Special Functions*. Academic Press, New York, 1974.

[87] R. E. O'Malley. On boundary value problems for a singularly perturbed differential equation with a turning point. *SIAM Journal on Mathematical Analysis*, 1:479–490, 1970.

[88] R. E. O'Malley. *Introduction to Singular Perturbations*. Academic Press, New York and London, 1974.

[89] R. E. O'Malley. *Singular Perturbation Methods for Ordinary Differential Equations*. Springer-Verlag, New York, 1991.

[90] Robert E. O'Malley. *Singular Perturbation Methods for Ordinary Differential Equations*. Springer-Verlag, New York, 1991.

[91] R. E. O'Malley. *Historical Developments in Singular Perturbations*. Springer, 1974.

[92] K. C. Patidar. On the use of nonstandard finite difference methods. *Journal of Difference Equations and Applications*, 11(8):735–758, 2005.

[93] K. C. Patidar. Nonstandard finite difference methods: recent trends and further developments. *Journal of Difference Equations and Applications*, 22(6):817–849, 2016.

[94] K. C. Patidar and K. K. Sharma. Uniformly convergent non-standard finite difference methods for singularly perturbed differential-difference equations with delay and advance. *International Journal for Numerical Methods in Engineering*, 66(2):272–296, 2006.

[95] S. J. Polak, C. Den Heijer, W. H. Schilders, and P. Markowich. Semiconductor device modelling from the numerical point of view. *International Journal for Numerical Methods in Engineering*, 24(4):763–838, 1987.

[96] L. Prandtl. Uberflussigkeitsbewegungbeisehrkleinerreibungverh. III. Intern. Math. Kongr., 1905.

[97] S. Priyadarshana, J. Mohapatra, and L. Govindarao. An efficient uniformly convergent numerical scheme for singularly perturbed semilinear parabolic problems with large delay in time. *Journal of Applied Mathematics and Computing*, pages 1–23, 2022.

[98] P. Rai and K. K. Sharma. Singularly perturbed parabolic differential equations with turning point and retarded arguments. *IAENG International Journal of Applied Mathematics*, 45(4):305–312, October 2015.

[99] P. Rai and K. K. Sharma. A parameter-uniform numerical method for singularly perturbed parabolic differential-difference equations with turning points and deviating arguments. *International Journal of Computer Mathematics*, 97(12):2374–2396, 2020.

[100] P. Rai and S. Yadav. Robust numerical schemes for singularly perturbed delay parabolic convection-diffusion problems with degenerate coefficient. *International Journal of Computer Mathematics*, 98(1):195–221, 2021.

[101] V. P. Ramesh and M. K. Kadalbajoo. Upwind and midpoint upwind difference methods for time-dependent differential difference equations with layer behavior. *Applied Mathematics and Computation*, 202(2):453–471, 2008.

[102] G. Rao and R. Chakravarthy. Fitted numerical methods for singularly perturbed 1d parabolic partial

differential equations with small shifts arising in the modelling of neuronal variability. *Differential Equations and Dynamical Systems*, pages 1–18, 2017.

[103] K. Rathish and K. Sunil. Convergence of three-step taylor galerkin finite element scheme based monotone schwarz iterative method for singularly perturbed differential-difference equation. *Numerical Functional Analysis and Optimization*, 36(8):1029–1045, 2015.

[104] Hans-Görg Roos. Robust numerical methods for singularly perturbed differential equations: a survey covering 2008–2012. *ISRN Applied Mathematics*, 2012:1–35, 2012.

[105] Hans-Görg Roos, Martin Stynes, and Lutz Tobiska. *Robust numerical methods for singularly perturbed differential equations: convection-diffusion-reaction and flow problems*, volume 24. Springer Science & Business Media, 2008.

[106] Hans-Görg Roos, Martin Stynes, and Lutz Tobiska. *Numerical Methods for Singularly Perturbed Differential Equations: Convection-Diffusion and Flow Problems*. Springer, Berlin, 1996.

[107] K. Ku. Sahoo and V. Gupta. An almost second-order uniformly convergent finite difference method for singularly perturbed parabolic problems with a turning point. *Mathematics and Computers in Simulation*, 194:359–376, 2022.

[108] S. K. Sahoo and V. Gupta. Second-order parameter-uniform finite difference scheme for singularly perturbed parabolic problem with a boundary turning point. *Journal of Difference Equations and Applications*, 27:223–240, 2021.

[109] Hermann Schlichting. *Boundary-Layer Theory*. McGraw-Hill, New York, 1979.

[110] L. F. Shampine. Heat transfer by conduction and radiation. *Indiana University Mathematics Journal*, 1978.

[111] K. K. Sharma and K. C. Rai, P.and Patidar. A review on singularly perturbed differential equations with turning points and interior layers. *Appl. Math. Comput.*, 219(22):10575–10609, 2013.

[112] G. I. Shishkin. A difference scheme on a non-uniform mesh for a differential equation with a small parameter in the highest derivative. *USSR Computational Mathematics and Mathematical Physics*, 23(3):59–66, 1983.

[113] G. I. Shishkin. Grid approximations to singularly perturbed parabolic equations with turning point. *Differential Equations*, 37(7):1037–1050, 2001.

[114] Satpal Singh. *Quadratic Spline Based Numerical Schemes for Different Classes of Singularly Perturbed Problems*. Ph.d. dissertation, BITS Pilani, Pilani Campus, Pilani, India, 2024.

[115] D. R. Smith. *Singular Perturbation Theory*. Cambridge University Press, Cambridge, 1985.

[116] Hal L. Smith. *An introduction to delay differential equations with applications to the life sciences*. Springer, 2011.

[117] R. B. Stein. A theoretical analysis of neuronal variability. *Biophysical Journal*, 5:173–194, 1965.

[118] R. B. Stein. Some models of neuronal variability. *Biophysical journal*, 7(1):37–68, 1967.

[119] Thomas H. Stix. *Waves in Plasmas*. Springer Science & Business Media, 1992.

[120] M. Stynes and H.-G. Roos. The midpoint upwind scheme. *Applied Numerical Mathematics*, 23(3):361–374, 1997.

[121] Martin Stynes and Hans-Görg Roos. The midpoint upwind scheme. *Applied Numerical Mathematics*, 23(3):361–374, 1997.

[122] D. M. Tefera, A. A. Tiruneh, and G. A. Derese. Numerical treatment on parabolic singularly perturbed differential difference equation via fitted operator scheme. *Abstract and Applied Analysis*, 2021:Article ID 1661661, 2021.

[123] S. K. Tesfaye, G. F. Duressa, M. M. Woldaregay, and T. G. Dinka. A uniformly convergent numerical scheme for singularly perturbed parabolic turning point problem. *Journal of Mathematical Modeling*, 4:501–516, 2024.

[124] H. C. Tuckwell. *Stochastic Processes in the Neurosciences*, volume 56. SIAM, 1989.

[125] Henry C. Tuckwell. *Introduction to Theoretical Neurobiology. Volume 2: Nonlinear and Stochastic Theories*. Cambridge University Press, Cambridge, 1988.

[126] M. Villasana and A. Radunskaya. A delay differential equation model for tumor growth. *Journal of Mathematical Biology*, 47(3):270–294, 2003.

[127] R. Vulanović and P. A. Farrell. Analysis of a multiple boundary turning point problem. *Radovi Matematički*, 8:181–196, 1992.

[128] R. Vulanović and P. A. Farrell. Continuous and numerical analysis of a multiple boundary turning point problem. *SIAM Journal on Numerical Analysis*, 30(5):1400–1418, 1993.

[129] W. Wasow. *Linear Turning Point Theory*. Springer, New York, 1985.

[130] Wolfgang Wasow. *Asymptotic Expansions for Ordinary Differential Equations*. Interscience Publishers, New York, 1965.

[131] Wolfgang Wasow. *Linear Turning Point Theory*, volume 54 of *Applied Mathematical Sciences*. Springer, 1987.

[132] Wolfgang Richard Wasow. *ON BOUNDARY LAYER PROBLEMS IN THE THEORY OF ORDINARY DIFFERENTIAL EQUATION*. New York University, 1942.

[133] A. M. Watts. A singular perturbation problem with a turning point. *Bulletin of the Australian Mathematical Society*, 5:61–73, 1971.

[134] S. Yadav, P. Rai, and S. Natesan. A robust numerical method for solving a class of singularly perturbed parabolic turning point problems. *Computers & Mathematics with Applications*, 78(7):2285–2303, 2019.

[135] Swati Yadav and Pratima Rai. A higher order scheme for singularly perturbed delay parabolic turning point problem. *Engineering Computations*, 38(2):819–851, 2021.

[136] Swati Yadav, Pratima Rai, and Kapil K Sharma. A higher order uniformly convergent method for singularly perturbed parabolic turning point problems. *Numerical Methods for Partial Differential Equations*, 36(2):342–368, 2020.